PULSED REACTION STUDIES OF SIMPLE REACTIONS ON ALUMINA SUPPORTED RHODIUM .

Ph.D. Thesis

Timothy John Cassidy.

Liverpool University, December 1994.

Thesis submitted in accordance with the requirements of the University of Liverpool for the degree of

Doctor of Philosophy

by

Timothy John Cassidy.

December 1994.

This Thesis is Dedicated to

My Parents and family;
I cannot thank you enough for enabling, encouraging and supporting me throughout my life and education.

Isabella ,
thank you for bearing with me, ti voglio bene, amore mio .

December 1994.

ACKNOWLEDGEMENTS.

First and foremost my immeasurable thanks are extended to Professor Mike Bowker, who has encouraged and inspired me scientifically (not an easy achievement !) over the last three years, but more than this, he has also been a true friend.

In addition, my sincere thanks goes to:

British Gas Plc for providing the CASE award, and Dr Norman Parkyns and Dr Robert Judd for their supervision and the I.R.C. in Liverpool for providing the Ph.D. award.

All the members of Staff in the Chemistry Department and the I.R.C. in Liverpool, a special mention should go to Prof. R.W. Joyner, Prof. G. Hutchings, Alan Nicholson and Pat Gibbs, who helped me immensely along the way, and to all the Bowker Group members from '91-'94.

All the members of staff at Reading, academic, secretarial and most importantly the maintenance staff, who made me very welcome and ensured that the move from Liverpool was smooth and painless.

And last but not least, to all of my friends both in the 'Leverhulme Comprehensive for Inopportune Catastrophe', Liverpool as a whole (hole ?) and in Reading. I wish I could mention everyone who has contributed to making the last three years so brilliant but alas I'll have to be brief, so here's a selected few in no particular order: Members of Moose Lodge; Neil (N.O.T.B. etc,), Andy and Rob. Mansion Chicks; Karen (Brooko Baby) and Nikki, plus Rich of course. The Leverhulme Kids; Paul K. Steve, F., Justin, Stu, Saskia, Col., and all the rest. From Reading; Mat, Amanda, Rob and Jane (S.T.S !), plus the Burch and Hollins groups and not forgetting the golden oldies Miles, Annie and Jim (alias Scum).

ABSTRACT:

PULSED REACTION STUDIES OF SIMPLE REACTIONS ON ALUMINA SUPPORTED RHODIUM.

A pulse-flow microreactor has been used to study simple synthesis gas ($CO + H_2$) reactions and the decomposition of glacial acetic acid, over a rhodium and a promoted rhodium on alumina catalyst. The microreactor is capable of analysing the post-reactor gases continually in real time with a quadrupole mass spectrometer.

The microreactor has been successfully used to measure the metal surface area of the catalysts by means of oxygen up-take. The amount of up-take is measured directly by detecting the breakthrough point of the adsorbate gas by the mass spectrometer.

The reactor revealed useful information on the mechanism and rates of reaction through the temperature range from 150°C to 450°C. When 0.5 ml pulses of CO were eluted into a continuous stream of H_2/He, the rhodium catalysts showed ~100% selectivity towards the formation of methane and water between 160°C and 260°C. From ~260°C onwards, a change in reaction mechanism was apparent, with dry methanation beginning to dominate over wet methanation. The rates of product formation in a transient experiment decrease in the order $CO_2 > CH_4 > H_2O$. The predominant reason for the gross change in mechanism is the change in reactant stoichiometries brought about by the differing desorption rates of hydrogen and carbon monoxide. The presence of H_2 does not lower the activation energy to CO dissociation, the role of H_2 is to clean the rhodium surface of C(a) and O(a). The rate of both methane and water production increases with higher hydrogen concentrations.

Rhodium based catalysts have the ability to selectively produce oxygenates such as ethanol from synthesis gas ($CO + H_2$). Acetate groups are seen in large numbers on catalysts that possess good ethanol selectivities and therefore the acetate group may be of some importance to the reaction mechanism. The adsorption and decomposition of glacial acetic acid has been studied over the supported rhodium catalysts. It is found to decompose with unusual autocatalytic kinetics under certain conditions. This type of decomposition is termed a 'surface explosion' and is analogous to decompositions reported on single crystals. Surface explosions of carboxylates have not been reported before on supported catalysts and this discovery is an interesting example of a direct transfer of knowledge from surface science to catalysis. A molecular model is proposed to explain the explosion phenomena and the higher temperature decomposition processes which involve both the migration of acetates from the alumina support to the rhodium particles, and the availability of O(a) species on the rhodium.

The main effect of potassium promotion was to alter the CO hydrogenation reactions by increasing CO conversion. The up-take of O_2 was reduced and a higher temperature of oxygen and acetic acid adsorption was required in order to produce an 'explosive' acetate decomposition.

Timothy John Cassidy. December 1994.

CONTENTS.

CHAPTER 1

INTRODUCTION.

- 1.1. Catalysis in general.
- 1.2. Rhodium , the element and its chemistry.
- 1.3. General synthesis gas chemistry.
- 1.4. General methane chemistry.
- 1.5. The CO molecule, its bonding and reactivity.
- 1.6. Scope of the thesis.
- 1.7. References.

1.1. CATALYSIS in GENERAL.

Catalytic action was first widely reported in the early part of the nineteenth century as a result of some isolated and diverse observations. Such as :

(a) the ability of heated platinum wires or foils to caused oxygen to combine with coal gas, alcohol and ether (Davy 1807) and to promote the union of hydrogen and chlorine (Turner, 1822);

(b) the oxidation of hydrogen to water at room temperature, caused by the presence of a platinum sponge (Dobereiner, 1822);

(c) the decomposition of hydrogen peroxide by platinum, gold and silver (Thenard, 1818);

(d) the conversion of starch to sugar on the addition of mineral acid (Kirchoff, 1812) and ,

(e) the dehydrogenation of alcohol to ether, in the presence of H_2SO_4 (which was found to be left unchanged); a reaction known since medieval times (Mitscherich, 1834).

Berzelius was the first to recognise a common theme and concluded that these observations heralded the discovery of a new phenomenon, and to describe it he used the word "CATALYSIS". The word is derived from two Greek words, the prefix *Kata* -meaning lower or down and *Lysein* , meaning to break or to loosen. His concept was however not exactly correct as he believed a catalytic "force" was responsible for the phenomenon as the catalyst

remained unchanged; the "force" he referred to, may be what we now call the surface free energy.

By the end of the nineteenth century the kinetic theory of gases and basic chemical kinetics had been formulated and through these developments a more rigorous view of catalysis emerged. In 1891 Ostwald re-defined a catalyst to be a substance which "changed the velocity" of a chemical reaction, thus laying to rest the rather ethereal "catalytic force" of Berzelius.

Ostwalds definition has stood the test of time and is very similar to the presently worded definition; 'a catalyst is a substance that increases the rate at which a chemical system approaches equilibrium, without being consumed in the process'[1].

The above definition leads to several general implications and these are as follows.

1 A catalyst cannot change the ultimate equilibrium position which is determined by thermodynamics, its role being restricted to accelerating the rate of approach to equilibrium. At any given temperature, the standard entropy and enthalpy changes of a reaction must be the same for both catalysed and uncatalysed reactions.

2 A catalyst can only increase the rate of a reaction that is already thermodynamically feasible.

3 A catalyst does not alter the equilibrium constant of a reaction, and so the quotients of the rates for the forward and reverse reactions must also remain unchanged at equilibrium. If therefore the catalyst increases the forward rate, it must also increase the reverse rate by the same factor at equilibrium.

4 A catalyst decreases the activation energy of a reaction. This means that the catalysed reaction proceeds by a new and energetically more favourable pathway.

The main branches of catalysis are heterogeneous, homogeneous and enzymatic catalysis. These disciplines are differentiated by whether or not the reactants and products share the same phase as the catalyst.

Heterogeneous catalysed processes are those systems in which the reactants, products and the catalyst exist in different phases; most commonly solid catalysts are used with gaseous or liquid reactants and occasionally both. Heterogeneously catalysed processes are convenient to use commercially indeed ~90% of industrial chemical processes make use of a heterogeneous catalyst, some of which are shown in Table 1.1[2]. Solid industrial catalysts are manufactured as pellets which are normally packed into tubes through which reactants flow, satisfying process requirements of simple construction and stable operation. Many variations exist on this simple approach including the shape of the catalyst pellets, the length of the catalyst bed, the flow rate and pressure of the reactants, and the temperature of the reaction. More recently, advances have been made in industrial reactor design with the development of 'fluidised beds' where the catalyst is a powder and is suspended in a upward flow of the reactant gases.

Homogeneous catalysis relates to a reaction where the catalyst, reactants and products are all in the same phase: either gas, liquid or solid. The liquid phase is the most common and most important industrially. Some industrially important homogeneous processes are; the Monsanto process, producing acetic acid from the carbonylation of methanol with carbon monoxide, and the Wacker process for oxidising ethene to acetaldehyde. However liquid phase operation places restrictions on temperature and pressure and subsequently the catalyst must be separated from the products, imposing additional difficulties.

Enzymes fall somewhere in between molecular homogeneous catalysts and macroscopic hetergeneous catalysts. They are proteins of colloidal size and are the driving force behind biochemical reactions. Present in an

enormous array of life processes they are characterised by their tremendous efficiencies and selectivities. There is enormous interest in studying the mechanisms and active sites within enzymes in the hope that the knowledge can be applied to improve the selectivity of industrial reactions.

Catalytic reactions are generally believed to pass through the following basic steps;

(1) Transport of reactants to the catalyst surface;

(2) Adsorption of the reactants on the catalyst;

(3) Reaction on the catalyst surface involving one or more adsorbed species;

(4) Desorption of products away from the catalyst;

(5) Transport of reactants away from the catalyst surface.

Steps (2) - (4) are chemical in nature and constitute the catalytic reaction, whereas steps (1) and (5) are not chemical. Any of steps (1) - (5) may be the rate-determining step for a reaction. If either step (1) or (5) is slower than the catalytic rate then we say the rate of reaction is diffusion controlled or mass-transport-controlled. The catalytic reaction steps involved in heterogeneous catalysis generally occurs at the gas /surface interface and are illustrated in Figure 1.1. overleaf.

Figure 1.1. Catalytic Steps Occurring at the Gas/Surface Interface and the Parameters Effecting Them.

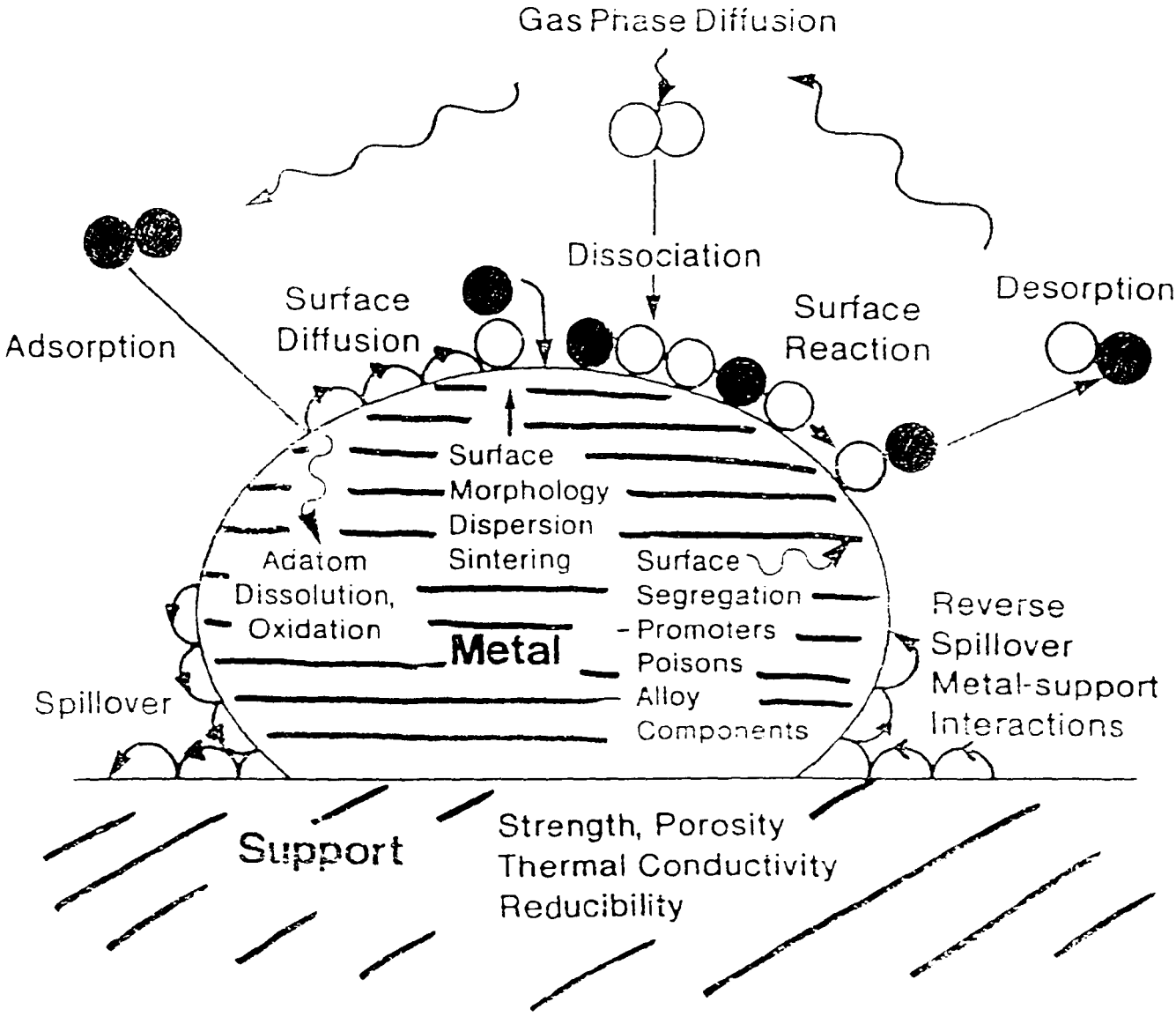

1.2. RHODIUM, the ELEMENT and its CHEMISTRY.

As a rhodium catalyst has been used throughout this thesis it is useful to cite some of the physical and chemical properties of the metal, see Table 1.2. overleaf, and to give a brief history of the element.

Rhodium was discovered in 1803 by W.H.Wollaston in England, and was named such because of the rose colour of aqueous acidic solutions of the metal salts. Rh has an atomic number of 45 and its relative atomic weight is 102.9. Rhodium is one of the platinum group of transition metals and shares their similar chemical and physical properties, it is found in small quantities in crude platinum ores, the majority of which are deposited in the river sands of the Urals and in North and South America. The gas phase atom has an electronic configuration of $4s^2\ 4p^6\ 4d^8\ 5s^1$. The ionic radius of Rh^{3+} is 66.4pm and the radius of Rh^0 is 134.5 pm. ^{103}Rh has a nuclear spin of $^1/_2$.

The major industrial use of rhodium is in car exhaust catalyts, which accounts for over 60% of its production, as shown in Table 1.3. overleaf[3]. Other major uses are in hydroformylation reactions (oxo reactions) in which H and HCO are formally added across a double bond using rhodium complexes such as $(Ph_3P)_3Rh(CO)H$ (used in the Union Carbide hydroformylation process). Today the vast majority of C_3 - C_{15} aldehydes are produced by oxo reactions and are subsequently converted into amines, carboxylic acids and above all , primary alcohols, the capacity world-wide for oxo compounds is ~5 x 10^6 t/a and as such represents the largest industrial scale homogeneous reaction[4]. In addition a rhodium complex catalyses the carbonylation of methanol to acetic acid, this is commercialised as the Monsanto process. A woven rhodium-platinum alloy gauze is an efficient commercial catalyst for the formation of nitric acid through ammonia oxidation. Rhodium-platinum alloys are also favoured for high temperature

Table 1-2 Physical properties of rhodium

Properties	Value
Crystal structure	Face-centred cubic
Lattice constant a, at 298K, nm	0.38031
Thermal neutron capture cross section, barns (10^{-28} m^2)	149
Density at 298K, g/cm^3	12.43
Melting point	1966K
Boiling point	3973K
Specific heat at 273K, cal/g (J/kg)	0.0589 (246)
Thermal conductivity, 273 - 373K, cal cm/cm^2 s K	0.36
Linear coefficient of thermal expansion, 293 - 373K, μm/(m. K)	8.3
Electrical resistivity at 273K, microhm-cm	4.33
Temperature coefficient of electrical resistance, 273 - 373K/K	0.00463
Tensile strength, $103lb/in^2$ (6.895MPa)	
Soft	120 - 130
Hard	200 - 230
Yung's modulus at 293K (GPa)	
Static	319
Dynamic	378
Hardness, diamond pyramid number	
Soft	120 - 140
Hard	300
ΔH_{fusion}, kJ/mol	21.6
$\Delta H_{vaporization}$, kJ/mol	494
ΔH_t monatomic gas, kJ/mol	556
Electronegativity	2.2

Table 1-3 Quantities of rhodium used in various applications (units: ounce)

Year	1988	1989	1990	1991	1992
Rh for autocatalyst	232	264	334	301	305
Total supply	317	324	370	348	378
Total demand	304	327	391	346	328

applications such as glass and glass fibre manufacture, furnace wiring and dies for pulling glass fibres, thermocoples and electrical contacts. Additionally, a small amount of rhodium goes into jewellery manufacture.

The dark red deliquescent $RhCl_3.H_2O$ (decomposing at above 373K) is the most commonly used compound of rhodium and is the usual starting point for the preparation of other rhodium compounds. The only stable oxide of the metal is the dark grey Rh_2O_3 , which has a corundum structure.

1.3. GENERAL SYNTHESIS GAS CHEMISTRY.

At present gasoline is the worlds most important fuel and it is not likely to be replaced in the near future. The oil crisis in the seventies demonstrated the dependence of the Western economies on the large crude oil resources in the Middle East. In order to become less dependent on these countries (desirable because of the political instability in that region) a general route for the production of gasoline and other added value hydrocarbon and oxygenated products was developed, using synthesis gas as the raw material, see Figure 1.2.

Synthesis gas (commonly referred to as syngas) is a mixture of carbon oxides and hydrogen, in various proportions. It can be made from coal or hydrocarbon feedstocks such as methane, oil residues or biomass , by steam reforming or selective oxidation. At present ~90% of the worlds hydrogen and syngas is produced by steam reforming of hydrocarbons, however in the future, methane and coal gasification will become the principal route due to the increasing cost and scarcity of liquid hydrocarbon feedstocks. One of the most promising new methods of producing synthesis gas from methane is by partial oxidation, using oxygen directly[5,6]. The reaction produces H_2 and CO in the ratio of 2:1 which is desirable for the synthesis of many hydrocarbons.

Figure 1. 2. General Synthesis Gas Conversion Routes Using a Variety of Transition Metals.

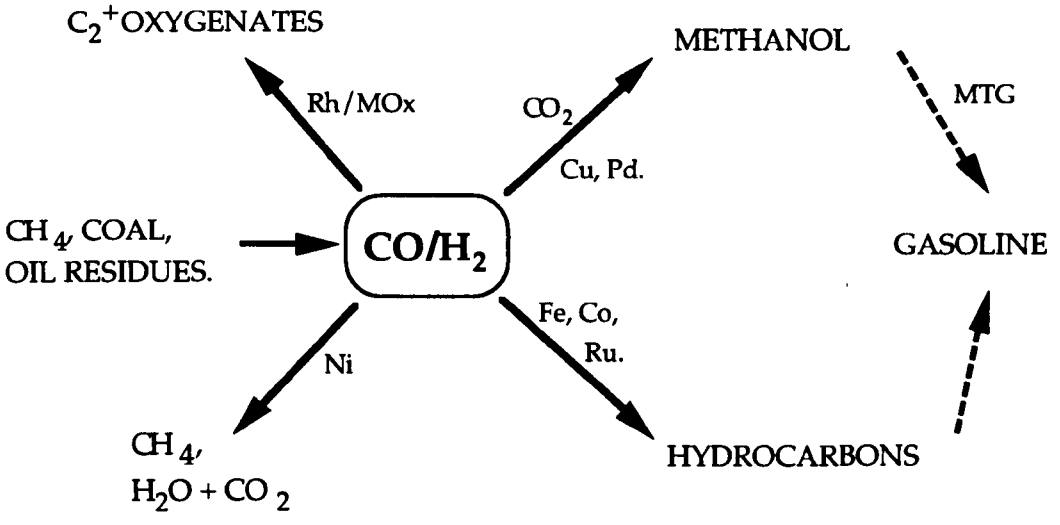

Synthesis gas owes its name to the ability to be converted selectively into a wide variety of products by using the right catalyst and reaction conditions. Some of the main industrial processes for which synthesis gas is produced are highlighted below:

(a) The production of H_2 - principally for ammonia synthesis, petroleum reforming and hydrogenation reactions - requires CO in the synthesis gas mixture to be converted into another molecule of hydrogen via the water gas shift reaction:

$$CO + H_2O <-----> CO_2 + H_2$$

and then removal of CO_2 by absorption. The water gas shift reaction is operated at two temperatures, the "high temperature shift" operates at ~700K and uses a magnetite (Fe_3O_4) and chromia (Cr_2O_3) containing catalyst. The "low temperature shift" operates at ~500K and uses a copper, zinc oxide and alumina catalyst.

(b) Methanation occurs over a nickel catalyst:

$$3H_2 + CO \text{ <-----> } CH_4 + H_2O$$

and is used as a method of purification to remove traces of carbon monoxide in the hydrogen production process and has been used to convert synthesis gas to pipeline gas.

(c) Production of higher hydrocarbons by Fischer-Tropsch chemistry. This process was developed to counter the shortage of crude oil in Germany during the first half of this century. The process is still being used in South Africa presently, using Fe-containing catalysts.

(d) Methanol synthesis, the majority of which is produced using a $Cu/ZnO/Al_2O_3$ catalyst, developed by I.C.I. Methanol can be directly converted to gasoline over zeolites via the M.T.G. process.

(e) Synthesis gas has been used in conjunction with other compounds such as the hydroformylation of alkenes for the production of aldehydes or alcohols and the carbonylation of methanol.

In addition to these industrial processes, synthesis gas has been converted into higher oxygenates via a heterogeneous reaction over promoted rhodium catalysts and this area of catalysis is one of the most topical today. Clearly the development of a one step selective heterogeneous process producing ethanol or acetic acid from synthesis gas will bypass the need for the expensive processes presently used and also reduce the use of toxic and volatile co-catalysts (such as methyl iodide in the Monsanto process).

1.4. GENERAL METHANE CHEMISTRY.

There are vast reserves of methane available world wide, however, the majority of it is located in remote areas such as Siberia, far from the chemical market . Presently the majority of methane is used as a domestic fuel or is 'flared' at oil rigs. It is a very useful fuel resource, however, because it is a gas

its energy density is low in comparison to coal and oil and it is both difficult and expensive to transport over long distances. Therefore there is great interest in developing ways of converting methane into more transportable and higher valued products. The most well known routes for methane conversion are summarised in Figure 1.3. below.

Figure 1. 3. Direct and Indirect Routes of Methane Conversion.

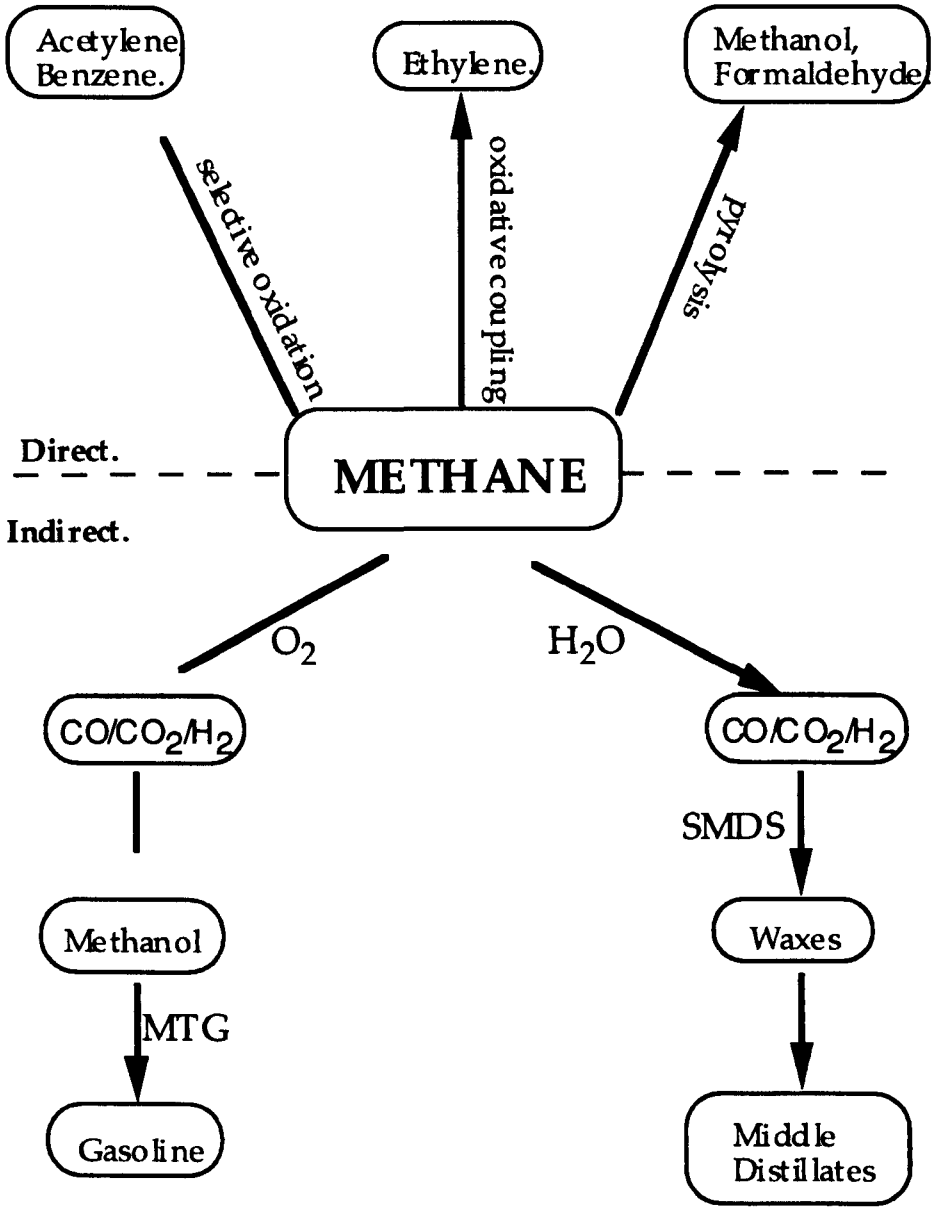

The direct selective oxidation of methane to methanol and formaldehyde is of interest as it by-passes the need to convert methane into synthesis gas. The perennial problem of selective oxidation processes is the rapid consecutive oxidation of the selective products to the fully oxygenated products, CO and CO_2 , limiting the overall yield of the reaction. For a review of selective oxidation routes of methane see Pitchai and Klier[7].

The oxidative coupling of methane to ethene and higher hydrocarbons has been achieved with yields approaching 30%, however prolonged activity has not been achieved and despite enormous efforts to crack this highly desirable process, it is proving very difficult to develop a catalytic system that is both stable and produces sufficient yields required to make it industrially feasible[8].

Methane pyrolysis to higher hydrocarbons occurs at high temperatures (above 1200^{o}C) by gas phase radicals. Graphite formation as well as the high operating temperature are the main limiting factors to this process, as well as low yields, commonly 12% at best.

At the present time only two indirect commercial processes have been realised for the transformation of methane into higher valued products. These are the Methanol To Gasoline (MTG) process, developed by Mobil and currently in operation in New Zealand[9], and the Shell Middle Distillate Synthesis (SMDS)[10] , which has been developed by Shell and began operating in Malaysia in 1991. Both processes transform methane via synthesis gas and because of the laboriousness of the multi-stage conversion schemes, new routes for methane tranformation are still of great interest.

In order to convert methane, one must activate the C-H bond and herein lies the difficulty. The fundamental reason why methane is available in such large quantities world wide is because it is thermodynamically very stable, it has a noble gas like configuration with strong tetrahedral C-H bonds which lack polarity. Most methane conversion reactions use reactants such as

water, oxygen or chlorine. These oxidants are corrosive and chlorine is highly toxic. The use of pure oxygen (as in the SMDS process) is extremely expensive as it must be separated cryogenically from air, and it ends up in the final products of CO_2 and H_2O. When water is used in steam reforming of methane the production of synthesis gas is expensive, approximately 80% of the total cost of the methane conversion route is due to the synthesis gas formation[11]. Clearly in view of these facts, methane routes to higher hydrocarbons that circumvent the high temperatures and expensive oxidants of the synthesis gas route are of world wide interest.

1.5. THE CO MOLECULE, ITS BONDING AND REACTIVITY.

The bonding and reactivity towards dissociation in the CO molecule is thought to be well understood and has been recently reviewed (see for instance Hindermann et al.[12] and references therein) and can be explained by consideration of the molecular orbitals. The electronic configuration of the molecule[13] in its' ground state is :

$$1\sigma^2 . 2\sigma^2 . 3\sigma^2 . 4\sigma^2 . 1\pi^4 .$$

The molecular orbitals are filled in the main as such, the 1σ and 2σ are essentially C1s and O1s respectively and are nonbonding, the 3σ orbital is essentially O2s in character and has a substantial bonding character. The 4σ and 5σ are situated, respectively, around the oxygen and carbon atoms and are analogous to the "lone pairs". The centre of the 5σ orbital is located along the CO bond axis but is largely outside its internuclear spacing and it is this orbital that is able to donate to unfilled d-orbitals on a metal and provides a means of strong adsorption. The O2p electrons predominantly form the doubly degenerate 1π orbital. This orbital is essentially bonding and with the

3σ orbital forms the triple bond in the CO molecule. Figure 1.4. shows the molecular orbital diagram for CO (adapted from[14]).

Figure 1. 4. The Molecular Orbital Diagram of CO.

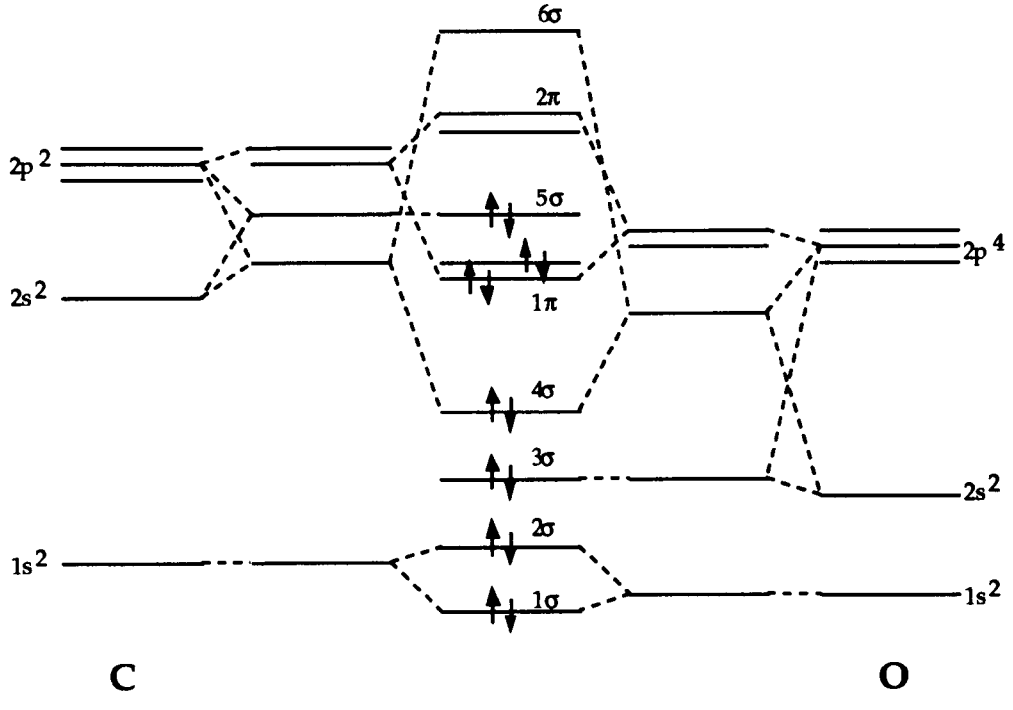

Unlike in a homonuclear diatomic molecule, the two atoms in the CO molecule have different nuclear charges. The O atom has a greater nuclear charge and results in its atomic orbitals being lower in energy than the corresponding orbitals in carbon, as shown in Figure 1.4. This results in certain molecular orbitals being strongly localised onto either the carbon or the oxygen atom.

The most common model by which CO is thought to bond to transition metals is known as the 'Blyholder' model. In this model the CO is attached carbon down and the molecular bond axis is perpendicular to the metal

surface. The metal to carbon bond results from charge transfer from the highest occupied molecular orbital of CO (the 5σ orbital) to a free σ symmetry d orbital of the metal, as noted by Broden et. al.[15], this does not weaken to any great extent the CO bond as the 5σ is essentially non-bonding with respect to the carbon and oxygen. The degree of population of the $2\pi^*$ orbitals is related to the activation energy of dissociation. Electron back-donation from an occupied s symmetry d orbital of the metal into the unoccupied $2\pi^*$ orbital of the CO leads to a weakening of the CO bond as the $2\pi^*$ orbital is antibonding with respect to carbon and oxygen and thus aids dissociation.

In the 'Blyholder' model of CO adsorption[16], the molecule is imagined to be oriented perpendicular to the surface, however, more recent studies of CO adsorbed on many transition metals, especially those with a low number of d-electrons, show that prior to dissociation, the CO passes through a tilted CO geometry. De Koster et.al.[17] during a theoretical molecular orbital model study of CO dissociation on different faces of rhodium, in agreement with the statement above, found that the first step in CO dissociation was a tilting of the CO molecule to the surface , until the CO is at an angle of approximately 70^o to the surface normal.

1.6. THE SCOPE OF THE THESIS.

As the title suggests, the work presented in this thesis is related to simple reactions of synthesis gas, predominantly the methanation reactions, over an un-promoted and promoted alumina supported rhodium catalyst. All the results in the thesis have been obtained on a specialised pulsed flow microreactor built 'in house' which was designed to study the transient products of catalytic reactions. Questions related to the initial reaction

mechanism of CO and CO_2 hydrogenation over rhodium and the mechanistic changes that occur with changes in temperature and reactant concentration have been addressed. The work, as well as investigating the usefulness of the micoreactor, has also tested the value of it in terms of how it yields information normally gained through other techniques - such as metal surface area measurements and activation energies.

The second theme of the thesis is related to the unusual behaviour of acetate groups adsorbed onto the small rhodium particles. It has been observed in surface science studies, that under certain conditions, carboxylate groups decompose with unusual autocatalytic kinetics. It has been found in this present study, that these phenomena, termed 'surface explosions' do infact translate directly to the high area supported rhodium catalyst. Acetate groups are important in the general field of methane and synthesis gas chemistry as they are found to be present in large numbers on promoted rhodium surfaces , active in the formation of ethanol from synthesis gas, under reaction conditions.

Finally, the rhodium catalyst was promoted with potassium and the effect of the promoter was studied in relation to the above reactions.

1.7 REFERENCES

1 Bond, G.C., "*Heterogeneous Catalysis: Principles and Applications*", Clarendon Press, Oxford (1987)

2 Mross, W.D., *Catal. Rev.-Sci. Eng.*, **25**(4), 591 (1983).

3 "*Platinum 1993*" Johnson Matthey.

4 Elschenbroich, C. and Salzer, A. "*Organometallics - A Concise Introduction*", VCH, Weinheim, Germany (1989).

5 Ashcroft, A.T., Cheetham, A.K., Foord, J.S., Green, M.L.H., Grey, C.P., Murrell, A.J. and Vernon, P.D.F., *Nature*, **344**, 319 (1990)

6 Hickman, D.A. and Schmidt, L.D., *Science*, **259**, 343 (1993)

7 Pitchai, R. and Klier, R., *Catal. Rev.,-Sci. Eng.*, **28**, 13 (1986)

8 Amenomiya, Y., Goledzinowski, M., Birss, V., Galsuszka, J. and Sanger, A.R., *Catal. Rev.-Sci. Eng.*, **32**, 63 (1990)

9 Chang, C.D. and Silvestri, A.J., *J. Chemtech.*, **17**, 624 (1987)

10 Sie, S.T., Senden, M.M.G. and Wechem van, H.M.H., *Catal. Today*, **8**, 371 (1991)

11 Michel, S., Linde, A.G. and Hoëllriegelskreuth, W., *Hydrocarbon Processing*, **68**, 37 (1989)

12 Hindermann, J.P., Hutchings, G.J., and Kiennemann, A., *Catal. Rev.-Sci. Eng.*, **35**(1), 1 (1993).

13 Ishi,I., Ohno, Y. and Viswanathan, B., *Surf. Sci.*, **161**, 349 (1985).

14 Hollins, P., *Ph.D. Thesis*, University of London (1980).

15 Broden, G. Rhodin, T.N., Bruckner, C.F. Benbow, R. and Hurych, Z., *Surf. Sci.*, **59**, 593 (1976).

16 Blyholder, G., *J. Phys Chem.*, **68**, 2772 (1964).

17 De Koster, A., Jansen, A.P.J. and van Santen, R.A., *Faraday Discuss. Chem. Soc.*, **87**, 263 (1989).

CHAPTER 2.

EXPERIMENTAL.

2.1. INTRODUCTION

Most experimental techniques used in academia and industry that measure catalytic parameters such as activity, selectivity and rates of reactions, monitor reaction systems that are operating under steady state conditions. In Chapter 1 the main processes involved in a heterogeneous catalytic step were illustrated. There are a number of steps, including adsorption, surface reaction and desorption. By using a conventional experimental technique operating at steady state, the overall parameters, for instance the overall rate of reaction from reactants to products, can be obtained. The direct determination of individual rate constants for each intermediate step in a reaction is obviously highly desirable as it leads to a detailed understanding of the mechanism of the reaction. In principle, measurements of the dynamics of adsorbed species and product molecules can lead to the determination of rate constants of individual steps.

The first transient method was used by Wagner and Hauffe[1] in 1939 when they perturbed the concentration of H_2 and O_2 on a palladium electrode. In 1955 a pulse method of transient experimentation was developed by Kokes, Tobin and Emmett[2], since then the method has formed the basis of numerous investigations. Useful information on the kinetics and mechanisms taking place during a reaction can be probed with transient methods by studying the dynamic response of the catalytic system under examination to a controlled change in its steady state or equilibrium state reaction. The most common variable used to change the reaction state is a change in the temperature, however any practical variable which, in part, defines the chemical state of the system may be used, and a number of transient techniques have been successfully developed[3,4]. The other most common variables are pressure and concentration. Mori et al. for instance, makes use of emissionless infrared diffuse reflectance spectrometry to monitor the

dynamics of the adsorbed species and flame ionisation detection to monitor the dynamics of the products[5,6,7]. A reactant is pulsed into a gas stream (possibly a second reactant) and its adsorption and reaction is monitored. Clearly when using this method no dispersion of the reactant or product pulses can be permitted otherwise false decay curves will be registered that do not lead to the true reaction rate constant. In order to do this, the dead volume of the reactor should be minimised.

2.2. EQUIPMENT.

2.2.1. THE PULSED FLOW MICROREACTOR.

The majority of experimental data presented in this thesis was collected on a specialised transient pulsed flow microreactor, originally built in-house by D. Law, S. Francis and M. Bowker. A schematic diagram of the reactor is given in Figure 2.1. and the following is a description of it.

The microreactor flows a diluent gas over a catalyst. A reactant gas mixture can be introduced into the diluent line and 'dosed' continuously onto the catalyst or for a pre-determined time period. A second reactant gas mixture can be 'pulsed' into the diluent, or diluent/'dosed' gas mixture, in set quantities (in this work 0.5 ml was normally used). Analysis of the post reactor gas stream is performed continually in real time, by quadrupole mass spectrometry, the travel time of the gas from the reactor to detector being approximately nine seconds. The rig passes gases supplied by B.O.C. PLC, with a purity of not less than 99.995%, from a bank of high pressure cylinders down $^1/_8$ inch stainless steel tubing connected with air tight Swagelok fittings and through stainless steel 'peritubes' supplied by Phase Separation Ltd. These contain a 5Å molecular sieve which reduces the water content of

FIGURE. 2.1. THE PULSE FLOW MICROREACTOR.

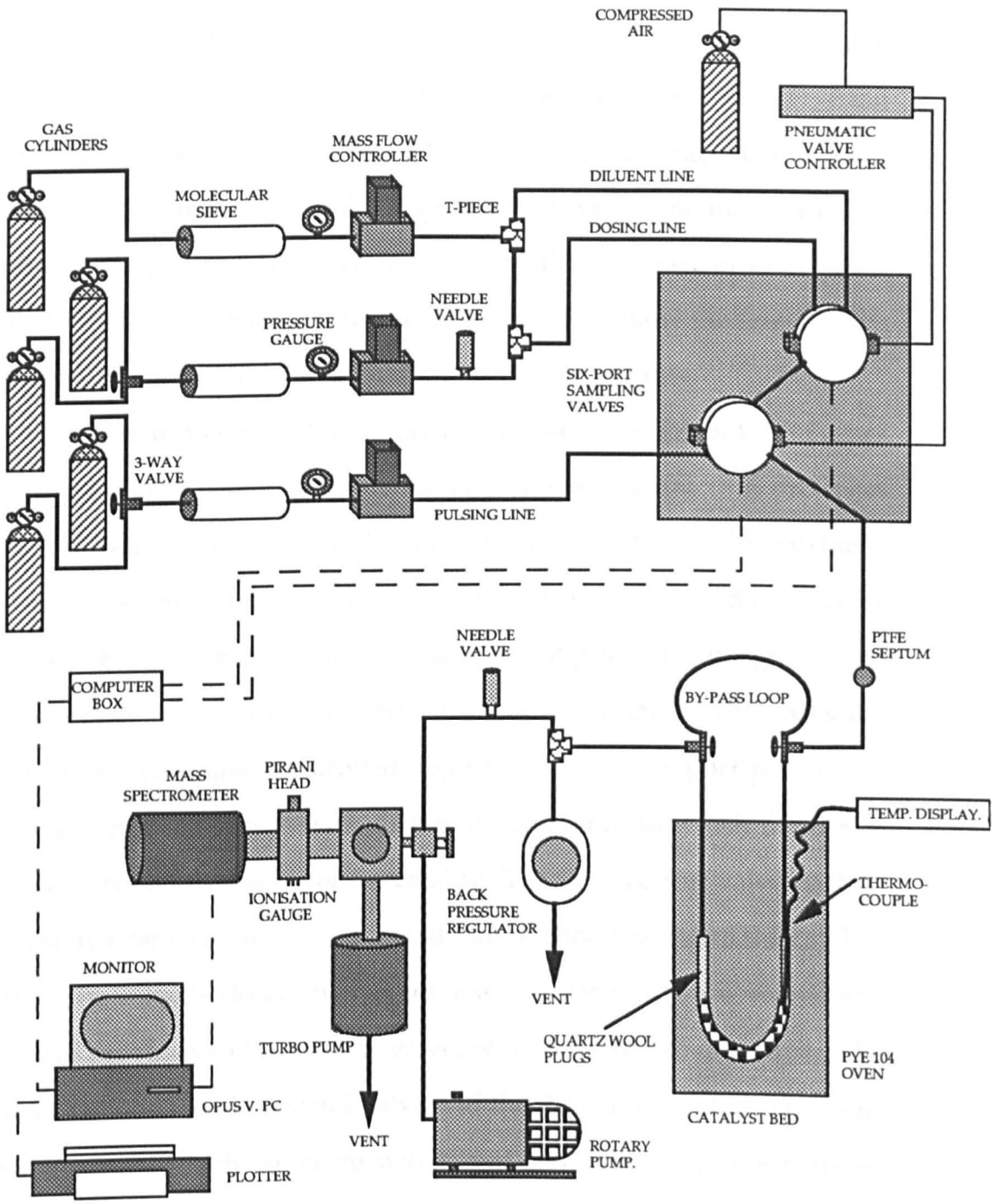

the gases to less than 1ppm. The peritubes also remove carbon dioxide and hydrogen sulphide therefore when carbon dioxide is used as a reactant, the molecular sieve is by-passed. In addition, the diluent helium gas passes through a 2 micron sieve. In this work, the gases used are; helium as the diluent, hydrogen, carbon monoxide, carbon dioxide, methane and oxygen as reactants, compressed air is used to operate the pneumatic valves which control the switching of flows. The hydrogen line has a Witt C_2H_4/H_2 flash back arrestor and the oxygen line has a B.O.C. Saffire flash back arrestor and each is attached to the outlet of the respective cylinder regulator head. The gases pass through Fisher pressure gauges and the flow rate of each gas is controlled by a Brooks 5580 mass flow controller. These allow the flow of each gas to be controlled to within an accuracy of 0.1 ml per minute.

The diluent line is split, one line acts as the main diluent , the other line is joined to the 'dosing' line by a T-piece. The dosing line thus produces an intimate mixture of helium and the reactant gas to be dosed. This mixing is necessary to ensure that the required amount of reactant gas is dosed across the catalyst while maintaining the total flow rate of gas when the gas stream is switched from only helium to a helium/reactant mixture. The gases are then led to two computer controlled Taylor-Servomex six port pneumatic valves, positioned in series, which dictate the sequence in which the dosed and pulsed gases are passed over the catalyst. The first six port valve enables the helium/reactant gas mixture to be fed into the line leading to the catalyst bed. When the valve is closed the helium/reactant gas mixture is vented and only helium proceeds to the second valve, when it is switched to open, the 'dose' reactant is fed to the second valve and the diluent is vented. The exact time in seconds at which the valve switches in and out can be programmed from the Opus V P.C. keyboard at the start of each experiment. The second six port valve enables a reactant gas to be 'pulsed' into the gas stream leading to the catalyst bed. The valve consists of a 0.5 ml. sample loop through which

the reactant gas to be pulsed continually flows. When the valve is closed the gas is vented. When the valve is switched open, the 0.5ml of gas in the loop is pushed into the mainstream leading to the catalyst bed, by either the diluent or the helium/reactant mixture, depending on whether the first valve is open or closed. The resulting 'pulse' flows over the catalyst with a narrow, defined shape, allowing the line shapes of the products evolving from the catalyst to be analysed continuously in real time. The timing of the first pulse, the duration of the pulse and the periodicity of each pulse can be programmed to an accuracy of 1 second from the P.C. before each experiment (see software description). The gases then pass either to the catalyst bed or can be directed by two Whitey 3-way valves through a by-pass loop and flow directly to the mass spectrometer unit. A Phase Separation triple silicone /PTFE septum is located immediately before the first 3-way valve allowing gases or liquids to be manually injected into the gas stream. Calibrations were made by injecting known quantities of a gas and recording the sensitivity of the mass spectrometer , see section 2.4.

The catalyst (normally 0.5 g) is located in a stainless steel U-tube reactor with 3mm i.d. and held in place at both ends of the bed by quartz wool plugs. A sheathed thermocouple is inserted into the catalyst bed which is ~6 cm in length. The whole U-tube ensemble is housed in a Pye 104 fan circulation oven, capable of heating the bed uniformly to 500°C. The oven can be ramped at rates from 1°C/minute up to a maximum of 40°C/minute and can be held at isothermal temperatures. Located after the oven is a Tescom back pressure regulator, in this work the pressure was kept at around ambient. To ensure that products do not condense, the post reactor gases pass down a heated capillary line kept at 120°C, the temperature of the heating tape can be varied using a Variac. A needle valve then reduces the total flow of gas, most of it is vented, the remainder passes to the mass spectrometer unit. At the mass spectrometer unit, the majority of the gas mixture is vented

FIGURE. 2.2. THE MASS SPECTROMETER ASSEMBLY.

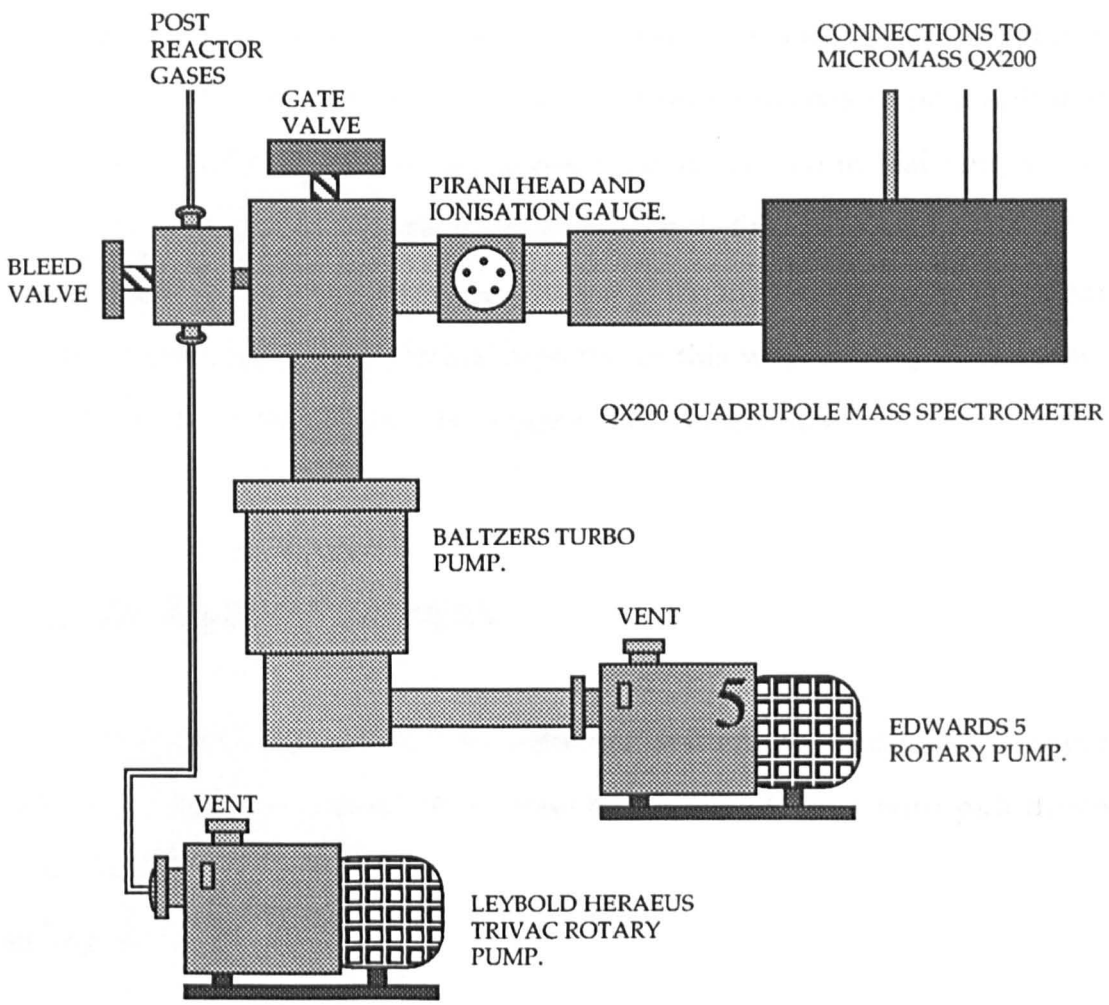

via a Leybold Heraeus TriVac rotary pump and only a small fraction is bled into the mass spectrometer itself. The latter is a V.G. QX200 quadrupole mass spectrometer, and the mass spectrometer assembly is shown in Figure 2.2. It is pumped by a Baltzers Turbo pump with a pumping speed of 170 litres per second, an Edwards 5 rotary pump continually backs the Turbo pump. The background pressure in the mass spectrometer is approximately 8.0×10^{-8} Torr, with the bleed valve open allowing the post reactor gases in the pressure rises to approximately 2×10^{-5} Torr. The mass spectrometer is generally run in the multiplexed mode allowing up to six different masses to be monitored continually. The output of the mass spectrometer is seen in real time on the P.C. screen. Software written in-house by Dr S. Francis enables the mass spectrometer to scan the voltage at which a given mass is expected to appear and then lock onto the maximum intensity. In this way, drifting of the mass spectrometer is corrected and the required mass is scanned.

2.2.2. SOFTWARE DESCRIPTION.

The microreactor is run on software written, 'in-house' at Liverpool University by Dr S. Francis. It is presented in table format with pull down menu items (see table 2.1.).

Table 2.1.

FILE	ACQUIRE	REVIEW	OUTPUT	VALVES	OTHERS
Load	Comments	Comments	Clear Comments	Manual	R.G.A.
Save	Set time	Time/date	Print Data	Remote	
Quit	Masses	Change time basis.	Plot Data	Cleaning cycle	
	Take data	Masses	Integration		
		Display			

To take data, the experimental parameters must first be set. In the Acquire column, the total time in minutes of the run, up to a maximum of 15, and the masses to be analysed, are specified. The software enables the quadrupole mass spectrometer to 'lock on' to each mass by comparing the theoretical voltage at which a given mass is transmitted and the actual voltage at that mass. The mass spectrometer scans either side of the theoretical voltage and the maximum voltage found is locked onto in the scan, this helps to compensate for any drifting of the mass spectrometer sensitivity. The sequence in which reactants are introduced into the diluent stream is set by entering the Remote menu item in the Valves column. A time is specified, in seconds, after the start of the run when the dosing valve is to be switched in and out, and when the first pulse is to be eluted. The duration of the pulse and the time interval between pulses can be set. Text or notes, normally the experimental parameters, are recorded in the Comments menu item, and are printed out when a hard copy is plotted. All data are saved onto the hard disk of the P.C. by going to the File column and pressing Save. Data can be manipulated in the Review column. The time basis can be altered to show an enlarged section of the spectrum. Masses can be multiplied to take into account sensitivity factors, or to enhance a peak or desorption profile, and they can also be deleted from the plot. From the Output column the raw or manipulated data can be plotted on a Hewlett Packard ColorPro flat bed plotter. The software also allows integration of peak areas to be carried out by finding the total area beneath a given peak between two specified times, then subtracting the corresponding trapezoidal area. For more accurate integration calculations and for higher quality data presentation, the data was converted into an Apple Macintosh file and displayed using Kaleidagraph 3.0.2. software.

2.2.3. METHODOLOGY

To ensure that results taken at different times during the course of this research were reproducible and comparable, the microreactor and the catalysts were conditioned in the same way before experiments were carried out. The mass spectrometer filament was degassed so that all desorption products seen during an experiment were from the catalyst and not from residual gas on the filament itself. The background gases, namely carbon monoxide and residual water vapour, were checked so that their levels could be subtracted from experimental amounts. With the gas flowing through the by-pass the gas lines were purged and their masses analysed by the mass spectrometer to ensure that no foreign residual gases were present, this was especially important when the gas passing through the dosing or pulsing lines had been changed.

Once the lines were fully purged, the gas flow was switched to flow across the catalyst bed and the oven was ramped from room temperature to between 400°C and 450°C. This cleared the catalyst and the walls of the reactor vessel of water. The catalyst was then cleaned of any contaminants by reduction in flowing hydrogen for ten minutes at >400°C. Generally the total flow rate was 60 mls per minute and the ratio of hydrogen to helium was 1:10. The catalyst was then cooled in helium to the required temperature. Before an experiment could be carried out, the sensitivity of the mass spectrometer was tuned so that the height of a reactant pulse, passed through the by-pass, was maximised on the computer monitor.

Every two to three months, or after a new catalyst had been loaded into the reactor, the flow rate indicated by the mass flow controllers and the actual flow rate of gas was calibrated. This was done by closing the post reactor needle valve , thus diverting the total gas flow into the vent line. A bubble meter was attached to the vent line and the flow rate was manually recorded

Figure 2.3.
Mass flow controller reading versus actual flow rate.
for H_2 through the gas dosing line.

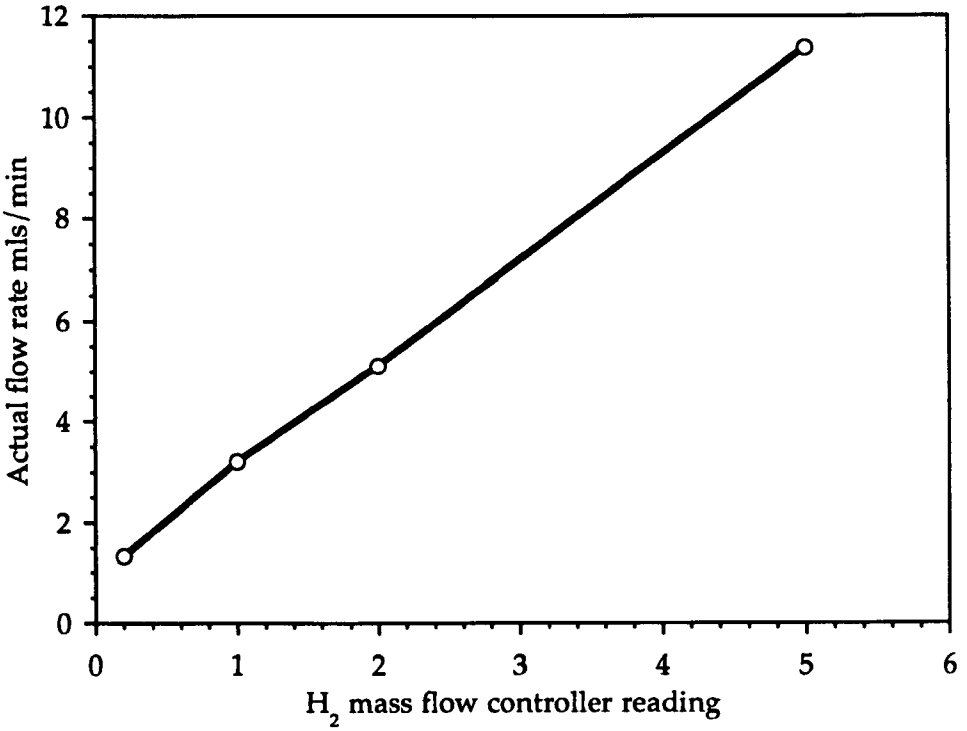

Figure 2.3. is a plot of the mass flow controller reading versus the actual flow rate of hydrogen through the dosing line. A significant discrepancy between the flow rate through the catalyst bed and through the by-pass indicates that there is a blockage in the catalyst bed and gas cannot flow freely through it, thus altering the amount of reactants passing over the catalyst and the area of catalyst available for reaction. If a catalyst powders and becomes compacted it can form a plug, this can lead to a severe pressure drop across the catalyst bed which in turn may lead to a change in the product distribution due to an elevated pressure.

After conditioning the catalyst, as described above, the oven was then cooled to the required temperature, keeping the flow of helium passing over the catalyst. Depending on the experiment to be carried out, the masses to be monitored were set and the mass spectrometer peak locked. The mass spectrometer was most sensitive to masses that were in appreciable quantities during the peak locking process. If H_2 was flowing during peak locking, it was more sensitive than the other masses being monitored. The experimental sequence determining the point at which the reactants were dosed and/or pulsed was set, as was the total duration of the run, up to a maximum of fifteen minutes. The data from each run was saved onto the hard disk of the computer immediately. Once the data was collected the software allows individual mass gains to be changed for output purposes.

2.3. EXPERIMENTAL MODES of the PULSED FLOW MICROREACTOR

2.3.1. ISOTHERMAL PULSED MODE.

In this experimental mode the temperature of the catalyst is held constant while a sequence of reactants are dosed and/or pulsed over the

catalyst. A variety of experimental parameters can be altered, such as the temperature of the catalyst bed, the total flow rate which determines the contact time of the reactants on the catalyst surface, the partial pressure of individual reactants and of the total system, the concentration of the dosed reactant, which will alter the surface concentration of the dosed reactant and therefore the products formed. The catalyst can be dosed prior to, after or during the pulsing sequence yielding different information in each case. When one reactant is pulsed into a continuous flow of the dosed reactant the result is an accurate reaction profile at a given temperature, see Figure 2.4. This yields information on the activity, selectivity, the conversion of the reactants and the yield of products under defined conditions. The most obvious visible information is revealed by the position and shape of the product peaks as they appear after a reactant pulse. As described in the introduction, a fast sharp product peak appearing coincident with the reactant pulse is indicative of a kinetically favourable reaction and of a fast surface step. A product which is the result of a slower surface reaction will (a) be separated from the reactant pulse by a time difference and (b) will yield a broadened peak relative to the incident pulse. The rate of reaction and the selectivities to products can be altered by raising the temperature or altering the ratios of the reactants.

2.3.2. TEMPERATURE PROGRAMMED PULSE REACTION (T.P.P.R.).

Essentially this experimental mode is the same as the isothermal pulse mode, except the temperature of the oven is ramped while carrying out the measurement see for example Figure 2.5. Normally the temperature range is from room temperature to 450°C over a 15 minute reaction run. The result is

Figure 2.4.
H_2/He = 1:20. Flow = 60 mls/min

Temperature = 435° C

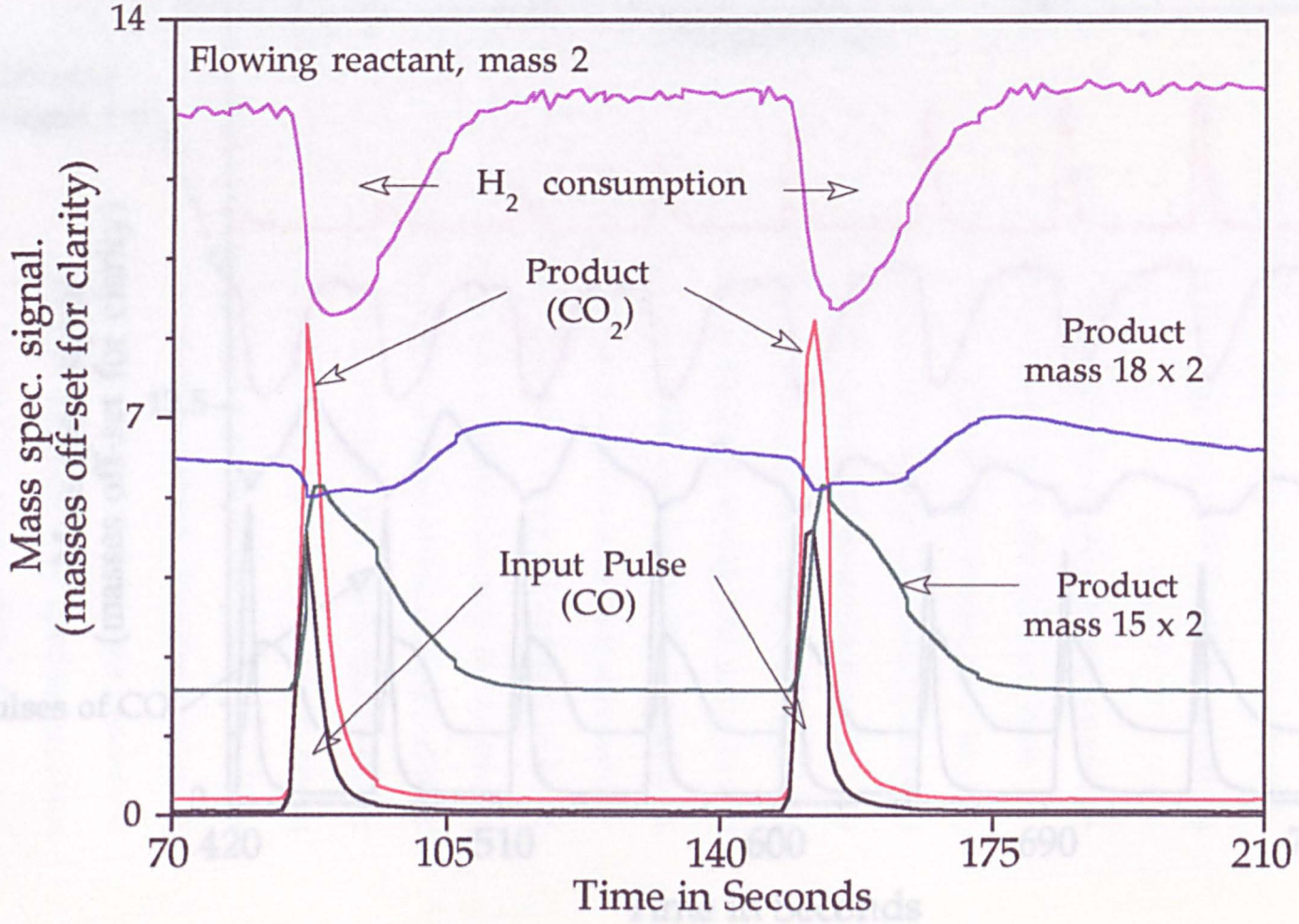

Figure 2.5.
Temperature Programmed Pulsed Reaction (T.P.P.R.).
0.5 ml Pulses of CO into a 1:20 H_2/He mixture.

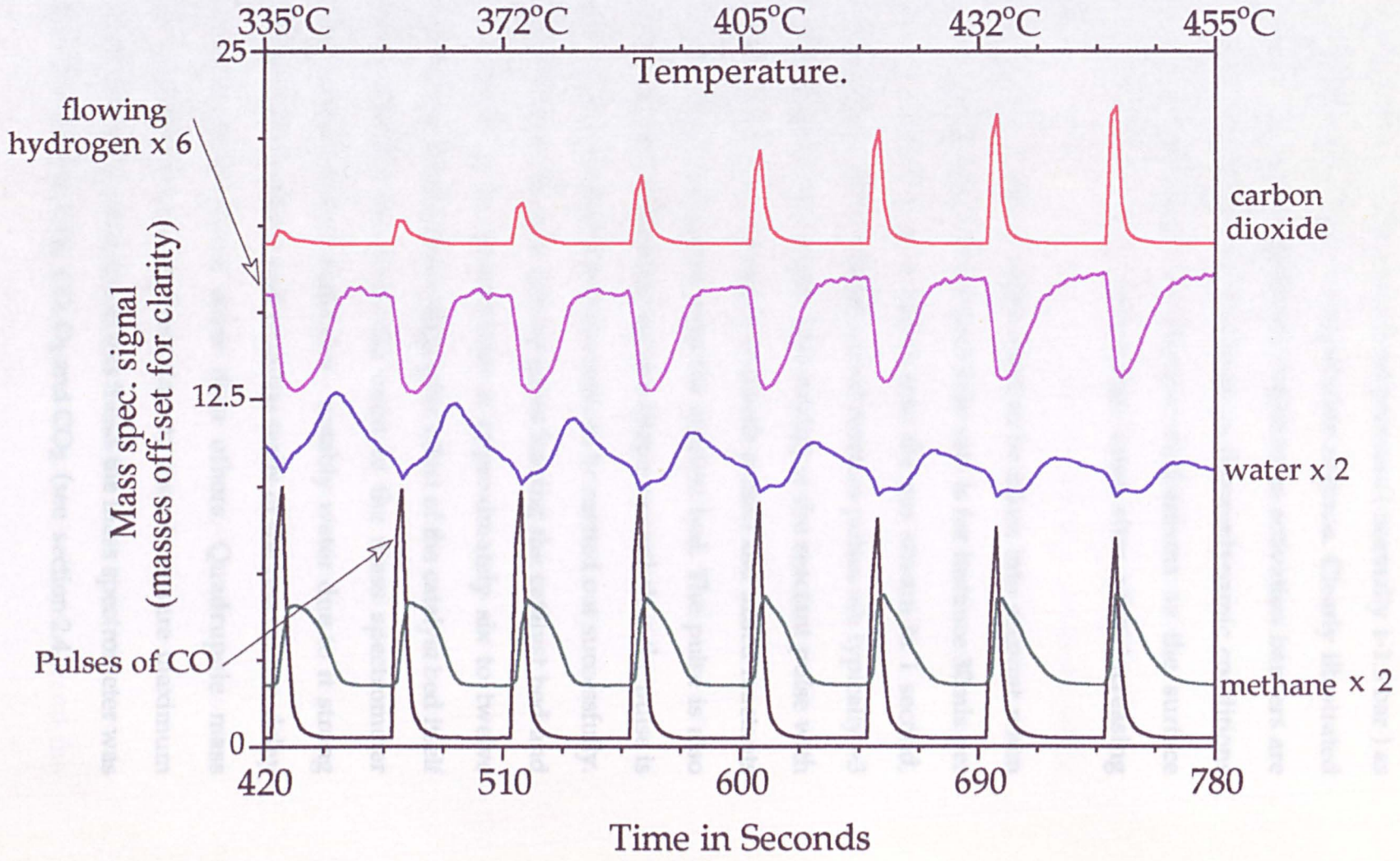

a total reaction profile in real time, at a fixed pressure (normally 1-1.5 bar) as the reaction goes through different temperature regimes. Clearly illustrated using this mode is the onset of different reactions as activation barriers are overcome, the rise and decline of products as thermodynamic conditions change and also the changes in reaction mechanisms as the surface concentration of reactants and desorption rates alter with increasing temperatures.

Certain features of the machine need to be taken into account when studying all the reaction plots. If the total flow rate is for instance 30mls per minute, the 0.5 ml sample loop is eluted into the gas stream in 1 second, however under these conditions the observed reactant pulses are typically ~3 seconds in width at half peak height. This mixing of the reactant pulse with the main gas flow is necessary to ensure that both pulsed and dosed reactants are present when the pulse passes over the catalyst bed. The pulse is also more of a Lorenzian shape rather than square shape, nevertheless the pulse is sufficiently narrow for transient measurements to be carried out successfully. The time delay between the post reactor gases leaving the catalyst bed and being analysed in the mass spectrometer is approximately six to twelve seconds, coupled to that is the chromatographic effect of the catalyst bed itself and the heated capillary line from the oven to the mass spectrometer assembly. Interactions between molecules - notably water due to it strong dipole - and the catalyst support and with the walls of the reactor can delay the analysis of some products more than others. Quadrupole mass spectrometers require fine tuning from time to time to ensure maximum accuracy. During the work presented in this thesis the mass spectrometer was calibrated regularly with H_2, CH_4, CO, O_2 and CO_2 (see section 2.4.).

2.4. GAS and LIQUID INJECTION and CALIBRATION.

The microreactor has a PTFE septum located in the diluent line immediately prior to the PYE 104 oven (see Figure 2.1.), allowing both gases and liquids to be dosed onto the catalyst accurately by manual injection. The septum was replaced regularly to ensure it remained air tight. Gases were injected to an accuracy of .025mls and up to a maximum of 10mls using Dynatech Precision Sampling Corp. gas syringes, fitted with high precision 'air-lok' valves. Gas samples for calibration where taken from a gas bomb, containing a continuous flow of the calibration gas, fitted with a rubber septum to enable the gases to be withdrawn with a syringe. In the case of liquids, SGE micro volume syringes were used, giving an accuracy of 0.01µl. When injecting a liquid it is necessary to ensure that the aliquot evaporates completely into the diluent gas stream before the syringe is withdrawn from the septum. When calibrating the mass spectrometer several injections of different volumes of a given gas were made. At very large quantities, the fragmentation pattern and the sensitivity of the mass spectrometer can be different than for smaller quantities of gas, this is caused by saturation of mass spectrometer due to the sudden influx of gas. A volume of gas similar to the volume produced during a reaction run gave the most accurate signal for calibrating the mass spectrometer for that gas. The peaks were integrated and the average area for a given volume of gas was taken. The integrals of product and reactant peaks were taken and compared to the calibrated integral to allow the yields, conversions and selectivities to be calculated.

Experiments involving the injection of oxygen in this way to measure the metal surface area of the catalysts are described in Chapter 3 and the dosing of acetic acid are described in Chapter 4.

2.5. QUADRUPOLE MASS SPECTROMETRY.

All quadrupole mass spectrometers operate by causing ions of different mass to charge ratios (m/e) to follow different spatial trajectories by subjecting them to three dimensional electromagnetic fields[8]. The potential variation required to produce the required electric field can be set up by the use of accurately machined stainless steel cylindrical electrodes, mounted symmetrically so that r/ro is approximately 1.16, where r is the radius of the electrode and ro is the radius of the inscribed circle. Figure 2.6. illustrates the general assembly of a quadrupole mass spectrometer.

Figure 2.6. A Quadrupole Mass Spectrometer

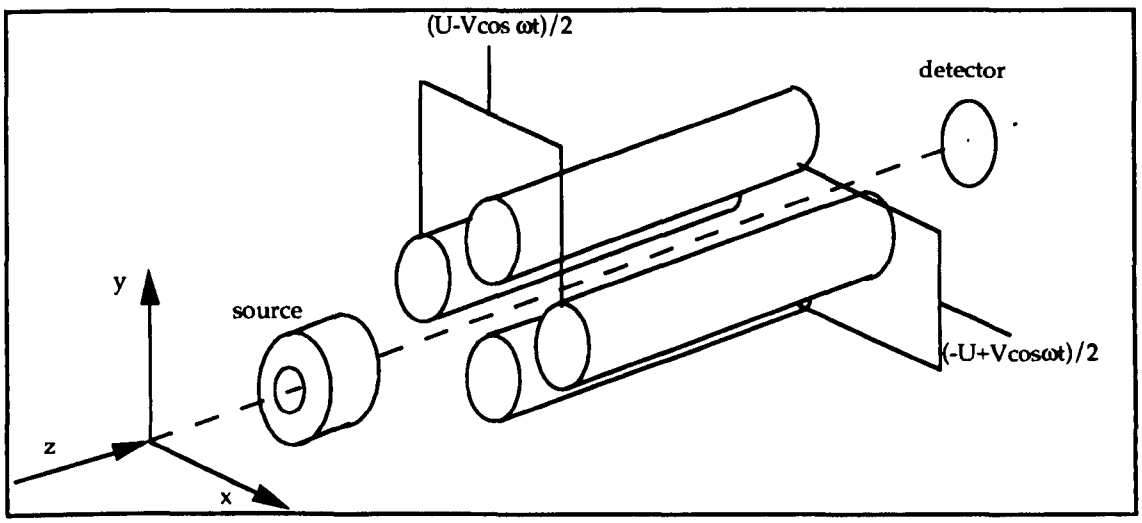

In quadrupole mass spectrometry, molecules are bombarded with electrons emitted from a filament, thus producing positive ions in a characteristic fragmentation pattern. An alternating electric field generates the

Figure 2.7.(a) Mass Spectrometer Stability Diagram

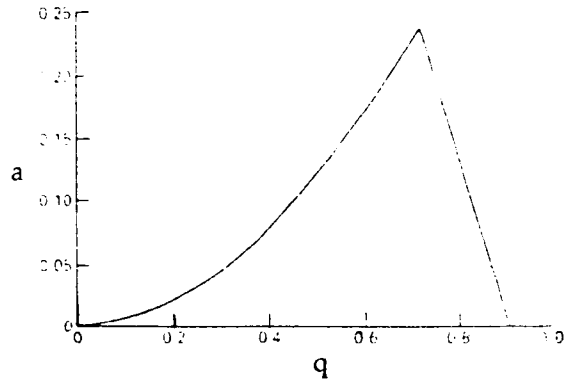

Figure 2.7.(b) Mass Spectrometer Stability Diagram Expressed in Terms of U(dc) and V(rf)

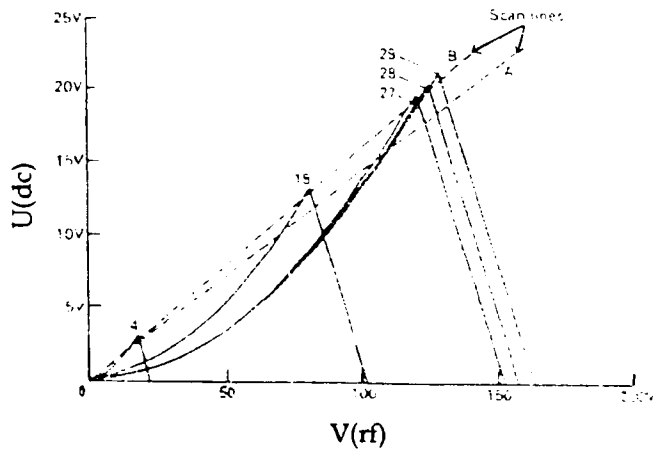

Radio frequency = 2 MHz

Quadrupole r_o = 2.75 mm

required mass selection operation. In order to generate a mass spectrum, an alternating voltage V is scanned, with a direct voltage U following it, so that V and U follow a' scan line' as shown in Figure 2.7. - this type of plot is called a 'Stability diagram' . If the transmitted ion current is monitored whilst U and V are scanned, a mass spectrum results, with the mass scale being linearly related to V . Depending on the voltages chosen, only certain masses will be stable and so able to travel down the quadrupole and reach the detector, in this way the quadrupole acts as a mass filter. The scan line is chosen so that it is parallel to the tops of the stability regions , but is displaced downwards so that peaks of approximately equal widths are obtained over the mass range. At higher masses the scan line approaches the apex of the stability region. The amplitude of the oscillations of the ions at this point are large, and so there is a higher probability that they will collide with an electrode or be ejected from the filter, this results in a lower sensitivity for higher masses[9].

2.6. TEMPERATURE PROGRAMMED DESORPTION (T.P.D.).

Temperature programmed desorption (T.P.D.) is a sensitive analytical method for looking at surface coverage's of adsorbates, their desorption energies and kinetics of desorption. It has been used extensively in studies on real catalysts but more especially on single crystals. In T.P.D. a sample is dosed with an adsorbate at a temperature where the adsorbate is stable on the surface. The temperature is then raised and the desorption products are analysed continuously, resulting in desorption profiles, from which a wealth of information can be gained. The so called 'complete' analysis of the desorption profiles is complex[10] as the activation energy of desorption E_d, and the pre-exponential factor A, can both depend on the coverage due to repulsive or attractive interactions, so they need to be calculated separately,

this is usually only done for UHV single crystal systems. The process of desorption can be viewed in simple terms as follows - where S is a surface site;

$$A\,(a) \text{ ----------> } A\,(g) + S$$

The energetics of this process can be described as follows;

$$Rd = -dq/dt = A.\,q^{n}.\,e\{-Ed/RT\} \qquad \text{Eqn. 2.1.}$$

Where Rd = Rate of desorption.

q = Fractional surface coverage.

A = Pre-exponential factor.

n = Order of desorption.

E_d = Activation energy of desorption.

R = Gas constant.

$T = T_O + ßt$ (where T = temperature and t = time)

At the onset of desorption the rate is determined by the $e\{-Ed/RT\}$ term, as the amount of desorption initially is very small compared to the total coverage of adsorbate. As desorption proceeds the surface coverage diminishes and so the q term begins to determine the desorption profile. These two terms compete and the result is a characteristic desorption profile with a peak maximum, as shown in Figure 2.8. More detailed reviews of T.P.D. can be found in the literature[11,12,13].

However in real catalyst systems, quantitative analysis is relatively simple. The integral of the desorption peak gives the surface coverage. The temperature of desorption relates to the activation energy of desorption - a strongly bound adsorbate will desorb at a higher temperature than a weakly held one. An adsorbate bound for instance at different sites on the surface,

Figure 2.8. A typical temperature programmed desorption profile.

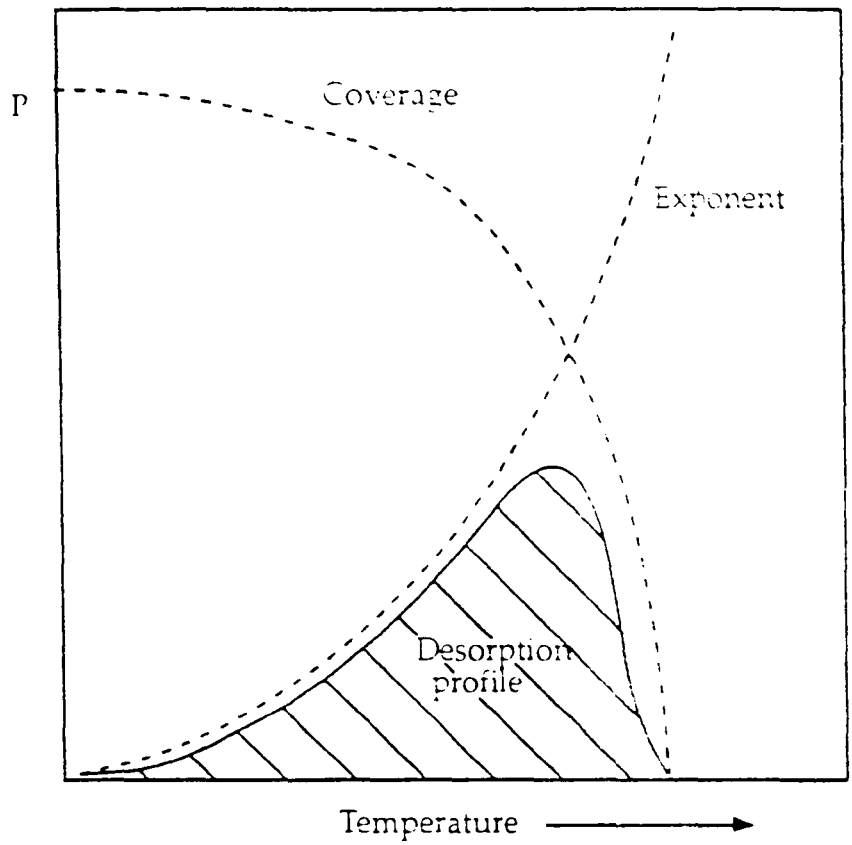

may desorb at different temperatures giving information on the relative population of that adsorbate and will give an indication of the surface heterogeneity. The surface area of a sample can be measured using T.P.D. provided an appropriate adsorbate is used, ideally one complete atomic monolayer should be adsorbed so that the number of molecules adsorbed is equal to the number of surface atoms. Two or more species desorbing at the same time and with the same desorption profile indicate that they probably came from a common surface species, in this way the reactive intermediate can be postulated. T.P.D. analysis carried out relatively simply using the Redhead method[11], in which the activation energy is equated to the desorption peak maximum temperature. This is done by assuming Ed is independent of coverage and approximating that A $=1x10^{13}$, then solving equation 2.1. to find the temperature at which the desorption rate is at a maximum (Tmax). This yeilds Eqn. 2.2.

$$\frac{Ed}{RT^2max} = \frac{A}{\beta}.\exp[\frac{-Ed}{RTmax}] \qquad \text{Eqn. 2.2.}$$

This can be rearranged to yield the following expression;

$$\frac{Ed}{RTmax} = \ln\frac{A.Tmax}{\beta} - \frac{\ln Ed}{RTmax} \qquad \text{Eqn. 2.3.}$$

Redhead found that the relationship between Ed and Tmax is very nearly linear and so Eqn. 2.3. can be approximated to

$$Ed = RT_{max}[\ln[\frac{A.Tmax}{\beta}]-3.64] \qquad \text{Eqn. 2.4.}$$

E_d= Activation energy of desorption.

R = Gas constant.

T_{max} = peak maximum temperature.

A = Pre-exponential factor.

β = the heating rate.

T.P.D. was performed in the rig previously described (Figure 2.1), in a continuous stream of He to carry the desorption products to the mass spectrometer unit. Accurate T.P.D. analysis requires the increase in temperature to be constant, the Pye 104 oven was not entirely linear , however the temperature was closely monitored by a thermocouple situated in the catalyst bed, so that an accurate temperature profile was recorded, see figures 2.9.(a) and (b). Accurate integrals of the desorption peaks were performed by converting the PC data into an Apple Macintosh file and then using Kaleidagraph 3.0.2. software for the calculations and presentation of data.

2.7. CATALYSTS DESCRIPTION and PREPARATION.

The catalyst system studied was 5% rhodium supported on g alumina. The catalyst was supplied by Johnson Matthey PLC. To reduce the risk of hot spots on the catalyst bed and to fill dead space inside the reactor tube, the catalyst was diluted four times by weight with finely ground a alumina, making a 1% by weight rhodium on alumina catalyst. The surface area of the g alumina was ~100 m^2 per gram and the metal surface area (S.A.) of the 5% rhodium catalyst was 12-15 m^2 per gram before reaction (values supplied by Johnson Matthey PLC). The metal particle size plays an important role in determining the behaviour of a supported metal catalyst. It

Figure 2.9.(a).
Temperature profile of catalyst bed.
Ramp rate = 0.5°C/minute.

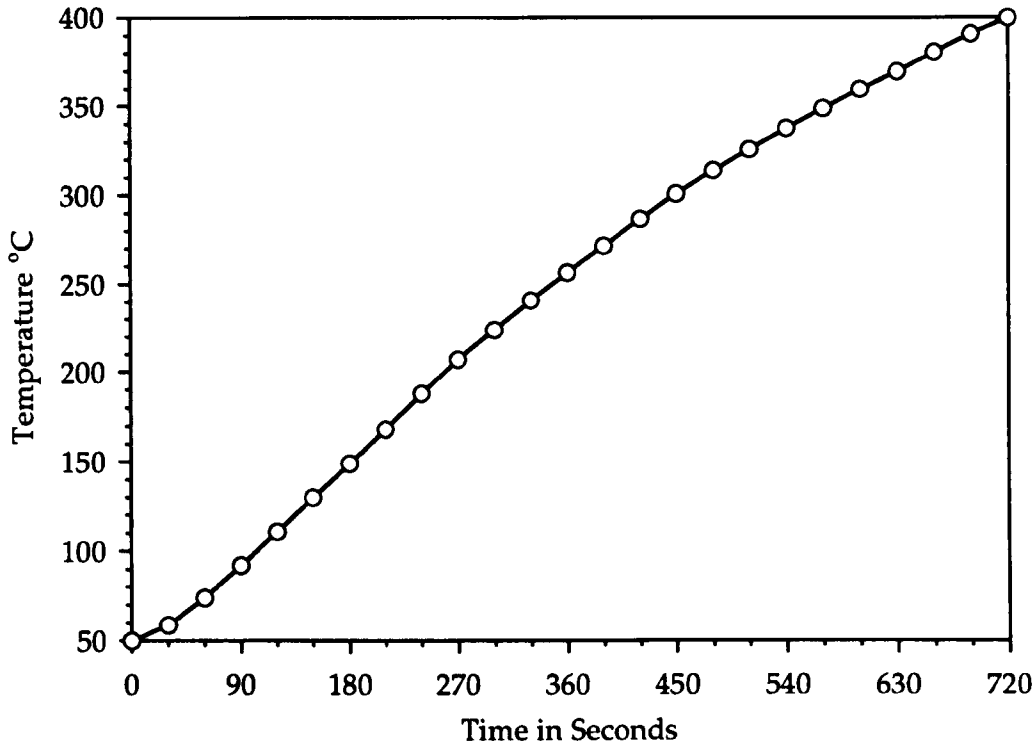

Figure 2.9.(b).
Temperature profile of catalyst bed.
Ramp rate = 0.4°C per second.

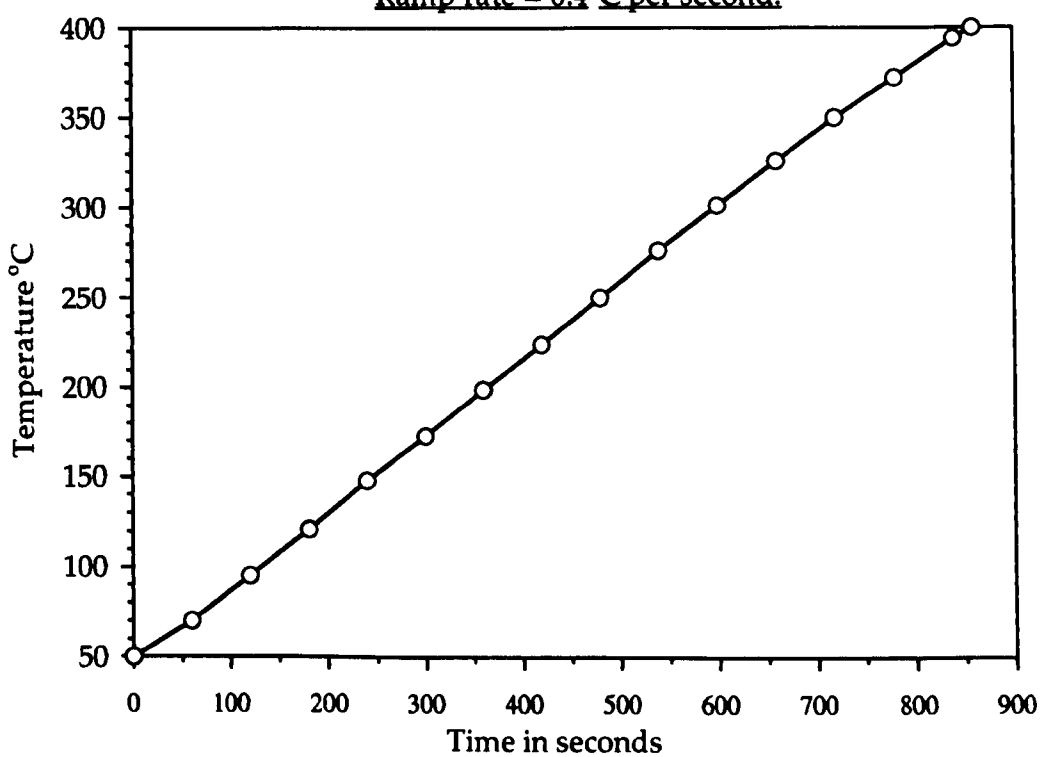

is the size and shape of the metal particle which determines the geometry in which surface atoms are available for reaction. The difference in the electronic state of the bulk metal and that of the small metal particle plays a critical role in the binding of adsorbed surface species, due to variations in the valence band electrons. Supported rhodium catalysts with very high dispersions show a remarkable diversity of morphology, forming 'rafts' or platelets[14]. The nature of adsorbed species on small supported rhodium particles relevant to this thesis are discussed in Chapters 3 and 4. The average rhodium metal particle size of the catalyst used in this work was calculated as follows:

$$\text{Metal S.A. of 5\% } Rh/Al_2O_3 = 12 m^2 g^{-1}$$

$$\therefore \frac{12}{0.05} m^2 g^{-1} = 240 m^2 g^{-1} Rh$$

$$S.A.m^2 = \frac{3v}{r} = \frac{3w}{\rho . r}$$

$$240\ m^2 = \frac{3x1(g)}{12.4x10^6 (g.m^3) x r(m)}$$

$$r = \frac{3x10^{-6}}{12.4x240} = 1.008^{-9} m \sim 10Å$$

Where;

S.A. = Surface area.

Rh = Rhodium.

v = Volume .

r = Radius .

w = Weight

r = Density

The rhodium particles are remarkably small for a supported metal catalyst and some irreversible sintering of the metal phase was expected. The surface area, however, remained the same throughout the course of the experiments even though the catalyst was repeatedly heated and cooled.

All fresh catalysts were first heated for 3-6 hours in air at 130°C to drive off any residual moisture. The catalysts were then pressed into thin discs approximately 1-2 mm in depth and 10mm in diameter, at a pressure of 8-10 tons. The discs were then crushed and sieved to a uniform particle size of between 1000-600μm. By granulating the catalyst, one ensures that the gases can pass easily through the catalyst bed minimising the risk of a pressure drop across it and also the dead volume of the reactor is reduced by increasing the catalyst bed volume. Furthermore the risk of loosing catalyst particles in the gas stream is greatly reduced by granulation . The bed is held in place with plugs of quartz wool at each end.

2.7.1. PROMOTING the CATALYST

The activity of a catalyst can be modified by the use of promoters. A body of empirical knowledge about the promoting effect of many elements has been available since the development of the iron ammonia synthesis catalyst, for which over 8000 different catalyst formulations were tested. In broad terms promoters fall into two categories. Structural promoters help to stabilise certain surface structures of the catalyst or may prevent sintering. They do not play a direct role in the catalytic reaction and do not interfere with reacting species. Chemical promoters, on the other hand, do have a direct influence on the reacting surface species. Potassium is clearly a chemical promoter in that it alters the electron density of the surface metal atoms, the role of promoters and potassium in particular, is discussed in Chapter 5.

Potassium promoted catalysts were prepared using the incipient wetness technique. In this preparative technique the pore volume of the catalyst was determined by adding water to the dry catalyst powder and

noting the amount taken up at the point when the powder turned from dry to a paste-like consistency, this point is termed the 'incipient wetness point'. Using this volume, a solution of the promoter, for instance a solution of its nitrate, is prepared such that when the promoter solution is added to the dry catalyst a known amount of promoter is dosed into the catalyst at the incipient wetness point. The procedure for promoting the 5% rhodium on g alumina with 25% surface coverage of potassium is shown below. In this procedure potassium nitrate was the salt used.

surface area of g alumina = $100m^2$ per gram.

= 10^{21}surface sites.

for a 25% coverage = $2.5x10^{20}$ surface sites.

the pore volume of 1g = 0.5 ml.

we require $2.5x10^{20}$ K atoms in 0.5 mls. of solution.

= $5x10^{20}$ K atoms in 1ml of solution.

= $5x10^{23}$ K atoms in 1 litre.

$$= \frac{5x10^{23}}{6.02205x10^{23}} = 0.8303M$$

= 83.94g of KNO_3 / litre

= 2.099g / 25 ml.

The assumptions made in relation to the calculation above are that the potassium is laid down evenly across the catalyst, both on the support and the metal phase and that the solution was able to permeate fully into the pores of the support.

The loading of a chemical promoter can have a drastic effect on the catalytic behaviour of the promoted metal, altering the selectivity to products and the overall activity[15]. A good example being the hydrogenation of CO on nickel, where the selectivity to higher alkanes is greatly increased with an

alkali metal promoter[16]. In a catalytic sense the effect of a promoter is to shift the chemical behaviour of the promoted metal towards the left in the transition series.

2.8. REFERENCES.

1 Wagner, C. and Hauffe, K. Z. *Electrochem.*, **45**, 409 (1939).

2 Kokes, R.J., Tobin, H. and Emmett, P.H., *J. Am. Chem. Soc.* **77**, 5860 (1955).

3 Kobayashi, H. and Kodayashi, M., *Cat. Rev.-Sci. Eng.* **10(2)** 139 (1974).

4 Bennett, C.O., *Cat. Rev.-Sci. Eng.*, **13**, 121 (1976).

5 Mori, T., Niizuma, H., Takahashi, N., Hattori, T. and Murakami, Y., *J. Phys. Chem.*, **90**, 109 (1986).

6 Mori, T., Miyamoto, A., Takahashi, N., Niizuma, H., Hattori, T. and Murakami, Y., *J. Catal.*, **102**, 199 (1986).

7 Mori, Y., Mori, T., Miyamoto, A., Takahashi, N., Hattori, T. and Murakami, Y., *J. Phys Chem.*, **93**, 2039 (1989).

8 Beynon, J.H., '*Introduction to mass spectroscopy*', University of Wales Press, Cardiff (1981).

9 Batey,J.H., *Vacuum*, **37**, 659 (1987).

10 King, D.A., *Surf. Sci.*, **47**, 384 (1975).

11 Redhead, P.A., *Vacuum.*, **12**, 203 (1962).

12 Morris, M., Bowker, M. and King, D. " *Comprehensive Chemical Kinetics*" **Vol. 19**., Elsevier Science Publishers, (1984).

13 Woodruff, D.P. and Delchar, T.A., "*Modern Techniqus of Surface Science*," Cambridge University Press, p279 (1989).

14 Yates, D.J.C., Murrell, L.L. and Prestridge, E.B., *J.Catal*. **57**, 41 (1979).

15 Nonneman, L.E.Y., Bastien, A.G.T.M., Ponec, V. and Burch, R. *Appl. Catal*. L23 (1990).

16 Goodman, D.W. and Campbell, C.T., *Surf. Sci.*, **123**, 413 (1982).

CHAPTER 3.

CO AND CO_2 HYDROGENATION OVER Rh / Al_2O_3.

3.1. INTRODUCTION.

3.1.1 PREAMBLE

Due to the increase in demand for energy, especially since the oil crisis in the early seventies, there has been a huge interest in utilising sources of carbon other than oil. Coal gasification and methane reforming into synthesis gas have been examined in great detail. More recently and indeed more relevant to this thesis, is the catalytic and surface science research carried out on the simple reactions of synthesis gas. This introduction serves as a short summary of the present literature, concentrating on CO and CO_2 hydrogenation over supported group VIII metals, in particular the Rh/Al_2O_3 system. A broader review of methane and synthesis gas chemistry on supported group VIII metals is given in Chapter I.

Rhodium holds a very interesting position in the periodic table, in that it lies between metals that can dissociate molecular CO spontaneously such as Fe and Re and the elements to the left of the periodic table and those metals that cannot dissociate CO to any great extent i.e. Pd, Pt and the metals in the 11th and 12th groups. Table 3.1. refers to CO dissociation on transition metals at 273 K.

Table 3.1.

Mn^	Fe^	Co**	Ni^o	Cu$^-$
Tc^	Ru**	**Rh^o**	Pd$^-$	Ag$^-$
Re^	Os**	Ir^o	Pt$^-$	Au$^-$

^ = efficient CO dissociation. ** = dissociation on some crystal planes.

^{o} = dissociation only on special sites. $^-$ = no CO dissociation.

Table adapted from reference[1]

Some early studies relating to the hydrogenation of CO over rhodium samples revealed product distributions and determined some kinetic data, but revealed little information on the surface species present during the reaction[2,3,4,5] . Several groups in Europe, America and Japan have further elucidated detailed information on the reaction and on the effects of particle size, and the identity, reactivity and concentration of surface species.

3.1.2 CO / CO_2 ADSORPTION and DISSOCIATION on RHODIUM.

CO and CO_2 dissociation on rhodium has been an ongoing topic of research for many years. In the late seventies and early eighties Yates et al.[6,7] reported that the probability of CO dissociation on Rh(111) between 300-870 K is negligible, and concluded that CO adsorbs molecularly and desorbs, even on stepped and polycrystalline surfaces, before dissociation occurs. Somorjai and co-workers[8,9,10] however disagreed and reported that rhodium foil, and certain surfaces of rhodium that contain irregularities such as steps, kinks or defects, do dissociate CO in appreciable quantities, the C(a) and O(a) were found to recombine and the resulting CO(g) desorbed at far higher temperatures than molecularly adsorbed CO.

It is now well established that CO does dissociate on certain facets and on irregularities on the surface of rhodium. Solymosi[11] detected CO dissociation on a 1%Rh/Al_2O_3 catalyst at temperatures above 473K. He used the yield of CO_2 as a measurement of the amount of CO dissociation and found that the carbon, formed upon dissociation, reacted with hydrogen to form methane at temperatures as low as 300K and that different forms of carbon are produced, the ratios of which depend upon the temperature of dissociation. They are identified by their hydrogenation temperatures, the more reactive carbon being hydrogenated at lower temperatures. The carbon

was found to age into a less reactive form and this ageing process is increased by a rise in temperature.

There is a large body of data on the nature of CO on supported rhodium surfaces. The orientation of CO has been probed most successfully by infra-red spectroscopy that has revealed that numerous different forms of CO(a) can exist[12,13,14,15,16] . The most common forms are illustrated in Figure 3.1. below, they are linear (I), bridged (II) , bridged(III) and geminal dicarbonyl(IV), other forms[17,18] have also been detected on supported rhodium or promoted rhodium, such as (V).

Figure 3.1. Modes of CO adsorption on rhodium .

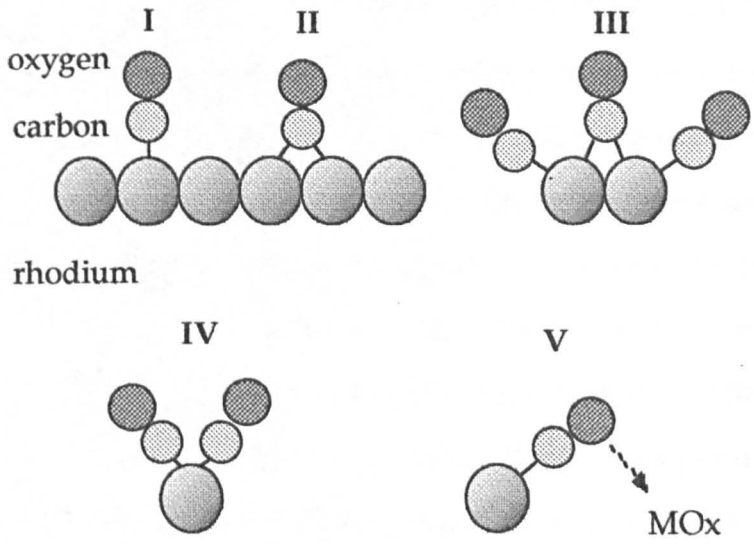

The geminal dicarbonyl species (IV above) forms on isolated rhodium atoms. The low temperature <373K interaction of CO with highly dispersed rhodium can cause disintergration of the small rhodium particles resulting in the highly uncoordinated atoms most being stripped away from the cluster, forming the geminal dicarbonyl species. The oxidation state of the geminal dicarbonyl rhodium atoms[19] is +1 and Basu et al.[20] provided infra-red evidence that -OH groups are involved in the oxidation step, reacting with a mononuclear neutral rhodium carbonyl. Basu's mechanism is shown below.

$$Rh_n + CO(g) \text{ -----> } Rh_{n-1} + [Rh^0CO](a)$$

$$[Rh^0CO](a) + OH^-(s) \text{ -----> } [O^{2-}\text{---}Rh^+\text{---}CO]_S + \frac{1}{2} H_2$$

$$[O^{2-}\text{---}Rh^+\text{---}CO]_S + CO(g) \text{ -----> } [O^{2-}\text{---}Rh^+\text{---}(CO)_2](s)$$

In the mechanism , Rh_n is a small rhodium particle, and the subscripts (s), (a) and (g) stand for support, adsorbed and gas respectively.

This phenomenon has only been observed on particles less than ~1.5nm and can be explained by the strength of the Rh-CO bond, which is stronger (~145kJ/mol) than a Rh-Rh bond[21](121kJ/mol). The first step in the mechanism above is thought to proceed on coordinatively highly unsaturated rhodium atoms only, which explains why this process has only been observed on highly dispersed particles. CO adsorption on larger sized particles shows that CO adsorption energies are significantly smaller than the bond energies of Rh-CO carbonyls, implying that the activation energy for particle disintegration becomes too high when they are above ~1.5nm.

The geminal dicarbonyl forms in the low temperature interaction but takes no part in the hydrogenation reactions as it is unstable in the presence of hydrogen at temperatures well below those required for CO hydrogenation[22]. Fujimoto[23] found that the onset of methane production at 373-423K coincided with the disappearance of the infra-red band due to bridged CO(a) and found that linearly bonded CO(a) was hydrogenated at slightly higher temperatures 423-573K. Solymosi et al.[24] found similar results when probing the surface species present under CO/H_2 conditions. They found that methanation occurred at a considerable rate above 473K and that at the reaction temperature, linear bonded CO was the only CO(a) species present in appreciable quantities. It's frequency shifted down slightly in the

presence of H_2. The work of Mori et al.[25] in Japan has gone a long way to elucidating changes in the reaction rates and they have concluded that the rate of CO dissociation is much smaller than that of CHx hydrogenation and that on highly dispersed Rh/Al_2O_3, with a rhodium particle size of ~10-15Å diameter, the predominant adsorbed CO species leading to methane is linear (species I from Figure 3.1.) whereas with larger rhodium particles, and consequently larger rhodium ensembles, the bridged CO species (species III from Figure 3.1.) predominantly leads to methane.

In a comprehensive review Ponec[26] focuses on the catalytic active centres in synthesis gas reactions, the three most important aspects for a strong adsorption and high activation of CO are reported to be;

(i) partially occupied d-orbitals in the metal allowing binding with the lowest anti-bonding orbitals of CO (most commonly called π^*, 2π or $2\pi^*$).
(ii) a low work function of the catalyst - the work function generally decreases with an increase in surface heterogeneity.
(iii) a definite co-ordination between CO and the metal surface atoms.

It is apparent that for CO dissociation to take place a group of metal atoms (an ensemble) is required[27]. Clearly from a physical point of view, in order for CO to dissociate a vacant site must be available for the O atom to adsorb. Manipulation of the size of active metallic ensembles by alloying with an inactive metal (e.g. Ru-Cu) has a dramatic negative effect on the synthesis of hydrocarbons - termed the "suppression factor". The numerical value of the "suppression factor " caused by alloying however can appear too high, requiring the existence of unreasonably large ensembles[28] . An explanation that fits well in the case of highly dispersed catalyst systems, is that there are a variety of active sites, some with higher activity than others. When the sites are more active due to a stronger CO adsorption, it is probable

that these sites would be poisoned first upon the addition of an inactive metal as the metal would preferentially adsorb at the strong binding site. An alloying metal that shows strong surface segregation could likewise do the same. Bond proposed that in the case of ruthenium, four atoms are required for CO dissociation and subsequent methanation. From quantum chemical calculation it was suggested that at least five free metal atoms are necessary for successful separation of the CO bond. Especially the moving oxygen atom needs space and free rhodium atoms with which to bind[29].

In early studies of CO_2 adsorption[21,30,31] on polycrystalline films, Rh foils and on supported rhodium, the adsorption of CO_2 was found to be weak and non-dissociative. Somorjai[8] however showed that CO_2 can dissociate on several Rh single crystal faces and that EELS of chemisorbed CO and CO_2 gave identical spectra on Rh(111) however CO_2 required a five fold increase in exposure to achieve the same surface structure this is indicative of the lower heat of adsorption.

3.1.3 CO AND CO_2 DISSOCIATION WITH H_2 PRESENT.

In a catalytic study into the dissociation of CO_2 over a Rh/Al_2O_3 catalyst[32,33] Solymosi observed that hydrogen vastly increased the adsorption of CO_2, this was found to be due in the main, to the formation of a formate ion. As the surface concentration of the formate was found to be 1.3 times the number of surface Rh atoms, it was concluded that the formate must reside on the alumina and that Rh was vital to the formation of the formate entity. The rate of methanation of CO_2 was found to be 20 times greater than that of CO hydrogenation at 275°C and this is in agreement with the observations of Somorjai and others[8]. The surface concentration of CO detected by infra-red spectroscopy, taken at the reaction temperature, however remained at a very

low level, and disappeared when CO_2 was removed. This suggests that the methanation of CO_2 passes through CO(a). The same effect of hydrogen was not observed with CO adsorption on alumina supported rhodium, in that H_2 did not increase the up-take of CO and the infra-red spectra of the linearly bonded molecule changed little in the presence of H_2 in the temperature range 298-373K . Recently Solymosi[34] has studied the effect of photo-illuminescense on the activation of CO_2 on TiO_2 and Rh/TiO_2. His results show that photo-induced activation does occur and that illumination induced a charge transfer from the Ti to the Rh, this leads to more back bonding from the metal to the $2\pi^*$ anti-bonding orbitals of the CO_2 molecules and hence facilitates the cleavage of a carbon- oxygen bond. Solymosi assumes that CO_2 is bound with the carbon bonded to the Rh and one oxygen linked to an oxygen vacancy on the TiO_2 .

Infra-red studies illustrate that the structure and the reactivity of the CO derived from CO_2 differs markedly from that observed in CO/H_2 studies. With CO derived from CO_2/H_2, the molecule is most likely to be bonded exclusively in the linear form on a rhodium atom that has one or possibly two H atoms co-ordinated to it. This conclusion comes from the observed shift in frequencies, CO derived from CO_2 appeared at lower frequencies (2030-2020 cm^{-1}) than the Rh-CO species (~2060 cm^{-1}) . Hydrogen acts as an electron donor and so increases the π-donation from the rhodium into the anti-bonding orbitals of CO. Solymosi[24] proposed a hydrogen assisted CO dissociation mechanism and this route is illustrated in Figure 3.2. below. Calculations however suggested that electron transfer from hydrogen cannot account for all of the observed shift[16] and so other surface species, most probably surface carbon formed in the CO dissociation step, also contribute to the shift. No geminal dicarbonyl formation has been observed from CO_2 studies and the bridged form was found to be scarce (only a very weak ir band was observed). An earlier suggestion for the H-assisted CO dissociation

was proposed by Vannice[35,36] , whereby hydrogen attacks the CO double bond and forms a hydrogenated acyl type intermediate (see below). Sachtler and Biloen[37] however discounted this mechanism as kinetically it seems highly unlikely. The two hydrogen assisted CO dissociation mechanisms are illustrated in Figure 3.2. below.

Figure 3.2. Proposed Hydrogen Assisted CO Dissociation Mechanisms.

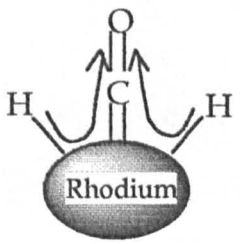

H_2 assisted CO dissociation.
Solymosi. F.

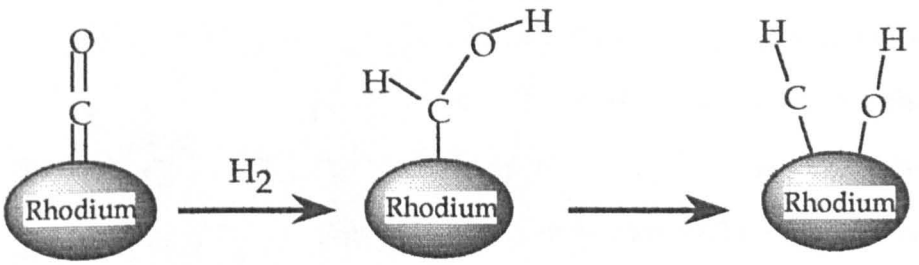

H_2 assisted CO dissociation. Vannice, M.A.

The necessity of Rh ensembles for CO dissociation suggests that the CO molecule bends down towards the surface in order to be activated towards dissociation[38,39]. Clearly when the coverage of CO is high, dissociation is more difficult. The support plays a major role in the activity of rhodium catalyst towards dissociation[40,41], arguments point to the formation of new adsorption sites with different supports. Solymosi argues that a strong

electronic interaction can occur between the support and metal particle so that when the isoelectric point of the support is sufficiently below that of the metal, electrons flow from the support to the metal. In doing so they allow more back bonding from the metal to the anti-bonding orbitals of the CO, resulting in easier dissociation. The majority of supports are insulators and show very limited electrical conductivity, however, n-type TiO_2 has a high electron concentration in comparison to most other common supports and shows superior initial activity. Solymosi [39] found the activity for CO dissociation decreased in the order:

$$TiO_2 > Al_2O_3 > SiO_2 > MgO$$

The enhanced activity of TiO_2 cannot be accounted for entirely by electron flow contributions. Other effects such as adsorbed species on the surface also contribute to the back donation. It has been widely suggested that a bent CO entity (species V in Figure 3.1) bridging the rhodium and support is the most activated CO surface species and therefore the one that leads to the majority of products[42]. There is substantial evidence that gives credence to the theory of Strong Metal- Support Interaction[43] S.M.S.I. however for the purposes of the research presented in this thesis, S.M.S.I. is not considered to be an influencing factor as alumina shows very poor S.M.S.I. characteristics[44]. Some metal-alumina systems do however show S.M.S.I.-like chemisorption behaviour (e.g. the high temperature reduction of Pt/Al_2O_3) but rather than migration of Al_2O_3 moieties at high temperature it is thought that the Al_2O_3 deposits are derived from the preparation step i.e. dissolved alumina attaching to the metal particles during the drying and calcination steps. The enhanced activity is seen after high temperature reduction processes in which the clusters of Al_2O_3 are reduced to AlO_x moieties, and the oxygen deficient species then aid CO dissociation because they have a strong affinity for O atoms. In the case of rhodium, no enhanced reactivity was observed after high temperature reduction. The reason given by Taniguchi et al.[45] is that a Rh-Rh

ensemble is more active towards CO hydrogenation than a Rh-Al ion ensemble whereas in the case of Pt/Al_2O_3 catalysts, the methanation rate is faster on Pt- AlO_x groups than on Pt-Pt ensembles. In the research presented in this thesis, the reduction temperature was consistently between 680-700K which is below the high temperatures required for a considerable S.M.S.I.-like behaviour.

Sachtler and Ichikawa[46] classify oxidic supports / promoters into two distinct groups;

(a) Those which are "oxophilic" -these promote CO dissociation, stabilise surface acyl groups and therefore show enhanced CO conversion with high selectivity to oxygenates. Oxides of Mn, Ti, Zr and Nd are in this category.

(b) " Basic" metal ions which break up the rhodium ensembles required for CO dissociation. As a result there is a depression of both methane and CO_2 production with promoted CO insertions favoured. Oxides in this class commonly used are Fe and Zn .

3.1.4 SURFACE SPECIES FORMED WITH CO/H_2 OVER Rh/Al_2O_3.

There are many surface species that can be formed on a supported transition metal catalysts from synthesis gas. We will confine this discussion to the species that lead to the formation of methane, water and carbon dioxide on supported rhodium catalysts . During the hydrogenation of CO_2 Solymosi et al.[32,33] observed the formation of a formate ion at low temperatures (298-373K) . In a flow of CO and H_2 over Rh/Al_2O_3, no surface formate complex was formed at low temperatures[24] however at reaction temperatures (423-573K) the formate species became evident, although in lower concentrations than in the CO_2 case. The formate can be hydrogenated to methane in a

stream of pure hydrogen at 425K, which is below the methanation temperature of CO and CO_2 but is relatively stable at this temperature in He[47].

As the surface concentration of the formate is fairly high even at 523K and is located on the alumina support, Solymosi concluded that it was not an important reactive intermediate in the formation of methane. However as the concentration of the formate group remained constant after 5 hours and up to 13 hours of reaction, it must be consumed at the same rate as being formed, therefore it cannot be viewed as being totally inactive. The formate was not seen on a blank alumina catalyst, therefore the role of rhodium in the formation of the species is crucial. It was proposed that hydrogen, activated on the rhodium, migrates onto the support forming an OH^- group which react with CO(a) to form the formate, as shown below.

$$OH^- + CO \text{ <====> } HCOO^-$$

Solymosi concludes that the formate ion is methanated at low temperatures ~423K, possibly through the formation of a different surface complex;

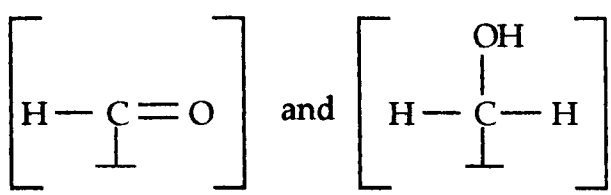

at high temperatures the formate is less stable and may be in equilibrium with absorbed formic acid, through the addition of an activated H atom. The formic acid is proposed to move to the rhodium particles where it decomposes to give CO_2(CO) and H_2(H_2O). As the decomposition of adsorbed formate yields CO and CO_2 at these temperatures, a conclusion as

to the pathway to methane could not be made - it could either be produced by the dissociation and hydrogenation of CO /CO_2, or it could be via the hydrogenation of a surface complex, as in the low temperature case. In any case, formate appears to play a minor role in the production of methane from CO hydrogenation.

The presence of CH_x (x=1-3) on Rh/Al_2O_3 was proved by a number of authors, notably Solymosi and Bell[24,48], by the use of probe molecules. They used ethylene and propylene as probe molecules, introducing small amounts of these into the reactant gas mixture. When ethylene was the additive, an increase in propylene was immediately observed, with propylene as the additive, butene and butane production increased. The production of the higher hydrocarbons rapidly decreased after the introduction of the probe molecules, indicating the concentration of the CHx species is low and their production is activated.

In a recent paper C.O.Bennett[49] has added further to his considerable contribution to the elucidation of the transient kinetics of the reaction[50,51,52,]. By FTIR and mass spectroscopy, the chemical composition and coverage of surface species formed under reaction conditions on a 1% Rh/Al_2O_3 catalyst was probed. He found that the concentration of surface CO was high θ_{CO} = 0.95, and the majority of it was linear and bridged. No geminal dicarbonyl was detected at 220°C. The surface coverage of H_2 was small as was the coverage of active carbon, θ CH_x = 0.025 where x=0 is denoted as Cα (carbon which is active in methane formation under CO/H_2 conditions at 220°C). The coverage of a less reactive carbonaceous species was found to be θ = 0.54 after 30 seconds of H_2/CO and its concentration rose with time on stream, Bennett ascribed this to CxHy species. These groups hydrogenated to methane at a faster rate than they desorbed and are therefore most likely to be located on the metal - this is in agreement with Bell et al.[53,54] . He found that after 30 seconds of reaction, 1.52 monolayers of carbon containing species

existed, as this represents more than 1 carbon per Rh atom, he interpreted this to mean that some species contained more than one carbon and indeed IR backed up this assumption. Also detected were more stable carbonaceous species denoted as Cβ, that formed but did not hydrogenate at 220°C. These were assigned to methylene groups (=CH_2) adsorbed either on the metal or the support.

Formates and carbonates were formed on the support and their concentration built up with time on stream. Through temperature programmed desorption, the formates were found to decompose between 220-380°C whereas the carbonates require temperatures exceeding ~380°C in order to decompose. He differentiated between stable carbonaceous surface species and labile $CO_{(a)}$ by exchanging the $CO_{(a)}$ with $^{13}CO_{(g)}$, then upon hydrogenation the stable carbon containing species yielded purely ^{12}C hydrocarbons and the labile $^{13}CO_{(a)}$ yielded $^{13}CH_4$. It was demonstrated that upon a switch from H_2/CO mixture to pure H_2, three types of carbon are hydrogenated. The most rapid is Cα, followed by the hydrogenation of adsorbed CO which passes through a carbidic carbon species, and then thirdly the hydrogenation of the (Cβ) methylene groups. The concentration and peak T_{max} for hydrogenation of the (Cβ) increased with time on stream whereas the Cα and CO(a) remained the same. By changing the time on steam, the build up of Cβ, formate and carbonate species could be probed, after 120 seconds virtually none had formed but after 10 minutes on stream, 0.21 monolayers in total had built up. The average rate constant k, for the active carbon;

$$k = \frac{T.O.F}{\vartheta CHx} = \frac{1}{Ave.lifetimeCHx}$$

(where T.O.F. is Turn Over Number and θCHx is the surface concentration of CHx) was found to be between 0.2 and 0.4 s^{-1} for the 1% Rh and in the order of 0.4-0.8 for a 5%Rh catalyst[49].

The predominant product was methane, and the vast majority of methane was formed through hydrogenation of $C_{(a)}$, and $CO_{(a)}$. The alkyl chains were not found to take part in the CH_4 formation during the methanation reaction, however they are hydrogenated to methane at 220°C in a stream of pure H_2 . They were assigned as spectator species along with the formate and carbonate groups.

A variety of mechanisms can explain the formation of CO_2, the most cited and supported mechanism is via CO disproportionation, known as the Boudouard reaction. Some other contributing mechanisms possible are from the decomposition of surface carbonates and formates and from a pseudo Langmuir-Hinshelwood mechanism proposed to occur on most transition metals by Engel and Ertl[55],

$$\text{i.e. } CO(g) + O(a) \text{ -----> } CO_{2\,(g)}$$

As will be demonstrated in the results section, the above reaction is extremely facile.

3.1.5. THE DIFFERENCE BETWEEN CO and CO_2 REACTIVITY.

The CO_2 molecule is less reactive than the CO molecule and consequently does not fully dissociate as readily. The under-lying reasons for the difference in the reactivity between CO and CO_2 is the availability of bonding orbitals in the respective molecules. As highlighted in Chapter 1, in the case of CO, the HOMO (5σ-molecular orbital) is located around the carbon atom and is available for bonding. It is in a favourable orientation (along the CO bond axis) and is able to donate electrons to the metal therefore providing a bond. With the CO molecule in this stabilised orientation the $2\pi^*$ anti-bonding orbital in the CO molecule can be partially filled by back-donation of electrons from the metal, weakening the CO bond

and therefore aiding dissociation. In the linear CO_2 molecule the carbon atom is saturated and is therefore unable to donate electrons to the metal. The HOMO is higher in energy and is therefore less favourable to molecular overlap with the d-electrons of the metal. However, the bond strength in CO_2 is weaker than that in CO, as it is a double bond rather than a triple bond.

The CO_2 hydrogenation reaction is inherently more simple than that of CO hydrogenation as there is only one reductant in the gas stream, namely hydrogen. No net CO_2 can be formed, therefore methane formation as a result of dry methanation does not take place. Wet methanation is the only straight forward route to methane and as can be seen from the equation below, twice as much water as methane is formed.

$$CO_2 + 4H_2 \text{ ---------> } CH_4 + 2H_2O \qquad 3.8.1.$$

CO_2 hydrogenation has been investigated over rhodium and supported rhodium catalysts by various authors[31, 32, 56, 57, 58, 59, 60] and has been reviewed here in order that comparisons to CO hydrogenation may be drawn and to probe further the mechanistic details of the reaction.

3.2. RESULTS.

Presented in the following section are the results from an extensive series of experiments to study the simple reactions of CO and H_2 over an alumina supported rhodium catalyst using the pulsed flow microreactor . Un-promoted rhodium is not selective towards higher hydrocarbons or oxygenates, and the intention of this study was to probe the mechanisms of the reactions, and to explore any changes in mechanism that occur.

Carbon monoxide can undergo two methanation reactions, wet methanation (equation 3.2.1.) and dry methanation[61,62] (3.2.2.). The wet methanation reaction is the back reaction of methane steam reforming - the industrial route to synthesis gas - and dry methanation is the back reaction of dry reforming[63], an industrial reaction known as the "Calcor" process[64]. Dry reforming is potentially an important route to synthesis gas formation[65] as it utilises two of the cheapest and most readily available forms of carbon, namely CH_4 and CO_2. The latter perhaps being provided as a waste product of a large scale industrial reaction (a selective oxidation process for instance). The main financial drawback in the dry reforming reaction is that high temperatures are required due to the high endothermicity of the reaction and little is known about the reaction mechanism and kinetics. Also conventional reforming catalysts deactivate through carbon build up in the absence of steam.

$CO + 3H_2$ ---------> $CH_4 + H_2O$ $\quad \Delta H_{1000K} = -225.4$ kJ mol^{-1} Eqn. 3.2.1.

$2CO + 2H_2$ ---------> $CH_4 + CO_2$ $\quad \Delta H_{1000K} = -260.5$ kJ mol^{-1} Eqn.3.2.2.

From looking at the equations above it can be seen that the stoichiometries of the reactants change markedly. In wet methanation (Eqn. 3.2.1.) three moles of hydrogen react with one mole of carbon monoxide, forming one mole of both methane and water. In dry methanation (Eqn. 3.2.1.), one mole of carbon monoxide reacts with one mole of hydrogen to form half a mole of methane and half a mole of carbon dioxide. Very little emphasis has been laid on this aspect of CO hydrogenation in the literature and as will be shown in this chapter, a change in the stoichiometries of the reactants causes a gross change in the mechanism by which CO and H_2 react.

A change in stoichiometry need not involve a change in the concentration of the reactants in the feed gas, as the surface concentration of adsorbed molecules varies with temperature as their desorption rates increase. In other words, by going up in temperature, the surface concentration of adsorbed species changes whereas the total amount of each reactant being fed into the reaction remains the same .

The methanation reactions do not require the high temperatures of the reforming reactions and were therefore more suited to the capabilities of the microreactor (maximum temperature 500°C). The main reasons for studying these reactions under transient conditions were; (i) to gain a detailed insight into the kinetics and mechanisms involved in the CO methanation reaction under different temperature regimes and under various reactant stoichiometries. By using a transient pulsed technique, the initial steps of the reaction can be probed to a greater degree than with a continuous flow microreactor, (ii) to use the CO hydrogenation reaction as a probe to study the capabilities of the pulse flow microreactor and (iii) to perhaps gain an insight into the dry reforming reaction by extrapolating back from the mechanisms involved in the methanation reactions.

The surface area of the catalyst was determined in a simple and novel way using the microreactor and these experiments are included in this section. The up-take of oxygen was used as a means of characterising the catalyst to some degree because the role of oxygen on the surface of rhodium is crucial in the formation of both water and carbon dioxide.

Carbon dioxide hydrogenation has been studied in order that comparisons may be made between the two reactions. The same experimental procedures were followed in both cases and indeed the same catalyst was also used.

Figure 3.1.

O_2 injections at 100°C, all injections 0.1 ml

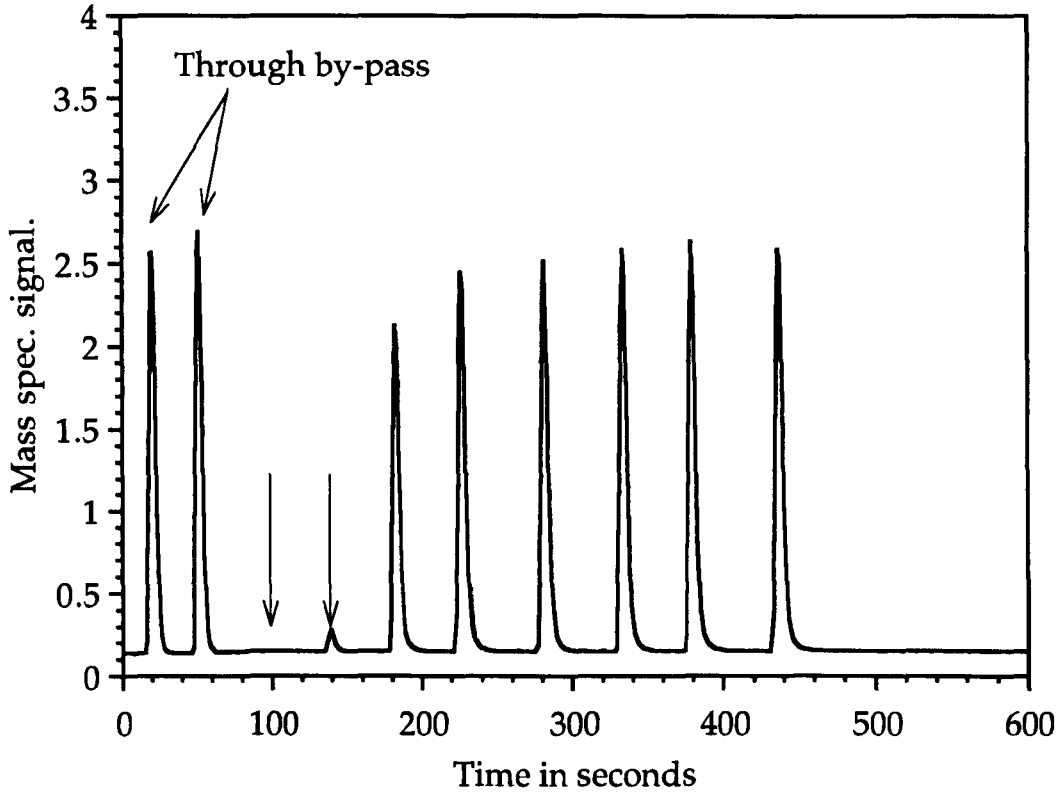

Figure 3.2.

O_2 injections at 200°C, all injections 0.1mls

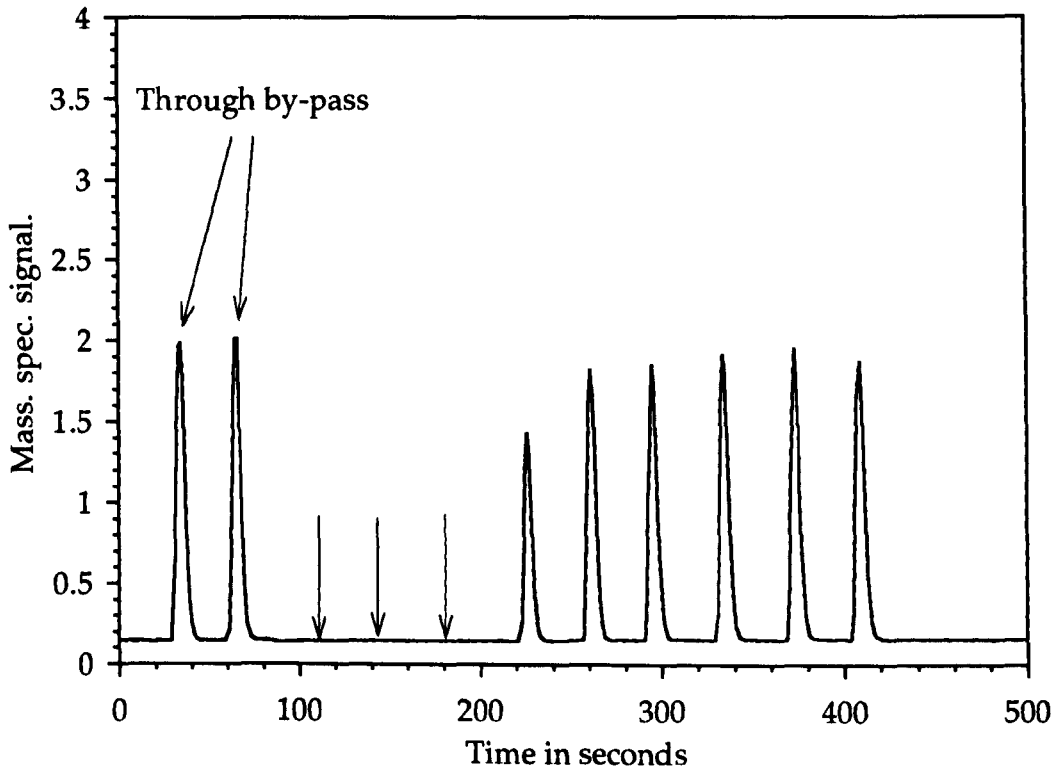

Figure 3.3.(a)

O_2 injections at 400°C.

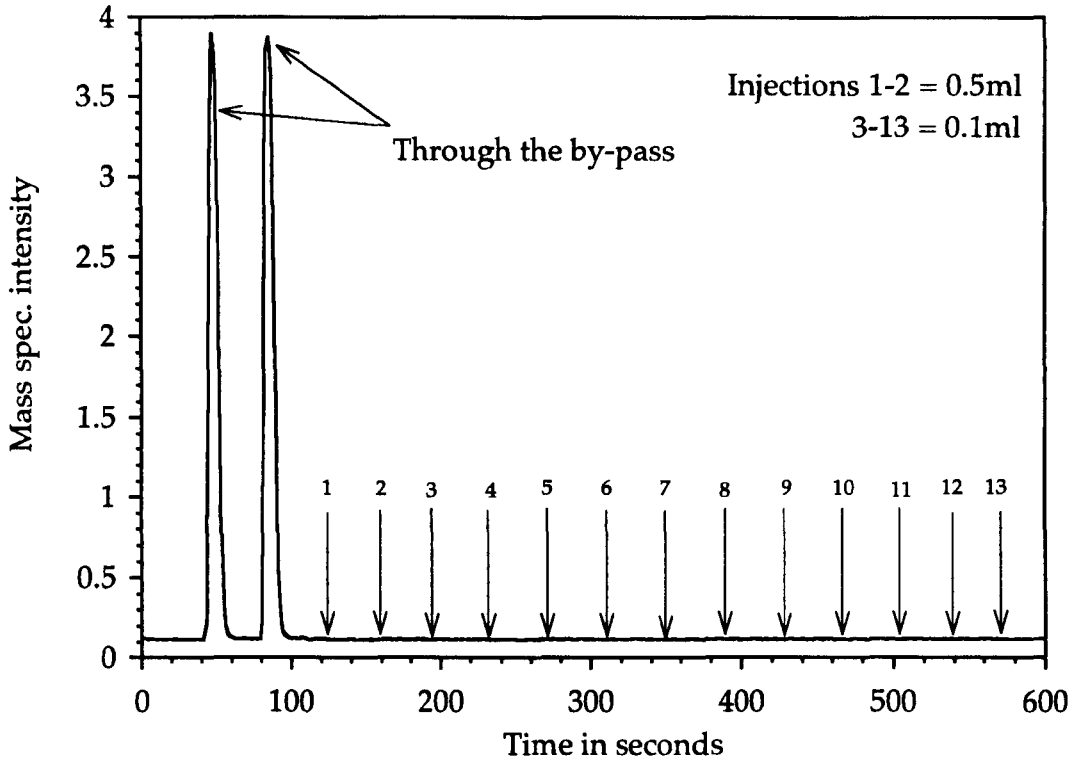

Figure 3.3.(b) the continuation of Figure 3.3.(a)

O_2 injections at 400°C.

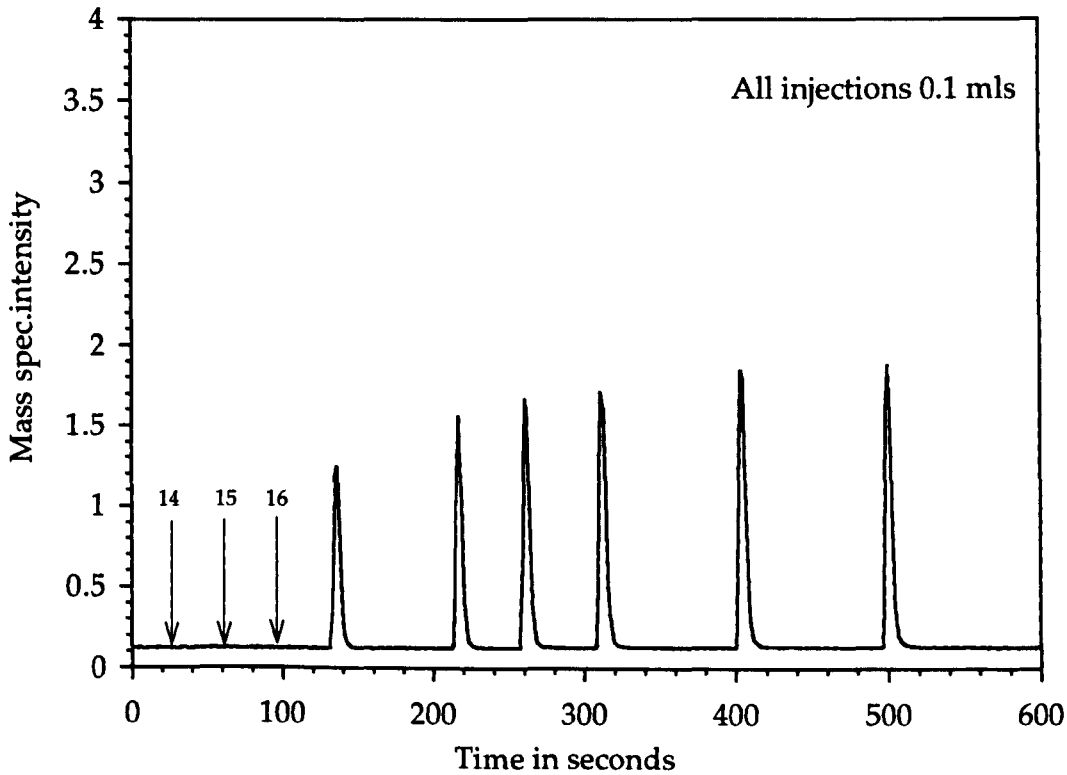

3.2.1. METAL SURFACE AREA MEASUREMENTS by OXYGEN ADSORPTION.

Dioxygen dissociatively adsorbs on all facets of rhodium at room temperature (equation 3.2.3.), each oxygen atom binding to a rhodium atom on the surface giving monolayer coverage[66]. The surface area of the rhodium component of the catalyst can therefore be determined by measuring the up-take of oxygen by the catalyst.

$$O_2\,(g) \quad \text{---------}> \quad 2\,O\,(a) \qquad 3.2.3.$$

$$O\,(a) + CO(a) \quad \text{---------}> \quad CO_2\,(g) \qquad 3.2.4.$$

Figures 3.1-3.3(b) show the up-take of oxygen at increasing temperatures on the 1% rhodium on alumina catalyst. The oxygen was dosed manually using an accurate gas tight syringe via a PTFE septum positioned just in front of the catalyst bed (see Figure 2.1.). Prior to the oxygen dosing, the catalyst was reduced in hydrogen at 410°C and cooled to the experimental temperature in a stream of helium. It can be seen as the temperature rises going from Figure 3.1 to 3.3., the oxygen up-take increases considerably . This is due in the main to the bulk oxidation of the rhodium particles by migration of the surface atomic oxygen species into the centre of the rhodium particles, forming rhodium oxides. This process has recently been studied using model rhodium catalysts by Tolia et al[67]. A second possibility is that the oxygen causes a change in the surface area of the rhodium by disrupting to some extent the crystallites, perhaps causing the three dimensional particles to change morphologically into two dimensional rafts. This type of behaviour was proposed by Kellner and Bell[68] to explain the increase in CO up-take over a Ru/Al_2O_3 catalyst, and is well documented in the case of CO adsorption on small rhodium particles[69] A considerable

amount of oxygen has been proposed to be adsorbed by the reduced alumina support as reported by Cho and Stock [70]. However in the present study, when a blank catalyst (a 1:4 mix of gamma:alpha alumina) was reduced at 400°C, cooled to 50°C, then subjected to 0.5 ml pulses of oxygen, no up-take of oxygen was detected. Figure 3.4. shows that the peak area of 0.5 ml pulses of oxygen passed over a blank alumina catalyst are the same as those passed through the by-pass. The up-take in this catalyst system is therefore entirely due to the rhodium component.

The surface atomic oxygen species formed upon dissociation of dioxygen may be titrated off the surface by CO(g). The titration of the $O_{(a)}$ by pulses of $CO_{(g)}$ yields $CO_{2(g)}$, equation 3.2.4. This reaction is shown in Figure 3.5. with the evolution of CO_2 when 0.5 ml of CO is pulsed over the catalyst after oxygen adsorption at 100°C. The yield of CO_2 compares well to the amount of O_2 adsorbed, in that 0.38 mls of $CO_{2(g)}$ is evolved from 0.2mls of adsorbed oxygen - (0.2 mls of O_2 = 0.4 O(a)). This reaction, the non-dissociative oxidation of carbon monoxide is a very facile reaction and goes at room temperature on rhodium single crystals. As CO dissociation requires elevated temperatures on rhodium (>150°C) all of the CO_2 produced comes from the reaction between adsorbed O(a) and the incoming CO molecules. In this way, two independent values related to the metal surface area of the catalyst can be found; (i) the up-take of dioxygen to form a monolayer of atomic oxygen and (ii) the yield of CO_2 produced by CO oxidation. The mass spectrometer was calibrated for oxygen, carbon monoxide and carbon dioxide in order that quantitative peak areas were obtained.

The volume of CO required to saturate the rhodium surface, provided that the CO:Rh=1 is calculated as follows;

$1m^2$ of rhodium $\approx 10^{19}$ surface sites

(assuming an interatomic distance of 3 .16Å)

Figure 3.4.
0.1 ml injections of oxygen over a reduced blank alumina catalyst - no oxygen adsorption.

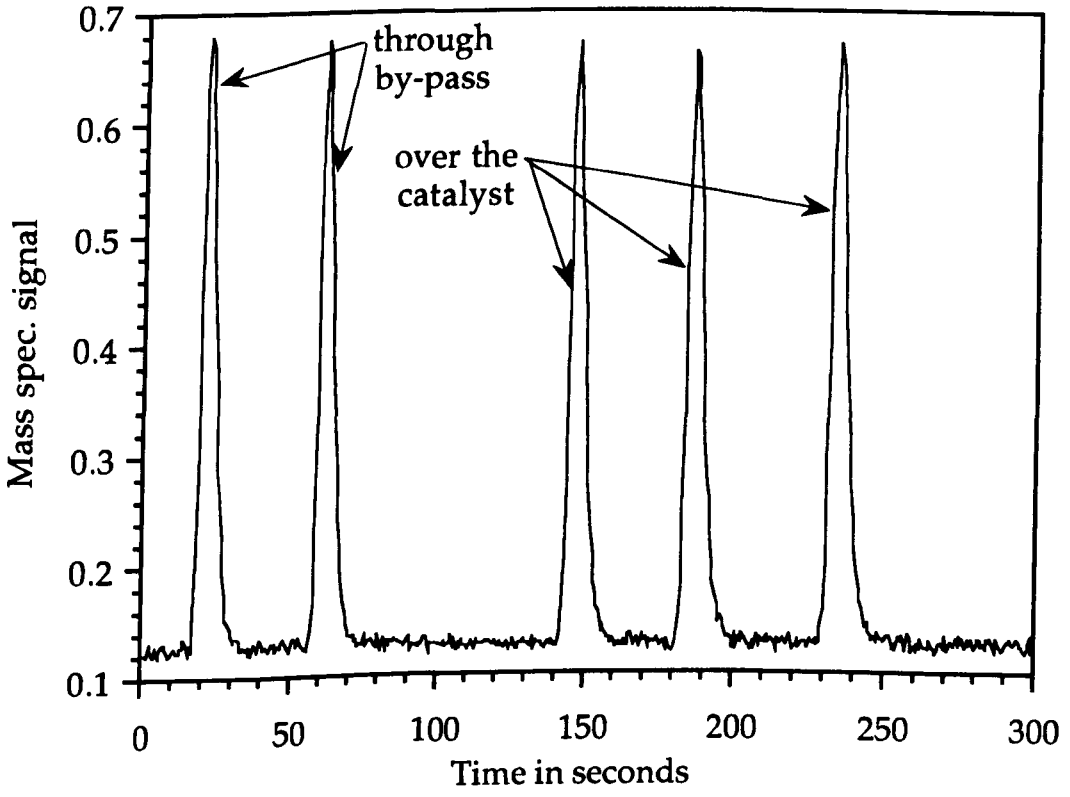

Figure 3.5.

CO pulses after O_2 injections at T = 100°C

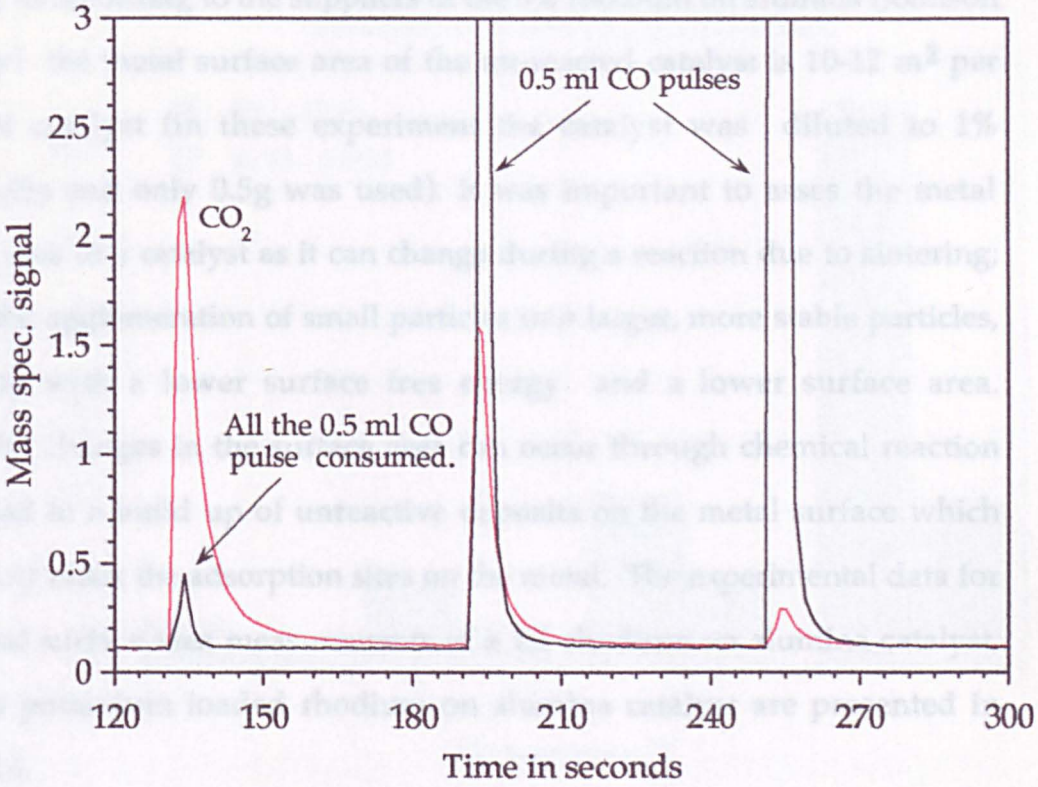

0.5 mls of CO $= 0.5/22400 \times 6.022 \times 10^{23} = 1.344 \times 10^{19}$

$10^{19} / 1.34 \times 10^{19} = 0.7439$

$0.7439 \times 0.5 = 0.37$ mls of CO required for 1 monolayer

Therefore 0.37 mls of CO contains approximately the same number of molecules as there are surface Rh atoms in 0.5 grams of the 1% Rh/Al_2O_3 catalyst, as according to the suppliers of the 5% rhodium on alumina (Johnson Matthey) the metal surface area of the un-reacted catalyst is 10-12 m^2 per gram of catalyst (in these experiment the catalyst was diluted to 1% Rh/Al_2O_3 and only 0.5g was used). It was important to asses the metal surface area of a catalyst as it can change during a reaction due to sintering; that is the agglomeration of small particles into larger, more stable particles, normally with a lower surface free energy and a lower surface area. Similarly, changes in the surface area can occur through chemical reaction that lead to a build up of unreactive deposits on the metal surface which effectively block the adsorption sites on the metal. The experimental data for the metal surface area measurements of a 1% rhodium on alumina catalyst, and the potassium loaded rhodium on alumina catalyst are presented in Figure3.6.

Clearly the addition of potassium has reduced the ability of the catalyst to adsorb oxygen. It can be envisioned that the promoter sits on the rhodium and alumina homogeneously and through simple site blockage, prevents the adsorption of the oxygen. At higher temperatures, two processes combine to increase the oxygen up-take, firstly, the O(a) species become more mobile, releasing the active sites of oxygen dissociation, therefore increasing the turn over number for dissociation, secondly oxidation becomes important, with O(a) have sufficient energy to bury into the bulk and in so doing, revealing clean rhodium for further oxidation.

Figure 3.6.
Oxygen take up versus temperature on promoted and un-promoted catalysts.

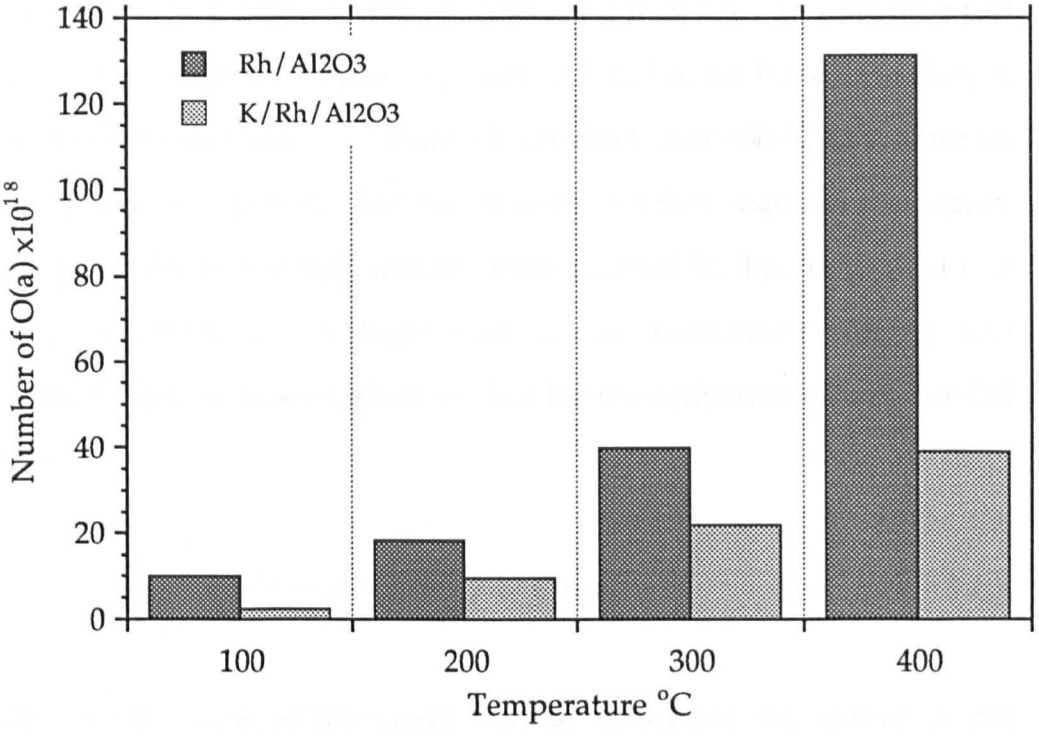

3.2.2 CO OXIDATION on RHODIUM on ALUMINA CATALYSTS.

Carbon monoxide may be oxidised to form CO_2 in a variety of ways. Two mechanisms are highlighted here; the disproportionation of CO, forming CO_2 and C(a), equation 3.2.5. where-by both oxygen atoms in the resulting carbon dioxide originate from CO. This reaction is commonly known as the Boudouard reaction. The second mechanism to be noted is non-dissociative oxidation, where an adsorbed oxygen atom combines with an adsorbed CO molecule to form carbon dioxide equation 3.2.4., i.e. no bond breaking is involved, (as demonstrated in Figure 3.5. conducted at 100°C, therefore no CO dissociation took place). The Boudouard reaction requires the highly activated CO dissociation step and has been studied in this work as it is a competing reaction to methane and water formation during CO hydrogenation and because it gives a value for the activation energy for CO dissociation.

$$2CO\,(a) \text{ ---------> } CO_2\,(g) + C\,(a) \qquad 3.2.5.$$

One of the aims of the study was to determine the extent of the dissociative oxidation route to CO_2 as opposed to other mechanistic routes such as the water gas shift reaction, equation 3.2.6.

$$H_2O + CO \text{ ---------> } CO_2 + H_2 \quad \Delta H\ -41 kJ\ mol^{-1} \qquad 3.2.6.$$

The water gas shift reaction is used industrially to alter the H_2 content in synthesis gas production (steam reforming) and to convert CO into CO_2 as CO is normally a severe poison in hydrogenation reactions. There are for instance two water-gas shift stages incorporated into the ammonia synthesis process (see for instance Twigg 'Catalysis Handbook'[71]).

Another aim was to calculate the activation energy for CO(a) dissociation over the highly dispersed rhodium catalyst, and to find the contribution, if any, of the alumina support in the overall reaction. Previous values for the activation energy of CO have been determined over a dispersed rhodium catalyst (for instance Ea=100.5 $kJmol^{-1}$., Solymosi et al.) and it was of interest not only to find the activation energy over the present catalyst but also to compare how well the pulse flow microreactor yields data that has been reported using other techniques.

After reducing the catalyst in H_2 at 400°C the temperature was dropped to 100°C with the catalyst under flowing He. The temperature was then ramped steadily to 400°C while 0.5 ml pulses of CO were introduced into the He diluent stream every 30 seconds, no H_2 was present. This experimental technique is referred to as **Temperature Programmed Pulsed Reaction** (T.P.P.R.). Figures 3.7. and 3.8.(a) and (b) show typical outputs from the microreactor between 200°C - 420°C. It can be seen that small peaks are seen at temperatures below 200°C, these were also present when the CO pulses were passed through the by-pass and are therefore discounted from any catalytic reaction. They are most likely to be due to the water gas shift reaction occurring on the hot mass spectrometer filament as there is always a small amount of residual water present in the vacuum chamber.

By plotting the natural logarithm of the CO_2 peak height versus the reciprocal temperature, being careful to eliminate the contribution by the mass spectrometer filament, an Arrhenius plot giving the activation energy for the dissociation of CO can be obtained. The reasoning behind this method is explained by the following logic;

Figure 3.7.
CO conversion from T.P.P.R.
with 0.5 ml CO pulses, no H_2.

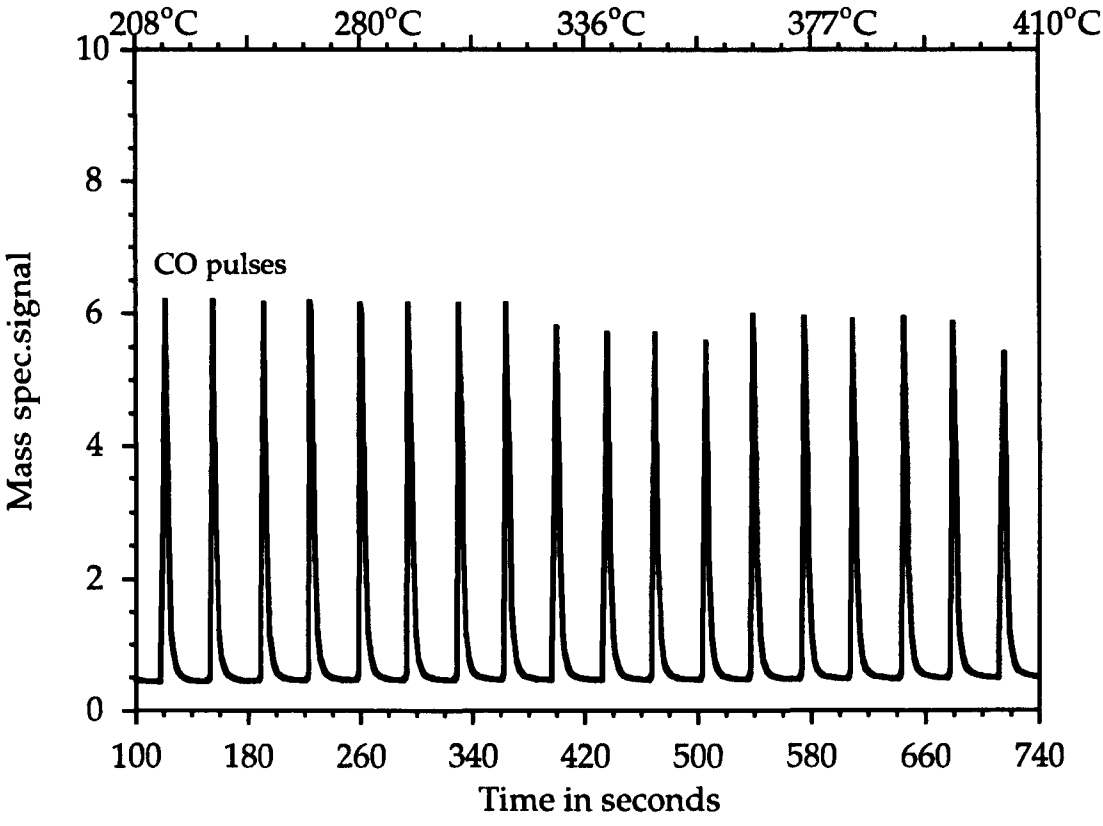

Figure 3.8.(a)
CO_2 production from T.P.P.R.
with 0.5 ml CO pulses, no H_2.

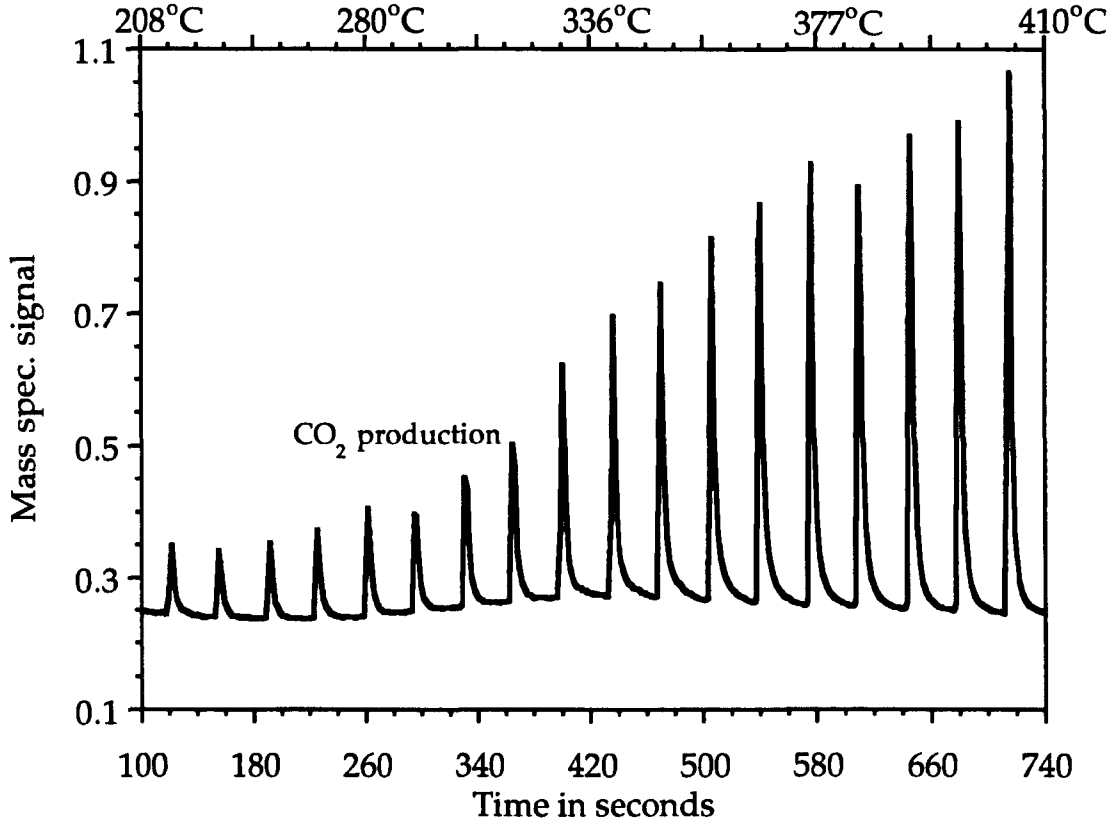

Figure 3.8.(b)
CO_2 production from T.P.P.R.
with 0.5 ml CO pulses into H_2. CO : H_2 = 1 : 1.8

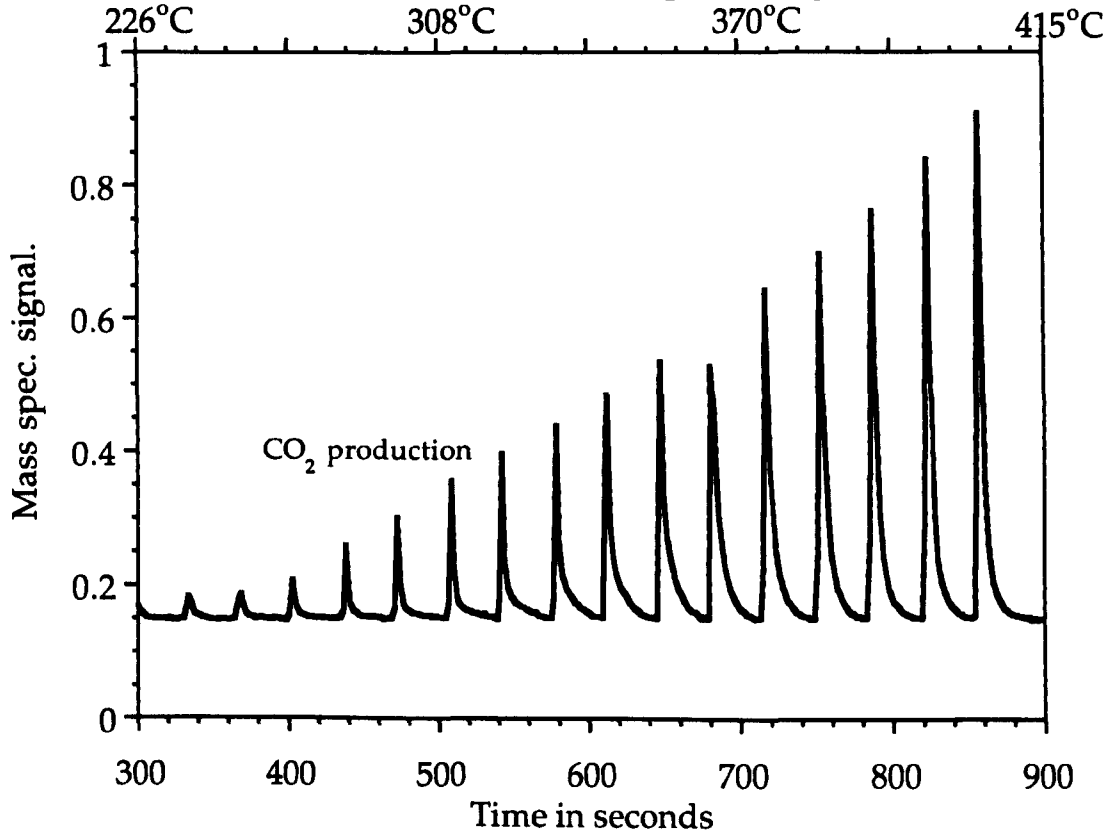

1(k) $CO(g) \Leftrightarrow CO(a)$

2(k2) $CO(a) \rightarrow C(a) + O(a)$

3(k3) $CO(a) + O(a) \rightarrow CO2(a)$

4(k4) $CO2(a) \rightarrow CO2(g)$

$$\frac{dCO_2}{dt} = k3[CO(a)][O(a)]$$

Assuming that $\theta CO(a) = 1$ and is also temperature independent and $[1 - \theta CO(a)]$ is constant, then,

$$\frac{dCO_2}{dt} = k3'[O(a)] \qquad \text{where } k3' = k3CO(a) = \text{constant}$$

$$\frac{dO(a)}{dt} = k2[CO(a)][1 - CO(a)] - k3[CO(a)][O(a)] = 0 \text{ if at steady state.}$$

$$[O(a)] = \frac{k2[CO(a)]}{k3[CO(a)]}[1 - CO(a)] \quad \therefore \quad \frac{dCO_2}{dt} = \frac{k3.k2[1 - CO(a)]}{k3} = k2$$

Certain assumptions have been made in the argument presented above. These are that the coverage of CO during the pulse is 1, that step 2 is the rate determining step, that the coverage of free sites during the pulse remains essentially constant and that reactions 3 and 4 are fast. In the present work only data relating to the initial onset of the Boudouard reaction has been used, that is at low CO conversion, thus avoiding complications due to the temperature dependence of CO(a) coverage at the higher temperatures and effect of carbon deposition poisoning the catalyst. The activation energy was found to be 103 $kJmol^{-1}$. Clearly, in the absence of hydrogen there is no water production, therefore all CO_2 comes from the dissociative oxidation of CO. This value compares well with others quoted in the literature[2,3,39] and illustrates that the microreactor provides useful information very readily, and that the assumptions made are not unreasonable.

When H_2 is present in the diluent stream, the surface is cleaned of C(a) between pulses, this leads to a higher CO conversion as more rhodium sites

are available for reaction. See for instance the CO conversion in Figure 3.7. (with no H_2 present) compared to the CO conversion in Figure 3.13.(a) where there is H_2 present . In Figure 3.7. the CO conversion is less than 10% at 400°C whereas with hydrogen flowing at 2mls per minute, the conversion of each CO pulse rises to over 50% at the same temperature (Figure 3.13.(a)). From inspection of the CO_2 produced from pulsing CO across the catalyst with no hydrogen, Figure 3.8.(a) it is interesting see note that a broad rise in the base line is evident between ~280 - 380°C, whereas with H_2 present, Figure 3.8.(b) the broad rise is replaced by a prominent shoulder developing at the base of the CO_2 peaks in the same temperature range. This observation will be expanded upon in the discussion. Small variations in the mass spectrometer sensitivity between the two experiments accounts for the change in scale on the y axis. As the CO conversion is very low in Figure 3.7., the build up of carbon deposits does not poison the metal surface during the course of the experiment, as shown by the continual rise in CO_2 production in Figure 3.8.(a). However, as will be shown in the following section, at higher CO conversions, carbon deposits do poison CO dissociation.

In isothermal experiments at 440°C, in which the H_2 flow rate is varied from 3mls per minute to 2mls per minute then to 1ml per minute - Figure 3.9. - it is evident that as the concentration of H_2 decreases the CO_2 production slightly increases. As the production of CO_2 is only slightly less with a tripling of the hydrogen concentration it must be that the surface coverage of H(a) in comparison to CO(a) remains low throughout the experiment, this is not surprising given the high temperature. When the concentration of hydrogen increases, the surface of the catalyst is cleaned at a faster rate via hydrogenation reactions, this is very apparent from Figure 3.9. where the rate of methanation and H_2O production is greatest with the highest H_2 flow rate. Clearly there is competition between CO(a) and H(a) for the O(a) and when the concentration of H_2 is increased, the better it competes.

Figure 3.9.

Temperature = 440°C

0.5 ml pulses of CO into 3, 2 and 1 mls per min. H_2.

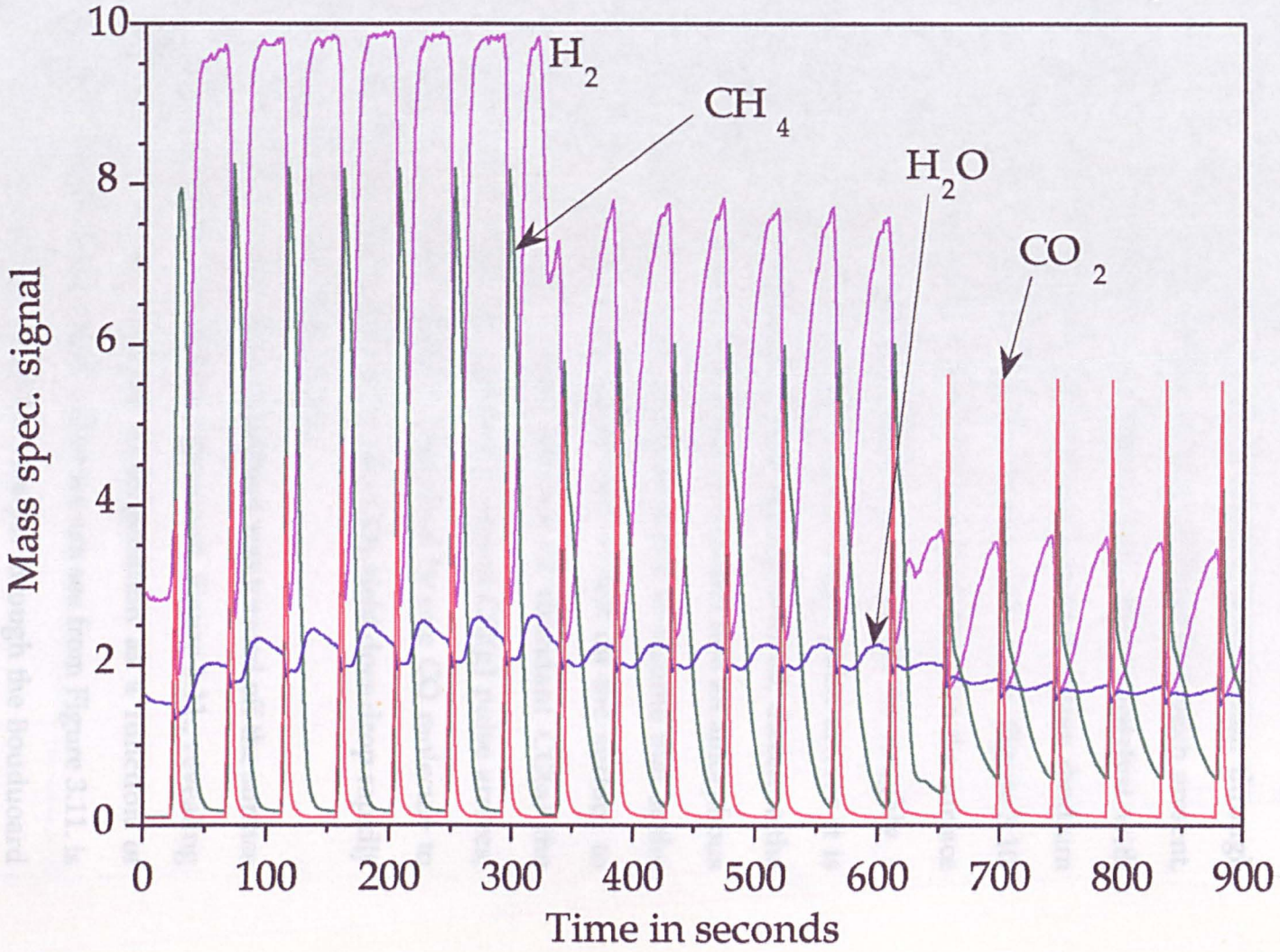

The implications of the CH_4 and H_2O signals in Figure 3.9., particularly regarding the prevalent methanation reaction (wet methanation as opposed to dry methanation) are discussed in section 3.3.

The Boudouard reaction was studied isothermally at 400°C to monitor the decay of CO_2 production as a result of catalyst deactivation through carbon deposition. A fully reduced, clean catalyst, without hydrogen present, is better at initial CO_2 production, see Figure 3.10., than a catalyst with hydrogen present. The first 0.5 ml CO(g) pulse arrives at the clean rhodium surface and is almost entirely converted to CO_2 and C(a) - from Figure 3.10. ~70% of the first pulse reacts, i.e. 0.35 mls of C(a) is laid down on the surface according to the Boudouard reaction, which corresponds to roughly 1 monolayer (see section 3.2.1.). When the second CO(g) pulse arrives it is apparent that a considerable amount of CO_2 is again produced, therefore the C(a) doesn't block all the surface and may group together into an amorphous carbon type at this temperature. Also, it is reasonable to assume that at the trailing end of the first pulse, some CO(a) will be left on the surface to dissociate to C(a) and O(a) and in the absence of abundant CO(a) the formation of CO_2 is slow. Therefore when the second CO(g) pulse arrives, any O(a) remaining will be very quickly consumed by one CO molecule to form CO_2. Apparent from Figure 3.10. is that the CO_2 yield does drop rapidly as the surface is poisoned by deposits of C(a).

The carbon laid down from this experiment was titrated off the surface in a temperature programmed reduction experiment, Figure 3.11., revealing the rhodium catalysts activity towards hydrogenation as a function of temperature and its carbon chain length. What we can see from Figure 3.11. is that C_1 and C_2 species have built up on the catalyst through the Bouduoard reaction at 440°C. A reactive species is gradually cleaned off as ethane between 50°C and 200°C. This reactive surface species leading to ethane formation was not formed under CO hydrogenation conditions. A less

Figure 3.10.

0.5 ml CO pulses at 440°C. No H_2 present.

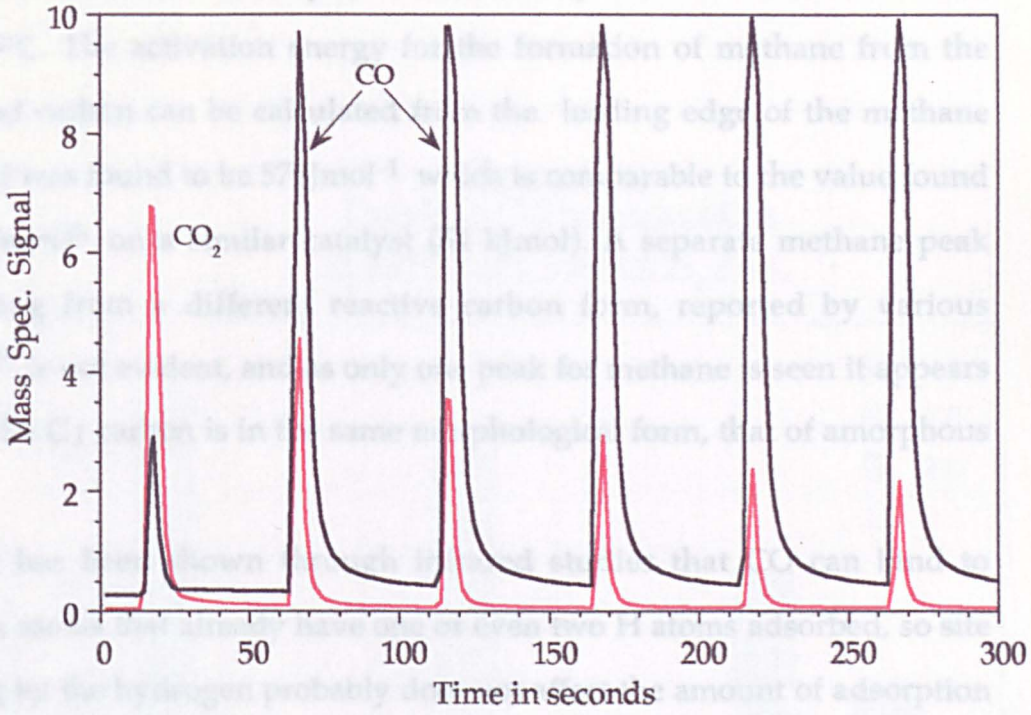

Figure 3.11.

T.P.R. with H_2 flowing at 1 ml per minute

after CO pulses at 440°C

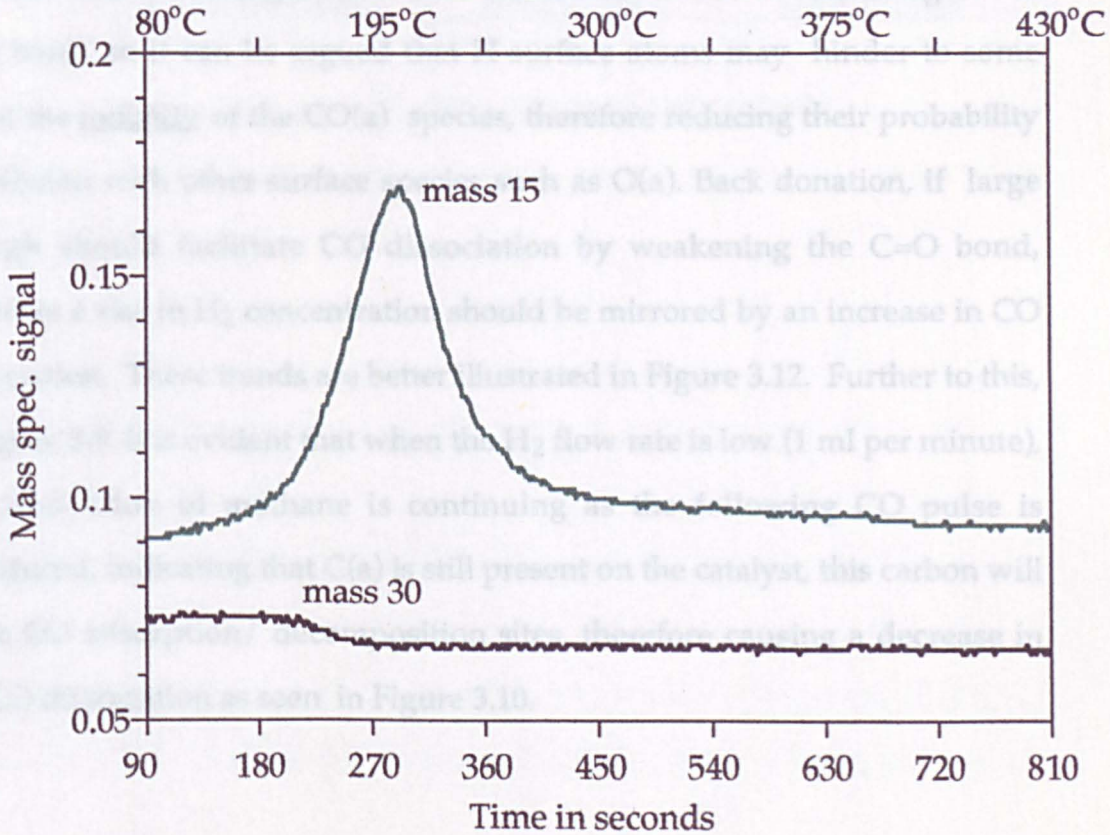

reactive C_1 species begins to be hydrogenated at ~90°C with the methane peak maximum at 205°C, the peak tails off slowly and is down to its base line by ~350°C. The activation energy for the formation of methane from the deposited carbon can be calculated from the leading edge of the methane peak and was found to be 57kJmol^{-1} which is comparable to the value found by Solymosi[35] on a similar catalyst (54 kJmol). A separate methane peak originating from a different reactive carbon form, reported by various authors[35] is not evident, and as only one peak for methane is seen it appears that all the C_1 carbon is in the same morphological form, that of amorphous carbon.

It has been shown through infrared studies that CO can bind to rhodium atoms that already have one or even two H atoms adsorbed, so site blocking by the hydrogen probably does not affect the amount of adsorption of CO. However, electron flow from the H atom into the electron deficient rhodium atom may contribute to electron back donation from the rhodium into the anti-bonding π-orbitals of the C=O bond as proposed by Solymosi[24]. This will cause a stronger bond between the Rh-C and a weakening of the C=O bond, so it can be argued that H surface atoms may hinder to some extent the mobility of the CO(a) species, therefore reducing their probability of collision with other surface species such as O(a). Back donation, if large enough should facilitate CO dissociation by weakening the C=O bond, therefore a rise in H_2 concentration should be mirrored by an increase in CO dissociation. These trends are better illustrated in Figure 3.12. Further to this, in Figure 3.9. it is evident that when the H_2 flow rate is low (1 ml per minute), the production of methane is continuing as the following CO pulse is introduced, indicating that C(a) is still present on the catalyst, this carbon will block CO adsorption/ decomposition sites, therefore causing a decrease in the CO dissociation as seen in Figure 3.10.

Figure 3.12.
Trends in CO hydrogenation
at 440°C with varying H_2 flow.

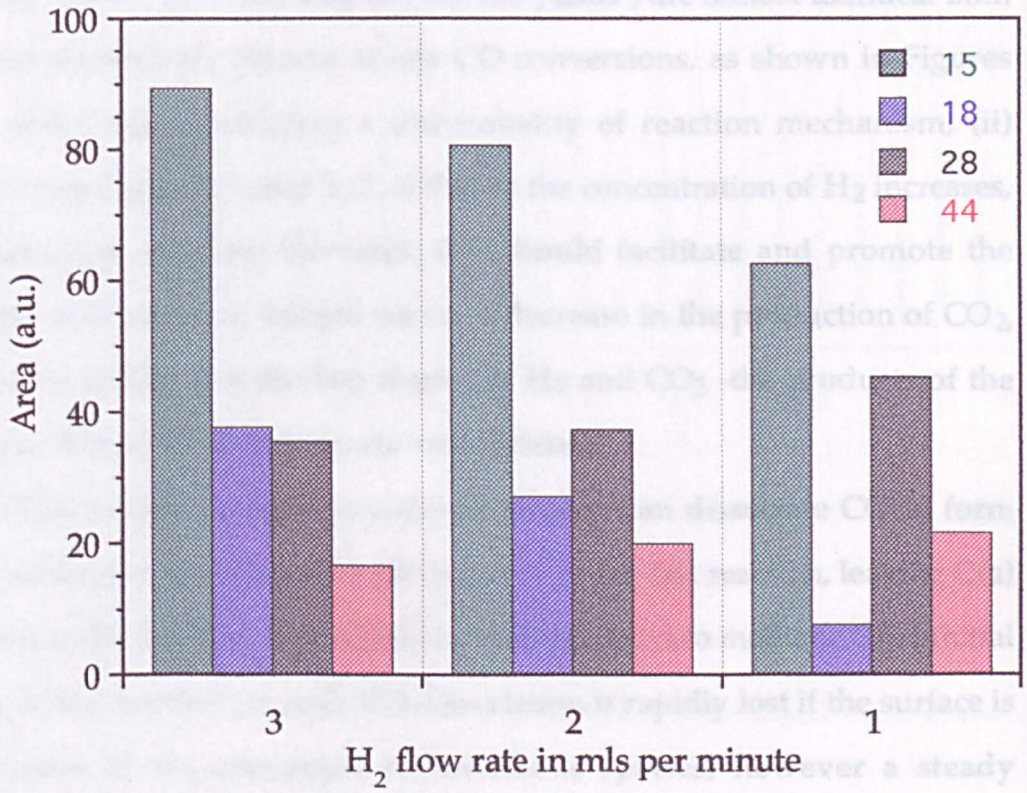

What is at first unclear is whether CO_2 production is due exclusively to more dissociative oxidation or due to the water gas shift reaction. This is a little difficult to determine precisely under the transient conditions employed in these experiments as a steady state of CO and water is not achieved. The results suggest, however, that the water gas shift reaction does not occur to any significant degree in this system. The following points back up this assertion; (i) the CO_2 line shapes (not the yields) are almost identical both with and without H_2 present at low CO conversions, as shown in Figures 3.8.(a) and 3.8.(b), indicating a commonality of reaction mechanism, (ii) evident from Figure 3.9. and 3.12. is that as the concentration of H_2 increases, the production of water increases, this should facilitate and promote the water gas shift reaction, instead we see a decrease in the production of CO_2, and further to this, (iii) the line shapes of H_2 and CO_2 -the products of the water gas shift reaction- are clearly very different.

What is clear is that the reduced catalyst can dissociate CO to form C(a) and O(a) and that CO_2(g) is produced in a very fast reaction, leaving C(a) adsorbed on the surface. This carbon is hydrogenated to methane. The initial activity of the catalyst towards CO dissociation is rapidly lost if the surface is not cleaned of the unreacted carbonaceous species, however a steady conversion of CO to CO_2 is maintained in these experiments when H_2 is present.

3.2.3. CO HYDROGENATION on RHODIUM on ALUMINA.

3.2.3.1. CO HYDROGENATION with $CO:H_2 = 1:1.8$

Figure 3.13.a and 3.13.b. shows a temperature programmed pulsed reaction T.P.P.R. experiment. Pulses of CO (0.5 ml) are introduced into the

Figure 3.13.(a)
T.P.P.R. showing
H_2 and CO consumption. CO:H_2 = 1:1.8

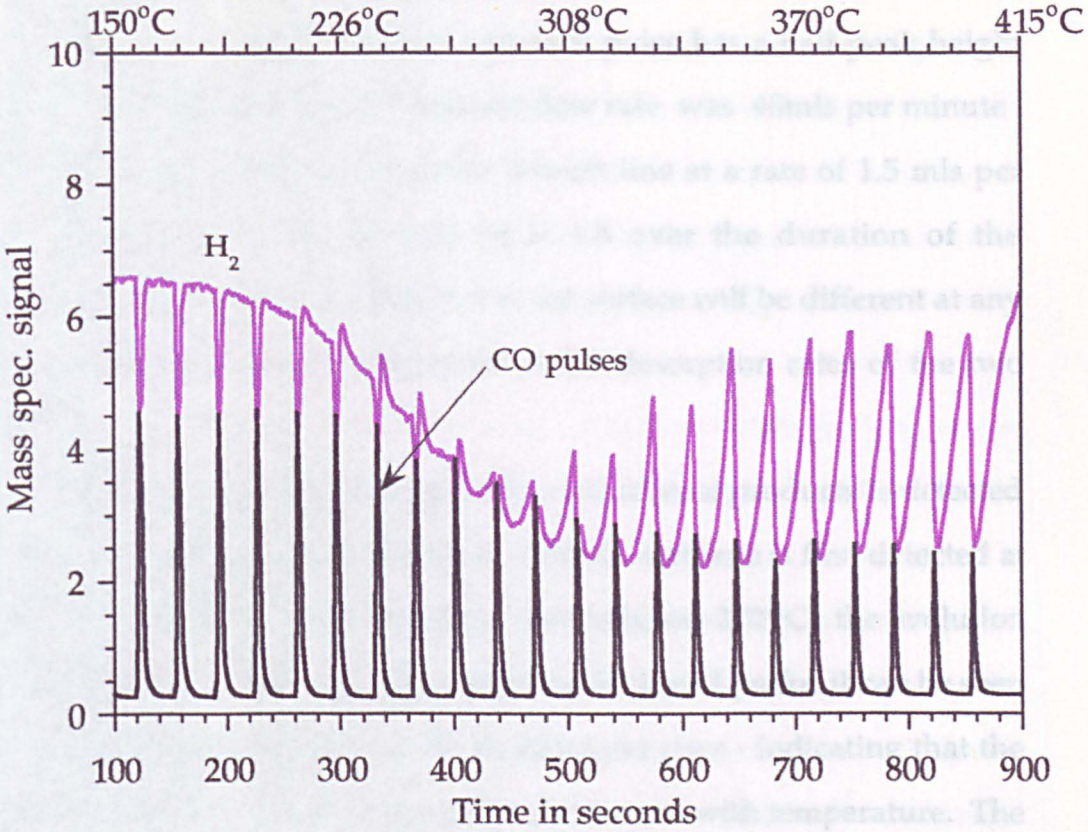

Figure 3.13.(b).
T.P.P.R. showing
evolution of products. CO : H_2 = 1:1.8

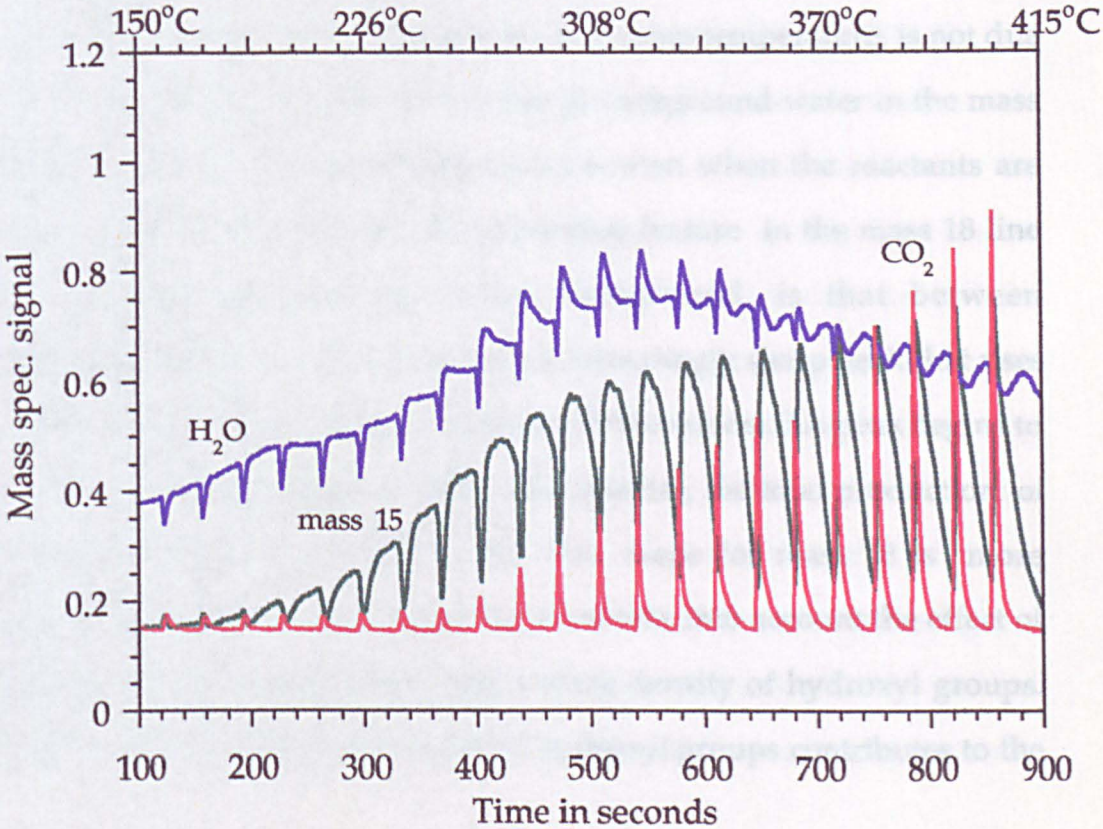

helium diluent line every 35 seconds, therefore in a fifteen minute run, 25 pulses are passed across the catalyst and each pulse has a half peak height width of ~ 5 seconds. The diluent (helium) flow rate was 40mls per minute . Hydrogen is dosed continually into the diluent line at a rate of 1.5 mls per minute thus giving a $CO:H_2$ ratio of 1: 1.8 over the duration of the experiment, however, the stoichiometry at the surface will be different at any given temperature due to the difference in the desorption rates of the two reactants.

As the temperature rises the gradual evolution of products is detected and the first product to appear is H_2O at ~150°C, methane is first detected at ~165°C. In the lower temperature range , that is below 270°C , the evolution of CH_4 (mass 15) is at first very slow resulting in broad peaks, it can be seen that the peaks begin to sharpen as the temperature rises - indicating that the rate of methanation is initially very slow but increases with temperature. The production of H_2O also begins very gradually, the line shape is similar to that of the CH_4 peak, in that it begins as a very shallow rise but as the temperature increases the rate of water production increases too. It should be noted that the high mass 18 background level seen even at room temperature, is not due to water formation on the catalyst, it is due to background water in the mass spectrometer unit as the same background is seen when the reactants are passed through the by-pass line. An interesting feature in the mass 18 line shape, noticeable despite the broad background, is that between approximately 250°C and 320°C there is an increasingly sharp peak that rises rapidly after each CO input pulse. At higher temperatures this peak begins to decline and is not discernible at 400°C and likewise, the total production of water begins to fall above 320°C. The line shape for mass 18 is more complicated than that for the CH_4 as one must take into account the effect of the alumina support which has a high surface density of hydroxyl groups. The hydrogenation and desorption of the hydroxyl groups contributes to the

water production at high temperatures. The extent of desorption of water from the support depends upon whether the support is fully reduced prior to a reaction run; if it is reduced then water will be seen to desorb only at high temperatures as illustrated in Figure 3.14., a T.P.P.R. on blank alumina. If however the support has a high density of hydroxyl groups then more water will desorb between 100-280°C . The catalyst was generally reduced prior to each reaction run.

It can be seen, particularly in the line shapes of hydrogen and water, that as the CO pulse passes across the catalyst bed, there is a sudden drop in the mass spectrometer signal. In the case of H_2 the perturbation is approximately 15% at maximum. This effect was touched upon in Chapter 2 and it is due to a partial displacement of the hydrogen/helium flow by the incoming CO pulse, there evidently is sufficient mixing of the reactants in the gas line prior to them reaching the catalyst bed to ensure that both are present at the catalyst surface, otherwise the H_2 signal would be reduced to it's zero level with each CO pulse. At the same time, the CO pulse is sufficiently narrow to allow line shape analysis to be carried out.

Under the hydrogen deficient conditions employed here, CO : H_2 = 1: 1.8, the maximum production of methane produced between pulses occurs between 300-325°C, from then on it begins to slowly decline as the temperature rises. This decline can be explained due to the Boudouard reaction, which consumes CO(a) which at lower temperatures could have reacted to form CH_4. The intrinsic rate of the methanation reaction clearly continues to rise with temperature, as illustrated by the sharper leading edge of the methane peaks . It can be seen upon inspection of the methane base-line in Figure 3.13.(b), that under these conditions even at 400°C, it is still being produced at the time the subsequent CO pulse is introduced, indicating that there are still surface carbonaceous species present. There was however no evidence of any higher hydrocarbons or oxygenates formed in appreciable

Figure 3.14.
Showing H_2O lineshape on a
blank Al_2O_3 catalyst. CO : H_2 = 1 : 6

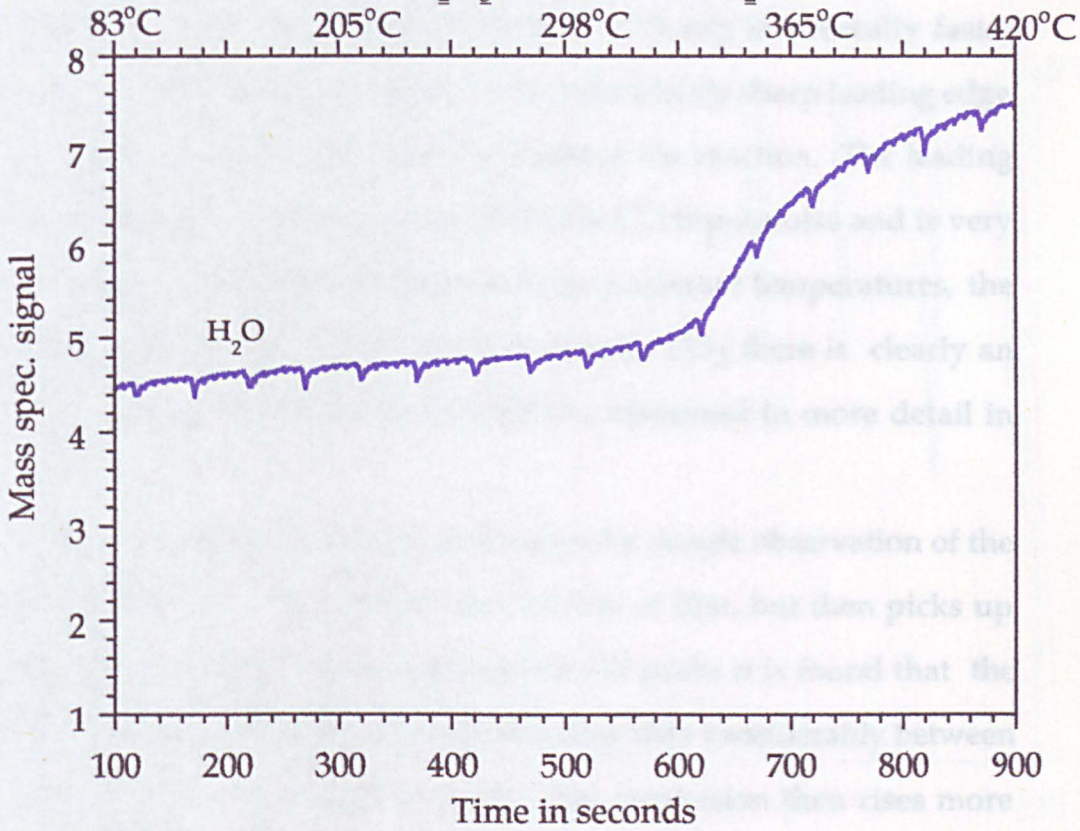

quantities. The relevant masses for ethane (30), propane (29) , methanol (31) and ethanol (31,45) were monitored. Water is produced at a slower rate than methane at higher temperatures. This observation is better illustrated in the following section.

Continuing with Figure 3.13.(b), the production of CO_2 begins at ~270°C at this temperature there is a very low yield. The production rises with temperature. The rate of CO_2 production is clearly intrinsically faster than that of CH_4 and H_2O as evidenced by the remarkably sharp leading edge of the mass 44 line shape, right from the onset of the reaction. The leading edge of the CO_2 peak is near coincident with the CO input pulse and is very narrow in width, indicating that even at these moderate temperatures, the rate of reaction is very fast. With the production of CO_2 there is clearly an affect on the product distribution. This will be discussed in more detail in section 3.3.

By following the CO pulses it can be seen by simple observation of the peak heights, that conversion begins very slowly at first, but then picks up considerably above 220°C . By integrating the CO peaks it is found that the conversion is between 0.5% and 1% at 220°C, then rises considerably between 220°C and 310°C by which time it is 33%. The conversion then rises more gradually, at 400°C it is found that 43% of each CO pulse is reacted under these conditions. These conversions were calculated by integrating the peak area of an un-reacted CO pulse (through the by-pass) and comparing that value to the integrals of the CO pulses from the reactor run. It is interesting to note that the temperature at which CO desorption occurs from the catalyst is between 150°C and 250°C, evident from the expanded CO base-line shown in Figure 3.15. The implications of this observation will be considered in the discussion.

The line shape of the hydrogen illustrates very clearly how its consumption increases with temperature up to a maximum at ~320°C; the

Figure 3.15.
An expanded view of a T.P.P.R. of CO hydrogenation, showing CO desorption.

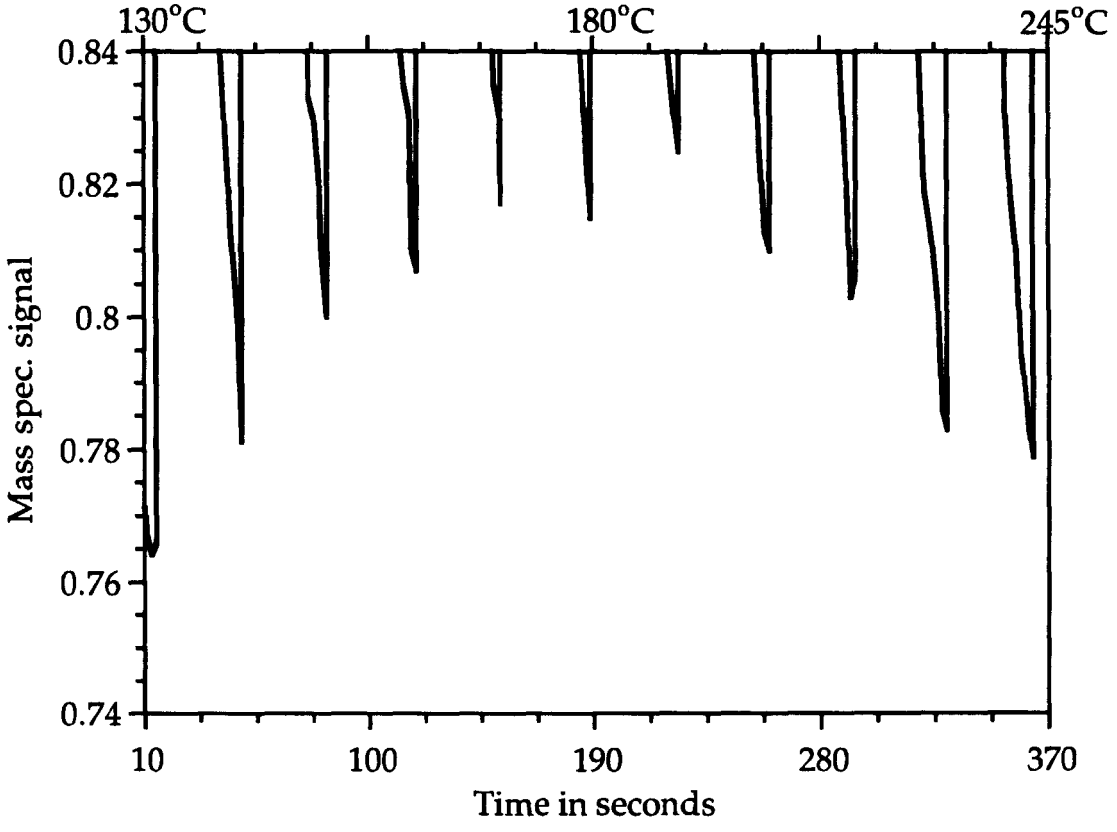

line shape can be seen falling gradually at lower temperatures as it is consumed in slow surface reactions, then at higher temperatures, it falls sharply, immediately after the CO pulse, illustrating that it is reacting at a fast rate. It rises back towards its unreacted level as the surface concentration of C(a) and O(a) is reduced, however under these H_2 deficient conditions the H_2 concentration doesn't reach it's maximum level between pulses, indicating just as the methane peak does, that hydrogenation of surface species is still taking place at the time of the subsequent CO pulse. Above ~320°C the hydrogen consumption begins to decrease, with the line shape rising up towards its unreacted level faster, this is in line with the observation that methane production is increasing in rate but decreasing in yield. It is apparent that the hydrogen line shape mirrors that of methane and isn't as noticeably affected by the production of water. Figure 3.16.(a) illustrates the trends in CO and H_2 consumption and Figure 3.16.(b) the trends in the product yields of the CO/H_2 reaction.

3.2.3.2. ISOTHERMAL CO HYDROGENATION WITH VARYING H_2.

In Figures 3.17.(a)-(d) a more detailed study into the rate of product formation and the product distribution as a function of hydrogen flow rate (concentration) is presented. The temperature was kept constant at 440°C. The H_2 flow rate was increased in the order 1.2/2.0/5.0/20 mls per minute in Figures 3.17.(a)-(d) respectively. The general trends apparent in the experiment are illustrated in Figure 3.18. and are discussed in section 3.3. (discussion). The high temperature, 440°C, was chosen in order to ensure that the dry methanation was favoured, as the rate of desorption of hydrogen at this temperature is very fast.

Figure 3.16.(a)
CO and H_2 conversion from T.P.P.R. CO:H_2 = 1:1.8

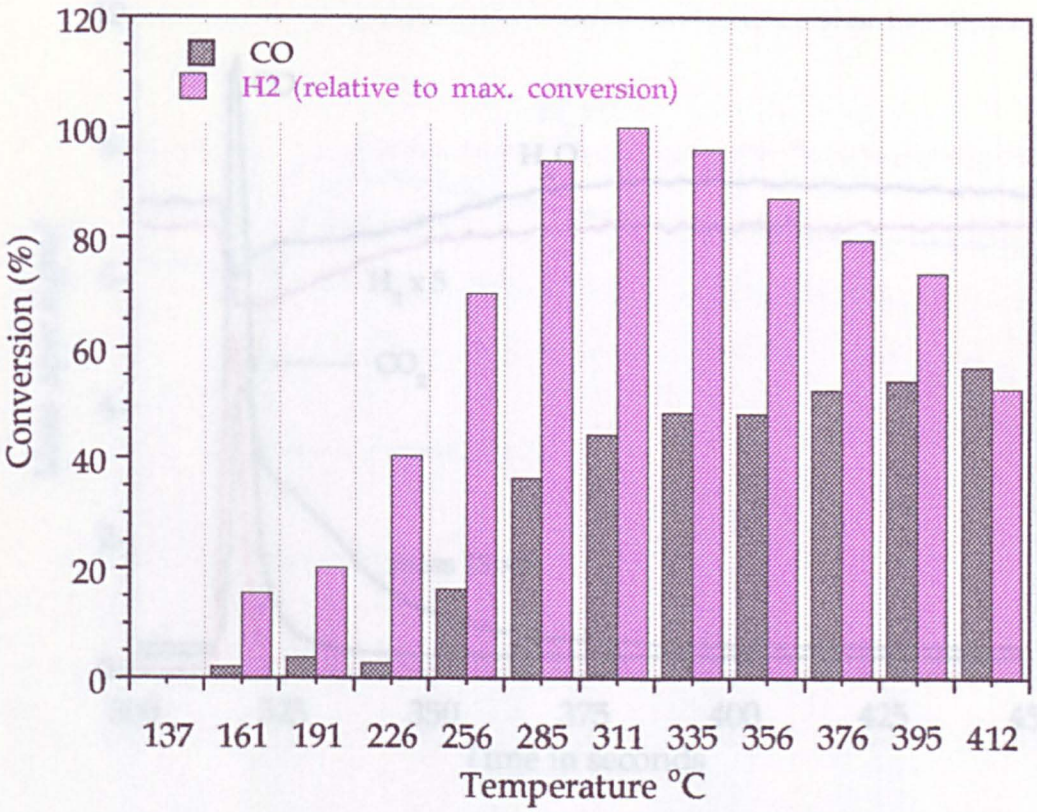

Figure 3.16.(b)
Yield of products from T.P.P.R. CO:H_2 = 1:1.8

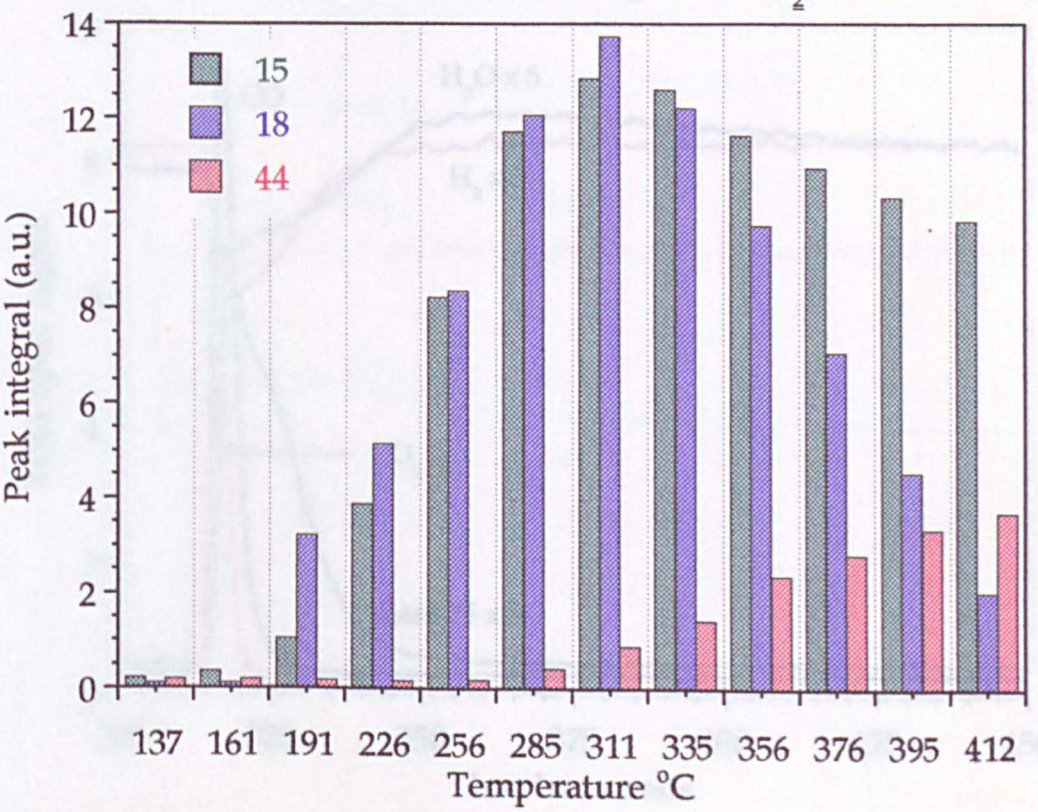

Figure 3.17.(a)

Temp. = 440°C. 1 x 0.5ml CO pulse.
He = 60 mls/min. H_2 = 1.2 mls/min.

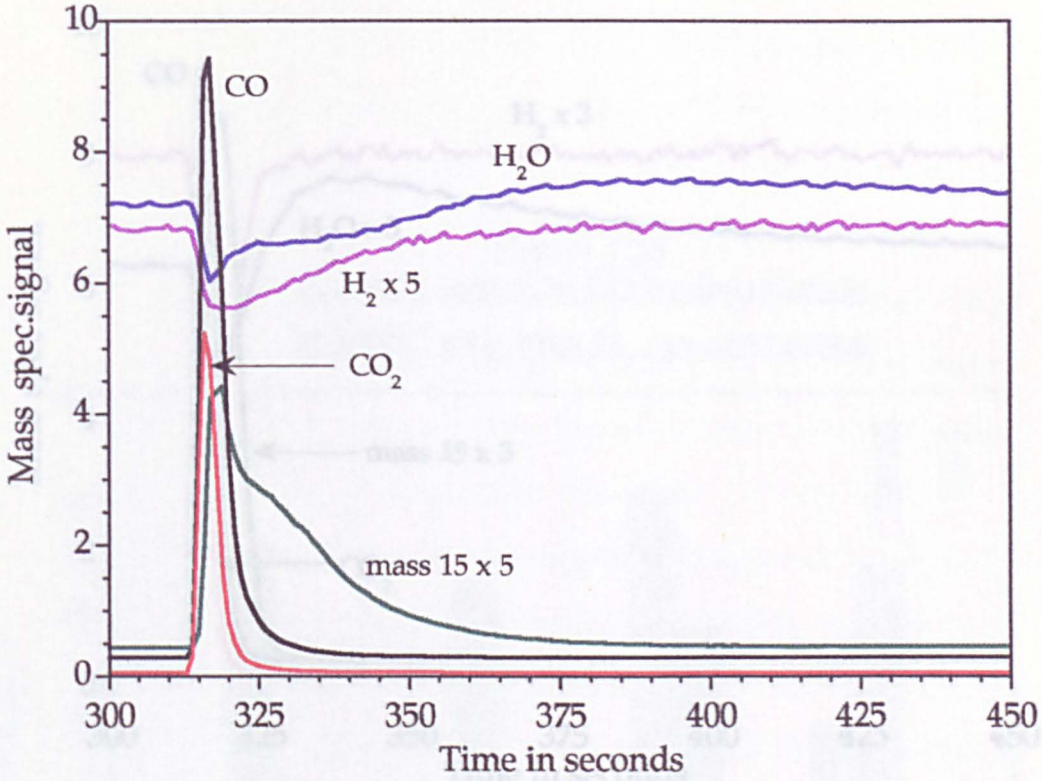

Figure 3.17.(b)

Temp. = 440°C. 1 x 0.5ml CO pulse.
He = 60mls/min. H_2 = 2mls/min.

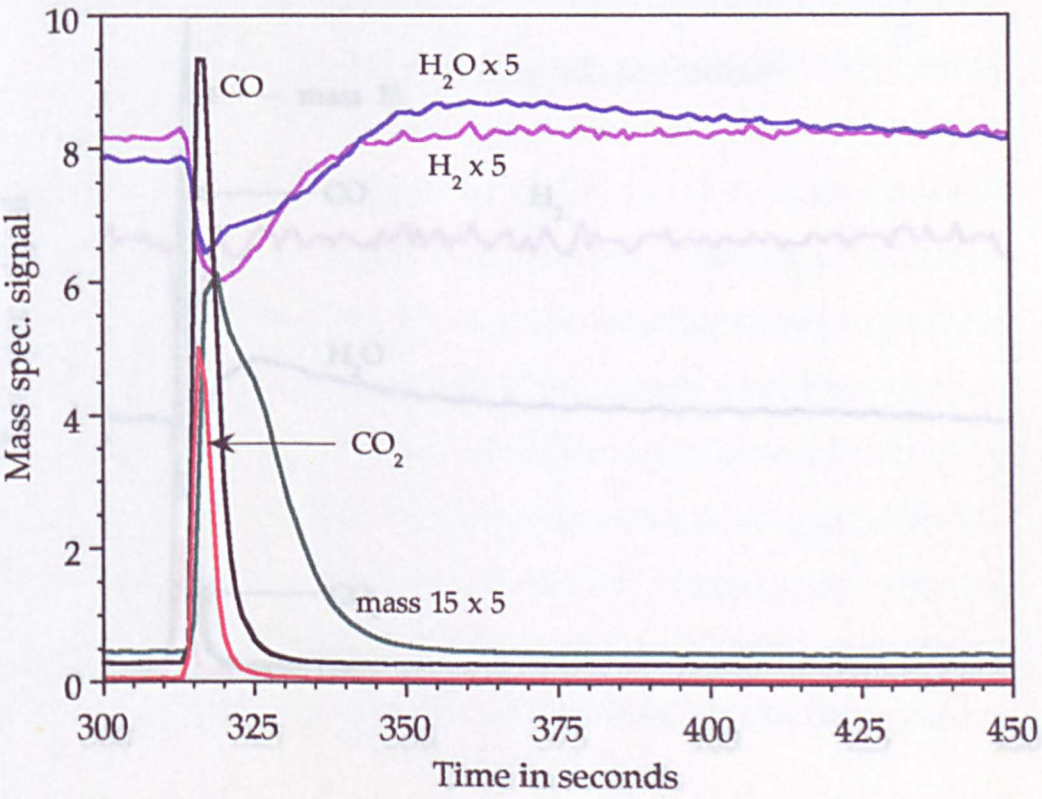

Figure 3.17.(c)

Temp. = 440°C. 1 x 0.5ml CO pulse.
He = 60 mls/min. H_2 = 5 mls/min.

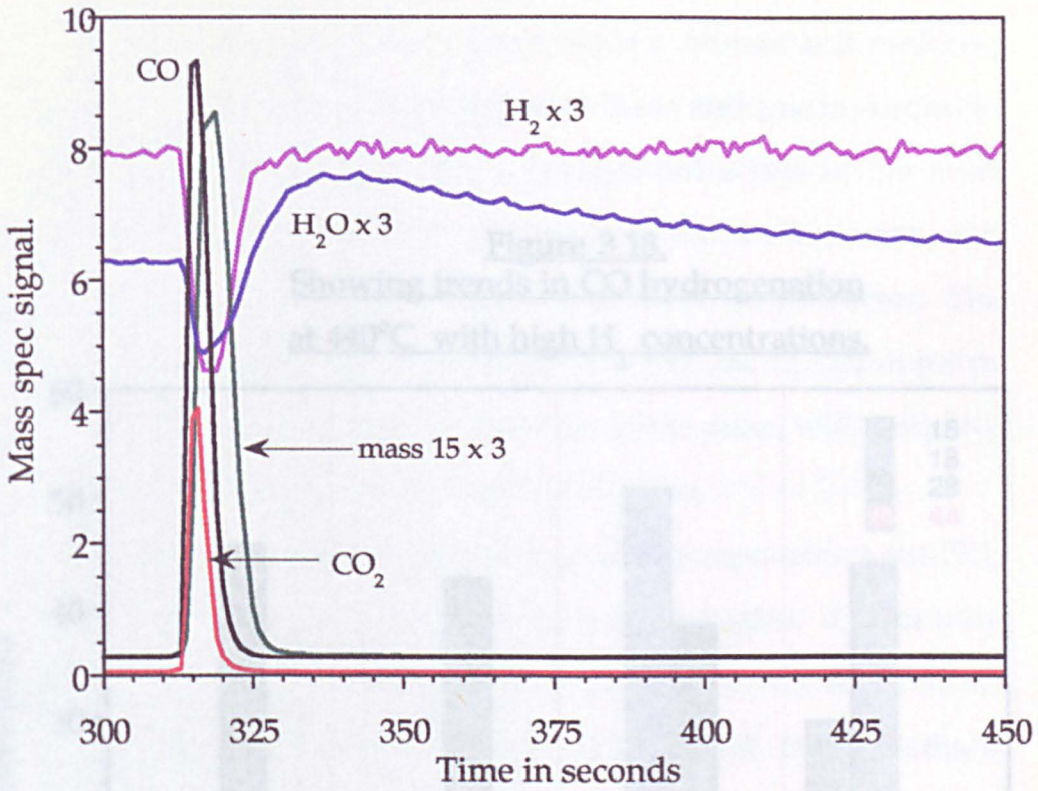

Figure 3.17.(d)

Temp. = 440°C. 1x0.5ml CO pulse.
He = 60 mls/min. H_2 = 10 mls/min.

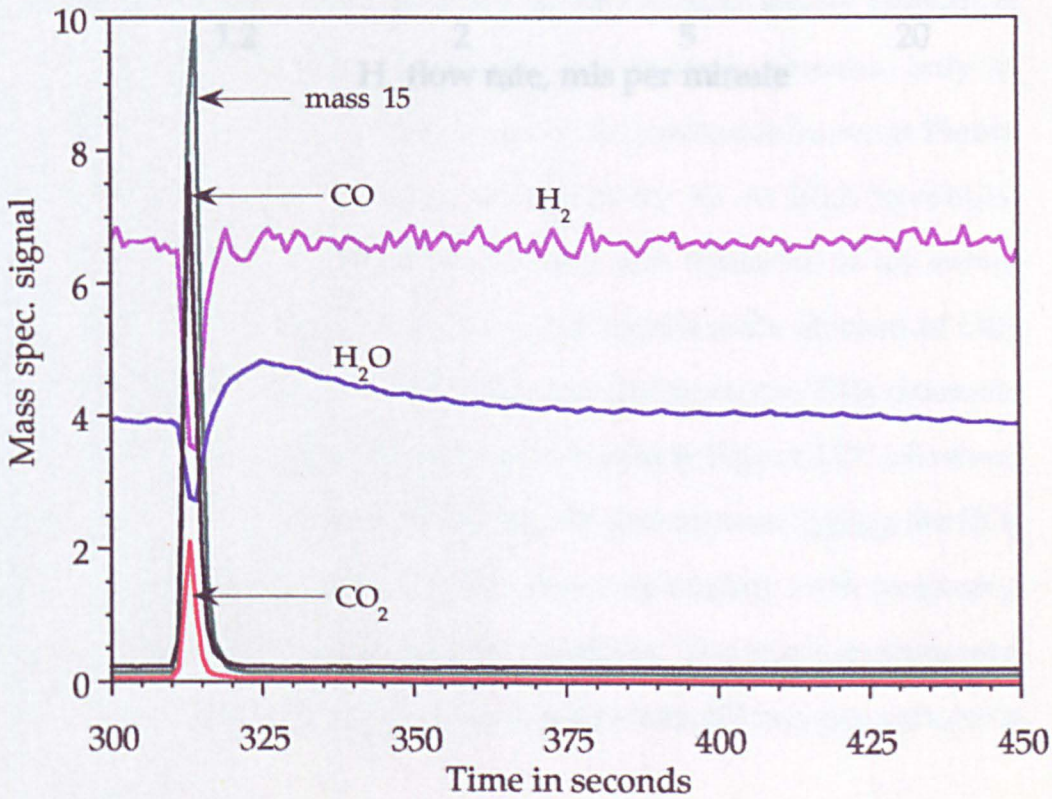

Figure 3.18.
Showing trends in CO hydrogenation
at 440°C with high H_2 concentrations.

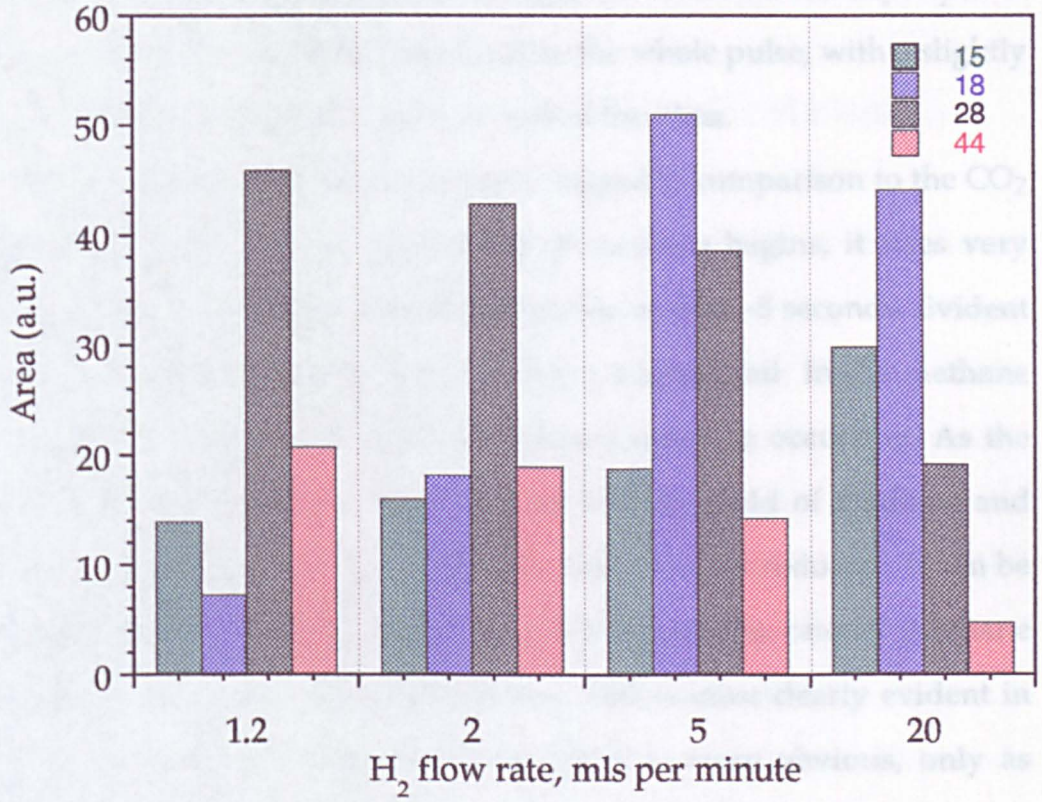

Looking first at Figure 3.17.(a) (H_2 flow rate = 1.2 mls per minute) it is apparent that only two products are formed, carbon dioxide and methane. Water production is small and indeed appears to fall as methane is produced, presumably as water is predominantly a background signal in the mass spectrometer and as hydrogen is consumed in the methanation, the background water falls as less H_2 enters the mass spectrometer. The production of CO_2 is remarkably fast, rising in line with the CO input pulse. It is near coincident with the CO signal across the whole pulse, with a slightly narrower width than for the CO peak in each of the plots.

The production of methane is clearly lagged in comparison to the CO_2 in Figures 3.17. (a)-(c). Once production of methane begins, it rises very sharply, reaching a maximum rate of production within ~5 seconds. Evident also, particularly in Figures 3.17.(a) and (b) is a broad tail in the methane peak. It appears that two reactions of different rates are occurring. As the hydrogen flow rate increases, both the rate and the yield of methane and water increase and the slower reaction path to methane is reduced. It can be seen that under these high temperature conditions the rate of methane production is far greater than that of water. This is most clearly evident in Figures 3.17.(c) and (d) where the water peak is more obvious, only as methane production falls does water begin to be produced (note in Figure 3.17. (d) the mass 18 signal is <u>not</u> multiplied by 3). At high hydrogen concentrations, the wet methanation reaction rate increases to an extent where it competes with CO(a) for the O(a) and therefore the amount of CO_2 produced is reduced through competition for surface sites. This dramatic increase in the rate of methane formation can be seen in Figure 3.17. (d) where the mass 15 peak rises with the CO input peak and appears <u>before</u> the CO_2 peak. The overall conversion of CO increases only slightly with increasing hydrogen flow, the production of CO_2 decreases. The more pronounced decrease in the peaks at high hydrogen concentrations (20 mls per minute) is

somewhat distorted due to the increase in the total gas flow rate (i.e. from 60 to 80 mls per minute), the amount of gas entering the mass spectrometer is constant, therefore at higher flow rates the gas composition being analysed is diluted. The most apparent trend in the series is the huge increase in water production with increasing hydrogen and the synchronous decrease in the CO_2 yield.

3.2.3.3. CO HYDROGENATION WITH HIGH DILUENT and HIGH H_2

A series of experiments were carried out to examine the effect of further increases to the H_2 flow at higher diluent rates (H_2 = 3 mls per minute and He = 60 mls per minute). As can be seen from Figure 3.19. the line shapes are generally similar to those seen previously, however there are some important differences to be noted in each of the masses.

In the case of methane, production can be seen beginning at ~165°C and is obvious by 185°C, therefore by comparison with Figure 3.13.(b) it appears that the temperature of methanation is not lowered by an increase in the H_2 concentration. It must be inferred that hydrogen does not actively assist CO dissociation, if it did, then a lower light-off temperature for methanation would be seen, this is in agreement with Koerts[72] . By ~315°C the rate of methanation is sufficient to ensure that it is completed by the time the next CO pulse is introduced, therefore the increase in hydrogen does increase the rate of methanation. The leading edge of the methane peak is far sharper at these higher H_2 concentrations and by 300°C it is near coincident to the CO input pulse. The higher H_2 concentration ensures that the surface is cleaned of carbonaceous species faster.

No water production was seen until 225°C, a significantly higher temperature than with the lower hydrogen flow rate. This is somewhat of a

Figure 3.19.
T.P.P.R. showing evolution of products.
He = 60 mls/min. CO : H_2 = 1:6

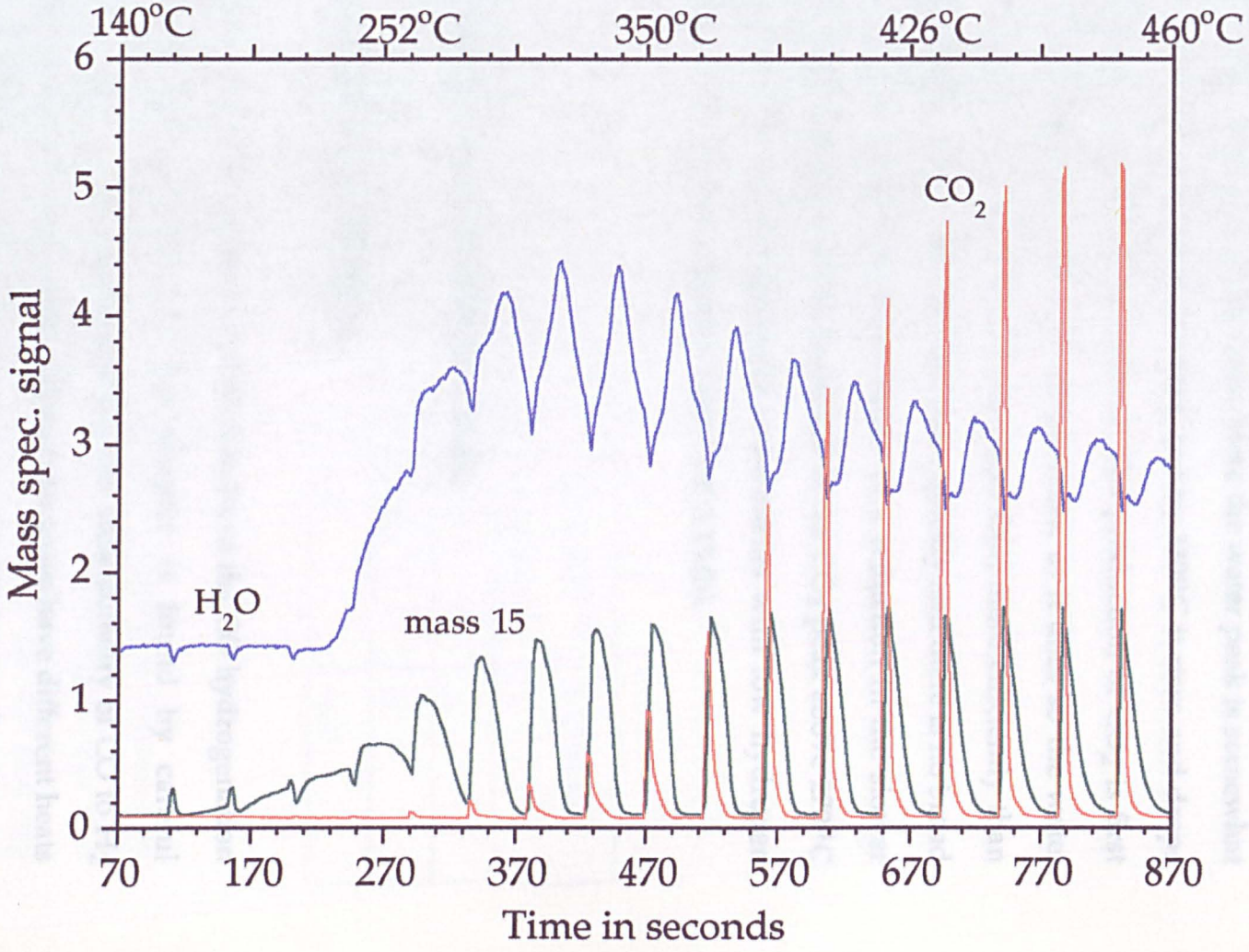

surprise especially as the H_2 is in abundant supply. It is perhaps indicative that the O(a) form a stable support species (a hydroxyl group) in a spillover mechanism that is hydrogenated at a higher temperatures. The sharp mass 18 peak seen near coincident with the CO peak between 270°C and 370°C in Figure 3.13.(b), can not be seen in this case. Here the water peak is somewhat lagged in comparison to the methane peak, but by 330°C it rises and drops quickly before the next pulse is introduced. The production of CO_2 is first seen at 290°C and rises linearly with temperature, as it does so the water production can be seen to drop as CO scavenges O(a) more efficiently than H(a). The CO_2 peaks drop to the base line more quickly and there is no broad rise in the base line, this may be indicative of a reduction in the slower secondary route to CO_2 causing the broad tail in the CO_2 peak above 270°C seen in the previous CO hydrogenation experiments with low hydrogen concentrations, see for instance Figures 3.8.(b) and 3.13.(b).

3.3. DISCUSSION of CO HYDROGENATION.

3.3.1. REACTION STOICHIOMETRY.

The key that holds together all of the results in the CO hydrogenation T.P.P.R. experiments reported in this chapter is found by careful consideration of the reactant stoichiometries. The stoichiometry of CO to H_2 changes with a change in temperature, because the gases have different heats of adsorption and therefore different desorption rates. Hydrogen desorbs at a faster rate than CO therefore as the temperature rises, its concentration on the surface of the catalyst, with respect to the CO concentration, declines.

At the onset of CO dissociation, at between 150°C-165°C, Figure, 3.13 (a) and (b), it is clear that only one reaction is taking place, that of wet methanation, as the only products detected are methane and water. The rate and yield of these products rise in a similar fashion, with fixed hydrogen flow rate, until they reach a maximum at ~320°C, Figure 3.16.(b). The rate at which water production declines at temperatures above 320°C is faster than that of methane, and as these two decline we see the emergence of a third product, carbon dioxide. If we take the integrals under the product peaks at the point where wet methanation is greatest - between 300°C and 320°C- and compare these to the corresponding integrals when CO_2 production is considerable, for instance at 412°C, the extent to which the reaction mechanism has change can be determined. This data is displayed in the table 3.2. below.

Table 3.2.

Product mass	Integral at T = 311°C	Integral at T = 412°C	% Change
15 (CH_4)	12.83	9.86	-23
18 (H_2O)	13.72	2.024	-42
44 (CO_2)	0.88	3.71	+422

In addition, to the data above, the consumption of hydrogen decreases by 48% and the conversion of CO increases by 21% between these two temperatures. Equations (3.3.1.) and (3.3.2.) below are the wet and dry methanation reactions. Equation (3.3.3.) illustrates the change from all wet methanation to 50% dry methanation keeping the CO conversion constant . The data clearly show that at 311°C wet methanation dominates where as at 412°C under these conditions, dry methanation is becoming dominant.

(3.3.1.) $CO + 3H_2$ ---------> $CH_4 + H_2O$

(3.3.2.) $CO + H_2$ ---------> $\frac{1}{2}CH_4 + \frac{1}{2}CO_2$

(3.3.3.) $CO + 2H_2$ ---------> $\frac{3}{4}CH_4 + \frac{1}{2}H_2O + \frac{1}{4}CO_2$

Figures 3.17. (a)-(d) show how keeping the temperature constant but varying the concentration of hydrogen results in a swich from dry methanation in hydrogen deficient gas mixtures to wet methanation in hydrogen rich reactant mixtures. Figure 3.18. is a bar chart which illustrates the trend more clearly. Take for example the 1.2 mls per minute H_2 flow rate, the reaction is almost entirely dry methanation with very little water production. With an increase in H_2 flow rate to 5 mls per minute there is a 32% increase in the production of methane, coupled with a 32% decrease in the production of CO_2 . From equation (3.3.1.) and (3.3.2.) above, a four fold increase in the hydrogen concentration should determine that the reaction swings in favour of wet methanation. However, as mentioned previously, the concentration of reactants in the gas stream is different to that on the catalyst surface and as the rate of hydrogen desorption is faster than the rate of CO desorption at high temperatures, a higher concentration of H_2 in the gas stream is required to alter the ratios of reactants on the catalyst surface.

3.3.2. CO_2 PRODUCTION.

Figure 3.20. shows an expanded T.P.P.R. experiment identical to Figure 3.13.(a) and (b). The initial reaction sequence of CO and H_2 can be clearly deciphered. Below ~260°C, very little evidence for the production of CO_2 is seen. Once carbon dioxide is produced it is clear that the reaction has by far the fastest rate, as the production can be seen to rise with the CO input pulse. Indeed in some cases (though not apparent here) CO_2 has been detected

Figure 3.20.
T.P.P.R. - Expanded view.
CO:H_2 = 1:2 He=40 mls/min

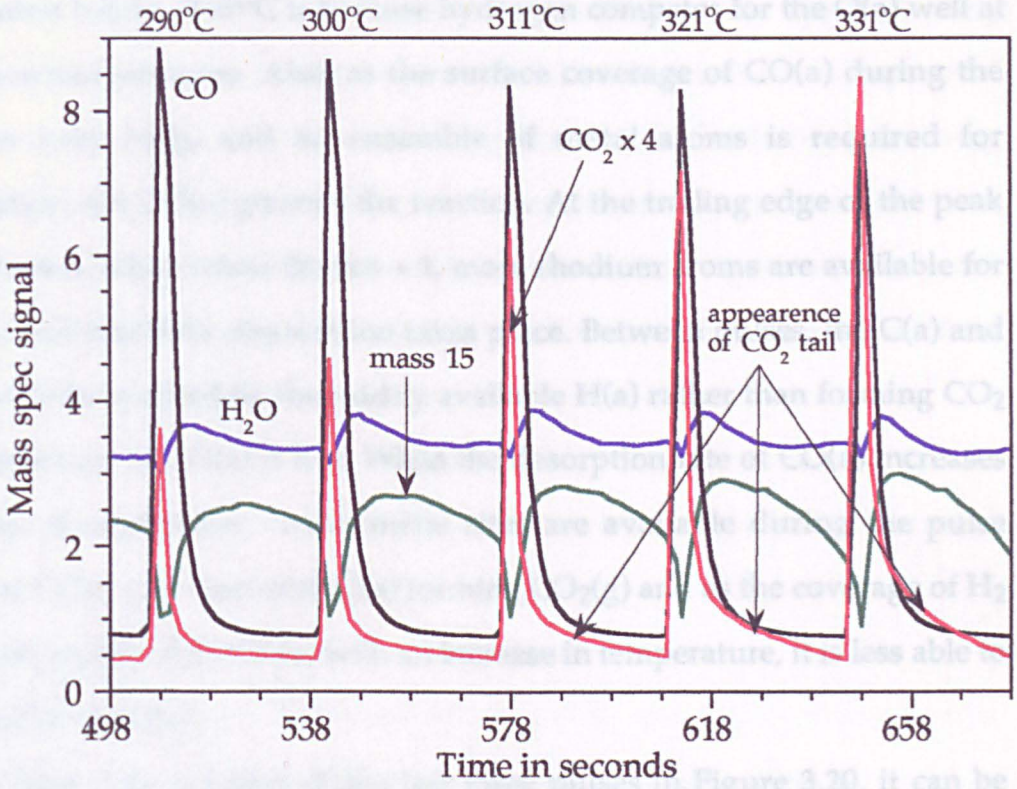

fractionally before any mass 28 is seen, indicating that the front end of the CO pulse reacts to form CO_2. In addition the width at half maximum height of the CO_2 pulse is slightly narrower than the corresponding CO pulse width, which is indicative of the faster desorption rate of CO_2. Clearly CO dissociation is occurring below the onset of CO_2 as methane and water are seen. The reason why CO_2 is not produced immediately upon CO dissociation below ~260°C is because hydrogen competes for the O(a) well at the lower temperatures. Also, as the surface coverage of CO(a) during the pulse is very high, and an ensemble of metal atoms is required for dissociation, the CO(a) poisons the reaction. At the trailing edge of the peak and between pulses when the $\theta_{CO} \ll 1$, more rhodium atoms are available for reaction and therefore dissociation takes place. Between pulses, the C(a) and O(a) are hydrogenated by the readily available H(a) rather than forming CO_2 as the coverage of CO(a) is low. When the desorption rate of CO(a) increases at higher temperatures, more metal sites are available during the pulse therefore CO(a) can react with O(a) forming $CO_2(g)$ and as the coverage of H_2 falls more rapidly than CO(a) with an increase in temperature, it is less able to compete for the O(a).

Upon close scrutiny of the last three pulses in Figure 3.20. it can be seen that there is more than one route to CO_2 taking place. Evident is the fast route producing the sharp and dominant initial peak (as seen exclusively in the first CO_2 peak) and in addition a slower route producing the obvious tail to the last three peaks is seen. The fast route to CO_2 has been ascribed to the Boudourd reaction, as noted above and in section 3.2.2. on CO oxidation. The mechanism of the slower route to CO_2 is not as easy to pinpoint. If CO_2 was formed via the water gas shift reaction, then there should be a comparable drop in the mass 18 signal near coincident with the rise in CO_2 (although somewhat lagged due to chromatographic effects) . This is not evident in the data - the slight drop in the water peak is also seen at temperatures below

that where CO_2 production occurs, and is therefore most likely to be due to temporary CO(a) site blockage preventing hydrogen getting to the surface. The molecular heat of adsorption of CO on Rh is higher than that of H_2 therefore as the CO passes across the catalyst it covers the Rh surface and in so doing reduces the surface coverage of hydrogen. A second reason to doubt the water gas shift reaction in this case becomes obvious upon consideration of the surface life time of a CO(a) molecule. This can be approximately calculated by using the Frenkel equation, 3.3.5. The heat of adsorption of molecular CO on Rh catalysts is essentially the same as the desorption energy since adsorption is non-activated, the desorption energy is measured to be between 100 - 130 $kJmol^{-1}$ for single crystals as well as supported catalysts[1]. In the calculation below, the enthalpy of chemisorption was taken to be 120$kJmol^{-1}$ as an average value.

$$\tau = \tau_0 \, e^{(\Delta H/RT)} \qquad 3.3.5.$$

τ = Life time on surface.

$\tau_0 = 10^{-13}$ seconds.

ΔH = 120$kJmol^{-1}$ (Enthalpy of chemisorption.)

R = Gas constant

T = Temperature of surface.

At 300°C the life time of a CO molecule was found to be in the order of ~ 3×10^{-2} seconds, clearly, once the CO pulse has passed through the bed, there is very little CO(a) left on the surface. There should certainly be none present after a few seconds, however by way of the tail, we can see that CO_2 is produced. Fujimoto[23], when looking at the same reaction on alumina supported rhodium, concluded that between 100-200°C any CO_2 production was via the water gas shift reaction but above 300°C the Boudouard reaction

dominated the production. The present work agrees with the latter half of this conclusion, as for the water-gas shift, no evidence was found for it.

When CO hydrogenation was performed over a blank catalyst (1:4 γAl_2O_3 : αAl_2O_3 by weight) Figure 3.21.(a) and (b), the similar trends in CO_2 production were seen, in that sharp peaks appeared with the CO input pulse followed by a tail, it must be noted however that the amount of CO_2 produced over the support was minuscule compared to that over the supported rhodium catalyst - this is evident when one compares the units on the y-axis (mass spectrometer signal (V)). In Figure 3.21.(b) one can see that between ~310°C and 420°C there is a rise in the mass 44 base line and a broadening at the tail of the CO_2 peak. The background rise visible in this expanded plot is also seen in the T.P.P.R. over the rhodium catalyst with no H_2 flowing - see Figure 3.8.(a), and is most likely to be caused by the decomposition of a support species, evidently one that does not exclusively require rhodium for its formation or decomposition. As there is very little product formation on blank alumina it is clear that the rhodium plays by far the most important part in the production of all the species.

It is known that many surface species can exist on an alumina supported Rh surface under synthesis gas conditions (see Chapter 4 section 4.1.). Some reside on the metal component, other species migrate to the support and remain in high concentrations as spectators. From the literature[49] it is known that at 220°C the most concentrated surface species under a continuous flow of CO/H_2 on the rhodium is linearly bonded CO(a). Formate and carbonate groups are produced under CO/H_2 conditions over Rh/Al_2O_3 catalysts and they reside on the support where their coverage builds up with time. In addition methoxy groups have been reported to form on the support through a spillover process in syngas reactions over Pt/Al_2O_3 catalysts[73].

Figure 3.21.(a)
T.P.P.R. showing CO pulses and CO_2 production over a blank alumina catalyst.

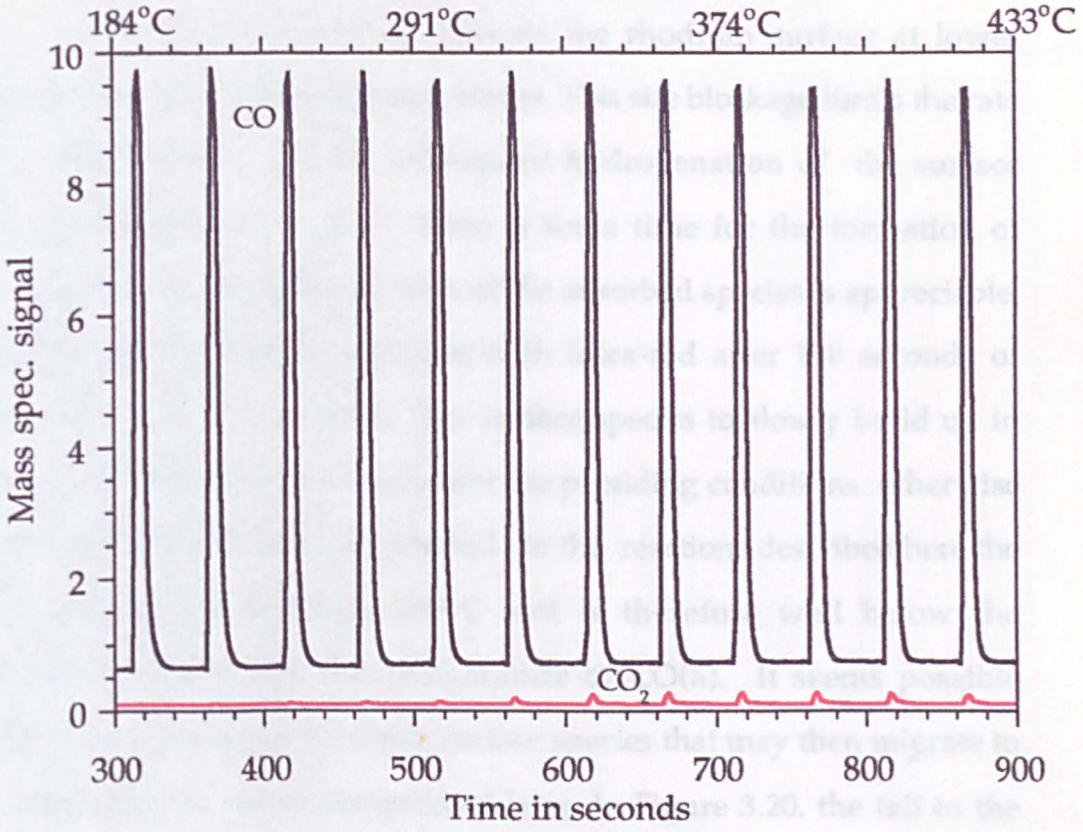

Figure 3.21. (b)
Expanded T.P.P.R. showing CO_2 (x4) production over a blank alumina catalyst

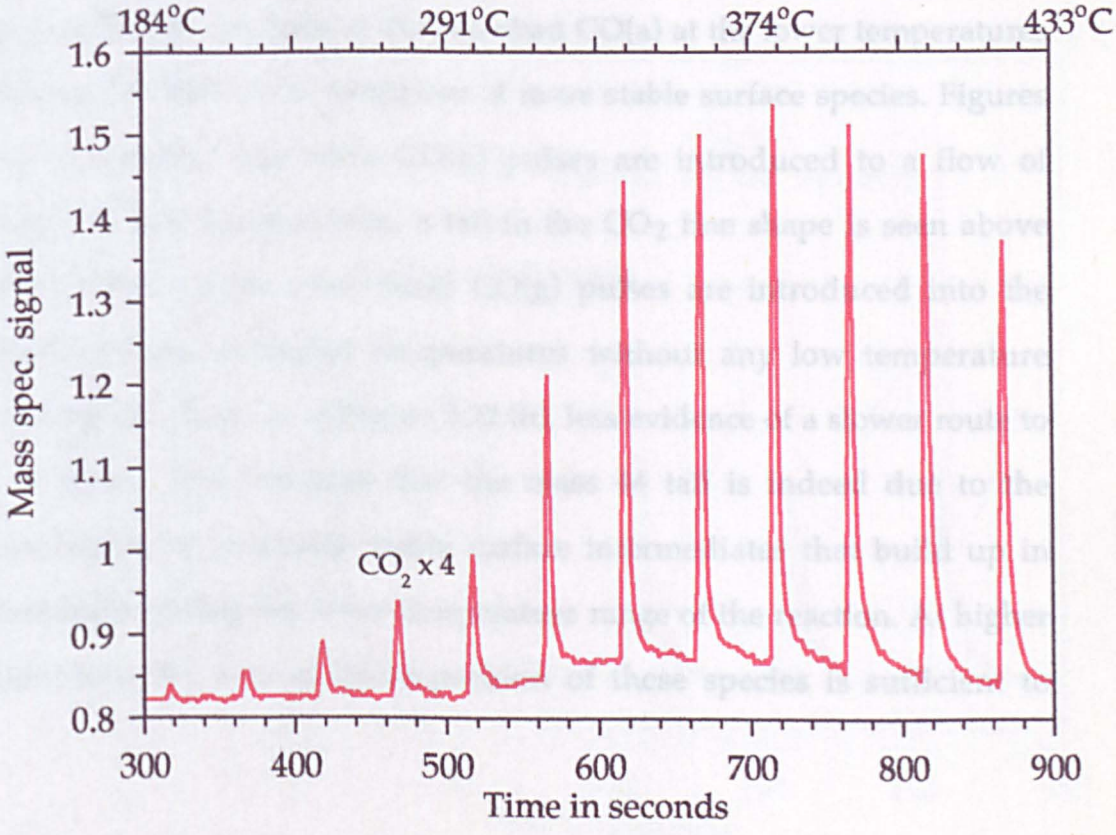

In the experiments presented here, the population of CO(a) on the catalyst is such that it effectively poisons the rhodium surface at lower temperatures as very little desorption occurs. This site blockage limits the rate of CO(a) dissociation and the subsequent hydrogenation of the surface oxygen and carbon. As a result there is some time for the formation of surface species to occur as the life time of the adsorbed species is appreciable. Efstathiou et al.[49] observed formates with infra-red after 120 seconds of CO/H_2 continuous flow at 220°C. For surface species to slowly build up in concentration, they must be stable under the presiding conditions otherwise they will desorb or will be hydrogenated . In the reactions described here the starting temperature is below 120°C and is therefore well below the desorption and hydrogenation temperature of CO(a). It seems possible therefore to have formation of stable surface species that may then migrate to the support and are only hydrogenated later. In Figure 3.20. the tail to the CO_2 peak doesn't manifest itself until approximately 8-9 minutes after the first pulse of CO passed across the catalyst and at a temperature of ~320°C, this corresponds to a total reactant mass flow of 8 mls of CO and 16mls of H_2. It appears that the life-time of the adsorbed CO(a) at the lower temperatures is sufficient to lead to the formation of more stable surface species. Figures 3.22.(a) illustrates that when CO(g) pulses are introduced to a flow of hydrogen at low temperatures, a tail in the CO_2 line shape is seen above ~330°C. When on the other hand CO(g) pulses are introduced into the hydrogen stream at higher temperatures without any low temperature reaction taking place , as in Figure 3.22.(b), less evidence of a slower route to CO_2 is seen. This indicates that the mass 44 tail is indeed due to the decomposition of relatively stable surface intermediates that build up in concentration during the lower temperature range of the reaction. At higher temperatures the rate of decomposition of these species is sufficient to

Figure 3.22.(a)

T.P.P.R. CO : H_2 = 1:1 Starting temp. = 35°C

Showing evolution of CO_2 tail

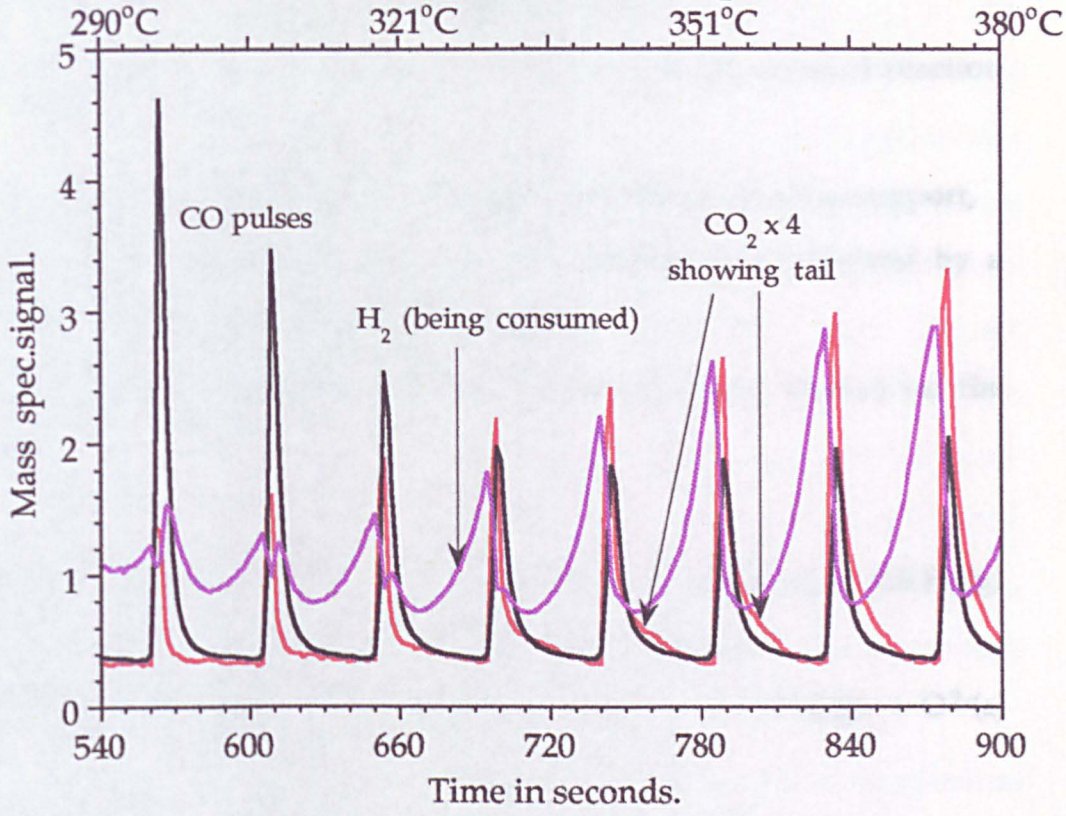

Figure 3.22.(b).

T.P.P.R. CO : H_2 = 1:1 Starting Temp. = 360°C

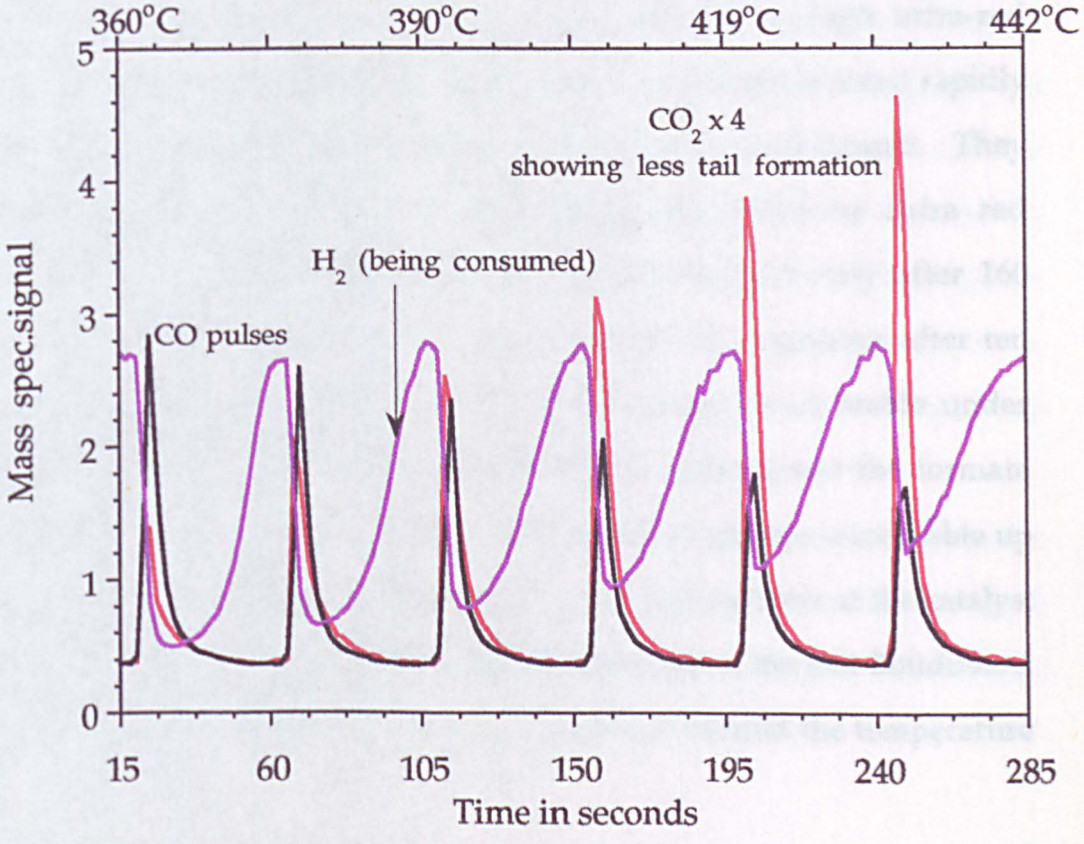

suppress their build up. What is more with an increase in hydrogen concentration there is a decrease in the size if the tail.

Three possible routes to CO_2 other than via the Boudouard reaction are;

(a) via the decomposition of fomate groups located on the alumina support,

(b) via the slow recombination of C(a) and O(a) groups followed by a subsequent oxidation step on the rhodium metal,

(c) via the formation and decomposition of a carbonate located on the support.

[a] $CO(a) + OH(a) \text{-----} > [X] \text{------} > HCOO(a) \text{---------} > CO_2(g) + 0.5\, H_2(g)$

[b] $C(a) + O(a) \text{---------} > CO(a) + O(a) \text{---------} > CO_2(g)$

[c] $COOH(a) + OH(a) \text{---------} > CO_3^{2-}(a) + H_2 \text{---------} > CO_2(g) + O^{2-}(a)$

Where [X] is a transient intermediate, formed via an activated CO spillover process from the rhodium onto the alumina where the hydroxyl groups reside.

In a recent paper[49], Efstathiou et al. showed through infra-red spectroscopy that most of these surface species can be hydrogenated rapidly and in the absence of hydrogen they can decompose and desorb. They showed that formate and carbonate groups, detectable by infra red spectroscopy on the alumina surface, were first detected only after 160 seconds of reaction at 220°C and only in appreciable quantities after ten minutes under continuous CO/H_2 flow. These groups were stable under hydrogen at 220°C, the temperature required to hydrogenate the formate groups was found to be 270°C - 365°C. The carbonate groups were stable up to slightly higher temperatures -365-450°C. As a pulse arrives at the catalyst bed at temperatures above ~250°C, the initial reaction is the fast Bouduoard reaction, then the broad CO_2 tail becomes evident at around the temperature

that formate groups are expected to decompose ~ 300°C therefore the formate group is the most likely species responsible for tail to the CO_2 peak. An explanation for the tail rather than a broad rise in the base line is to assume that formates are formed most rapidly during the pulse, this is reasonable as the concentration of adsorbed species is at its highest. At lower temperatures (less than ~300°C) however they have a sufficient life-time to migrate and remain on the support and it is envisages that they decompose and are hydrogenated by migrating to the rhodium. In the absence of rhodium, but with hydrogen flowing, the surface species occupying the support decompose causing the broad background rise in mass 44, seen clearly in Figure 3.21.(b). In the presence of rhodium but in the absence of hydrogen, the same broad decomposition is seen, therefore rhodium acts as a centre through which hydrogen reacts with the surface species.

Another possible mechanism to be considered is the sequential oxidation of C(a) - scheme [b] above. The production of methane continues until the following CO(g) pulse is introduced so clearly CHx(a) is an abundant surface species. As water is continuously being produced then likewise O(a) or OH(a) are present also. It is likely that at higher temperatures, where CO dissociation is easier, recombination will take place many times over the contact time in the bed. This ensures that a CO molecule can effectively sample the catalyst, increasing the chance of reacting with an O(a) or an OH group to form the CO_2. It is known that O(a) burrows into rhodium at a fast rate and so the second oxidation step is expected to be slow, and may be the cause of the tail. This scenario however seems somewhat unlikely as the same trends were seen on the blank catalyst.

The rate of carbonate build up is slower than that for formates and is thought to occur exclusively on the support (Solymosi). Carbonate formation / decomposition could therefore contribute to both the back-ground CO_2 rise

and the broadening of the CO_2 peak following the CO pulse however, Bennet reports the temperature of carbonate decomposition to be 380°C and above.

The most probable mechanism outlined above is the formation of formate groups that reside on the support and decompose between 310°C and 420°C, although the other mechanisms may occur to some degree. The dominant pathway to CO_2 is via the Boudouard reaction. In the absence of rhodium the CO_2 production is greatly reduced as CO dissociation is negligible, however support species do contribute to the broadening of the CO_2 peaks in the 310°C-420°C temperature range.

3.3.3. CH_4 PRODUCTION.

In Figure 3.20. methane is still being produced as each subsequent CO pulse comes in. Its level drops as the CO peak passes across the catalyst. This is due to a drop in the surface coverage of H_2 brought about by the higher heat of adsorption of CO on rhodium compared to H_2. The first sign of methane production from the CO input pulse can be seen after 3-4 seconds. The time delay is due to the rate of hydrogenation and the availability of hydrogen. As soon as the surface coverage of H_2 begins to increase with the desorption/reaction of the CO(a) after each pulse, hydrogenation of both C(a) and O(a) begins and as the temperature rises the rate of hydrogenation increases.

From the line shapes of the methane peaks in Figure 3.17.(a). and (b)., it appears that two routes to methane are occurring. A fast route that is manifest as the sharp peak, rising to a peak maximum approximately three seconds after the CO input peak maximum. The slower route is seen as a broad shoulder lagging after the initial peak. The methane tail shortens considerably as the flow rate of hydrogen is increased and is barely noticeable when the 5

mls per minute of H_2 is flowing - Figure 3.17.(c). The fast route can be ascribed to the reaction between incoming CO molecules and hydrogen atoms present at the metal surface. As its rate of formation (the time it appears after the CO input pulse) does not change with the different hydrogen concentrations, its rate of formation is not dependent on hydrogen availability, rather it is dependent on CO availability. The rate of hydrogenation in Figure 3.17.(d) is fast enough to ensure that methane is produced before the CO molecules self poison the surface through site blockage. In Figure 3.17. (a) and (b) the surface coverage of hydrogen is relatively very low during the pulse and only as the CO molecules desorb as CO(g) or react and desorb as either CO_2 or CH_4 , do more surface sites become available for H_2 to dissociate and hydrogenate the surface carbon, giving rise to the slower methane peak. When the hydrogen concentration is high more methane and water is produced, indicative of the switch from dry methanation towards wet methanation.

At this temperature (440°C), the hydrogenation of oxygen surface species to form water is a slow reaction, as can be seen from the mass 18 signal appearing as a very lagged broad peak. Also interesting to note is that water is only seen after the methane peak. The rate of methanation ensures that water production is not seen until all the C(a) has been hydrogenated, it appears therefore that hydrogen prefers to scavenge C(a) faster than it does O(a). It should be noted that at low hydrogen concentrations O(a) is scarce after the predominant CO_2 formation, but with an increase in hydrogen concentration, there is a decrease in CO_2 formation and a swing in favour of wet methanation. As the water peak is so lagged it is apparent that the activation barrier for water formation is higher than of methane formation and even though thermodynamically the two products are similarly favoured, the surface life-time of the H(a) species is such that the formation of methane is kinetically favoured over water.

These experiments illustrate accurately and in detail, the processes occurring when CO and H_2 react under various conditions over a supported rhodium catalyst. It is clear that under the transient conditions employed here, very little of the CO converted (less than 1%) forms C_2^+ hydrocarbons. No oxygenate formation was seen under these conditions. This is not surprising as no reducible oxide promoter is present and the pressure was ambient throughout. It is concluded that for the coupling of CHx(a) to occur there has to be;

(i) a high density of surface carbon species, and

(ii) a relatively long surface life-time for the surface species.

In the experiments presented here the conditions were such that methane carbon dioxide and water were the only products. The main mechanistic steps that lead to these products are concluded to be as follows:-

$$CO(g) \text{ <-----> } CO(a)$$

$$CO(a) \text{ <-----> } C(a) + O(a)$$

$$H_2(g) \text{ <-----> } 2H(a)$$

$$C(a) + H(a) \text{ <-----> } CH(a) \text{ <-----> } CH_2(a) \text{ <-----> } CH_3(a) \text{ <-----> } CH_4(g)$$

$$CO(a) + O(a) \text{ <-----> } CO_2(g)$$

$$O(a) + 2H(a) \text{ <-----> } OH(a) + H(a) \text{ <-----> } H_2O(g)$$

In addition to these steps, minor routes leading to the same products occur due to the presence of the alumina support, these are as follows:-

$$CO(a) + OH^- \text{ <-----> } HCOO^-(a)$$

$$HCOO(a) \text{ <-----> } CO_2 + {}^1/_2 H_2$$

$$HCOO(a) + 7H(a) \text{ <-----> } CH_4(g) + 2H_2O(g)$$

$$CO_2 + O^{2-} \text{ <-----> } CO_3^{2-}$$

3.4. CO_2 HYDROGENATION : RESULTS AND DISCUSSION.

As can be seen from comparing Figure 3.23.(a) and Figure 3.23. (b), the line shapes for both methane and water from CO_2 hydrogenation, are more simple than those seen in CO hydrogenation. The line shapes of both products in CO_2 hydrogenation change relatively little from 250°C onwards. This indicates that the reaction mechanism likewise is not changing and that there are no competitive reactions occurring. The rate of reaction changes and the yield of both methane and water increases upon heating, up to approximately 310°C above which there is little change in the total yield of water and methane.

The onset of methane production is seen starting very slowly at 160°C-165°C, a comparable temperature to the on-set of methanation of CO - see Figure 3.13.(b) and 3.23.(b). The production of methane rises dramatically up to ~310°C, then above this temperature, under these T.P.P.R. conditions, the rate of methanation begins to fall. The integral of the methane peak at it's maximum rate of production, between 310-320°C, is 15% more than the integral of the peak arising from hydrogenation at 390-400°C over a time interval of 40 seconds, this is not due to less CO_2 dissociation at higher temperature . Below 300°C the rate of methanation is insufficient to clear the surface of CHx(a) species, as evidenced by the continuing methane production at the time the subsequent CO_2 pulse comes in. However above this temperature and upto approximately 390°C under these conditions the surface is cleaned of carbon in between pulses, note that at this temperature the methane peak is down to its base line before the following CO_2 pulse is introduced. As the temperature rises further, the concentration of hydrogen on the surface of the catalyst continues to decrease due to faster desorption and is insufficient to hydrogenate away all of the CHx(a) between pulses as shown more clearly in Figure 3.24.

Figure 3.23. (a)
T.P.P.R. 0.5 ml CO_2 pulses into flowing H_2.
$CO_2 : H_2 = 1 : 1.8$

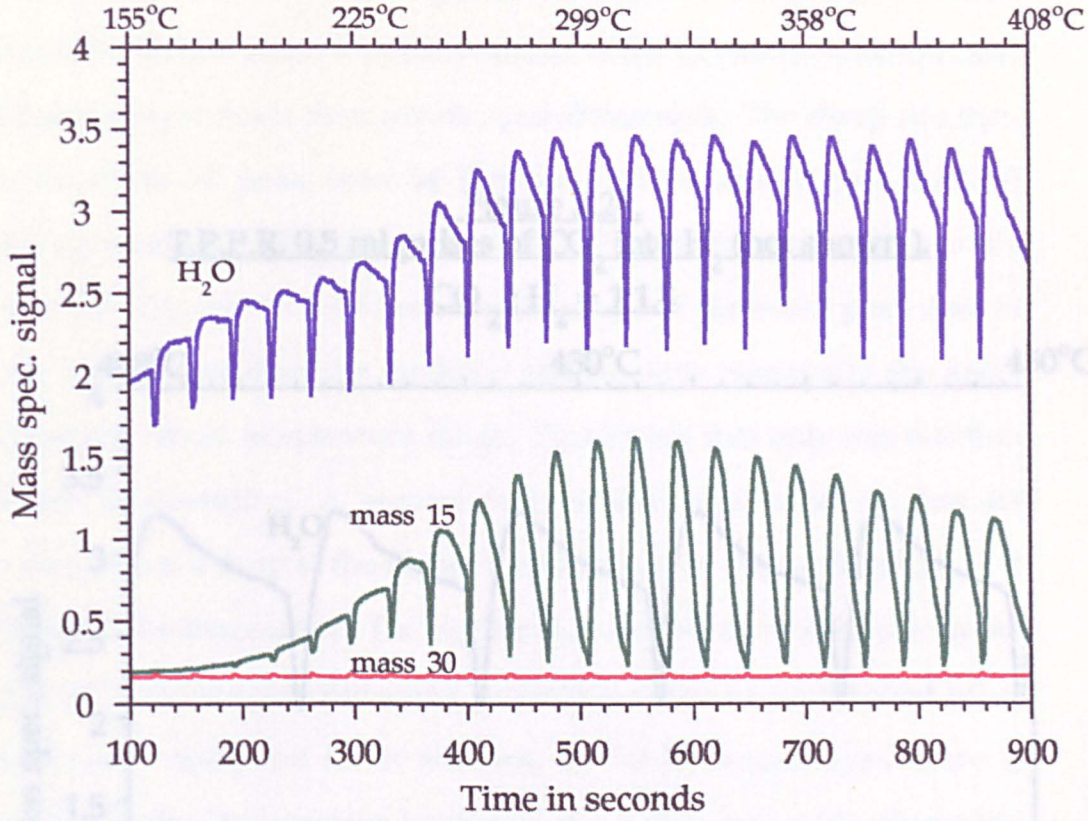

Figure 3.23. (b)
T.P.P.R. 0.5 ml CO pulses into flowing H_2.
$CO : H_2 = 1 : 1.8$

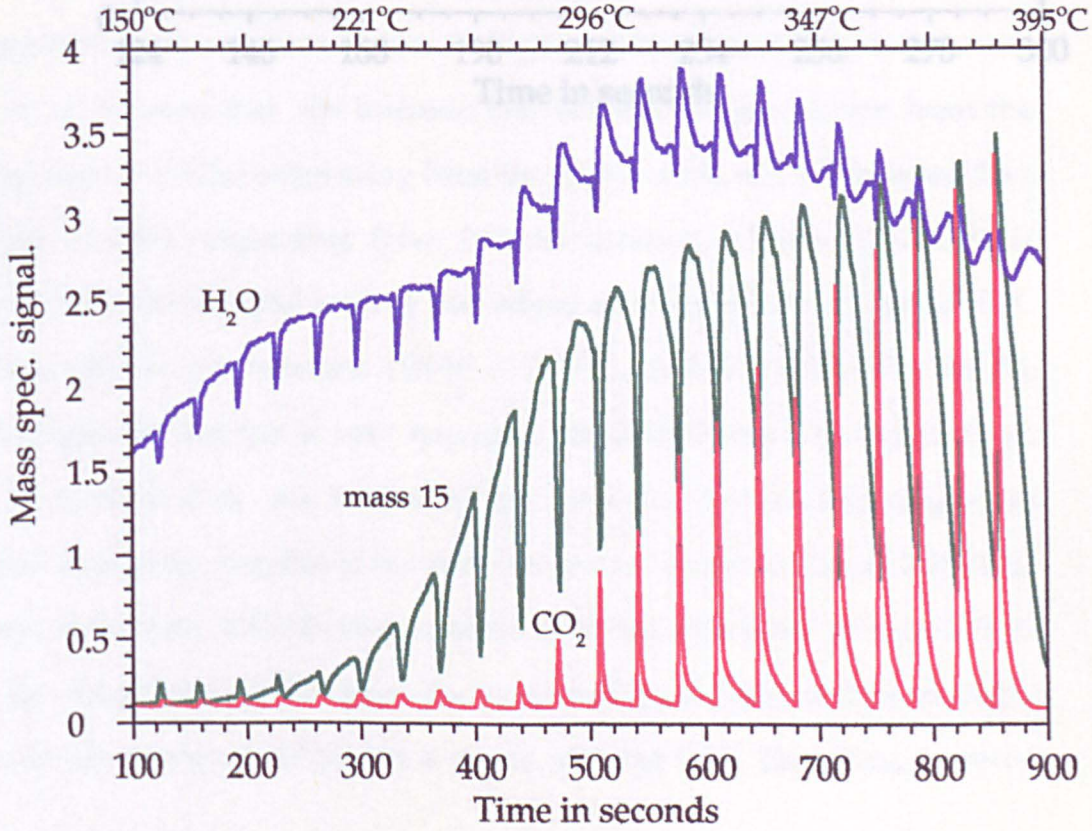

Figure 3.24.

T.P.P.R. 0.5 ml pulses of CO_2 into H_2 (not shown).

$CO_2 : H_2 = 1:1.8$

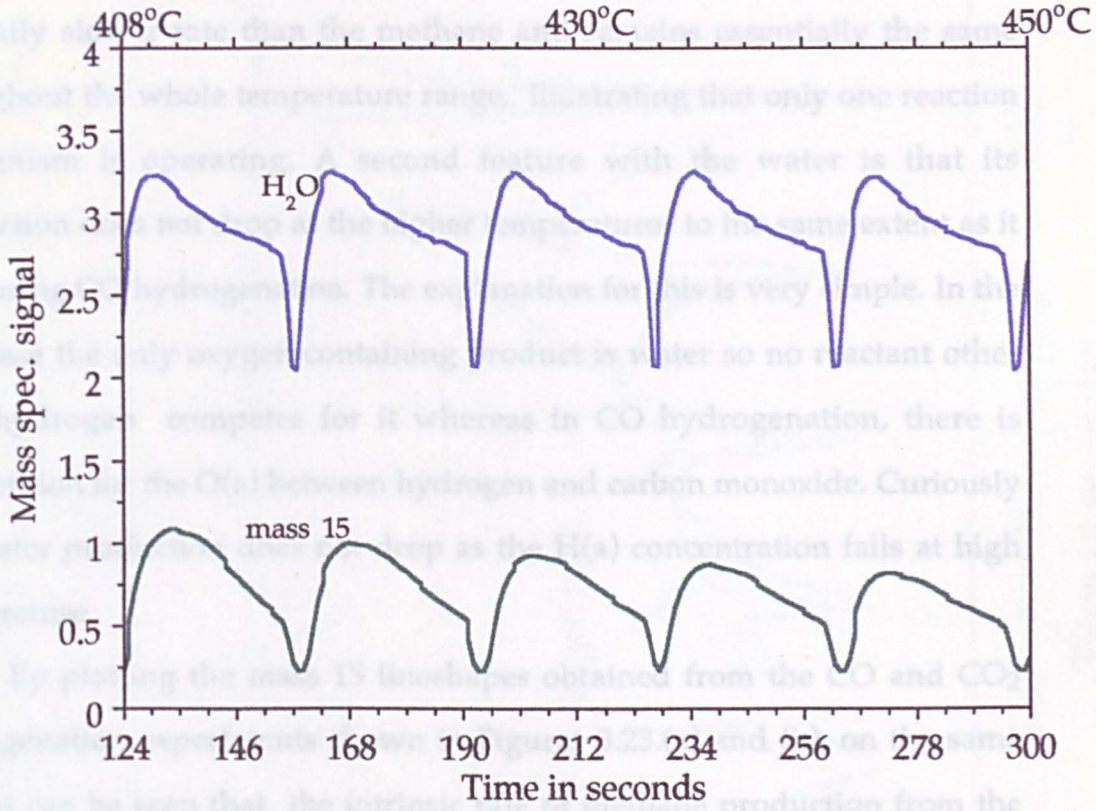

The production of water begins at around 150°C, somewhat earlier than with CO . Its line shape is initially similar to the CO hydrogenation case, but at higher temperatures there are obvious differences. The sharp rise then fall in the mass 18 peak seen in Figures 3.13.(b) and Figure 3.23.(b) immediately after each CO pulse in the 250-350°C temperature range is not present in the CO_2 case. We see here that the shape of the water peak rises at a slightly slower rate than the methane and remains essentially the same throughout the whole temperature range, illustrating that only one reaction mechanism is operating. A second feature with the water is that its production does not drop at the higher temperatures to the same extent as it did during CO hydrogenation. The explanation for this is very simple. In the CO_2 case the only oxygen containing product is water so no reactant other than hydrogen competes for it whereas in CO hydrogenation, there is competition for the O(a) between hydrogen and carbon monoxide. Curiously the water production does not drop as the H(a) concentration falls at high temperature.

By plotting the mass 15 lineshapes obtained from the CO and CO_2 hydrogenation experiments shown in Figures 3.23.(a) and (b), on the same page it can be seen that the intrinsic rate of methane production from the hydrogenation of C(a) originating from the dissociation of CO_2 is faster than the rate of C(a) originating from CO dissociation, Figure 3.25. This is evidenced by the sharper leading line edges after each pulse . The T.P.P.R. reactions shown are between 195°C - 280°C, and the difference in the methane production rate is very apparent. By 260°C however, the intrinsic rates of methanation are very similar - note that the leading edges are practically superimposeable in the final two pulses shown in Figure 3.25. This increase in the rate of CO hydrogenation coincides, as we saw in section 3.3., with the desorption of CO from the surface (Figure 3.15) and in so doing opens up the surface to H(a) which reacts with the C(a). Therefore, it would

Figure 3.25.
A comparison between the rates of methanation of CO versus CO_2, with CO (& CO_2) : H_2 ratio = 1 :1.8

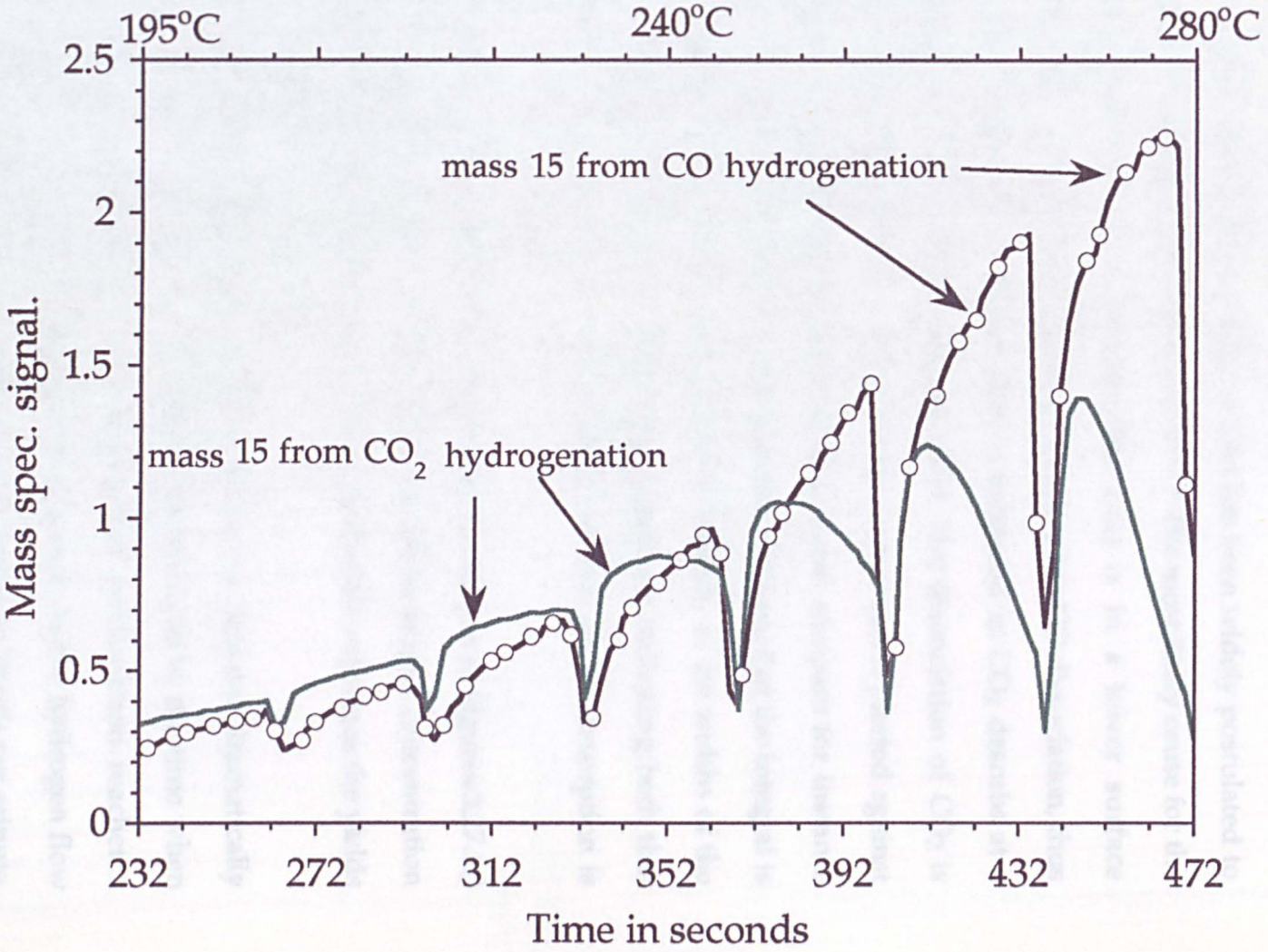

seem that CO(a) below ~260°C poisons the catalyst surface and it is only when it desorbs rapidly, above this temperature, that hydrogen is able to compete for surface sites and react efficiently. The adsorbed carbon from CO_2 dissociation is unlikely to be in a more reactive form than that from CO dissociation as the dissociation of CO_2 to C(a) has been widely postulated to pass through an adsorbed CO(a) species[32,69,72,74] The most likely cause for the faster hydrogenation rate is because the C(a) is in a lower surface concentration due to less CO_2 dissociation compared to CO dissociation, thus the hydrogen to C(a) ratio is higher, this is enhanced as CO_2 desorbs at a lower temperature than CO (see Figure 3.30.). The dissociation of CO_2 is clearly seen to be less than that of CO when the conversion is plotted against temperature, with the hydrogen concentration equal, compare for instance Figures 3.26.(a) and (b). It should be noted in these figures that the integral is difficult to gauge visually by judging the peak heights, as the widths of the peaks vary (they are narrower at higher temperatures, indicating both that the front end of the pulse reacts more readily and the rate of desorption is faster).

A series of isothermal pulsed experiments are shown in Figures 3.27.(a) -(c). The experiments show the effect of varying the hydrogen concentration on the product yield and rates of production. Figure 3.28. expresses the yields more clearly in a bar chart format.

The rate of both methane and water formation increases dramatically with an increase of hydrogen concentration. Taking t_o to be the time when CO_2 is first seen and t_{max} to be the time when methanation reaches a maximum, the rates of methanation can be compared. As the hydrogen flow rate is increased from 1.2 mls per minute to 5 mls and then 20 mls per minute, the t_{max} falls in the order 15 seconds/6.5 seconds /4 seconds , so in effect the rate of methanation roughly doubles with a quadrupling of the H_2 concentration under these experimental conditions. The rate of water

Figure 3.26.(a)

T.P.P.R. $CO_2 : H_2 = 1 : 1.8$ CO_2

Showing an 8% increase in CO conversion from 160°C to 395°C.

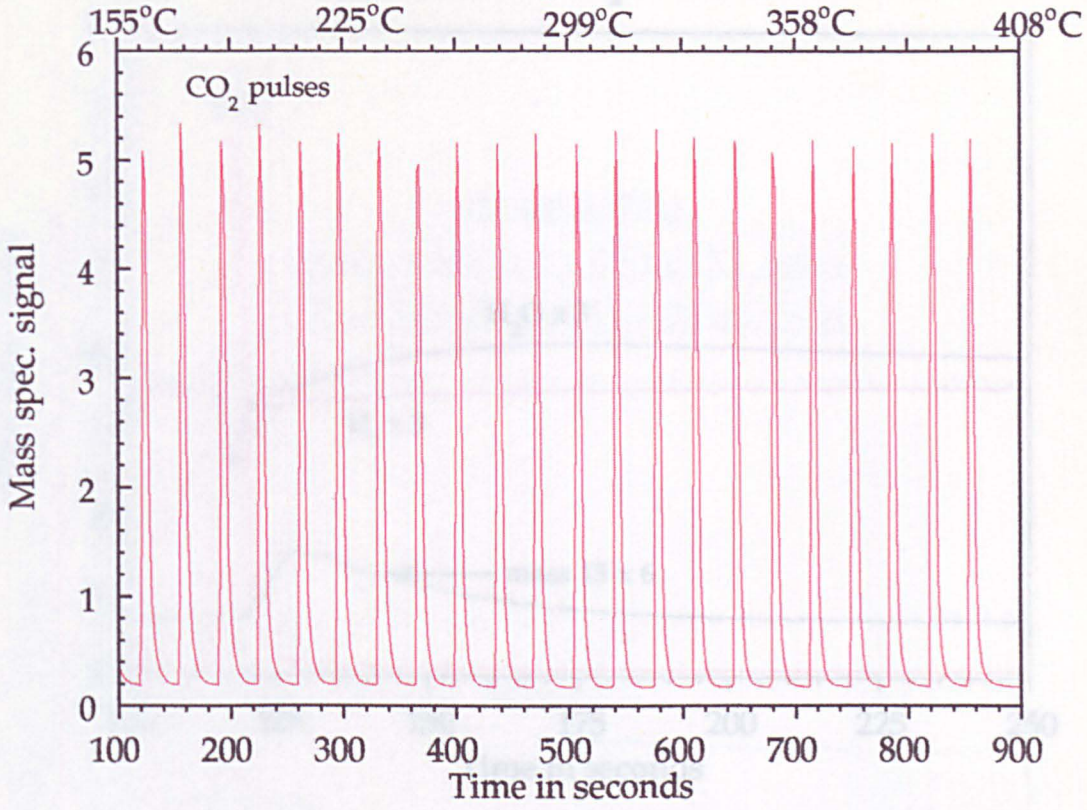

Figure 3.26.(b)

T.P.P.R. $CO : H_2 = 1 : 1.8$

showing a 45% increase in CO conversion from 160°C to 395°C.

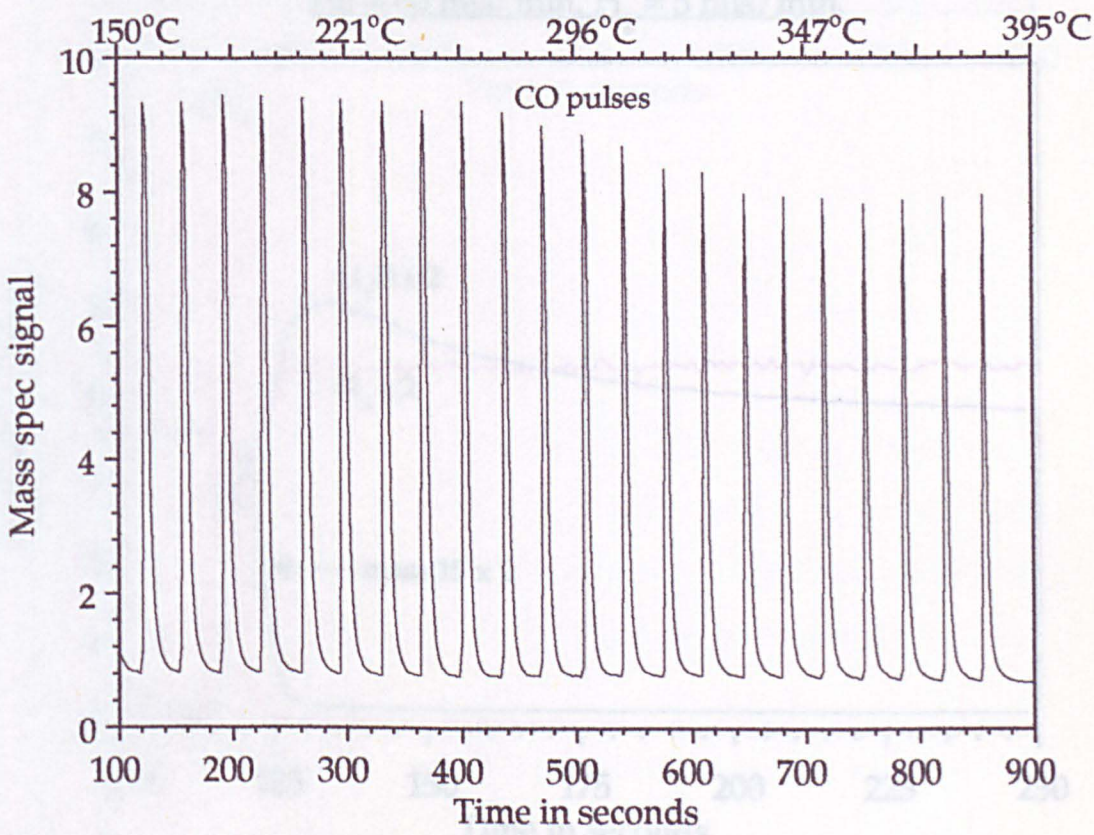

Figure 3.27.(a)

Temp. = 440°C. 1 x 0.5 ml CO_2 pulse.

He = 60 mls/min. H_2 = 1.2 mls/min.

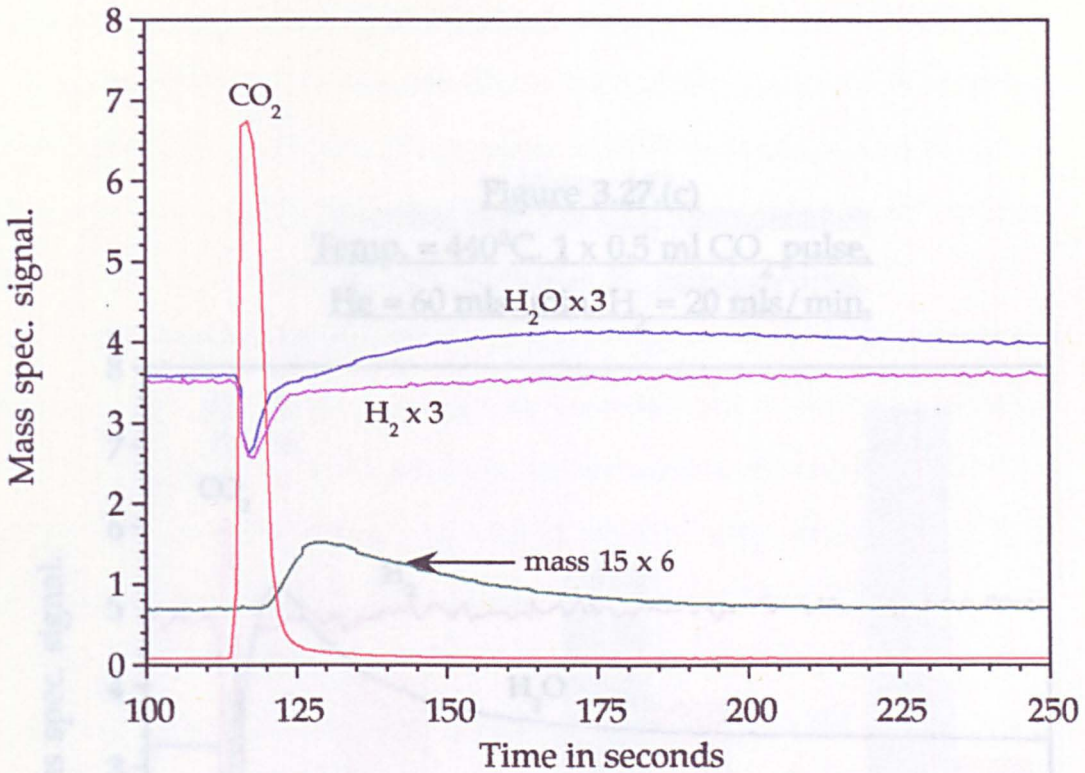

Figure 3.27.(b)

Temp. = 440°C. 1 x 0.5 ml CO_2 pulse.

He = 60 mls/min. H_2 = 5 mls/min.

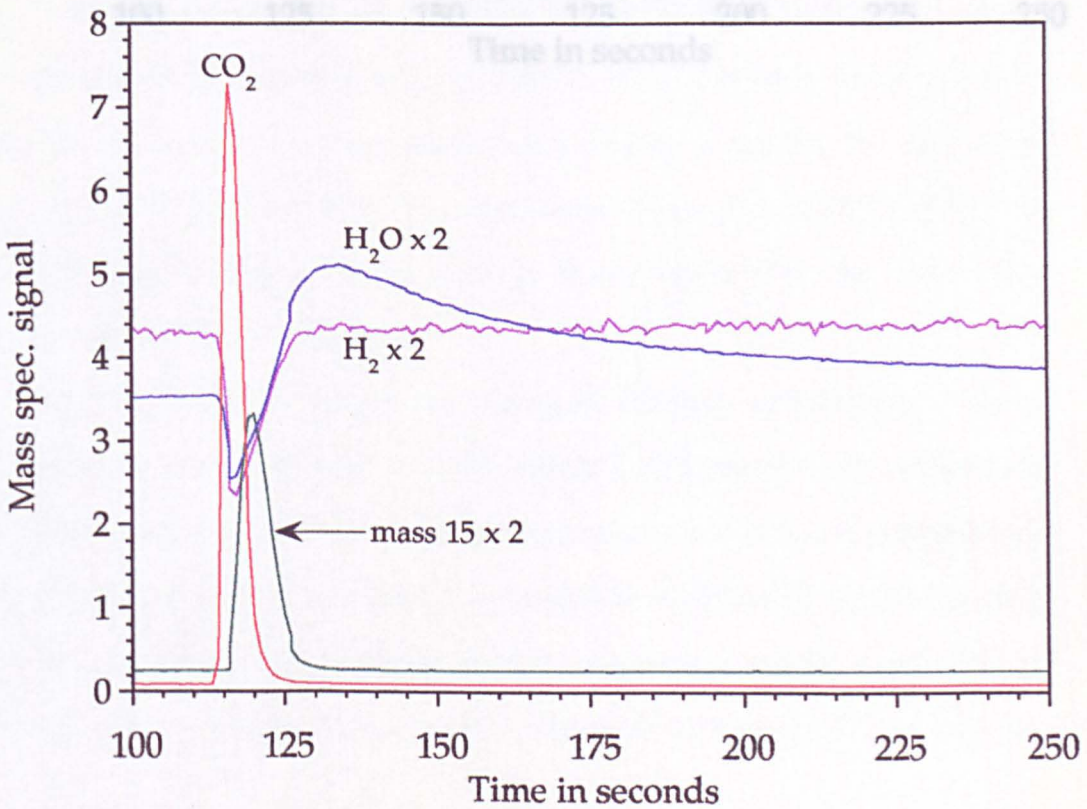

Figure 3.27.(c)

Temp. = 440°C. 1 x 0.5 ml CO_2 pulse.

He = 60 mls/min. H_2 = 20 mls/min.

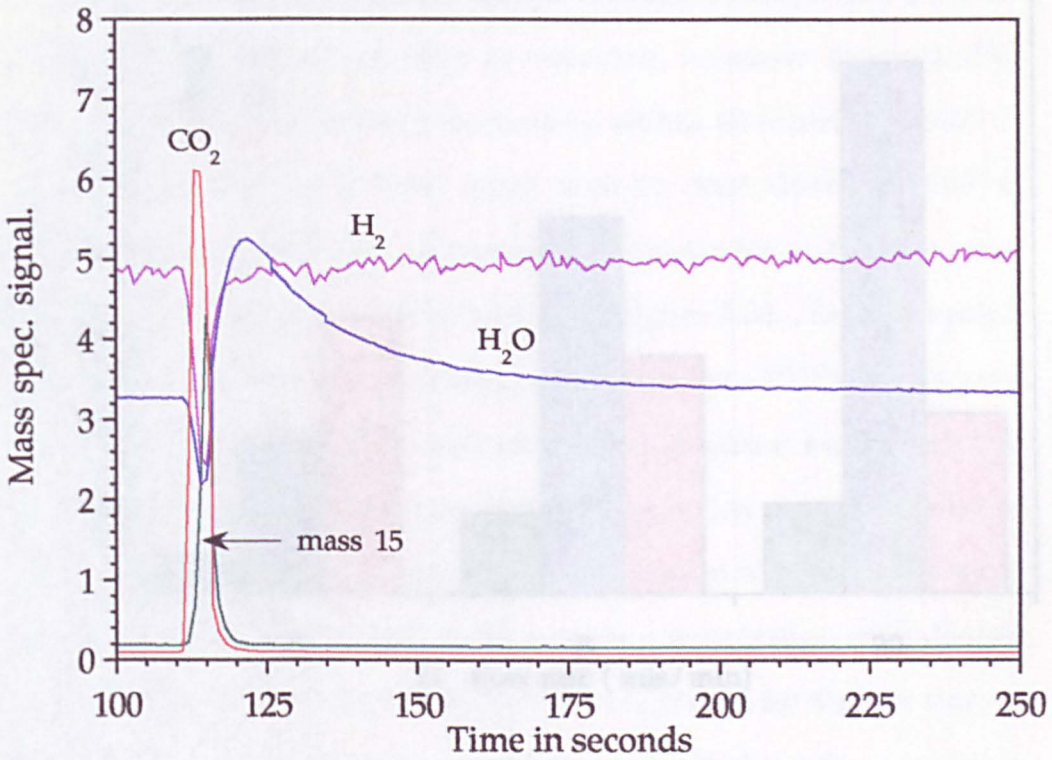

Figure 3.28.
Showing trends in CO_2 hydrogenation
at 440°C with high H_2 concentrations.

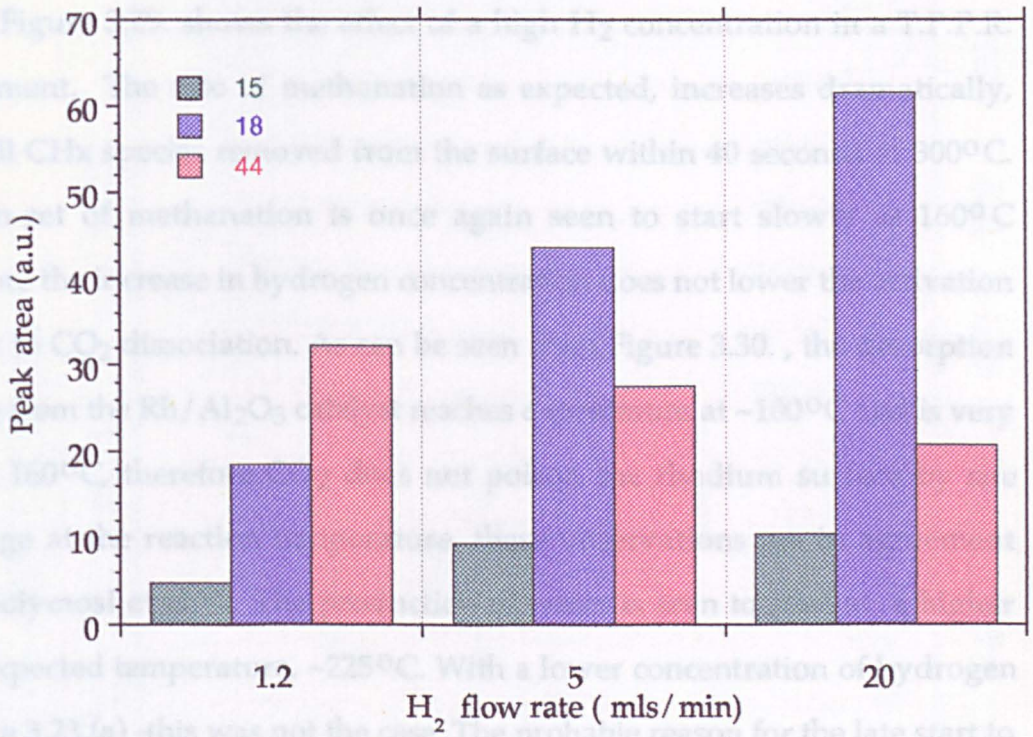

production is particularly slow, as was seen it the case of CO hydrogenation, Figures 3.17.(a)-(d), which suggests that under these conditions the formation of water is not kinetically favourable due to the surface life time of H(a) being extremely short. Also because the support is fully reduced it may have a larger capacity for retaining hydroxyl groups and their reaction to water is limited by hydrogen availability.

Figure 3.29. shows the effect of a high H_2 concentration in a T.P.P.R. experiment. The rate of methanation as expected, increases dramatically, with all CHx species removed from the surface within 40 seconds at 300°C. The on-set of methanation is once again seen to start slowly at 160°C therefore the increase in hydrogen concentration does not lower the activation energy to CO_2 dissociation. As can be seen from Figure 3.30. , the desorption of CO_2 from the Rh/Al_2O_3 catalyst reaches a maximum at ~100°C and is very fast at 160°C, therefore CO_2 does not poison the rhodium surface by site blockage at the reaction temperature, these observations are in agreement with Solymosi et al.[32]. The production of water is seen to start at a higher than expected temperature, ~225°C. With a lower concentration of hydrogen - Figure 3.23.(a) -this was not the case. The probable reason for the late start to water desorption is that with high hydrogen concentrations the support is more reduced and as a consequence has a higher capacity for retaining surface hydroxyl groups. The inference from this is that water formation occurs through a support species such as a hydroxyl group when the hydrogen concentration is high.

As with the CO hydrogenation reaction, the only carbon product seen was methane, no evidence of any higher hydrocarbon or oxygenate formation was found under the conditions employed. This is not surprising if the experimental mode is carefully considered; each pulse of CO_2 is only about six seconds wide (width at half maximum height) and this is combined with a stream of hydrogen. The surface intermediates that are

Figure 3.29.
T.P.P.R. showing CO_2 hydrogenation.
$CO_2 : H_2 = 1 : 6$

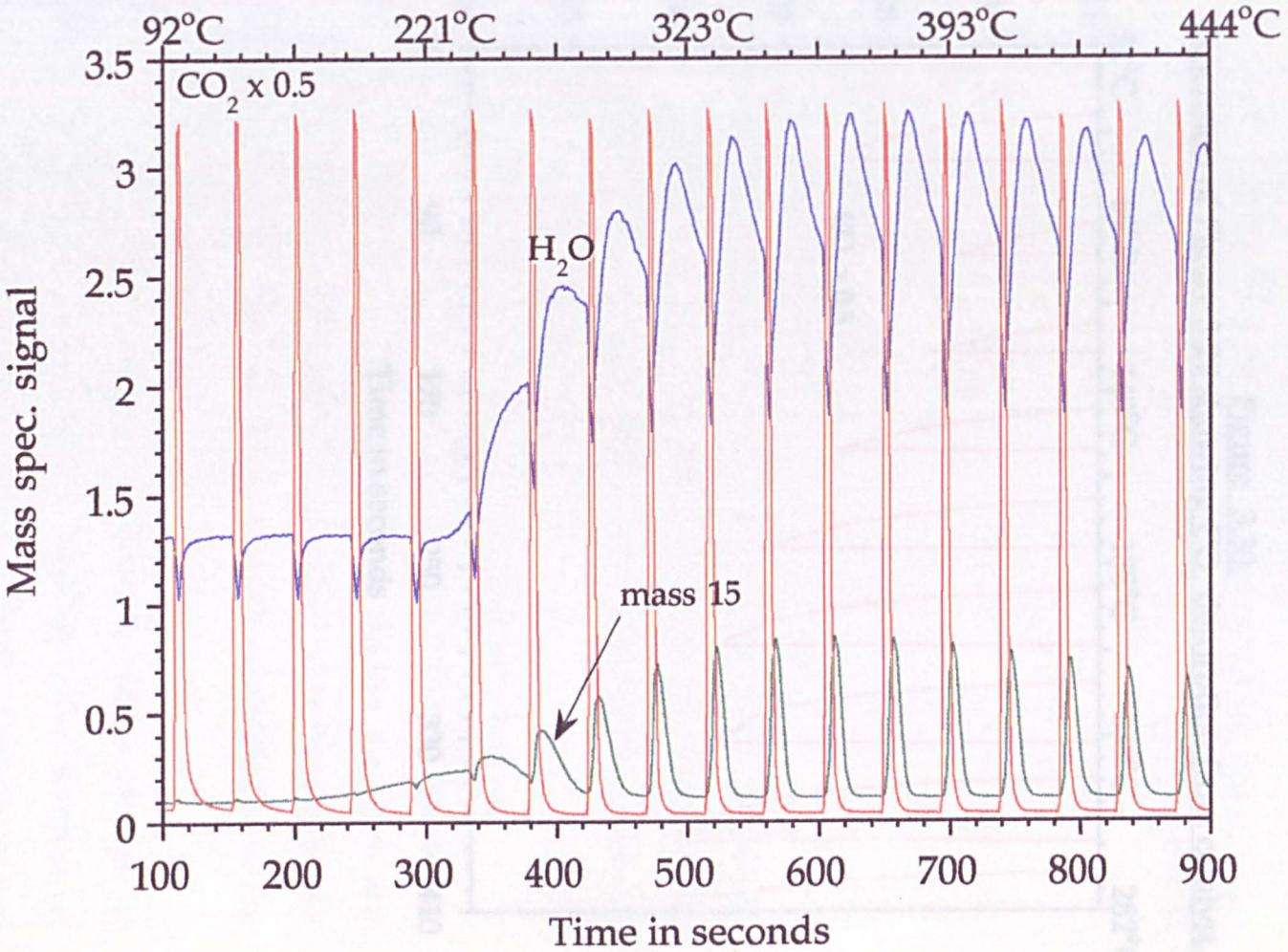

Figure 3.30.
Expansion of Figure 3.29 showing CO_2 desorption from catalyst.

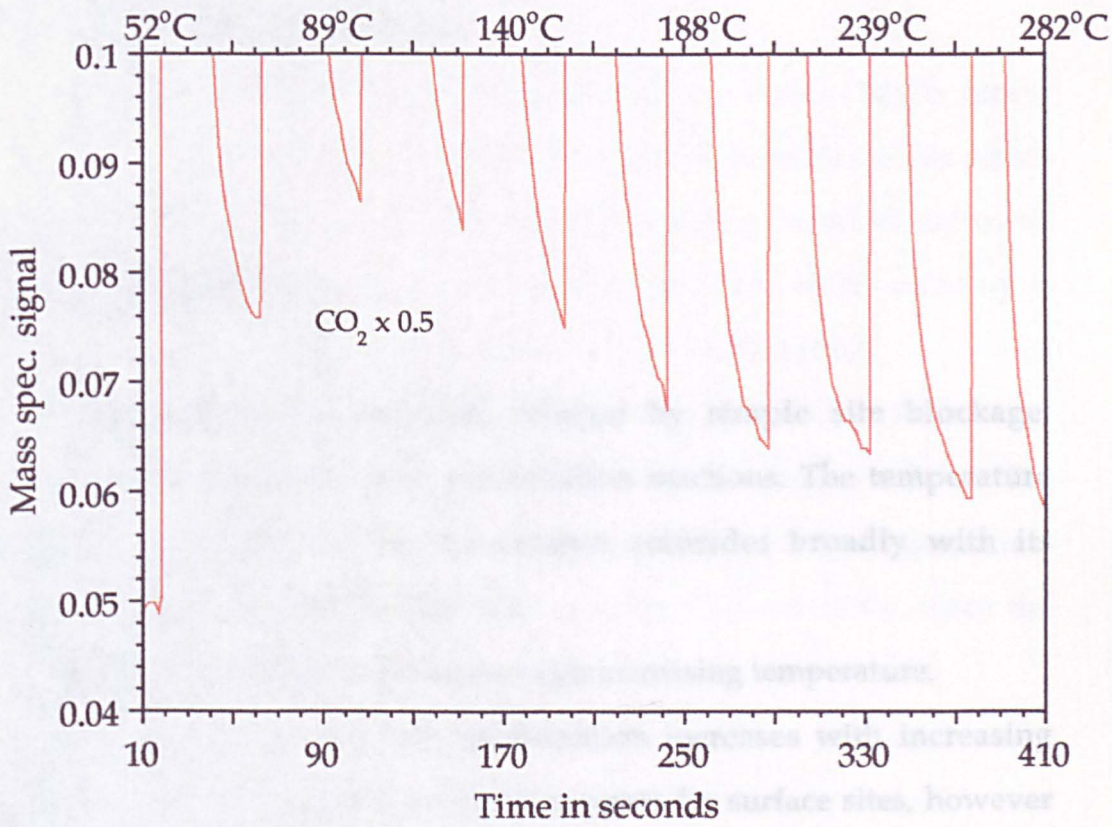

responsible for higher hydrocarbon synthesis and oxygenate formation are, it would seem, not given the time to build up into a sufficient concentration for coupling or insertion reactions to take place. It should also be remembered that the reactions have been conducted at atmospheric pressures whereas higher pressures favour higher hydrocarbon and oxygenate formation[4] and that the catalyst is not promoted with any reducible oxides widely reported to promote the synthesis of oxygenates.

3.5. CONCLUSIONS.

(1) CO(a) poisons the rhodium catalyst by simple site blockage, preventing CO dissociation and methanation reactions. The temperature required to dissociate CO on the catalyst coincides broadly with its desorption temperature (130°C - 230°C).

(2) The rate of methanation increases with increasing temperature.

(3) The rate of CO and CO_2 methanation increases with increasing hydrogen concentration as H_2 is able to compete for surface sites, however the temperature at which both CO and CO_2 dissociates is not effected by the hydrogen concentration therefore hydrogen does not markedly lower the activation energy to CO dissociation.

(4) The mechanism of CO methanation changes with a change in hydrogen concentration. At high hydrogen availability (either through an increased flow rate or through slower desorption at lower temperature) wet methanation dominates. At low hydrogen availability dry methanation dominates.

(5) The mechanism of CO_2 hydrogenation is not altered with a change in temperature or hydrogen concentration. The only products detected with T.P.P.R. were CH_4 and H_2O

(6) In the absence of hydrogen the catalyst looses activity towards CO dissociation through the build up of amorphous surface carbon. This carbon can be hydrogenated to methane between 100°C - 350°C with an activation energy of 57kJmol^{-1} .

(7) Carbonaceous surface species are produced over the Rh/Al_2O_3 during the hydrogenation of CO(a), these are most likely to be formate species which reside on the support. They decompose to CO_2 with a broad background between 320°C - 420°C in the absence of hydrogen, and their build up is prevented at high hydrogen concentrations through methanation.

(8) The rate of hydrogenation of C(a) originating from CO_2 in faster than that from CO between 160°C and 300°C. This is due to a higher ratio of H(a) to C(a) as a result of less CO_2 dissociation, in the case of CO hydrogenation a higher concentration of surface species , primarily C(a) and CO(a), block the surface to H(a).

3.6. REFERENCES.

1. M.Bowker, *Catalysis Today*, **15** , 77 (1992).
2. Vannice, M.A., *J.Catal.*, **37**, 449 (1975).
3. Vannice, M.A., *J.Catal.*, **37**, 462 (1975).
4 Bhasin, M.M., Bartley, W.J., Ellgen, P.C. and Wilson, T.P., *J.Catal.*, **54**, 120 (1978).
5 Ichikawa M., *Bull. Chem. Soc. Japan.* **51**, 2268, (1978).
6 Thiel, P.A., Williams,E.D., Yates Jn. J.T. and Weinberg,W.H., *Surf. Sci.* **84**, 54 (1979).
7 Yates, J.T., Williams, E.D. and Weinberg, W.H., *Surf. Sci.* **91**, 562 (1981).
8 Sexton,B.A., and Somorjai,G.A., *J.Catal.*, **46**, 167 (1977).
9 Castner, D.G.,and Somorjai,G.A., *Surf.Sci.*, **83**, 60 (1979).
10 Castner, D.G., Dubois,L.H.,Sexton,B.A. and Somorjai, G.A., *Surf.Sci.* **103**, L134 (1981).
11 Solymosi, F. and Erdöhelyi, A., *Surf. Sci.*, **110**, L630 (1981).
12 Primet,M., *J. Chem. Soc. Faraday Trans. I.* **74**, 2570 (1978).
13 Arai, H., and Tominaga, H., *J. Catal.*, **43**, 131 (1976).
14 Solymosi, F., and Sarkany, J., *Appl. Surf. Sci.* , **3**, 68 (1979).
15 Yates,J.T., Duncan,T.M., Worley, S.D., and Vaughan, R.W., *J. Chem. Phys.*, **70** , 1219 (1979).
16 Yates,J.T., Worley, S.D., Duncan,T.M., and Vaughan, R.W., *J. Chem. Phys.* , **70** , 1225 (1979).
17 Bredikhin, M.N., Lokhov, Y. and Kunznetsov, V.L., *Kinet. Katal.*, **28** 671 (1987).
18 Bredikhin, M.N. and Lokhov, Y.,*Kinet. Katal.*, **28** 678 (1987).
19 Rice,C.A. and Worley,S.D., *J.Chem. Phys.*, **74**, 6487 (1981).
20 Basu,P., Panayotov,D. and Yates, J.T., *J. Phys. Chem.*, **91**, 3133 (1987).

21 H. Knözinger, in Cluster Models for Surface and Bulk Phenomena, Pacchioni, G., Bagus, S.P. and Parmigiani, F. (Eds). *NATO ASI Series B: Physics.* Vol. **283**, Plenum, New York, 131, (1992).

22 Yang.A.C. and Garland, C.W., *J. Phys. Chem..*, **61**, 1504 (1957).

23 Fujimoto, K., Kameyama, M. and Kunugi, T., *J.Catal .*, **61**, 7, (1980).

24 Solymosi,F., Tombacz,I. and Kocsis, M., *J. Catal.* **75**, 78 (1982).

25 Mori, Y., Mori, T., Miyamoto, A., Takahashi, N., Hattori, T., Murakami, Y., *J. Phys. Chem.*, **93**, 2039 (1989).

26 Ponec,V., *Cat. Today.* ,**12**, 227 (1992).

27 De Koster, A. and van Santen, R.A., *Surf. Sci.* **233**, 366 (1990).

28 Bond.G.C., *J.Catal.*, **45**. 128, (1976).

29 Van Santen, R.A. and De Koster, A., in "New Trends in CO activation" ed. L. Guczi, *Studies in Surface Science*, **64**, 30 (1991).

30 Collins.A.C. and Trapnell, B.M.W., *Trans. Faraday Soc.* **53**, 1476 (1957).

31 Campbell, C. T., and White,J.M., *J.Catal.*, **54**, 289 (1978).

32 Solymosi, F., Erdöhelyi, A. and Kocsis,M., *J.Catal.*, **65**, 428 (1980).

33 Solymosi, F., Erdöhelyi, A. and Bansagi,T., *J.Catal.*, **68**, 371(1981).

34 Rasko,J. and Solymosi, F., *J. Phys. Chem.*, **98**, 7147 (1994).

35 Vannice, M.A., *J.Catal.* , **37**, 462 (1975).

36 Vannice, M.A., *Catal. Rev. Sci. Eng.*, **14**, 153 (1976).

37 Biloen,P. and Sachtler,W.M.H. *Adv. Catal.* **30**, 165 (1981).

38 N.D.Shinn and T.E. Madey, *J. Chem. Phys.* **83**, 5928 (1985).

39 Erdöhelyi, A. and Solymosi, F., *J.Catal.* **84**, 446 (1983).

40 Sachtler, W.M.H., Shriver, D.F., Hollenberg, W.B. and Lang, A.F., *J.Catal.*, **92**, 429 (1985).

41 Ioannides, T. and Verykios, X., *J. Catal.* **140**, 353 (1993).

42 Hindermann, J.P., Hutchings, G.J. and Kiennemann, A., *Catal. Rev.-Sci. Eng.*, **35**(1), 1 (1993).

43 Haller, G.L. and Resasco, D.E., *Adv. Catal.*, **36**, 173 (1989).

44 Tauster, S.J. and Fung, S.C., *J.Catal.* **55**, 29 (1978).

45 Taniguchi, S., Mori, Y., Hattori, T., Murakami, Y. and Mori, T., *J. Chem. Soc., Faraday Trans. 1*, **85**(10), (1989).

46 Sachtler,W.M.H., Ichikawa,M. *J.Phys. Chem.* **90**. 4752 (1986).

47 Solymosi, F., Bansagi,T. and Erdöhelyi, A., *J.Catal.* **72**, 166 (1981).

48 Erkerdt, J.G. and Bell, A.T., *J.Catal*, **62**. 19 (1980).

49 Efstathiou, A.M., Chafik, T., Bianchi, D and Bennett, C.O., *J. Catal.*, **148**, 224, (1994).

50 Efstathiou, A.M. and Bennett, C.O., *J.Catal.* **120**, 118 (1989).

51 Efstathiou, A.M. and Bennett, C.O., *J.Catal.*, **120**, 137 (1989).

52 Efstathiou, A.M. , *J.. Mol. Catal.* , **67**, 229 (1991).

53 Erkerdt, J.G. and Bell, A.T., *J.Catal.*, **58**. 170 (1979).

54 Kellner,C.S. and Bell, A.T., *J.Catal.* **71**. 296 (1981).

55 Engel, T. and Ertl, G., '*The Chemical Physics of Solid Surfaces and Heterogeneous Catalysis* ', (King, D. and Woodruff, D.P., eds.), Elsevier, Vol 4.

56 Solymosi, F., Erdöhelyi, A. and Kocsis,M., *J.Chem. Soc., Faraday Trans.1*, **77**, 1003 (1981).

57 Iizuka, T., Tanaka, Y, and Tanabe, K., *J.Catal.* **76**, 1 (1982).

58 Ichikawa, S., *J. Mol. Catal.*, **53**, 53 (1989).

59 Trovarelli A., Leitenburg de, C, and Dolcetti, G., *J. Chem. Soc., Chem. Commun.* **7**, 472 (1991).

60 Boffa, A.B., Bell, A.T. and Somorjai, G.A., *J.Catal.*, **139**, 602 (1993).

61 Vandervell, H.D. and Bowker, M., *Appl. Catal.* **30**, 151 (1987).

62 Bowker, M., Cassidy, T.J., Ashcroft, A. T. and Cheetham, A. K., *J. Catal.*, **143**, 308 (1993).

63 Ashcroft, A.T., Cheetham, A.K., Green, M.L.H. and Vernon, P.D.F., *Nature*, **325**, 225 (1991).

64 Teuner, S., *Hydrocarbon Process.* **64**, 106 (1985).

65 Richardson, J.T. and Paripatyadar, S.A., *Appl. Catal.* **61**, 293 (1990).

66 Ho, Y-S. and Yeh, C-Y. Adsorpt. Sci. Technol. **7**, 1 (1990).

67 Tolia, A.A., Smiley, R.J., Delgass, W.N., Takoudis, C.G. and Weaver, M.J., *J. Catal.* **150**(1), 56 (1994).

68 Kellner, C.S. and Bell, A.T., *J. Catal.* **71**, 296 (1981).

69 Kruse, N. and Gaussmann, A., *J.Catal.* **144**, 525 (1993)

70 Cho, B.K. and Stock, C.J., *J. Catal.* **117**, 202 (1989).

71 Twigg, M.V.,*'Catalysis Handbook.'* 2nd Edn., Wolfe Publishing Ltd (1989).

72 Koerts, T., Ph.D. Thesis, Eindhoven University of Technology, The Netherlands (1992).

73 Flesner, R.L. and Falconer, J.L., *J. Catal.* **139**, 421 (1993).

74 Takehira, K., Hayakawa, T. and Ishikawa, T., *Bull. Chem. Soc. Japan.* **51**, 1685 (1978).

CHAPTER 4.

SURFACE EXPLOSIONS ON A HIGH AREA SUPPORTED CATALYST.

4.1. INTRODUCTION.

Through the advent of ultra high vacuum (UHV) conditions over the past 30 years, the study of simple reactions between known quantities of reactants on well defined surfaces has been made possible. There has been much discussion as to the relevance and indeed the use of surface science UHV experiments with respect to catalysis. It is true that UHV conditions are different from the conditions of a working catalyst, however the piecing together of definitive reaction kinetics and mechanisms from UHV studies allows better and more informed propositions to be put forward when elucidating the exact processes occurring on the microscopic scale on a working catalyst. It is now clear that many species identified in single crystal surfaces are also implicated in catalysis on supported materials, a good example being the early observation of stable formate species on Cu single crystals[1,2] then their subsequent observation on supported Cu catalysts during high pressure methanol synthesis[3].

In this chapter, I briefly review the recent literature on simple carboxylate species formed from CO and H_2 mixtures over rhodium based catalysts and single crystals, highlighting the connection between synthesis gas and the existence of carboxylate groups on rhodium catalysts and single crystals. Secondly, I briefly review the literature on simple carboxylate groups (formates and acetates) that have been shown to have autocatalytic desorption kinetics, often referred to as surface 'explosions'.

In the results section, data are presented that represent a direct transfer of knowledge from surface science studies on single crystals, to a supported rhodium catalyst operating at atmospheric pressure[4,5]. These results are discussed in the light of the single crystal work.

4.1.1 HIGHER OXYGENATES AND SURFACE CARBOXYLATES.

There has been enormous interest over the past two decades on the direct synthesis of higher hydrocarbons from synthesis gas. The unique ability of supported rhodium catalysts to selectively produce C_2 oxygenates was first recognised in 1975 [6,7,8]. From a commercial view point, perhaps the most important C_2^+ oxygenated products are ethanol, acetaldehyde and acetic acid, as these are widely used in the production of plastics, paints and pharmaceuticals[9] . Ethanol is used primarily as a solvent in the varnish and perfume industries, it is used also as an alternative to gasoline in Brazil, where its annual production through fermentation of molasses exceeds 9 million tonnes. Higher alcohols, in particular ethanol, are excellent gasoline boosters and so could challenge MTBE (methyl terbutyl ether) as a gasoline additive.

At the present time, the major routes to C_2^+ oxygenates are through homogeneous liquid phase catalytic cycles, e.g. the Monsanto process for acetic acid production, or via high pressure reactions such as the hydration of ethylene to ethanol over supported phosphoric acid catalysts (280°C and 70 atmospheres pressure). A one step selective, heterogeneous catalytic process from synthesis gas, operating at intermediate temperatures and pressures (250-280°C and 10-15 atmospheres pressure) would bypass toxic and volatile co-catalysts, increase the turn over and reduce the cost of production, and would clearly be of enormous benefit to the petrochemical industry and indeed society at large.

The existence of carboxylate intermediates in catalysis is well known, their precise role is however a matter of some controversy. Their specific production, surface orientation and role in reactions are continued areas of research and debate both in academia and industry particularly as many industrial processes involve carboxylates. Carboxylate species have been

proposed as being reaction intermediates in a wide range of catalytic processes, among these are the water-gas shift reaction[10,11,12] , methanol synthesis[13,14,15], higher oxygenate synthesis[16,17], selective and unselective oxidations[18,19], ketone formation[20,21] and various condensation reactions[22] . It is not very surprising to find that they exist on the surfaces of working catalysts since carboxylate species are generally thermally stable, only decomposing above room temperature on metal oxides and on most metals[23,24] .

A large number of spectroscopic studies have been carried out on the surface orientation and the bonding of surface species. In chapter III the main adsorbed CO species were illustrated (Figure 3.1.), species V, the CO(a) co-ordinated to the metal and promoter via carbon and oxygen respectively, has been proposed as the key adsorbate in the production of C_2 oxygenates[25] . Also discussed in chapter III were the main C_1 carboxylates formed on un-promoted rhodium catalysts, namely the formate and carbonate species. Vibrational spectroscopies easily detect the large extinction coefficients of modes associated with vibrations and deformations of the carboxyl group and have therefore been used to great effect in elucidating the surface species present during reaction. Spectroscopic studies however reveal little about the kinetics of the formation, reaction and desorption of the carboxylate groups. There is much contention as to which carboxylates play an active role and which are simply present as spectator species, in the synthesis of oxygenates. The possible C_2 carboxylates on the surface during oxygenate synthesis[16] are; the acyl CH_3CO, acetyl CH_3CHO, ethoxy CH_3CH_2O, acetate CH_3COO and deoxyethyl CH_3CHOO species. There are two main candidates for the key carboxylate intermediate leading to ethanol synthesis - these are an acetyl like species that is hydrogenated first to acetaldehyde then further to ethanol[26,27,28,29,30]. and the acyl group has been proposed as the key intermediate in the synthesis of acetaldehyde and ethanol on promoted Pd

catalysts, through a CO insertion mechanism[31,32] Alternatively an acetate species, seen ubiquitously on promoted rhodium surfaces and single crystals under oxygenate synthesis conditions, has been proposed as the key intermediate[15,16,33,34,35,36,37]. The acetate group may be hydrogenated to ethanol in a step wise manner passing through an acetaldehyde intermediate, or alternatively may be hydrogenated to a dioxyethyl intermediate which can then undergo a concerted hydrogenation to an ethoxy intermediate, before being hydrogenated to ethanol. In this latter route, the implication is that two different intermediates are primarily responsible for acetaldehyde and ethanol production[38,39,40] . Others take the view that carboxylates reside solely on the oxide support and play a very minor role in oxygenate synthesis[41,42].

The role of carboxylates in the synthesis of ethanol on rhodium has recently been reviewed[16] by Bowker. He concludes that the most likely key carboxylate intermediate involved in the production of ethanol is an acetate group. This conclusion is centered around the fact that acetates are seen spectroscopically on catalysts that are good alcohol synthesis agents, whereas other proposed intermediates, such as an acyl group are not and that by-products of the acetate group are seen in the exit gases - most noticeably acetic acid. It is noted that acetates can form in a variety of locations on the catalyst, shown in Figure 4.1. below, but the likely active acetate is located at the Rh/metal oxide promoter interface, with one of the acetate oxygen atoms bound strongly to the promoter metal - in effect it can be described as a 'stabilised acyl species'. The other forms of acetate -i.e. those formed on the pure metal and on the support, can be considered as spectator species with respect to ethanol synthesis and he argues that these species have led to the confusion over the activity of the acetate intermediate.

FIGURE 4.1. Acetate species formed on promoted Rh catalysts. Adapted from Bowker, M.[16]

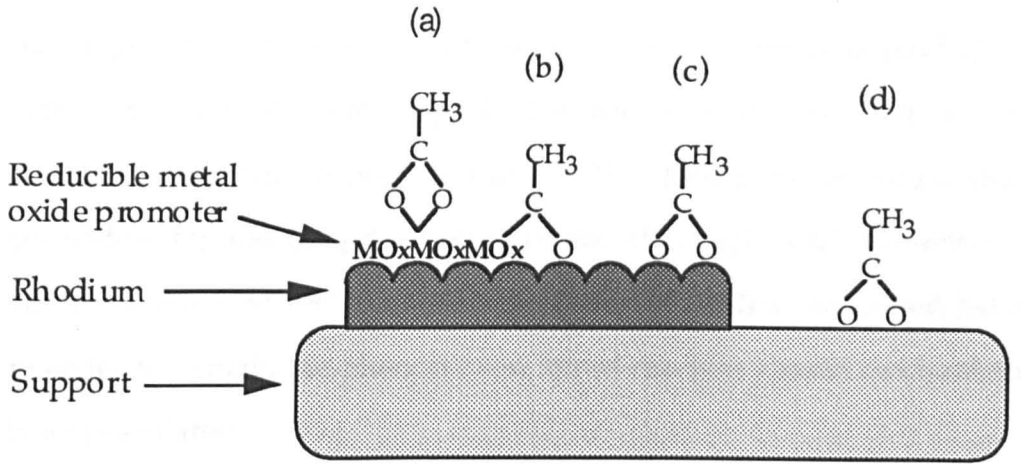

The detailed mechanistic scheme proposed by Bowker[16,38] acknowledges that the pathway to oxygenates is complicated by 'inter-connected' mechanistic schemes. The most dominant scheme depends upon the exact make-up of the rhodium particle, the metal support interaction and the effects of promoters.

4.1.2. SURFACE 'EXPLOSIONS' on SINGLE CRYSTALS.

The term " surface 'explosion' " encapsulates a number of unusual desorption phenomena ranging from CO oxidation processes to carboxylate decomposition. The most important aspect of a surface 'explosion' is that the adsorbate decomposes in an autocatalytic manner, i.e. the decomposition / desorption is catalysed by a product of the forward reaction. The autocatalytic nature of a reaction can be authenticated by checking that the adsorbate decomposition accelerates at a fixed temperature. The most obvious

manifestation of a surface 'explosion' is an unusually narrow peak width during temperature programmed desorption. The phrase surface 'explosion' was first coined by Professor Madix et al.[43], who when monitoring the decomposition of formic acid from a nickel (110) single crystal observed a remarkably fast desorption peak. The formic acid, adsorbed as a formate species on the Ni, decomposed at ~115°C giving rise to large, sharp and coincident H_2 and CO_2 desorption peaks. The 'explosion' phenomenon was studied further[44,45,46,47]most extensively on Ni(110) as described below, and in order to explain the phenomenon, novel reaction kinetic mechanisms have been postulated.

Falconer and Madix classified the T.P.D. peaks as either α peaks - those which did not occur at explosion temperatures and were relatively wide, and the explosive β peaks - the explosive desorption occurring at higher than expected temperatures and having a very narrow width. They found that at low coverages of formic acid (<0.2L) no explosion occurred - only the α peaks were observed. At higher coverages (≈0.4L) the β peak began to appear and concurrent with the appearance of the β peak there was a drop in the α peak area. The hydrogen and carbon dioxide peaks always occurred at the same temperature and the ratio of hydrogen molecules to carbon dioxide molecules was 1.0 ± 0.2 - indicative of the decomposition of formate groups. Using deuterated formic acid, DCOOH, it was found that no HD or H_2 peaks were observed unless the experiment was maintained under H_2 throughout the temperature ramp. An important result illustrated that there is little interaction between the formate species that desorbs as a broad peak (the α peak) and the formate that leads to the explosive β peak, as when the temperature was raised to a value in-between that of the two peaks then lowered again, the desorption process was quenched and upon subsequent temperature ramping, no α peak occurred but the β peak remained. The rate of formic acid dissociation was measured as a function of time at a fixed

temperature (95°C) and was found to accelerate and thus was classified as an autocatalytic process; a process in which a product of the forward reaction is also a reactant in the process itself. The question remaining was which product catalyses the reaction? As mentioned above, co-adsorption with hydrogen did not alter the desorption process, nor did co-adsorption with CO. Further to this, CO_2 and H_2 desorbed concurrently, indicating that they desorb quickly from the surface once dissociation occurs and therefore it seems unlikely that the presence of one of these as a co-adsorbate would catalyse the production of the other. Only one other product of the reaction remains, that is the liberation of an adsorbate site. The fact that there is little coverage dependence could be explained if the adsorbate is assumed to coalesce into 'islands' so that the local coverage is always close to one, they developed this idea with kinetic modelling.

4.1.3. THE 'ISLAND' MODEL.

Falconer and Madix attempted to confirm the 'island' model through various experiments. It is assumed in their 'island' model that the dissociation starts at an initiation site and then proceeds increasingly quickly outwards as bare metal is revealed. As two T.P.D. peaks occur, α and β, they postulated that islands of low density and of high density occurred. The low density ones resulting in the broad α peak and the high density islands resulting in the explosive β peak. They found that when DCOOH followed by HCOOH was adsorbed on the Ni(110) surface, the β CO_2 peak was found to occur at the temperature expected if only DCOOH were adsorbed. When HCOOH was adsorbed first, followed by DCOOH, two explosive CO_2 peaks were observed, the first at the temperature expected from adsorption of HCOOH

and coincident with H_2 desorption, the second indicative of DCOOH adsorption and coincident with D_2 desorption. Hence they concluded that adsorption took place preferentially on the initiation sites, thus molecules that were adsorbed later were incapable of initiating the dissociation.

A point in general to note, is that in normal temperature programmed desorption processes, the sequence in which adsorption sites are filled is in reverse order with respect to their desorption. This arises because the first sites filled are those with the highest binding energy and thus they desorb at elevated temperatures. However in temperature programmed dissociation, it is the activation energy towards dissociation that determines the order in which desorption occurs. It is possible therefore that the adsorption sites filled first, that is those with the highest binding energy, may also induce a weakening of the intramolecular bonds of the adsorbate and hence lower the activation energy required for dissociation.

Falconer and Madix considered two 'island model' possibilities; either the adsorbed formate is relatively free to move across the surface, so that the number of available sites depends upon the total amount of bare metal sites, or the formate species are not free to move and therefore, once the dissociation is initiated, the number of sites available for dissociation is determined by the circumference of the growing island of bare metal. In both cases, the rate of dissociation is also determined by the amount of adsorbate left. The two proposals were modelled mathematically. The rate equation describing the first proposal is;

$$-\frac{d\theta}{dt} = k\theta(1-\theta+f)$$

Where k is the rate constant, f is the proportion of adsorption sites which are initiation sites (≈ 0) and θ is the adsorbate fractional coverage, not at initiation sites.

In the second case, the rate equation is;

$$-\frac{d\theta}{dt} = kfN2\pi r(t)h$$

where N is the number of adsorbate sites per unit area on the surface (therefore fN is the number of initiation sites per unit area), r(t) is the radius of the island of clean surface surrounding an initiation site and h is the effective thickness of the reaction perimeter at the edge of the growing circle. They found that the first proposal could approximately fit some experimental data however the second approach did not give a good fit to the time dependence of the dissociation.

In an experiment where the formate was first adsorbed then the temperature was raised so that the explosive desorption just began then the reaction was halted through quenching the temperature, it was found that upon subsequent heating, the explosion did not occur. The T.P.D. peaks were broad, they occurred at lower temperatures and with a reduction in their total area. This 'interrupted flash' explosion data was successfully modelled by the first approach, i.e. the moving adsorbate auto-catalytic proposal. A further curious result was that if the formic acid was adsorbed at room temperature then 'explosive' decomposition occurred. If however the temperature of adsorption was below $0^{o}C$ then no 'explosion' occurred. A possible explanation put forward was that the low adsorption temperature affects the mobility of the adsorbate groups thereby hindering their ability to coalesce into islands.

Benziger and Schoofs[48] observed surface 'explosions' on a Ni(111) crystal however a direct comparison to the work of Madix et al. is difficult as Benziger et al. adsorbed dimerised formic acid, they however maintain that in the work of Madix, the formic acid dimer was the major adsorbate. They found that upon adsorption of the dimer 'explosive' dissociation occurred at

~360K with a peak width of ~8K. When the monomer was adsorbed no explosion was seen. It is clear that many similarities do exist between the Madix work on Ni(110) and Benzigers study on Ni(111) - perhaps most important to note is that the adsorbed species leading to the 'explosive' dissociation was proposed to be a dense formate species, formed on adsorption of the dimer as follows;

$$(HCOOH)_2 \text{ ---------> } HCOO(a) + HCOHOH$$

$$HCOHOH \text{ ---------> } H_2O + CO(a) + H(a)$$

They proposed that the CO(a) and formate groups were strongly repulsive causing the dense areas of formate to form through phase separation. In the case where the monomer was exclusively adsorbed, no CO(a) co-adsorbate was found and no explosive desorption occurred.

In 1976 Madix et al. discovered that the 'explosive' desorption of formate groups could be extended to C_2 carboxylates - namely acetates, CH_3COO. He performed T.P.D. experiments after dosing acetic acid onto a Ni(110) surface. The adsorbate formed upon adsorption behaved quantitatively in the same way as the formate groups described earlier. Broad α peaks occurred and narrow 'explosive' β peaks were seen if sufficient coverage of acetate was achieved ($\theta > 0.2$). Once again, CO_2 and H_2 desorbed concurrently and the ratio of H_2 to CO_2 was 1.5. Madix et al. proposed that the adsorbed species was acetic anhydride $CH_3CO_3CCH_3$, this was to explain the build up of carbon after the desorption, however the adsorbate is now considered to be an acetate group after the work of Bowker et al. There were differences between the acetate T.P.D. and the formate T.P.D. most notably, in the acetate case adsorption at low temperatures (-60°C) still lead to the explosive dissociation process whereas low temperature adsorption in the formate case leads to exclusively non-explosive dissociation. After the extensive work by Madix et al., there existed very little reported literature on explosive carboxylate groups until the observations of Bowker and Li[49].

They were studying ethanol decomposition and oxidation reactions on a Rh(110) single crystal with a view to revealing information on the direct route to ethanol from synthesis gas, via micro-reversibility. They found that through either co-adsorbing ethanol and oxygen, or by adsorbing acetic acid onto the Rh(110), an adsorbed acetate group was formed. Upon T.P.D. a surface 'explosion' occurred yielding very sharp (~5K), concurrent CO_2 and H_2 peaks (or if sufficient oxygen was present, water was observed rather than H_2). They proposed a modified island mechanism akin to the Madix proposal, whereby clean metal sites necessary for acetate decomposition were made available for reaction at the circumference of a growing patch of clean surface, that radiated out from initiation centres, such as steps or kinks, into dense areas of acetate. It should be noted that at this stage (1991) surface explosions involving carboxylate species were considered rare, they had only been conclusively seen in UHV conditions and were considered by many to be exclusive to the (110) surface. With further results from Bowker and Li[50], some important general trends were highlighted and it became apparent that the phenomenon was more wide spread, with the 'explosions being seen also on a Rh(111) surface[51].

By using a molecular beam system to dose acetic acid onto the Rh (110) crystal at 315K, it was found that initially the acid decomposed resulting in CO_2 and H_2 evolution and C(a) left on the surface. As the dosing continued, the evolution of CO_2 fell, but H_2 continued, indicating that acetate groups were forming - and it became apparent that the carbon contamination was stabilising the acetate groups. Upon T.P.D. the acetate 'explosively' decomposed. To further explore the role of the adatom, oxygen was dosed onto the surface prior to acetic acid, the amount of acid decomposition during adsorption fell and less beaming time was required for the formation of stable acetate species. Water was the by-product of the adsorption process rather than hydrogen. Upon T.P.D. the characteristic 'explosion' took place. It was

found that by increasing the amount of oxygen prior to the acetate formation, the temperature of the 'explosion' peak rose. The oxygen was therefore implicated in the stability of the acetate group. They also dosed nitrogen atoms prior to beaming acetic acid. This was done by beaming NO onto the surface at 393K at this temperature the majority of the NO decomposed to N(a) and O(a), the O(a) was removed by beaming CO, forming CO_2. As was found with O(a) adatoms, the presence of nitrogen was found to reduce the time required for stable acetates to form from acetic acid and explosive decomposition was seen upon T.P.D, therefore the conclusion was made that an adatom - either C(a), O(a) or N(a) - are able to bring about explosive desorption.

The investigation was widened with adsorption of acetic acid on Rh(111). On the clean Rh(111) surface, the acid adsorbed as acetate (only H_2 was seen upon adsorption) therefore, no C(a) was left behind. With subsequent T.P.D. no 'explosion' occurred, the CO_2 and H_2 peaks were 26K wide and at a temperature of 390K. When oxygen was pre-dosed onto the crystal, a stabilised acetate was formed upon acid adsorption (water was formed rather than H_2), if the oxygen coverage was small, the evolution of H_2 was seen following a fall in the water production, indicating that all the oxygen had been titrated off. When this was the case, upon T.P.D. the desorption was 'non-explosive' as with the clean crystal. When higher coverages of oxygen were pre-dosed, such that O(a) remained after acetate formation, the desorption became 'explosive'. A strong correlation was found to exist whereby higher doses of oxygen induced a higher explosion peak temperature, the explosive peaks varying from ~410K to ~500K. In comparison to the work done on Rh (110), the oxygen covered Rh (111) surface stabilised the acetate species by more than 100K in T.P.D. A further effect of acetic acid concentration in agreement with the work of Madix was

found, in that at low coverages of acetate no explosion was seen while at higher coverages the explosion dominated the desorption.

With the reporting of surface explosions occurring on Pd (110)[52] it became apparent that surface explosions were in fact more widespread than at first thought, occurring also on Ni(110) and (111) as well Rh(110) and (111). In agreement with the rhodium work above, Aas and Bowker found that no 'explosion' occurred after acetate formation on the clean Pd(110) surface, however if C(a) was allowed to build up by means of successive acid doses and T.P.D.'s the CO_2 peak became 'explosive' . The autocatalytic nature of the explosions was verified by an experiment where, after dosing acid on the oxygen covered crystal at 325 K, the temperature was raised to just below the explosion temperature maximum, then held constant. The decomposition became self-accelerating and required no further heating to reach completion. The effect of reversing the adsorption i.e. adsorb acetic acid then oxygen adsorption complicated the T.P.D. further. Two processes appeared to take place, the first yielding coincident CO_2 and H_2O and the second yielding CO_2 and H_2 . The decompositions occurred at lower temperatures than for the oxygen pre-dosed case.

Having concluded that adatoms are a necessary requirement for surface explosions to occur, Bowker and Li then asked the question : why is this so ? Three potential reasons were considered;

(i) Adatoms act as a simple poison by blocking the decomposition sites adjacent to the adsorbed acetate, i.e. they hinder the rotational mode of the molecule that leads to its decomposition.

(ii) There is a possibility that an atomic adsorbate may induce a surface reconstruction that creates different sites than those seen on the clean surface.

(iii) Adsorbate induced ordering occurs, where the atomic adsorbate is arranged in an ordered array and they induce the carboxylate adsorption to

be ordered with respect to the adatoms. The result is that the carboxylate species themselves largely poison the sites required for their decomposition.

Taking each in turn, the first suggestion seems unlikely as at high coverages of adatoms and low coverages of acid, no explosion occurs. One would expect an explosion proportional in size to the amount of carboxylate adsorbed. The second suggestion also seems highly unlikely as explosions are seen on a variety of different metals and crystal orientations with a number of adatoms. It is difficult to believe that such a medley produces a specific surface structure that induces the 'explosions'. In addition to this, surface reconstructions are normally an effect due to a change in the surface environment, not a cause of the change in the surface environment. Hence Li and Bowker preferred the third proposition where the adsorbates are ordered and normal decomposition is thwarted via site blockage by the neighbouring adsorbates.

In a recent paper[53] by Hoogers et al. surface 'explosions' were reported on a Rh(111) crystal, the reaction under scrutiny was acetic acid decomposition. With observations in agreement with Bowker et al. they found that adsorption of the acid at 200K on the clean surface led to a broad non-'explosive' decomposition at ~ 410K, whereas if oxygen was dosed prior to the acid then an explosion was seen at ~460K with a peak width of ~15K. They however disagreed with Bowker et al. on the absolute requirement of an adatom for an explosive decomposition after acetic acid adsorption at 300K. Hoogers reports that an 'explosion' occurs regardless of whether oxygen is pre-adsorbed or not provided enough carboxylate is adsorbed. Hoogers et al. explained the 'explosion' resulting from acid adsorption onto the clean Rh(111) surface by pointing out that hydrogen was found to desorb from the crystal at around 280K, therefore when adsorption below this temperature occurred each dissociated acid hydrogen atom formed, blocked an adsorption site, therefore reducing the density of acetates. Indeed their results show that

adsorbing at 200K then heating to 300K and allowing the H(a) to desorb as H_2 before cooling again to 200K and repeating the process, the yield of H_2 with each successive heating drops. The interpretation is that adsorption of acetic acid below the desorption temperature of H_2 does not produce a saturated layer of acetate.

It would appear that the fundamental reason that 'explosions' occur is that a sufficient density of adsorbate builds up. Adatoms stabilise the adsorbate and therefore encourage it to form dense areas where, through mutual site blockage as described by Li and Bowker, the conditions for 'explosive' decomposition are met. In addition it would appear that in some cases, a saturated layer of adsorbate can be obtained without the need of a co-adsorbate. The reaction has been successfully modelled in terms of large dense 'islands' of stabilised adsorbate. Once decomposition is initiated at perhaps a step edge or kink the acetates decompose rapidly in an auto-catalytic manner, leaving behind clean decomposition sites, themselves required for the decomposition.

In the light of the single crystal work, it was of considerable interest to study the decomposition of acetic acid on a high area supported catalyst, paying attention to the effect of adsorbed oxygen and to the alumina support. Could the explosion phenomenon be extended to more realistic reaction conditions of high pressure which occur in much of industrial and academic catalysis? It is particularly relevant to understand the behaviour of acetates since they are seen on high area rhodium catalysts under conditions where ethanol can selectively be formed from synthesis gas, furthermore, a rhodium complex is used in the homogeneous carbonylation of methanol to form acetic acid.

4.2. RESULTS.

4.2.1. DECOMPOSITION of ACETIC ACID on BLANK Al_2O_3.

A study was made of the decomposition of glacial acetic acid on a blank alumina catalyst. As with all experiments involving acetic acid presented in this thesis, the acid was dosed onto the catalyst by means of a manual injection of a tiny droplet of the liquid, typically 1 microlitre, via a PTFE septum located in the diluent line up-stream of the catalyst bed (see Figure 2.1.) . One microlitre of acid is equivalent to ~$1x10^{19}$ molecules, this is ample to cover the metal surface area, as 1 microlitre of acetic acid vaporises to 0.392 mls of gas in the diluent stream. The acid vapour was carried to the catalyst bed in the He stream where it was adsorbed. With the diluent stream diverted through the by-pass line, acetic acid vapour was detected by the mass spectrometer, Figure 4.1., as can be seen from the Figure, the majority of the acid vaporises in under two minutes. When the same experiment was conducted with the diluent flowing over the catalyst, Figure 4.2., no acetic acid vapour was detected, indicating it had adsorbed completely. To ensure that all the acetic acid had vaporised, the syringe was left in the diluent stream for approximately two to three minutes.

After heating the blank alumina catalyst to 400°C in flowing hydrogen, maintaining it at 400°C for 30 minutes and then cooling to 50°C, a series of 0.5 ml pulses of oxygen were passed over the catalyst followed by a one microlitre injection of acetic acid. The reason for the oxygen injections was to ensure the blank alumina experiments are directly comparable with the 'explosion' data reported in section 4.2.4. The desorption spectra obtained, Figure 4.3. shows that CO_2 desorption begins very slowly at ~270°C and a high temperature water peak is seen beginning at ~350°C and maximising at ~400°C . Mass 43, indicative of acetic acid (and seen when the vapour is

Figure 4.1.
1 microlitre injection of acetic acid through the by-pass. Temperature = 25°C

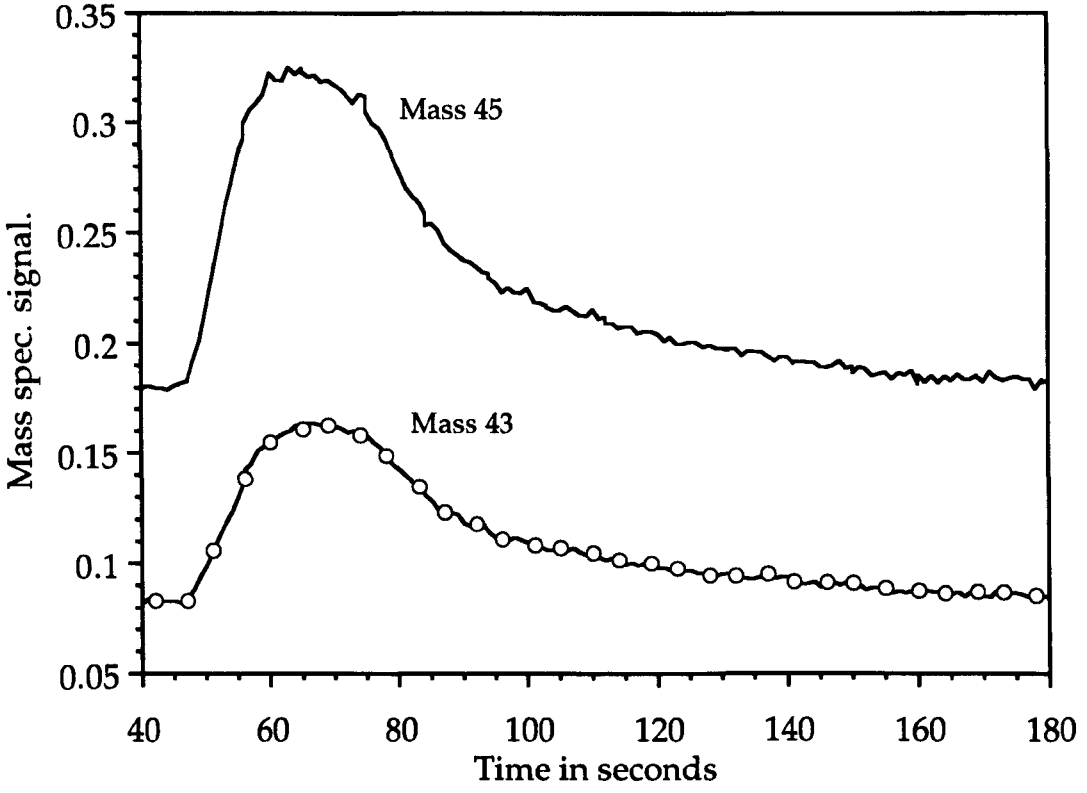

Figure 4.2.
1 microlitre of acetic acid over the catalyst .
Temperature = 50°C .

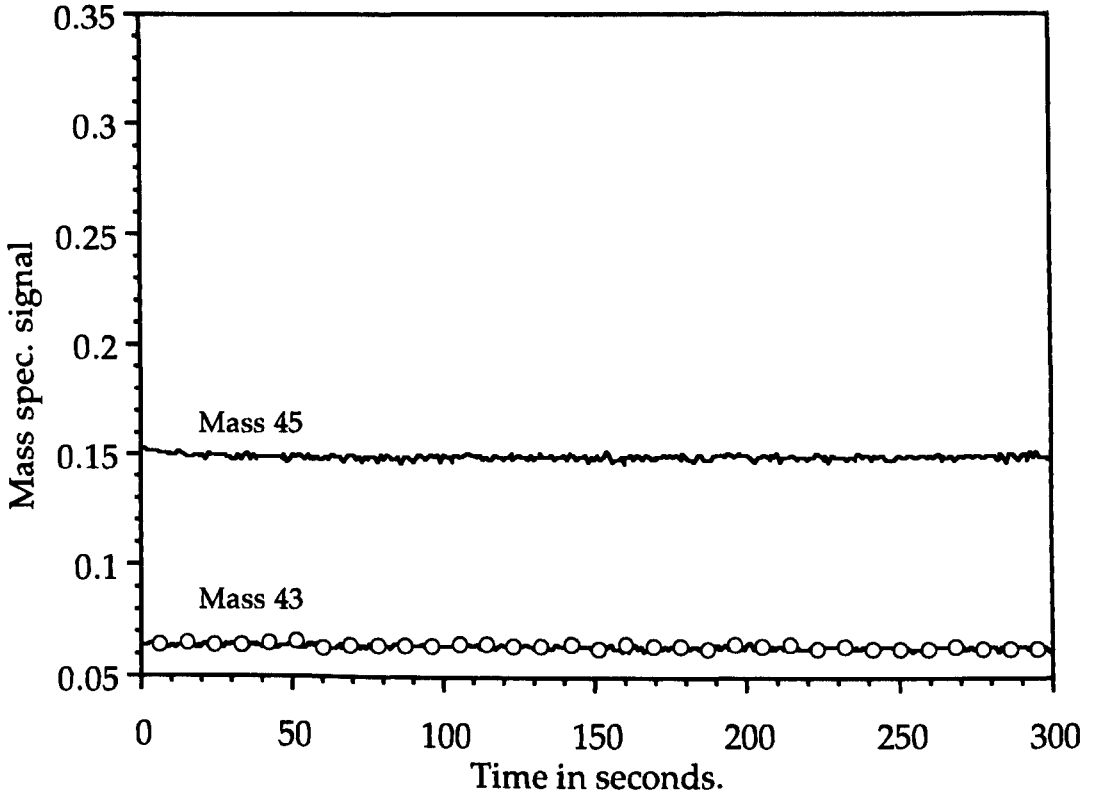

passed through the by-pass line), was seen to desorb in small amounts from the blank alumina under heating, coincident with a small mass 15 peak due primarily to methane desorption, however some is a cracking fraction of the acetic acid, mass 43. No desorption of hydrogen was seen to occur upon adsorption, which is indicative that the acid hydrogens are trapped on the alumina support as hydroxyl groups, which then either combine with a second hydrogen or disproportionate, both processes produce water which desorbs at higher temperatures .

Figure 4.4. shows the decomposition of acetic acid when injected over a hot blank alumina catalyst (catalyst bed temperature - 405°C). From Figure 4.3. it can be seen that the adsorbed surface species are readily decomposing at this temperature, therefore the acetic acid cannot form a stable surface species at 405°C and so decomposes upon adsorption. The evolution of products illustrates clearly the mechanism of the decomposition and is discussed in the results section.

From Figures 4.1-4.4 it is clear that the alumina support is capable of adsorbing acetic acid and the surface species decompose upon heating, forming predominantly water, carbon dioxide and methane. As will be shown in section 4.2.4. the 'explosive' acetate spectra are very different. The desorption profiles here are broad and no evidence is seen of 'explosive' decomposition behaviour, therefore the alumina support alone can be discounted when explaining the 'explosion' phenomenon on the Rh/Al_2O_3 catalyst.

Figure 4.3.
T.P.D. of 1 microlitre of acetic acid adsorbed onto blank alumina at 100°C

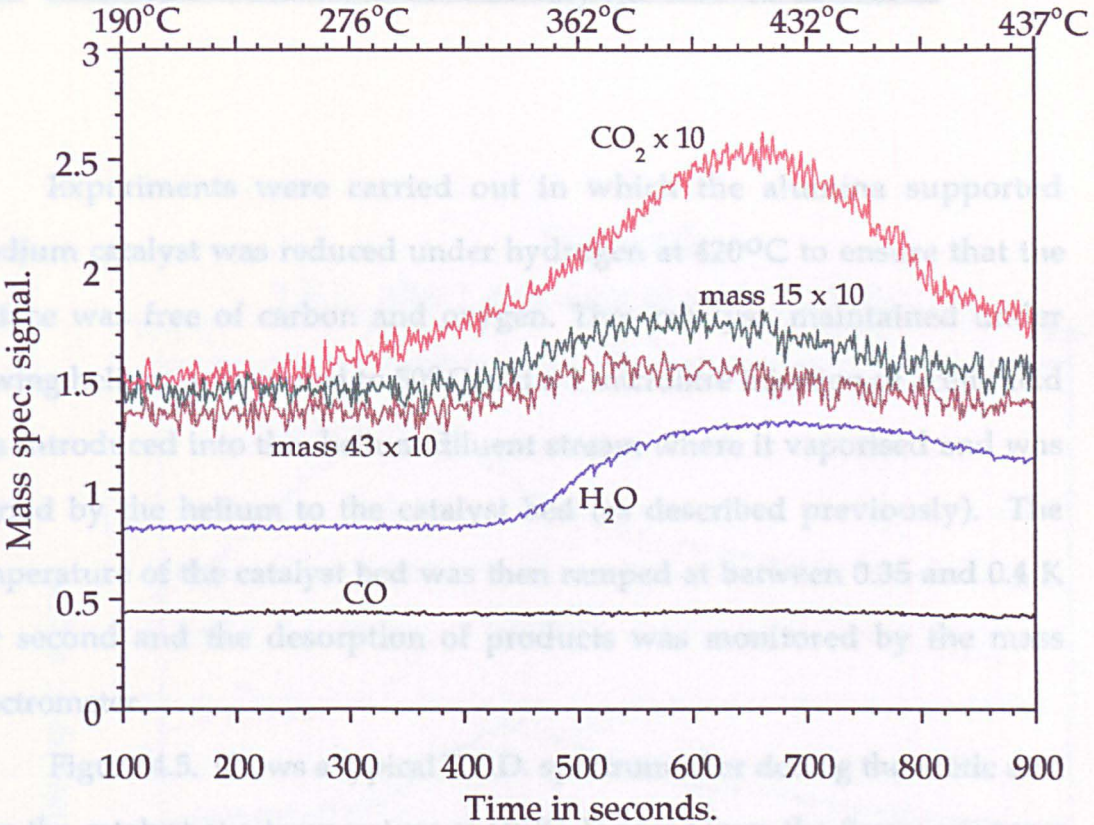

Figure 4.4.
1 microlitre of acetic acid injected over blank alumina.
Temperature = 405°C

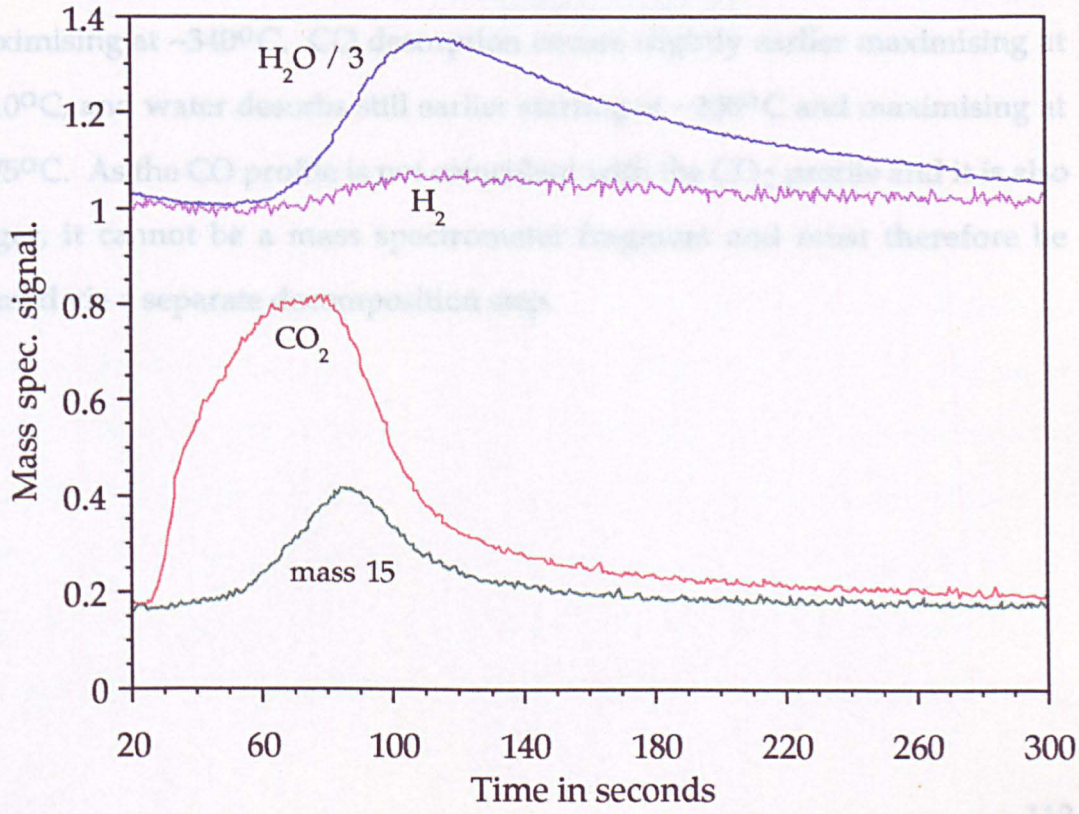

4.2.2. ACETIC ACID DOSES ONTO Rh/Al_2O_3 WITH NO OXYGEN.

Experiments were carried out in which the alumina supported rhodium catalyst was reduced under hydrogen at 420°C to ensure that the surface was free of carbon and oxygen. The catalyst, maintained under flowing helium, was cooled to 50°C and a 1 microlitre injection of acetic acid was introduced into the helium diluent stream where it vaporised and was carried by the helium to the catalyst bed (as described previously). The temperature of the catalyst bed was then ramped at between 0.35 and 0.4 K per second and the desorption of products was monitored by the mass spectrometer.

Figure 4.5. shows a typical T.P.D. spectrum after dosing the acetic acid onto the catalyst at a temperature of 60°C. Evident from the figure are some of the characteristic desorption profiles seen from the blank alumina catalyst namely CO_2 and CH_4 although the temperature of decomposition has been reduced by ~70°C. The majority of the adsorbed acetate begins to decompose at around 250°C with the broad desorption profiles for CO_2 and CH_4 maximising at ~340°C, CO desorption occurs slightly earlier maximising at ~310°C, and water desorbs still earlier starting at ~200°C and maximising at ~275°C. As the CO profile is not coincident with the CO_2 profile and it is also larger, it cannot be a mass spectrometer fragment and must therefore be formed via a separate decomposition step.

Figure 4.5.

T.P.D. after 1 microlitre of acetic acid at 60°C.

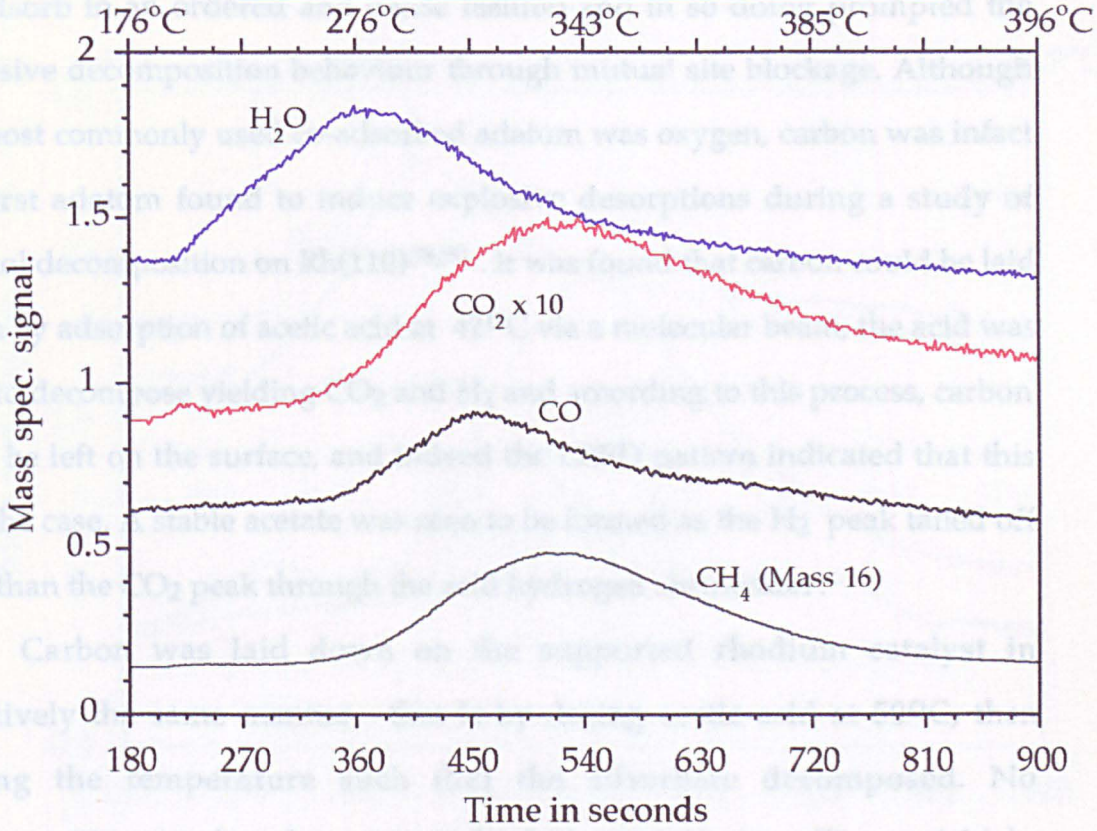

4.2.3. SUCCESSIVE ACETIC ACID DOSES WITH T.P.D. on Rh/Al_2O_3.

From the single crystal work of Bowker et al. it was shown that the existence of an adatom, co-adsorbed with the acetate group induced the latter to adsorb in an ordered and dense fashion and in so doing prompted the explosive decomposition behaviour through mutual site blockage. Although the most commonly used co-adsorbed adatom was oxygen, carbon was infact the first adatom found to induce explosive desorptions during a study of ethanol decomposition on Rh(110)[38,50] . It was found that carbon could be laid down by adsorption of acetic acid at 42°C via a molecular beam, the acid was seen to decompose yielding CO_2 and H_2 and according to this process, carbon must be left on the surface, and indeed the LEED pattern indicated that this was the case. A stable acetate was seen to be formed as the H_2 peak tailed off later than the CO_2 peak through the acid hydrogen abstraction .

Carbon was laid down on the supported rhodium catalyst in effectively the same manner, that is by dosing acetic acid at 50°C, then raising the temperature such that the adsorbate decomposed. No decomposition was found to occur at the dosing temperature. Figures 4.6.(a) - (e) show a series of experiments in which acetic acid was dosed at 50°C, then a temperature programmed desorption was conducted, before the catalyst was cooled to 50°C when the process was repeated, no hydrogen cleaning of the catalyst was carried out, therefore C(a) was successively laid down with each T.P.D. The onset of water desorption, mass 18, begins at 190°C, this is accompanied by a slight desorption of methane and carbon dioxide, masses 15 and 44. The water peak reaches a maximum at ~270-275°C and is not directly coincident with any other mass, although there are overlapping desorptions. A large and obvious mass 28 peak begins to desorb at ~272°C and reaches a maximum at ~308°C. Between 250-260°C

Figure 4.6.(a)
T.P.D. after 1 microlitre of acetic acid adsorbed at 50°C , onto clean catalyst.

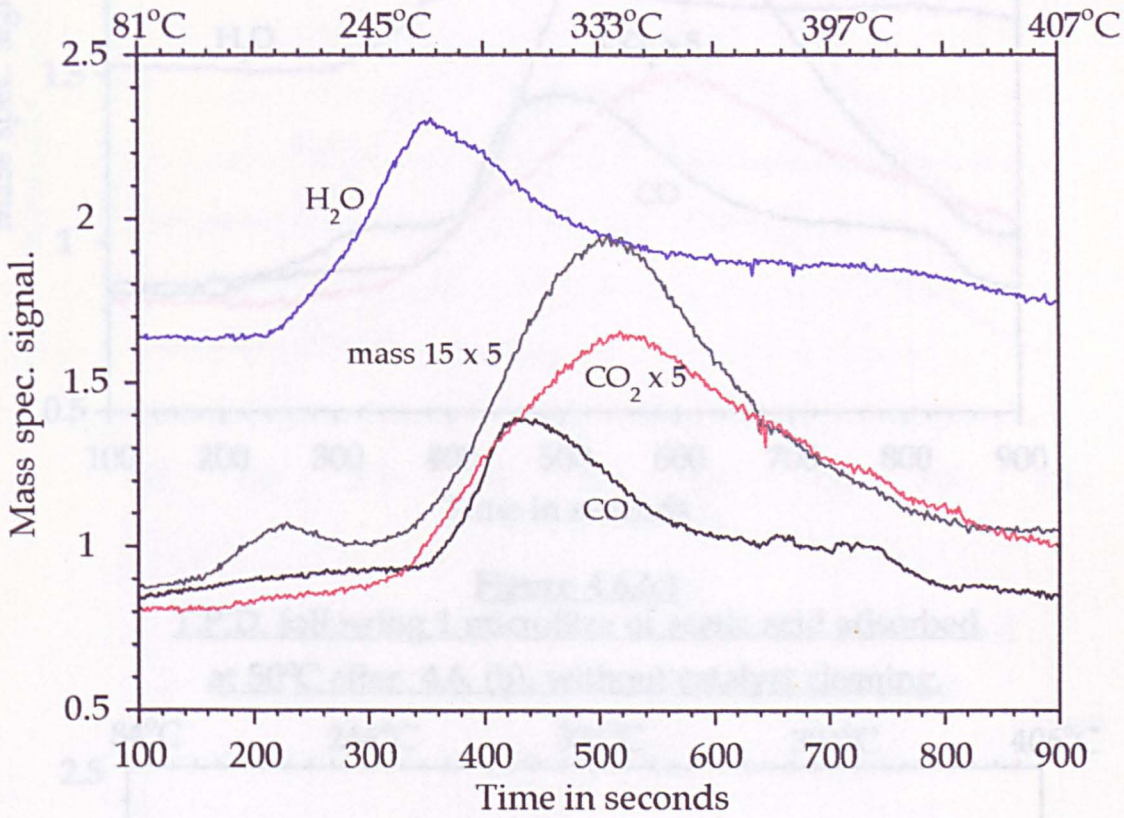

Figure 4.6.(b)
T.P.D. following 1 microlitre of acetic acid adsorbed at 50°C, after 4.6.(a) without catalyst cleaning.

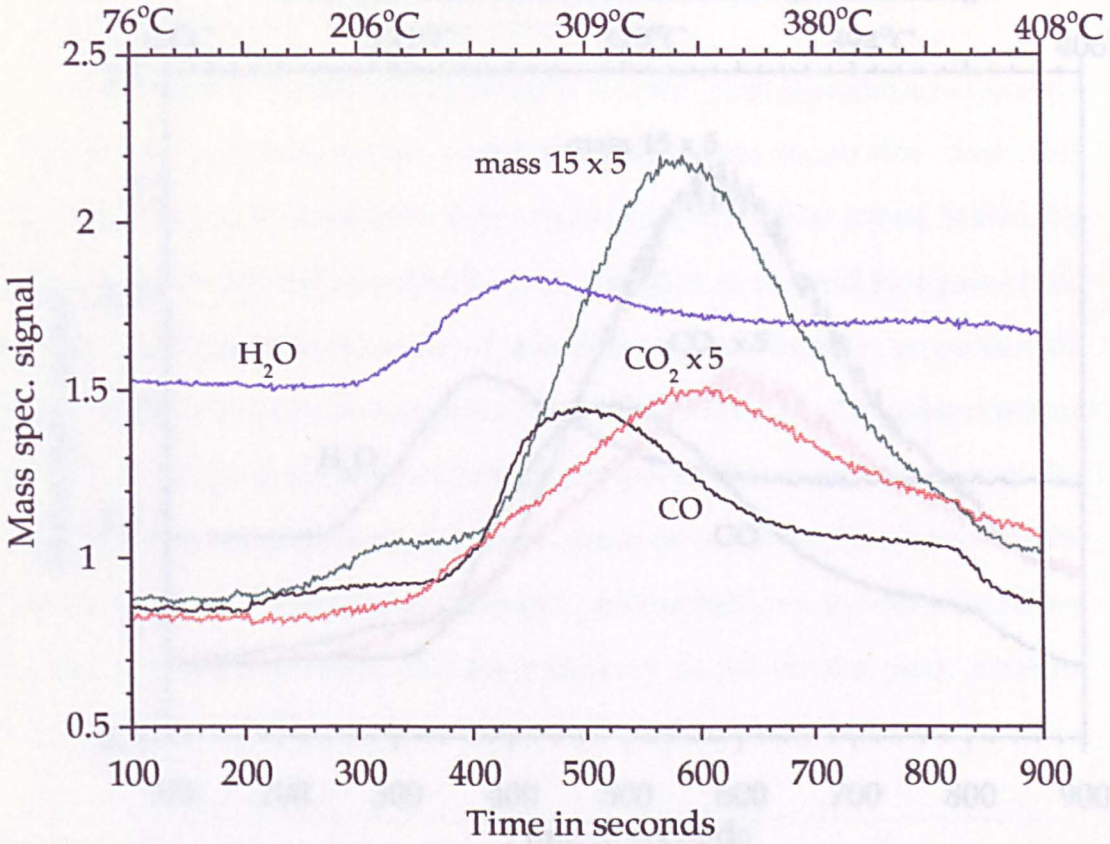

Figure 4.6.(c)
T.P.D. following 1 microlitre of acetic acid adsorbed at 50°C after 4.6. (b). without catalyst cleaning.

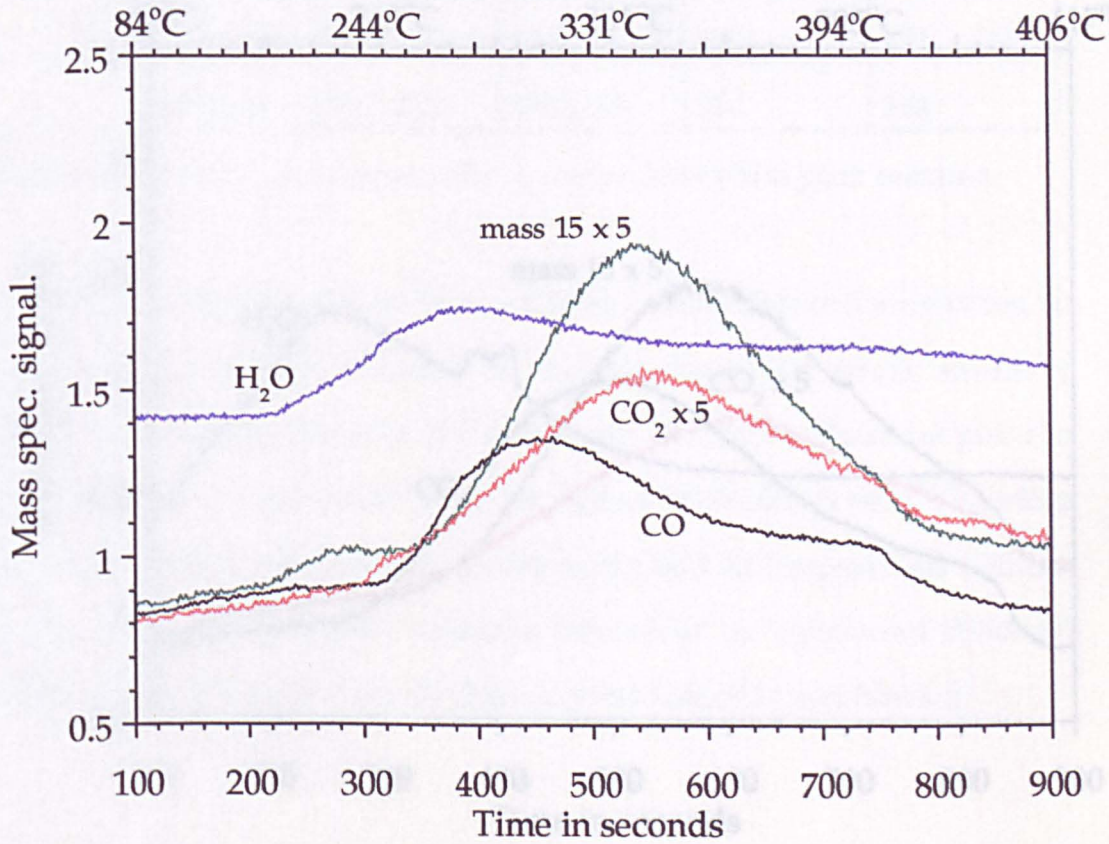

Figure 4.6.(d)
T.P.D.following 3 microlitres of acetic acid adsorbed at 50°C, after 4.6.(c) without catalyst cleaning.

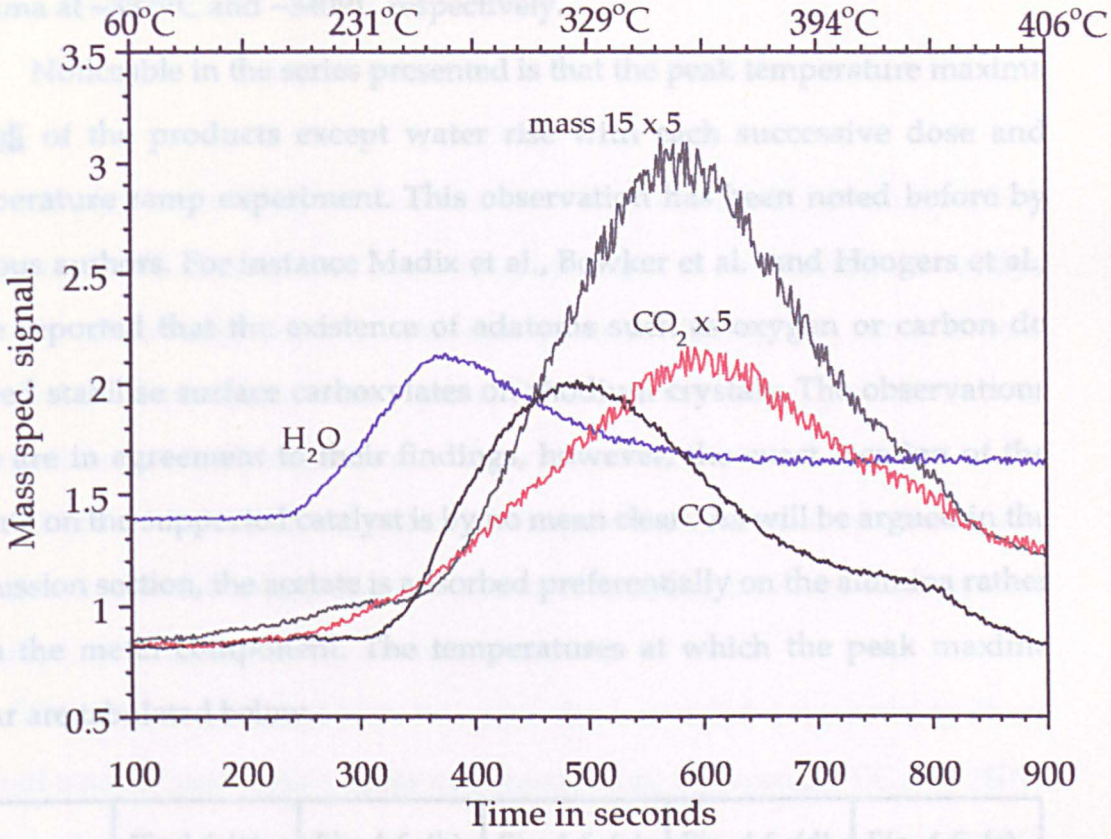

Figure 4.6. (e)
T.P.D. following 3 microlitres of acetic acid adsorbed at 50°C, after 4.6.(d) without catalyst cleaning.

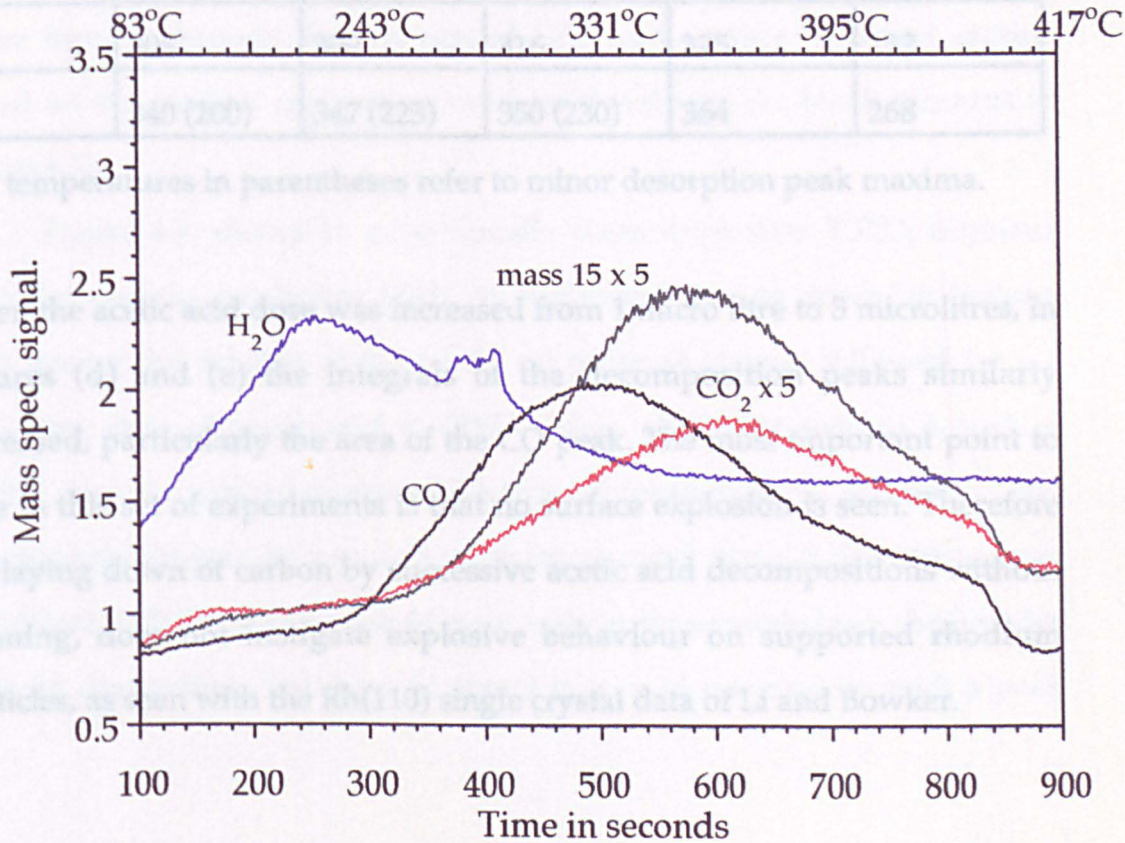

masses 15 and 44, (methane and carbon dioxide), begin to desorb, reaching maxima at ~337°C and ~340°C respectively.

Noticeable in the series presented is that the peak temperature maxima for all of the products except water rise with each successive dose and temperature ramp experiment. This observation has been noted before by various authors. For instance Madix et al., Bowker et al. and Hoogers et al., have reported that the existence of adatoms such as oxygen or carbon do indeed stabilise surface carboxylates on rhodium crystals. The observations here are in agreement to their findings, however, the exact location of the acetate on the supported catalyst is by no mean clear . As will be argued in the discussion section, the acetate is adsorbed preferentially on the alumina rather than the metal component. The temperatures at which the peak maxima occur are tabulated below.

Mass	*Fig 4.6 (a)*	*Fig. 4.6. (b)*	*Fig. 4.6. (c)*	*Fig. 4.6. (d)*	*Fig. 4.6. (e)*
15	337 (200)	341 (223)	346 (234)	357 (230)	355
18	272	285	285	272	220
28	308	309	316	325	232
44	340 (200)	347 (223)	350 (230)	364	268

The temperatures in parentheses refer to minor desorption peak maxima.

When the acetic acid dose was increased from 1 micro litre to 3 microlitres, in Figures (d) and (e) the integrals of the decomposition peaks similarly increased, particularly the area of the CO peak. The most important point to note in this set of experiments is that no surface explosion is seen. Therefore the laying down of carbon by successive acetic acid decompositions without cleaning, does not instigate explosive behaviour on supported rhodium particles, as seen with the Rh(110) single crystal data of Li and Bowker.

4.2.4. ACETIC ACID DOSES ONTO OXYGEN PRE-DOSED Rh/Al_2O_3 CATALYST.

Experiments were carried out in which the rhodium catalyst was heated to 420°C and reduced in flowing hydrogen to ensure that the catalyst was cleaned of any deposits and that prior to dosing the catalyst with adsorbates, the surface was standardised i.e. the same procedure was followed before each experiment. The catalyst was cooled to 50°C and a controlled number of 0.5 ml pulses of oxygen were introduced. Acetic acid was dosed onto the oxygen pre-covered catalyst using the same experimental technique as described in the above section.

The T.P.D. obtained after this procedure revealed a remarkably sharp peak of mass 44 seen over a range of temperatures, between 207°C and 260°C at the two extremes, but normally the peak temperature was between 220°C - 240°C. Near coincident with the mass 44 peak is a mass 18 peak, this peak is often masked by a broader mass 18 desorption, caused by the desorption of water formed through the reaction of H(a) and surface hydroxyl groups found on the catalyst support, as seen previously on the blank alumina in Figure 4.3.

Figure 4.7. shows an exceptionally clean 'explosive' T.P.D. acquired after cleaning the catalyst at 420°C in hydrogen, cooling down in helium, then dosing the catalyst with one 0.5 ml pulse of oxygen followed by a 1 microlitre dose of acetic acid at 45°C. Mass 18 is first seen to desorb at ~116°C forming a broad profile which tails off between 300°C and 400°C, it is interrupted mid-way by a second more pronounced mass 18 desorption near coincident with the sharp mass 44 peak and clearly separate from the broader mass 18 desorption. The mass 44 signal is seen to rise rapidly with a peak

Figure 4.7.
T.P.D. showing exceptionally clean acetate 'explosion'
after 1 microlitre of acetic acid at 45°C
on catalyst pre-dosed with 0.5 mls of oxygen.

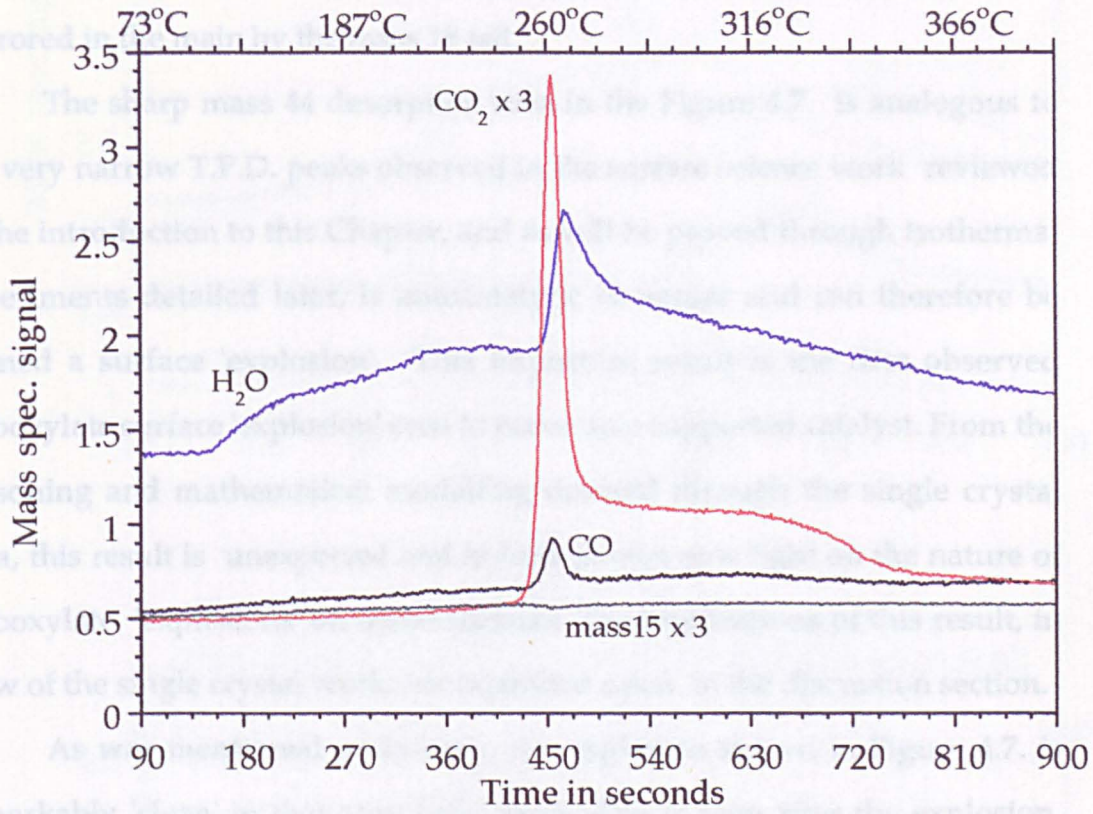

maximum occurring at 260°C and is only 7°C in width at half its maximum height.

This result is remarkable as desorption profiles of adsorbates from single crystals are typically around 30°C in width at half their maximum height, and supported catalysts often exhibit desorptions of ~100°C in width. Following this sharp rapid desorption peak is a broader mass 44 desorption mirrored in the main by the mass 18 tail.

The sharp mass 44 desorption seen in the Figure 4.7. is analogous to the very narrow T.P.D. peaks observed in the surface science work reviewed in the introduction to this Chapter, and as will be proved through isothermal experiments detailed later, is autocatalytic in nature and can therefore be termed a surface 'explosion'. This important result is the first observed carboxylate surface 'explosion' seen to occur on a supported catalyst. From the reasoning and mathematical modelling devised through the single crystal data, this result is unexpected and indeed throws new light on the nature of carboxylate 'explosions' on metal surfaces. The implications of this result, in view of the single crystal work, are expanded upon in the discussion section.

As was mentioned previously, the explosion shown in Figure 4.7. is remarkably 'clean' in that very little desorption is seen after the explosion. Two more typical 'explosive' T.P.D. are shown in Figures 4.8.(a) and (b). In Figure 4.8. (a), the 'explosion' occurs at ~210°C and in Figure 4.8.(b) at 230°C- considerably lower than in Figure 4.7. - and in contrast to it there is a more prominent mass 44 desorption profile after the explosion. In Figures 4.8.(a) and (b) an obvious dip is apparent in the broad mass 44 desorption peak seen above the explosion temperature. The dip is causes by the over-lap of two decomposition processes, each producing CO_2. The lower temperature process yields CO_2 (mass 44) in conjunction with water (mass 18), whereas the higher temperature process yields CO_2 and methane (mass 15). This was found to be a general trend when injecting acetic acid onto the oxygen pre-

Figure 4.8. (a)
A typical 'explosive' acetate desorption, with higher temperature desorptions due to contributions from the support.

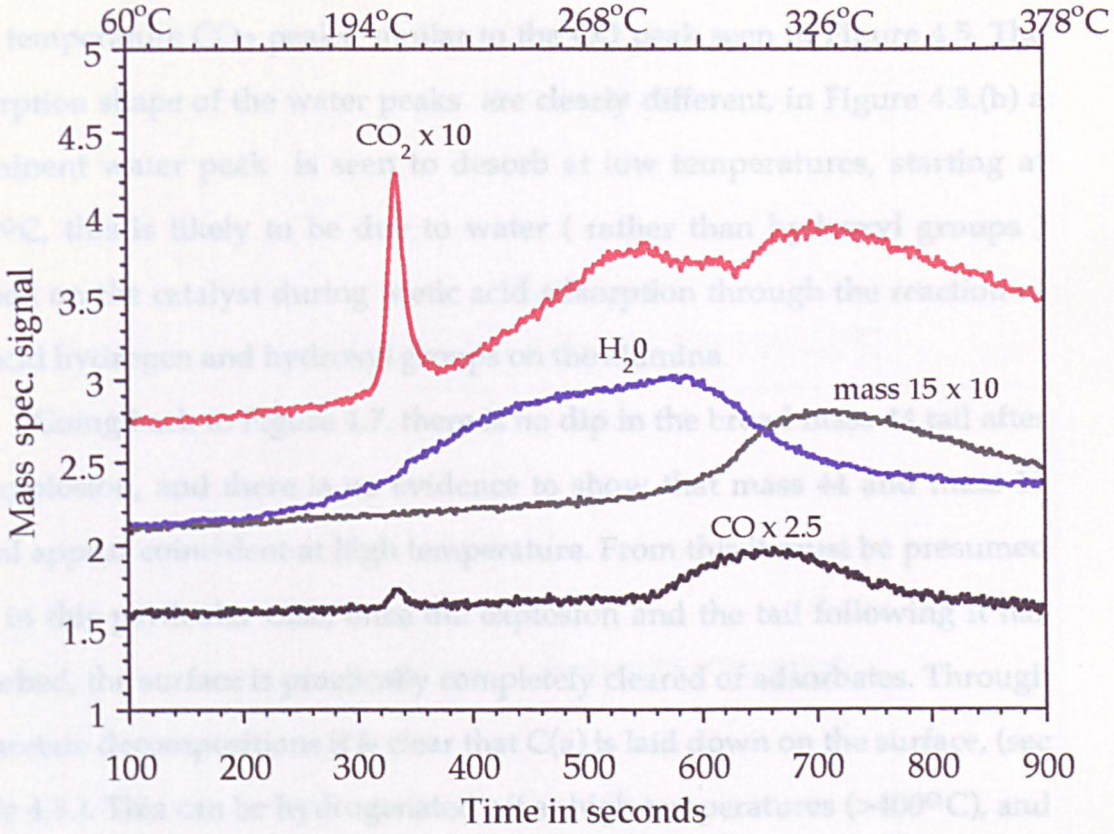

Figure 4.8. (b)
A typical 'explosive' acetate decomposition after dosing1.5mls of O_2 and 1 microlitre of acetic acid.

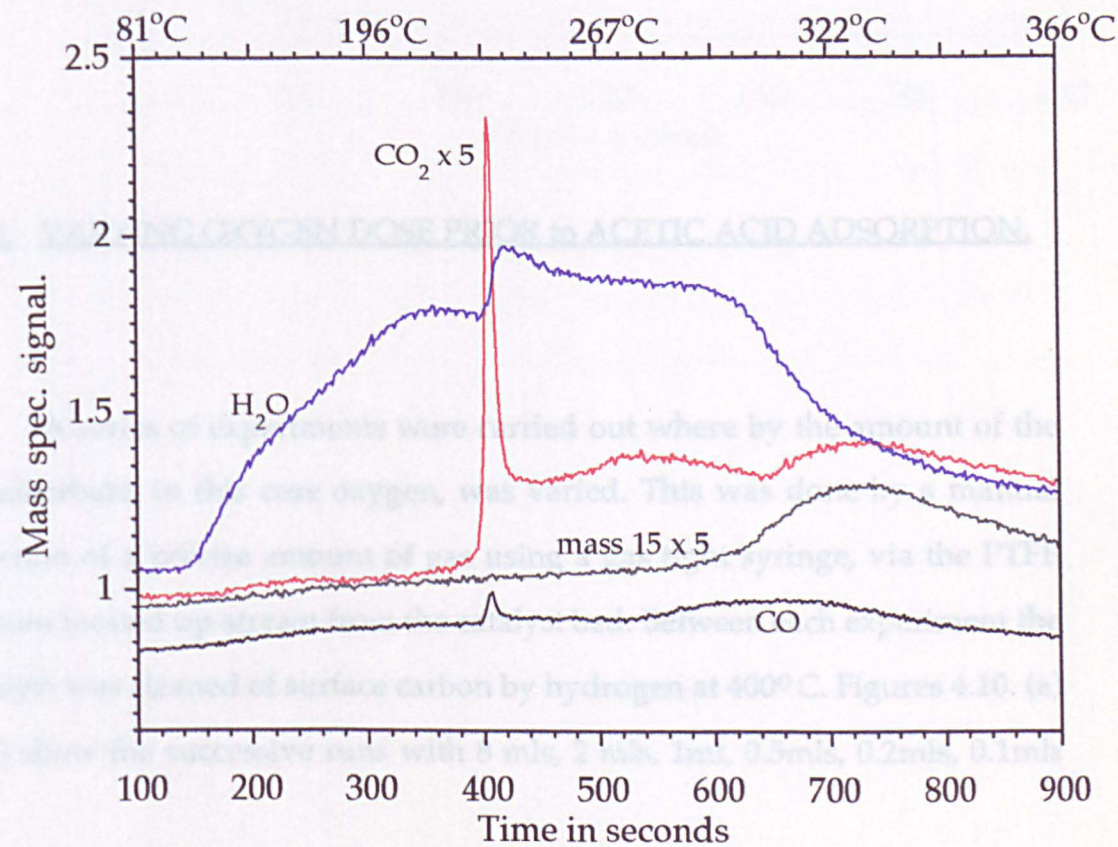

dosed catalyst. There is a CO desorption peak maximising between the two high temperature CO_2 peaks, similar to the CO peak seen in Figure 4.5. The desorption shape of the water peaks are clearly different, in Figure 4.8.(b) a prominent water peak is seen to desorb at low temperatures, starting at ~100°C, this is likely to be due to water (rather than hydroxyl groups) formed on the catalyst during acetic acid adsorption through the reaction of the acid hydrogen and hydroxyl groups on the alumina.

Going back to Figure 4.7. there is no dip in the broad mass 44 tail after the explosion, and there is no evidence to show that mass 44 and mass 15 signal appear coincident at high temperature. From this it must be presumed that in this particular case, once the explosion and the tail following it has desorbed, the surface is practically completely cleared of adsorbates. Through the acetate decompositions it is clear that C(a) is laid down on the surface, (see Table 4.3.). This can be hydrogenated off at high temperatures (>400°C), and Figure 4.9. shows the production of methane during cleaning following an explosive decomposition and it is apparent that the majority of the carbon is reacted to methane in the first ten seconds of hydrogenation.

4.2.5. VARYING OXYGEN DOSE PRIOR to ACETIC ACID ADSORPTION.

A series of experiments were carried out where by the amount of the co-adsorbate, in this case oxygen, was varied. This was done by a manual injection of a precise amount of gas using a gas tight syringe, via the PTFE septum located up-stream from the catalyst bed. Between each experiment the catalyst was cleaned of surface carbon by hydrogen at 400°C. Figures 4.10. (a) - (g) show the successive runs with 8 mls, 2 mls, 1ml, 0.5mls, 0.2mls, 0.1mls

Figure 4.9.

C(a) clean off with hydrogen at 400°C

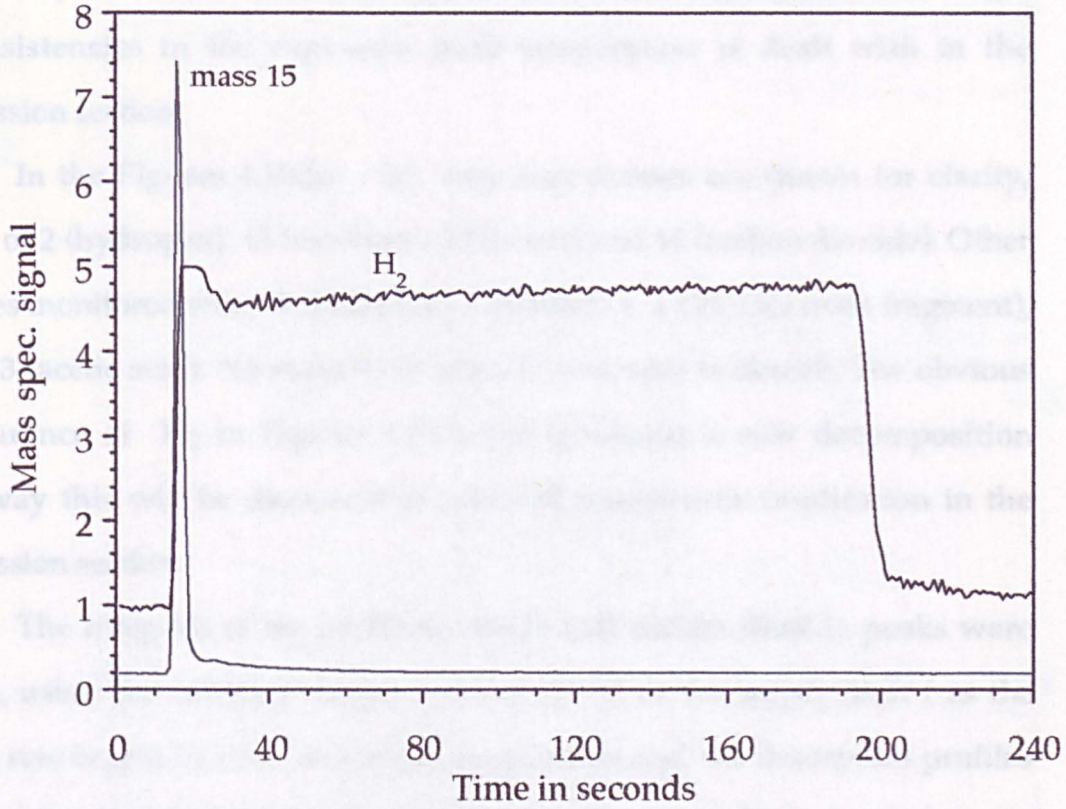

and 0.05 mls of oxygen respectively. The oxygen and acetic acid were dosed onto the catalyst at between 40°C and 50°C, the acid dose was 1 microlitre in each case. The explosion does not occur at exactly the same time after the start of the data acquisition, simply because the oven temperature at time = 0 varied slightly. The ramp rate however was equal in each experiment and indeed more importantly the temperature at which the explosion occurred is practically constant, centering around 228°C. The reasons for the slight inconsistencies in the explosion peak temperature is dealt with in the discussion section.

In the Figures 4.10.(a) - (g), only four masses are shown for clarity, those of 2 (hydrogen), 15 (methane), 18 (water) and 44 (carbon dioxide). Other masses monitored were 31 (methanol / ethanol i.e. a CH_2OH mass fragment), and 43 (acetic acid). No mass 43 or mass 31 was seen to desorb. The obvious appearance of H_2 in Figures 4.9.(f) and (g) marks a new decomposition pathway this will be discussed in terms of mechanistic implication in the discussion section.

The integrals of the methane, water and carbon dioxide peaks were taken, using the arbitrary temperature of 390°C as the upper limit (as the ramp rate begins to slow above this temperature and the desorption profiles elongate) and the start of each desorption as the lower limit. It can be seen that with oxygen doses from 8 mls to 0.5mls, the yield of all three masses does not change dramatically but drops slightly - mass 15 shows a 16% reduction from its maximum yield, water 14% and carbon dioxide 23%. When the oxygen dose is reduced to 0.2 mls a further change is seen, with water and methane production continuing to drop but carbon dioxide remaining near constant. When the oxygen dose is reduced to just 0.1ml and less Figures 4.9. (f) and (g), a change in decomposition mechanism is seen after the sharp 'explosive' peak, with a decline in the lower temperature carbon dioxide

Figure 4.10.(a)
Explosive T.P.D. after pre-dose of 8 mls of O_2
then 1 microlitre of acetic acid

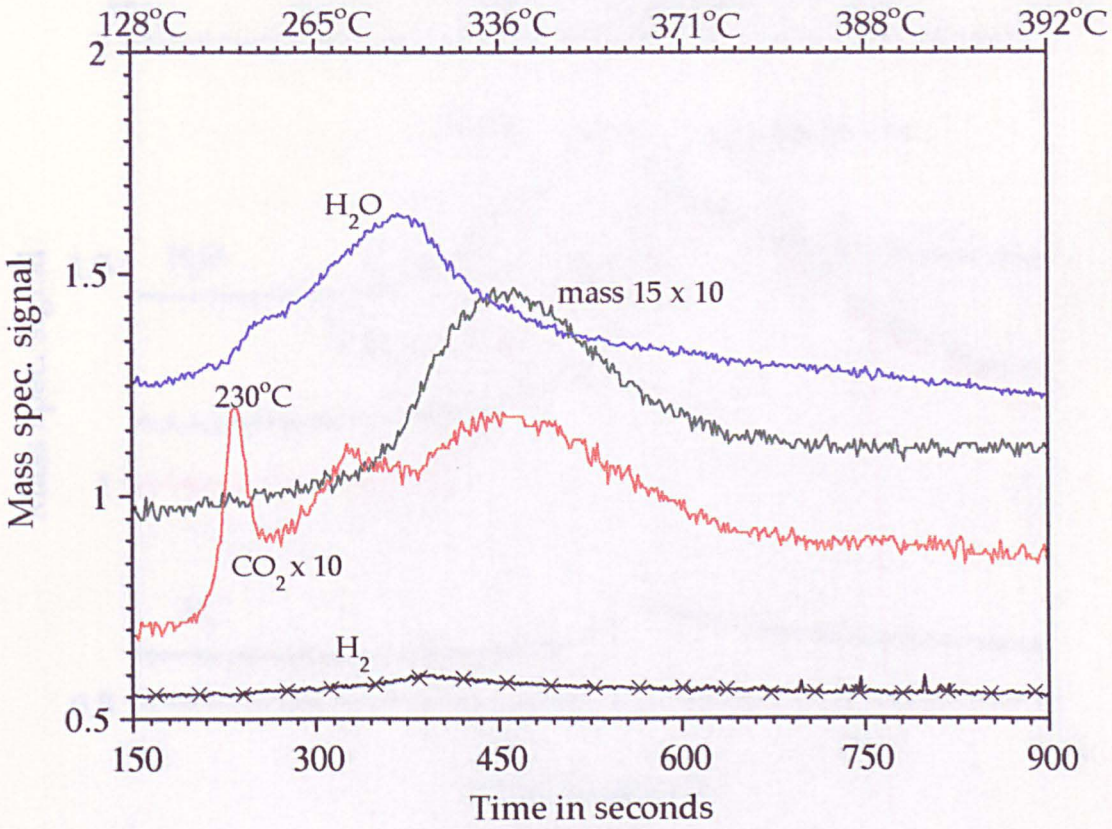

Figure 4.10. (b)
Explosive T.P.D. after pre-dose of 2 mls O_2
then 1 microlitre of acetic acid.

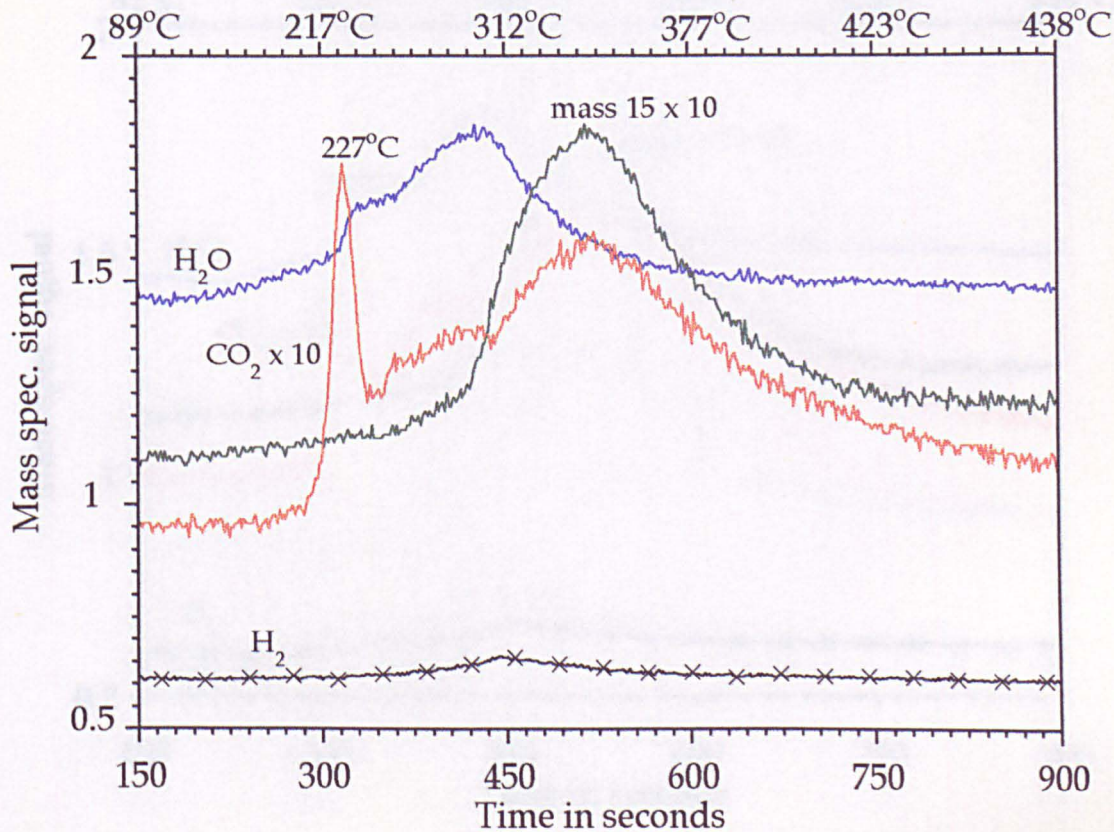

Figure 4.10.(c)
Explosive T.P.D. after pre-dose of 1ml of O_2
then 1 microlitre of acetic acid.

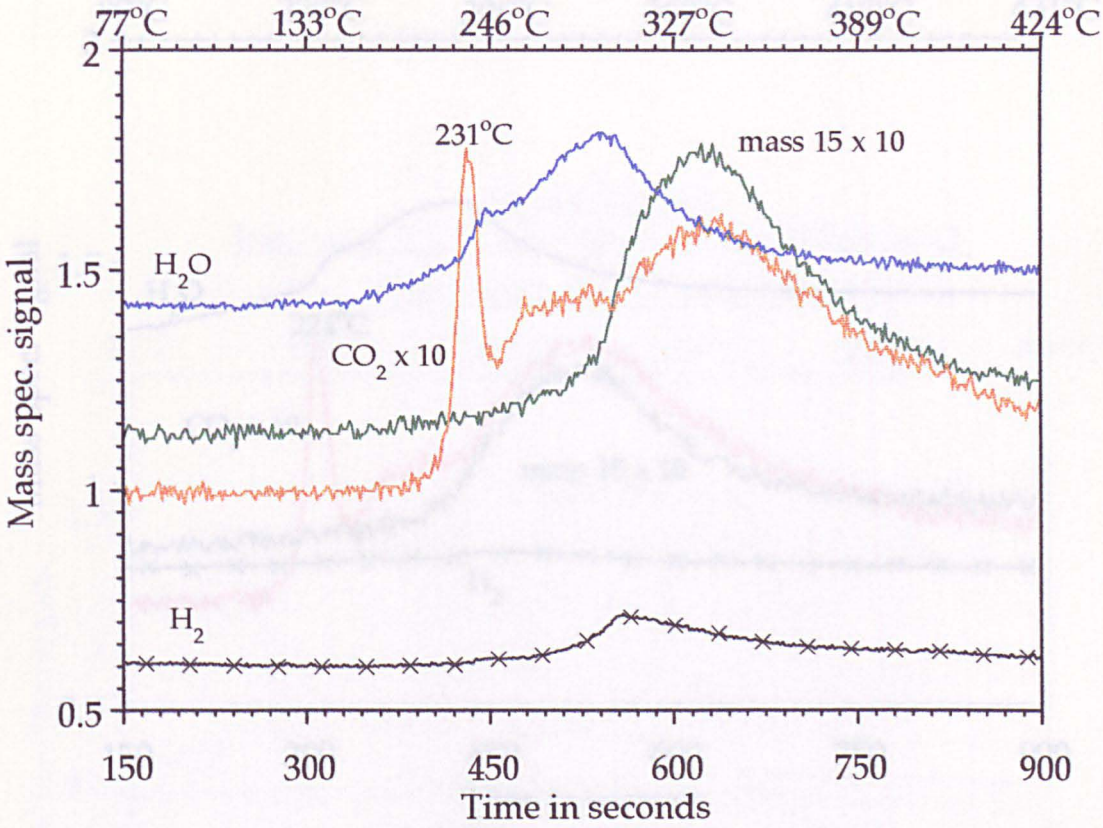

Figure 4.10. (d)
Explosive T.P.D. after pre-dose of 0.5 mls of O_2
then 1 microlitre of acetic acid.

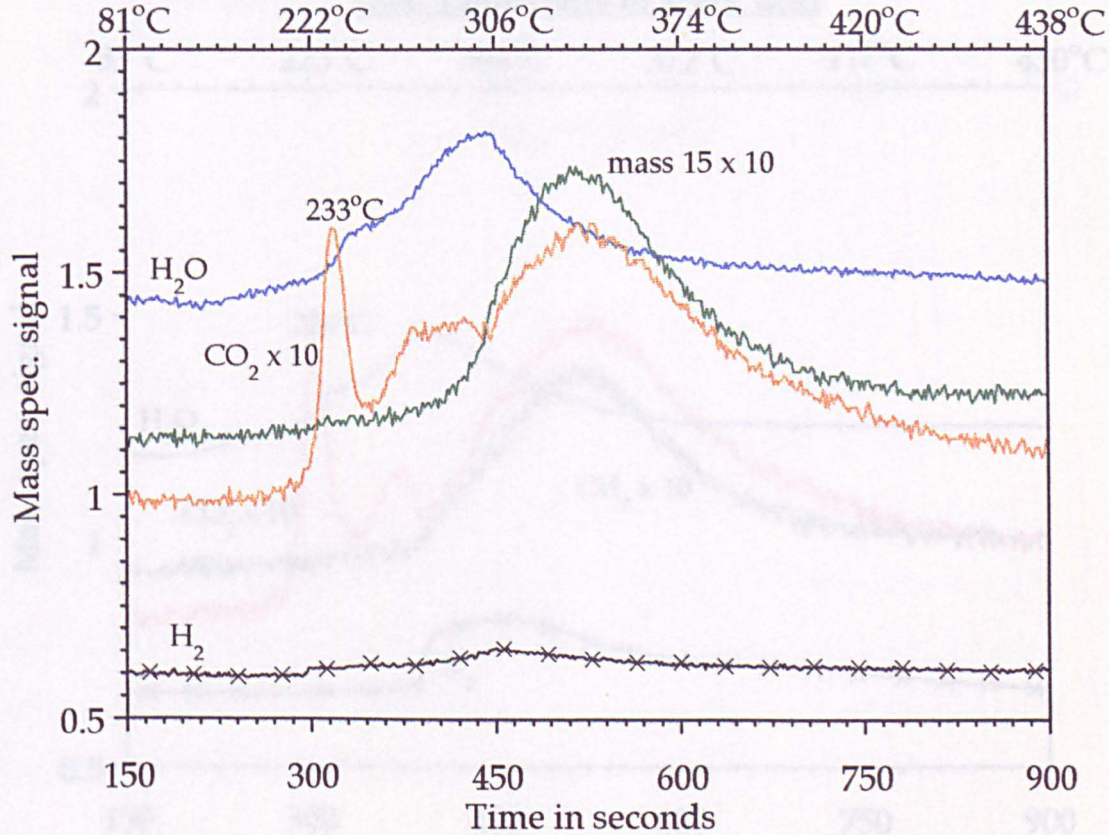

Figure 4.10. (e)
Explosive T.P.D. after pre-dose of 0.2 mls of O_2
then 1 microlitre of acetic acid.

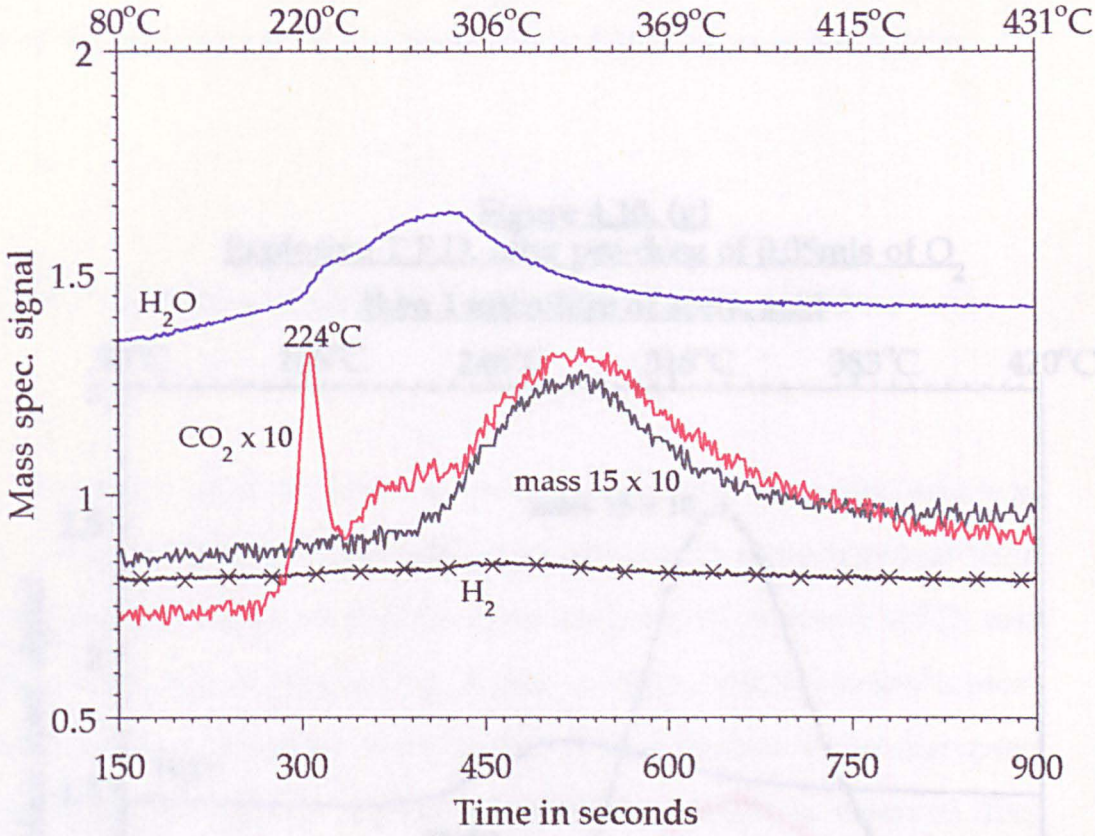

Figure 4.10. (f)
Explosive T.P.D. after pre-dose 0.1 mls of O_2
then 1 microlitre of acetic acid

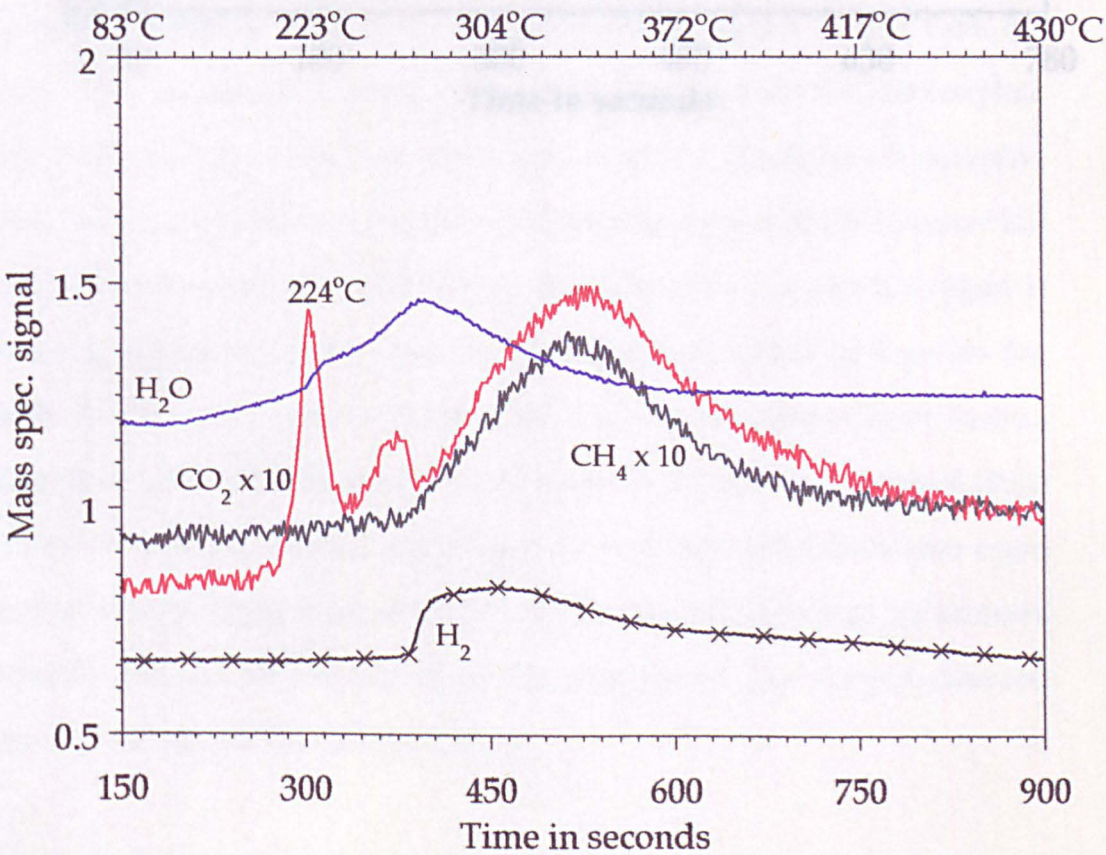

Figure 4.10. (g)
Explosive T.P.D. after pre-dose of 0.05mls of O_2
then 1 microlitre of acetic acid

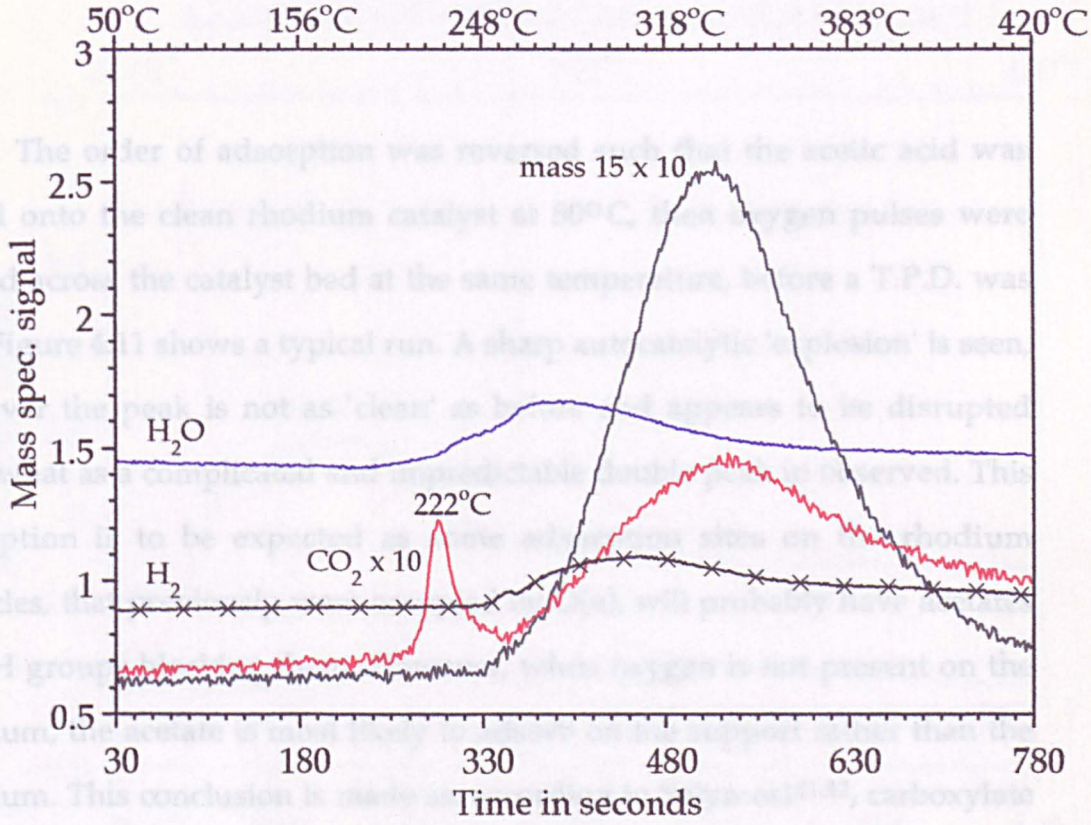

desorption and the emergence of a prominent hydrogen peak appearing at the on-set of the methane and higher temperature carbon dioxide desorption.

4.2.6. ACETIC ACID ADSORPTION PRIOR to OXYGEN ADSORPTION.

The order of adsorption was reversed such that the acetic acid was dosed onto the clean rhodium catalyst at 50°C, then oxygen pulses were passed across the catalyst bed at the same temperature, before a T.P.D. was run. Figure 4.11 shows a typical run. A sharp autocatalytic 'explosion' is seen, however the peak is not as 'clean' as before and appears to be disrupted somewhat as a complicated and unpredictable double peak in observed. This disruption is to be expected as some adsorption sites on the rhodium particles, that previously were occupied by O(a), will probably have acetates or OH groups blocking them. However, when oxygen is not present on the rhodium, the acetate is most likely to adsorb on the support rather than the rhodium. This conclusion is made as, according to Solymosi[41,42], carboxylate species preferentially reside on the support with a rhodium on alumina catalyst. In addition, the support does not adsorb oxygen (from Chapter III) however it does adsorb the acid (Figure 4.2), the order in which oxygen is adsorbed therefore will not effect the adsorption of acetate groups on the support and to add credence to this view, the higher temperature carbon dioxide, water and methane peaks are virtually unchanged in Figures 4.10.(a) - (g) despite the changes in the oxygen pre-dose. As an explosion is seen upon reversal of oxygen injections and acetic acid dosing, it is clear that the acetates are mobile enough to migrate from the support to the oxygen covered rhodium particles, and be stabilised there.

Figure 4.11.
Reversed order of adsorption resulting in distorted explosion
(1 microlitre of acetic acid followed by 4 ml O_2 dose)

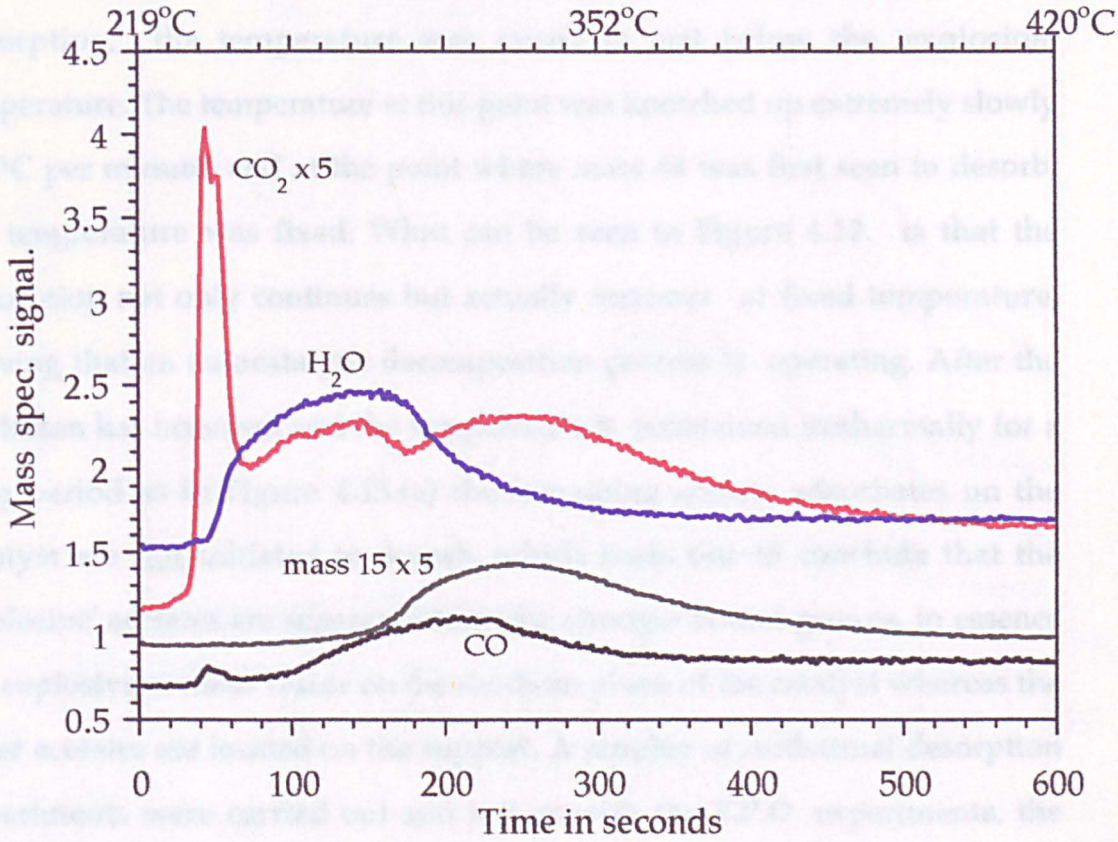

4.2.7. PROOF of AUTO-CATALYTIC EXPLOSION.

To test whether the 'explosive' decomposition was autocatalytic a carefully prepared experiment was carried out where-by after pre-treating the catalyst in the normal manner, that is reducing at high temperature, cooling to room temperature and dosing with oxygen followed by acetic acid adsorption, the temperature was raised to just below the 'explosion' temperature. The temperature at this point was knotched up extremely slowly (~1°C per minute) and at the point where mass 44 was first seen to desorb, the temperature was fixed. What can be seen in Figure 4.12. is that the desorption not only continues but actually *increases* at fixed temperature, proving that an autocatalytic decomposition process is operating. After the explosion has occurred and the temperature is maintained isothermally for a long period as in Figure 4.13.(a) the remaining acetate adsorbates on the catalyst are not initiated to desorb, which leads one to conclude that the 'explosive' acetates are separated from the stronger bound groups, in essence the explosive acetates reside on the rhodium phase of the catalyst whereas the other acetates are located on the support. A number of isothermal desorption experiments were carried out and just as with the T.P.D. experiments, the exact temperature at which the explosion occurred proved to be somewhat unpredictable, however the average temperature was found to be around 217°C. This is higher than the explosion temperature on Rh(110)[50] where the explosion temperature was ~100-120°C and slightly higher than the explosion temperature on Rh(111)[51] 120°C-220°C. which was found to be highly dependent on the amount of pre-adsorbed oxygen.

In Figure 4.12., and Figure 4.13(b) once the explosive peak had desorbed, the temperature was ramped again and the more strongly bound species associated with the support were seen to desorb. The two different

Figure 4.12. Isothermal desorption of acetate confirming the autocatalytic 'explosion' phenomenon.

[Pre-treatment; 4 mls O_2 then1 microlitre of acetic acid at 50°C]

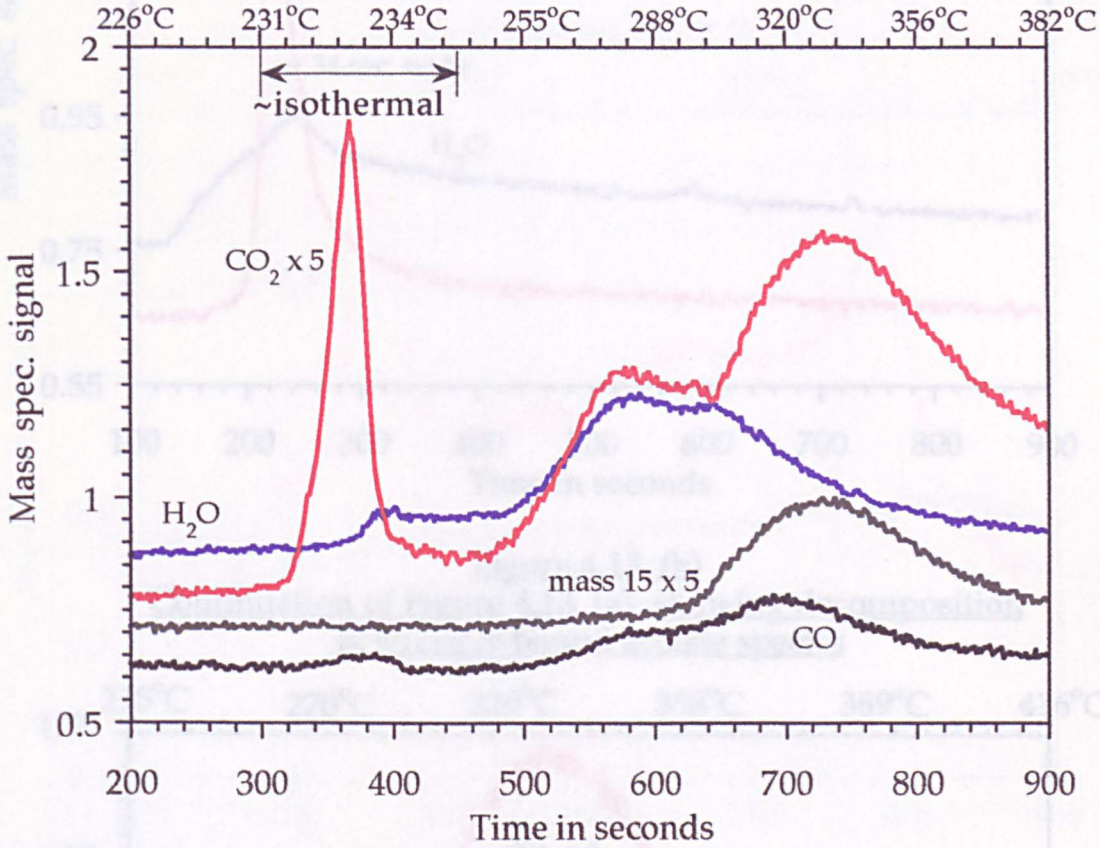

Figure 4.13. (a)
Isothermal plot showing no desorption after the explosion.

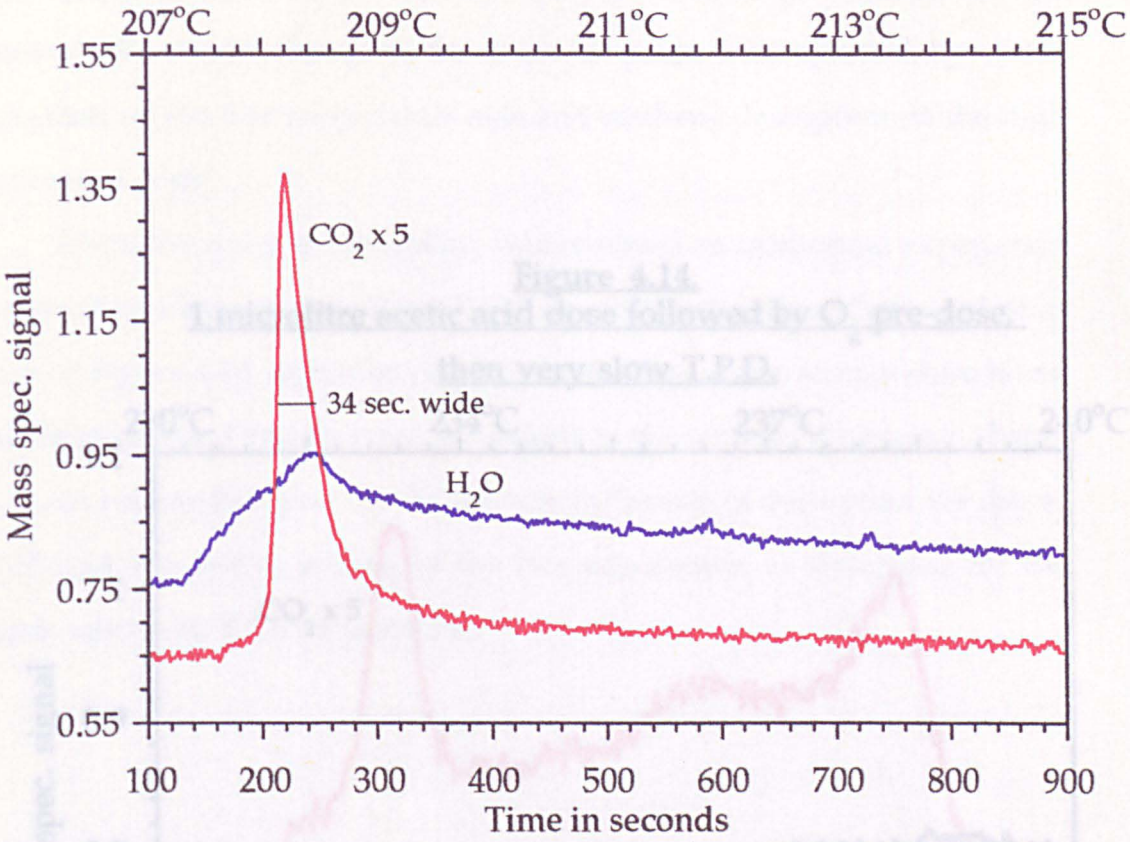

Figure 4.13. (b)
Continuation of Figure 4.13. (a) showing decomposition of strongly bound acetate species

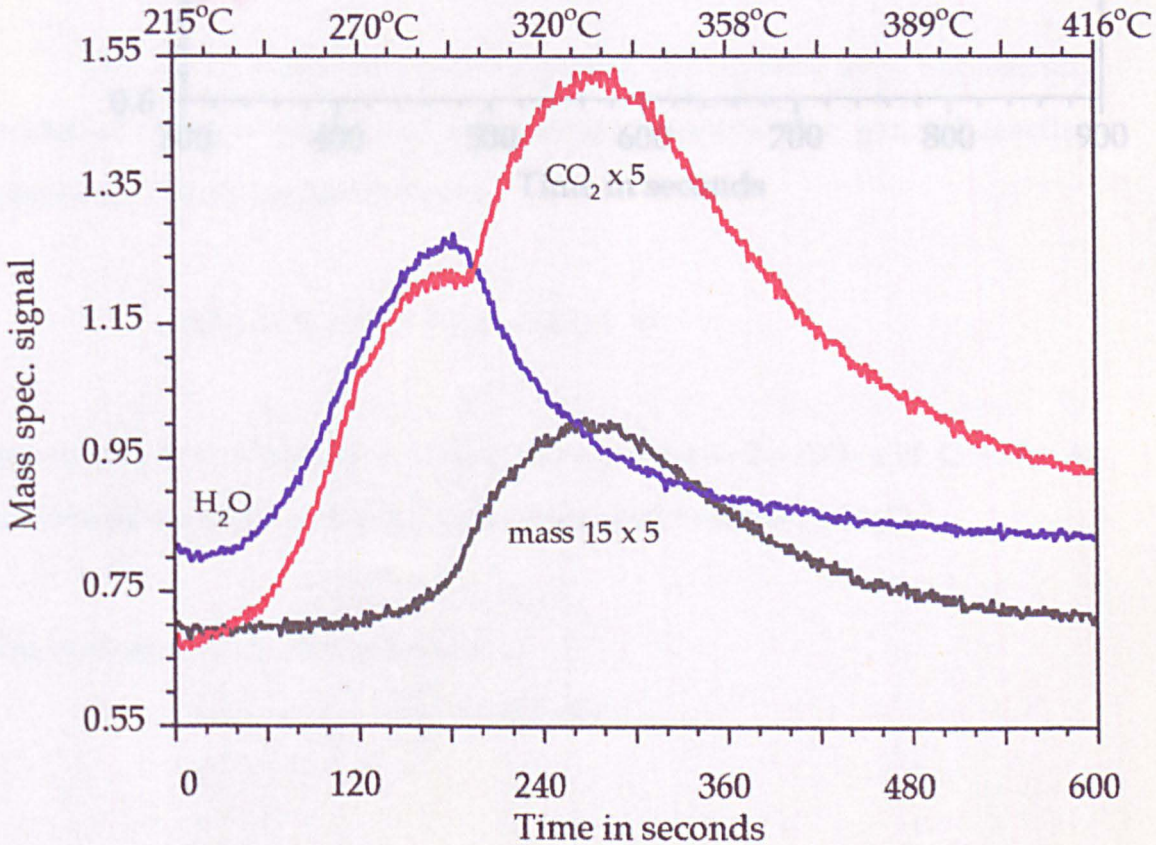

Figure 4.14.
1 microlitre acetic acid dose followed by O_2 pre-dose, then very slow T.P.D.

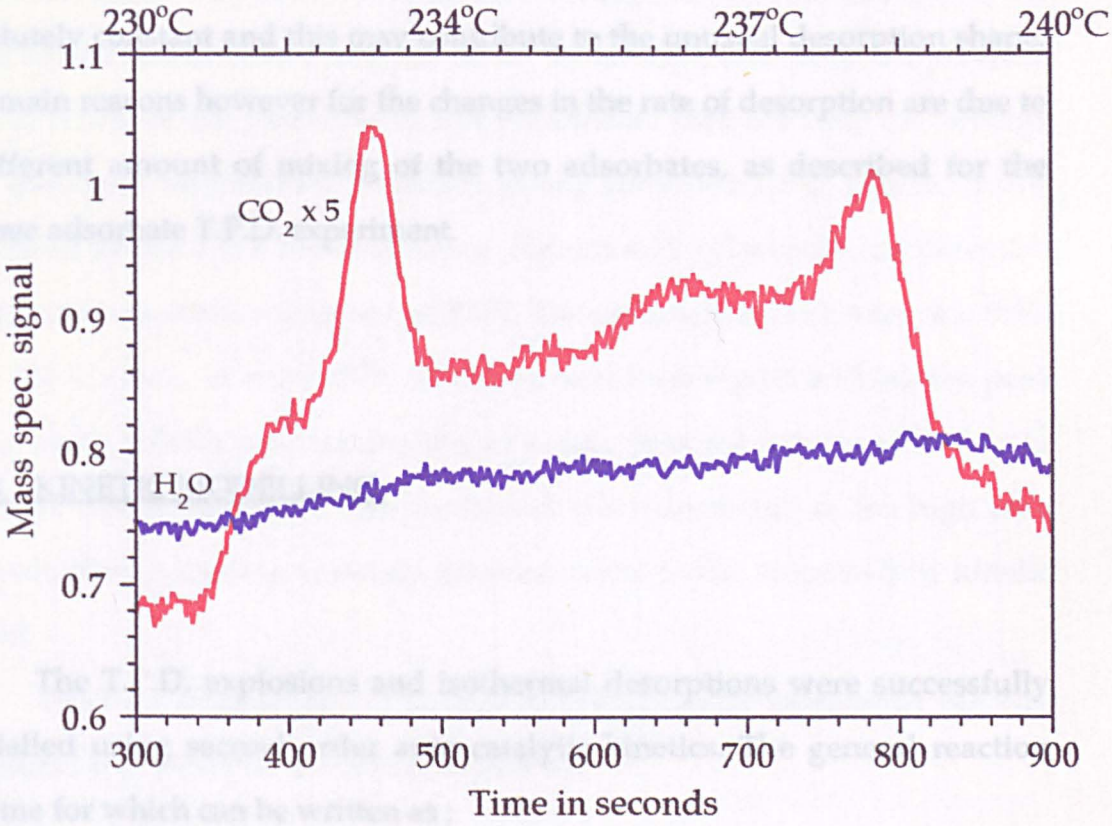

mechanisms of decomposition are clearly operating, leading to the characteristic double hump in the mass 44 peak, accompanied by water desorption on the low temperature side and methane desorption on the high temperature side.

When the order of adsorption was reversed an isothermal experiment attempted and a more complicated, but nevertheless autocatalytic explosion occurred Figure 4.14. as can be noted from the Figure, the temperature is not absolutely constant and this may contribute to the unusual desorption shape. The main reasons however for the changes in the rate of desorption are due to a different amount of mixing of the two adsorbates, as described for the reverse adsorbate T.P.D. experiment.

4.2.8. KINETIC MODELLING.

The T.P.D. explosions and isothermal desorptions were successfully modelled using second order auto-catalytic kinetics. The general reaction scheme for which can be written as ;

$$A(a) + \underline{S} \text{ ------> } B(g) + C(g) + \underline{S}$$

In our case, A = acetate, $\underline{S}$ + a clean rhodium atom, B = CO_2 and C = H_2. As previously mentioned, the hydrogen reacts and desorbes as H_2O.

The rate equation for the reaction is ;

$$-\frac{d\theta}{dt} = k\theta(1-\theta)$$

where k is the rate constant;

$$k = A.e^{\left[-\frac{Ea}{RT}\right]}$$

With this model, the vacancies on which the adsorbate decompose (free rhodium sites) must be averaged over the whole area, implying complete mixing over the time-scale of the experiment, at the high temperatures of the explosion, this is very likely to be the case. As explained in the text above, the exact kinetic parameters could not be fit as the explosive peak temperature varied, however using sensible kinetic parameters inferred from the average explosion peak temperature, a mathematically generated T.P.D. profile, can be generated by using the above equation. Figures 4.15. (a) and (b) compares the model to an explosion observed at 500K. The parameters used were $\theta = 0.99$, Ea = 150 kJ/mol., $A = 1 \times 10^{15}$. As can be seen from Figure 4.15.(a), the peak shape and width (in temperature) shows a close fit to the experimental data in 4.15.(b) . Given the added complexities of the system due to the high area support, this modelling certainly gives credence to the autocatalytic kinetic model.

The time dependence of the rate is calculated by integrating the rate equation , this yields the following expression;

$$1 - \theta = \theta \exp(kt)$$

When this expression is substituted back into the rate equation, the following time dependence is found,

$$-\frac{d\theta}{dt} = A\,\theta^2 \exp(kt)$$

Figure 4.15.
A comparison between a real T.P.D. explosive desorption and a mathematically generated desorption according to the second order autocatalytic model.

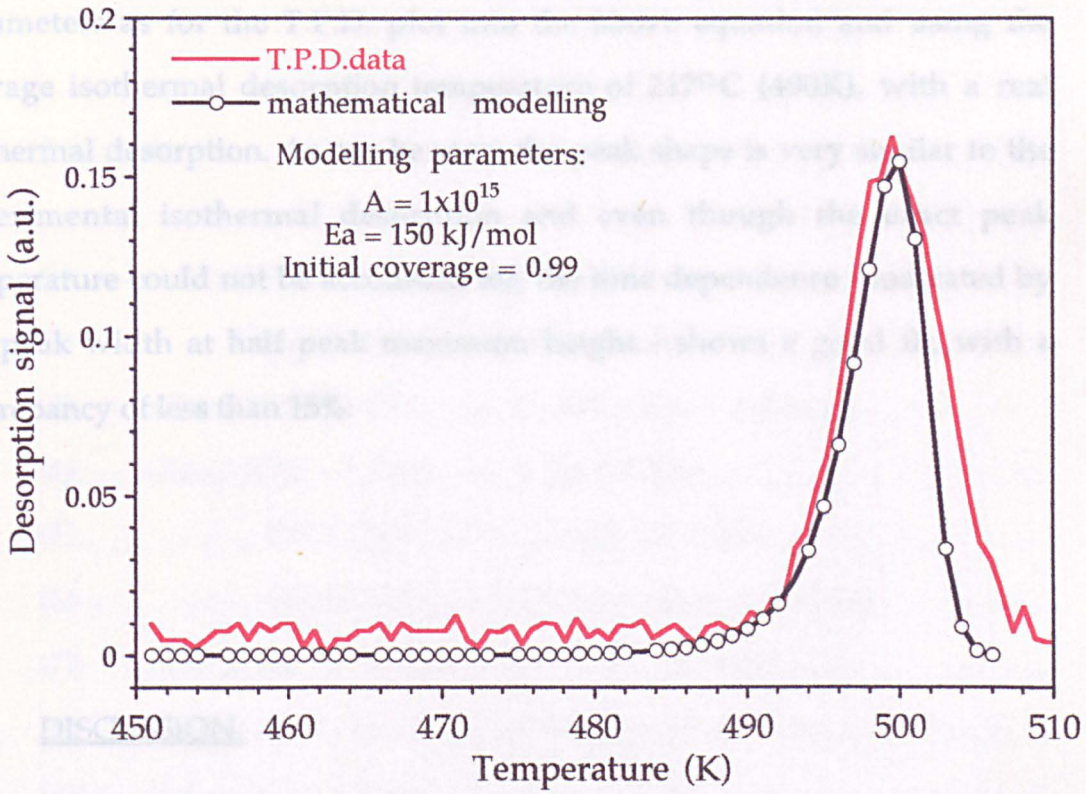

Figure 4.16.
A comparison between a real isothermal desorption (505K) and a mathematically generated desorption according to the second order autocatalytic model.

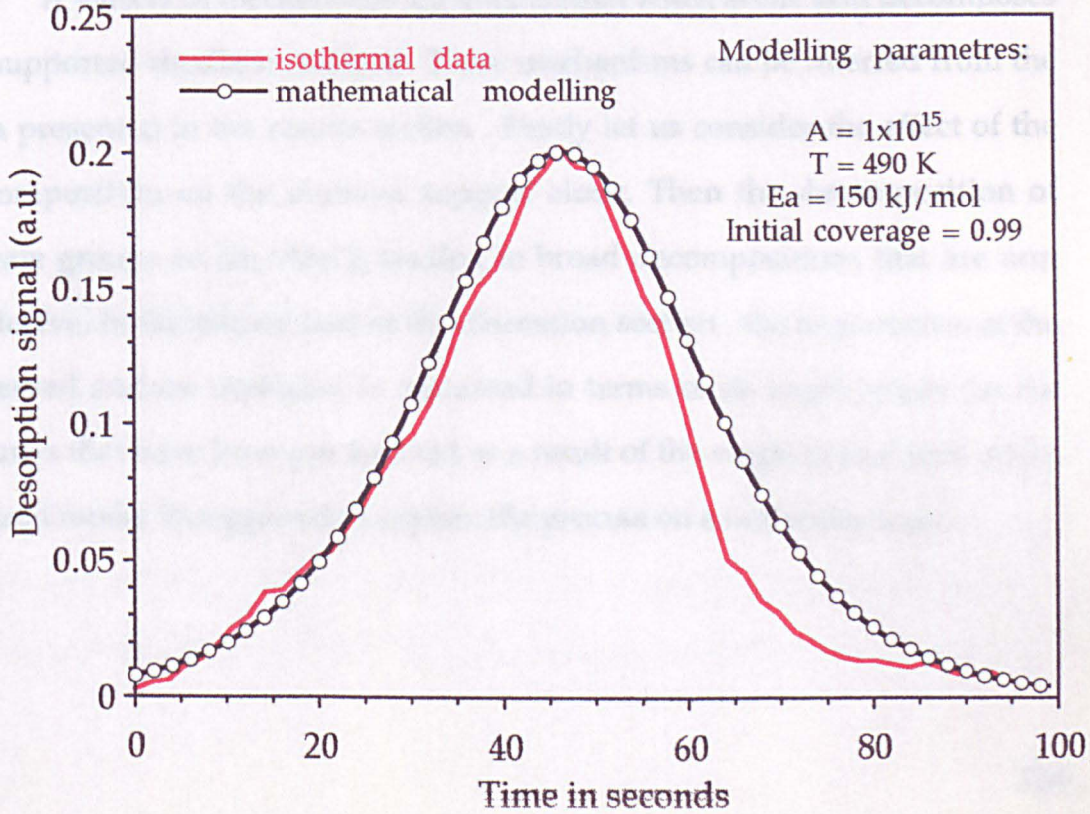

where A' is a constant at fixed temperature. Figure 4.16. compares the mathematically generated curve resulting from putting the same kinetic parameters as for the T.P.D. plot into the above equation and using the average isothermal desorption temperature of 217°C (490K), with a real isothermal desorption. As can be seen, the peak shape is very similar to the experimental isothermal desorption and even though the exact peak temperature could not be accounted for, the time dependence - indicated by the peak width at half peak maximum height - shows a good fit, with a discrepancy of less than 15%.

4.3. DISCUSSION.

4.3.1. PREAMBLE.

A variety of mechanisms are in operation when acetic acid decomposes on supported rhodium catalysts. These mechanisms can be inferred from the data presented in the results section . Firstly let us consider the effect of the decomposition on the alumina support alone. Then the decomposition of acetate groups on Rh/Al_2O_3 leading to broad decompositions that are non explosive. In the second part of the discussion section , the explanation of the observed surface explosion is discussed in terms of its implications for the theories that have been put forward as a result of the single crystal data and a revised model is suggested to explain the process on a molecular level.

The possible steps in the adsorption and decomposition of acetic acid on Rh/Al_2O_3 are shown in Table 4.3. below and they will be referred to in the text;

Table 4.3.

(1) $CH_3COOH(g) \longrightarrow CH_3COOH(a)$

(2) $CH_3COOH(a) \longrightarrow CH_3COO(a) + H(a)$

(3) $CH_3COOH(a)\ O(a) \longrightarrow CH_3COO(a) + OH(a)$

(4) $CH_3COO(a) + H(a) \longrightarrow CH_3COOH(g)$

(5) $CH_3COO(a) \longrightarrow CO_2(g) + CH_3(a)$

(6) $CH_3COO(a) \longrightarrow CO(g) + O(a) + CH_3(a)$

(7) $CH_3COO(a) + O^{2-}(a) \longrightarrow CO_3^{2-}(a) + CH_3(a)$

(8) $CO_3^{2-}(a) \longrightarrow CO_2(g) + O^{2-}(a)$

(9) $CH_3(a) \longrightarrow C(a) + 3H(a)$

(10) $H(a) + O(a) \longrightarrow OH(a)$

(11) $OH(a) + H(a) \longrightarrow H_2O(a)$

(12) $H_2O(a) \longrightarrow H_2O(g)$

(13) $H(a) + H(a) \longrightarrow H_2(g)$

(14) $CH_3(a) + H(a) \longrightarrow CH_4(g)$

4.3.2. DECOMPOSITION of ACETIC ACID on BLANK Al_2O_3

With acetic acid adsorption onto the alumina catalyst at 50°C and subsequent T.P.D., Figure 4.3. all the desorption products appeared as broad peaks at high temperatures with CO_2 desorption occurring from 270°C to

440°C [steps 5,8and 9], the other desorption products were H_20 [steps 10-12] starting at ~330°C and CH_4 [step 14] starting at ~320°C; there was also a small amount of acetic acid desorption [step 4] coincident with CH_4 desorption. As very little hydrogen production is evident (although a signal due to a mass fraction of water is evident) in neither Figure 4.3. nor 4.4. it is clear that the acid hydrogens and the methyl hydrogens must combine with the support to form hydroxyl groups and finally water and to a lesser extent methane.

Looking at the decomposition of acetic acid injected onto the hot (405°C) blank alumina catalyst , Figure 4.4., the first product seen is carbon dioxide, thus it can be inferred that a carbon-carbon scission [steps 5-7] is a relatively fast process at this temperature. The next two products, methane and water are not seen for a considerable time (>15 seconds), clearly the processes leading to these are slower surface steps on alumina [steps 11,12 and 14]. From Figure 4.4 , the initial decomposition step after removal of the acid hydrogen in the adsorption step, is a C-C bond scission [steps 5, 6 and 7] followed by some dehydration of the CH_3 group leading to water and methane production. The first acetate decomposition step on rhodium single crystals is normally a β-CH abstraction, not a C-C scission, the main observations leading to this conclusion were the coincident H_2 and CO_2 desorptions and the absence of methane production. Clearly if β-CH abstraction does preempt C-C scission then the likelihood of methane production is reduced as more H(a) have to be found to saturate the CHx moiety. For methane to form, the CH_3 groups need to find available hydrogen atoms, however the majority of hydrogens are strongly co-ordinated to the support as hydroxyl groups and desorb slowest of all through either disproportionation or reaction with H(a) to form water, therefore hydrogen atoms are scarce and one might imagine, considering the very short surface life-time of hydrogen at these temperatures, that methane formation must

occur when dehydration of either a CHx or a hydroxyl group occurs adjacent to a methyl group, therefore providing a hydrogen atom in close proximity to the CH_3 species. It is apparent that the methyl groups can follow more than one reaction path, with some desorbing as methane once an available hydrogen is found [step 14] and the rest dehydrogenating fully to C(a) [step 9]. From Figure 4.3. in can be seen that very little CO (mass 28) was seen in the T.P.D. of acetic acid on alumina and CO_2 is seen to desorb intact.

The state of adsorption for the acid is as an acetate group, formed via a scission of the acid hydrogen which rapidly forms a hydroxyl group [steps 1-3]. The acetate groups are likely to form at the surface Al^{3+} sites, as suggested in earlier studies of acetic acid on alumina[54,55,] . There is some debate over the precise mode of adsorption of the acetate species derived from acetic acid adsorption, however the two favoured forms are shown in Figure 4.17. below, they are a bidentate chelating species with both oxygen atoms bonding to the same Al^{3+} site and a bidentate bridging species, with two equivalent oxygen-metal bonds with the oxygen atoms being bound to separate metal atoms[56].

Figure 4.17. Two Modes of Adsorption for Acetate on Alumina.

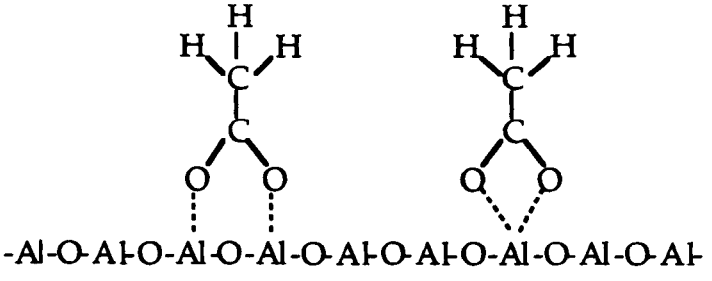

The most likely explanation for the confusion is that both species form and their relative concentration changes with coverage and temperature. At higher temperatures, some hydrogen atoms have been shown to migrate into

the alumina forming aluminium hydroxide (Evans.H.E. and Weinberg). This ties in well with the observation that no hydrogen was seen even at this high temperature where decomposition and desorption processes are fast.

4.3.3. DECOMPOSITION OF ACETIC ACID ON Rh/Al_2O_3.

With the presence of rhodium particles, the decomposition process is changed. From Figures 4.6.(a) - (e) it is apparent that as well as water, carbon dioxide and methane, carbon monoxide (mass 28) is definitely formed [step 6] during T.P.D. What is more, the entire decomposition process occurs at a lower temperature than on the blank alumina, take for instance the CO_2 and CH_4 peak maxima, in the presence of rhodium they appear at ~330-340°C, on the alumina alone they maximised at ~400-420°C. The rhodium therefore assists the decomposition of the acetate. This is to be expected as the rhodium single crystal data shows that acetate decomposition on the clean surface occurs at between 100°C and 120° C on Rh (111), Bowker et al. and Houtman[37].

The appearance of CO in the desorption spectra is interesting. It is certainly not a mass fraction of CO_2 as firstly it is larger than the CO_2 peak and secondly it is not coincident with it, although it should be noted that both desorptions begin at similar temperatures. A rhodium carbonyl hydride species (where a CO(a) and H(a) are bonded to the same rhodium atom) has been detected by infra-red spectroscopy, to form at ~200°C on Rh/Al_2O_3 after exposure to acetic acid (Anderson and Rochester) and also methanoic acid[57] , and its' infra-red band disappeared upon heating to 400°C. The CO desorption seen here could be the desorption of that same group, however the infra-red signal was weak and the CO(a) concentration small. In this case the CO peak is more likely to be as a result of either CO_2 dissociation, or an

inequality in the CO bond strengths in the acetate molecule, due to different environments (for instance as a result of the rhodium particle being closer to one side of the acetate), leading to a CO bond scission, releasing CO(g) and leaving O(a) behind on the rhodium particle [step 6]. In both scenarios, the rhodium is poisoned to some extent with O(a) which would tend to suppress the CO scission, this could explain the rise in CO_2 as CO desorption tails off. In the clean Rh(111) single crystal data of Houtman et al. 20% of the adsorbed acetates decomposed to yield CO(g) at 200°C with the remaining acetates decomposing through decarboxylation to CO_2 at lower temperatures.

The probable mode of reaction for the decomposition without an oxygen pre-dose is through a migration of the acetate species from the support to the rhodium particles where the dissociation takes place and intuitively one would not expect a migrating acetate group to have entirely equivalent CO bonds. This mechanism was first proposed to explain the decomposition of methanoate ions on Rh/Al_2O_3 by Solymosi[57] and it accounts for the lower temperature of decomposition. If the acetate decomposed separately from the rhodium then the desorption peaks would appear at higher temperatures as seen with solely the blank catalyst (Figures 4.3. and 4.4.) and if the acetates resided on the rhodium particles, decomposition would be seen at much lower temperatures, as in the single crystal work.

The desorption peak maxima rise to higher temperatures when successive doses of acid are adsorbed onto the catalyst in sequential T.P.D. experiments with no C(a) clean off, figures 4.6.(a) - (e). This effect has been widely reported in the single crystal data and the under-lying catalytic reasons for it is the poisoning of decomposition sites, and an increase in stability of the adsorbate through electronic interactions between the adatoms and the adsorbates. Adatoms that are electronic acceptors such as oxygen

stabilise the intramolecular acetate bonds whereas a metal such as potassium weakens the bonds[53].

4.3.4. EXPLOSIVE DECOMPOSITION'S - AN UNEXPECTED RESULT.

Surface explosions of carboxylates from a high area supported catalyst have never before been reported, to my knowledge. In the introduction to this Chapter, the history of this curious phenomenon has been mapped out and from being considered a peculiarity of the UHV and more particularly of the (110) single crystal world in the nineteen seventies, it is now a more wide-spread phenomenon. However, before this work, the mathematical kinetic modelling that has accompanied the experimental results and that has been used to explain the reactions, has all been built upon the assumption that the surface has long range order (as a single crystal has - certainly in comparison to a small metal particle) and that with this long range order comes the possibility of developing islands of densely populated adsorbate which then were prevented from decomposing through mutual site blockage. However with the results of the work presented here the situation is changed, the surface is no-longer flat with extended terraces, but instead is very heterogeneous. With this point alone one might expect the rhodium atom to be less co-ordinated at the surface of the particle, with a higher surface free energy and therefore be more reactive towards the decomposition of adsorbates . Furthermore, with an average particle diameter of ~20Å, the argument that the adsorbates forms large areas of dense stable islands becomes untenable as no such 'large areas' exist. In view of these reasons the observation of a surface explosion was indeed a surprise.

With the discovery of surface explosions on high surface area supported catalysts came the need for a re-think regarding processes which are occurring and the realisation that the explosion must be of a somewhat more localised nature than previously thought. As the explosions have most extensively been reported in UHV systems the process is certainly not mediated through the gas phase - however on the catalyst at atmospheric pressure, re-adsorption does take place and its effect is to broaden the peak widths and to block surface sites. In addition, re-adsorption of decomposition products may well be a cause of the high temperature at which the explosion occurs in comparison with the U.H.V. data, by blocking surface sites further.

With the absence of large flat terraces it is appropriate to consider the explosive reaction in a more simplified way through the formulation of classical kinetics for second order autocatalytic reactions[58]. In this scheme, one of the products of the reaction is itself necessary for the reaction to proceed, and the product involved in the first step is a clean rhodium atom , in the scheme below this is denoted by $\underline{S}$. In the case of the explosion we can write the decomposition as;

$$CH_3COO(a) + \underline{S} \text{ -----> } C(a) + 3H + CO_2(g) + 2\underline{S}$$

As oxygen is present on the rhodium particles as an adatom, water is formed immediately, such that no hydrogen gas is seen, the water desorbs immediately from the rhodium metal but can linger for some time on the support through re-adsorption processes. In the rhodium single crystal work, water formed on the adsorption of acetic acid on an oxygen pre-dosed surface desorbed at room temperature. It is clear from the equation above, that there is a net gain in the production of surface sites and it is this characteristic that causes the autocatalytic nature of the reaction. As no explosion is seen in the absence of rhodium and the explosions are clearly very similar to those seen

on single crystals, it is logical and appropriate to imagine that the acetates leading to the explosive decomposition reside on the rhodium particle. In the absence of oxygen as a co-adsorbate the explosion was not observed and it is likely that this is because the acetate is unstable on clean rhodium and prefers to reside on the support, either adsorbing directly onto the alumina or migrating onto it through a spill-over process. This view is shared by various authors who have reported carboxylate build up on the support phase rather than the metal during synthesis gas reactions on Rh/Al_2O_3 systems, such as Bennet[59] , Solymosi[57] and by Rochester et al. who reported little change between an infra-red spectra of acetic acid adsorption on alumina at 300K and on a Rh/alumina catalyst at the same temperature. The spill-over process is likely to be aided by heating.

From the single crystal work of Bowker et al. it is clear that the presence of oxygen causes the stability of the acetate to increase by blocking decomposition sites by site occupation, in effect smoothing out the surface by filling in clean surface sites (S) that would be left after only acetic acid adsorption - isolated empty sites always occur as acetates bridge two Rh metal atoms. Also, and in the catalyst case more importantly, the acetates are stabilised through electronic interactions, causing them to bind to the metal rather than residing on the support. The result is for densely populated patches of acetate groups to form covering the particles, with a less dense scattering of acetates on the high area support. So what in the single crystal work was envisaged as a flat terrace of densely populated acetate islands, is now translated as a 'cluster' of acetates drawn together on a particle through electronic interactions with surface oxygen atoms. A schematic representation of the adsorption of acetic acid on the Rh/Al_2O_3 catalyst with and without oxygen adatoms is illustrated in Figure 4.18.(a) and (b)., and the migration and 'cluster' of acetates on an oxygen pre-dosed catalyst is illustrated in Figure 4.19.

Figure 4.18(a).

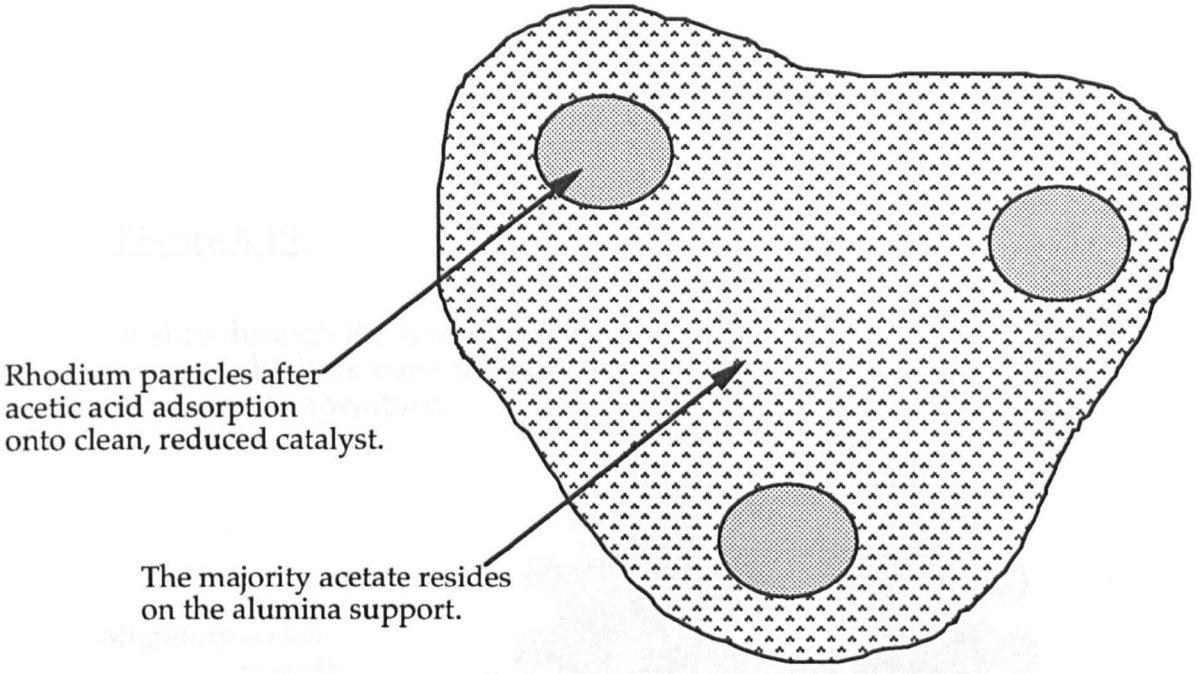

Figure 4.18.(b)

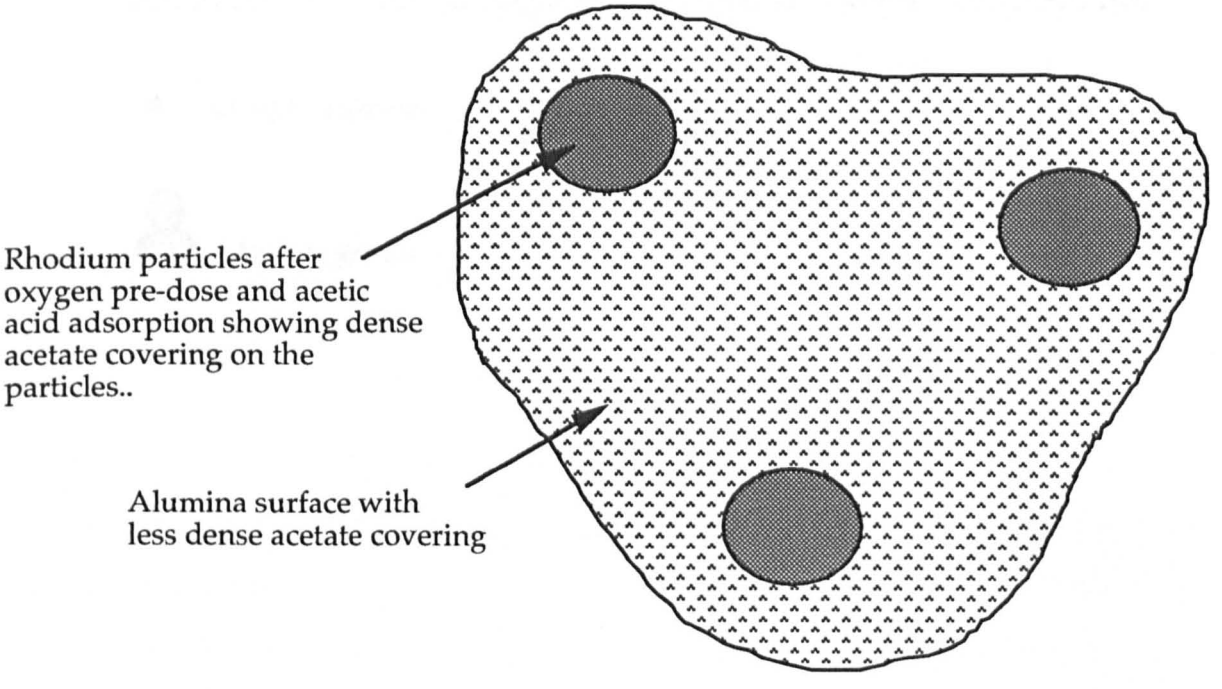

Figure 4.19.

A slice through the acetate/oxygen covered rhodium particle below the explosion temperature.

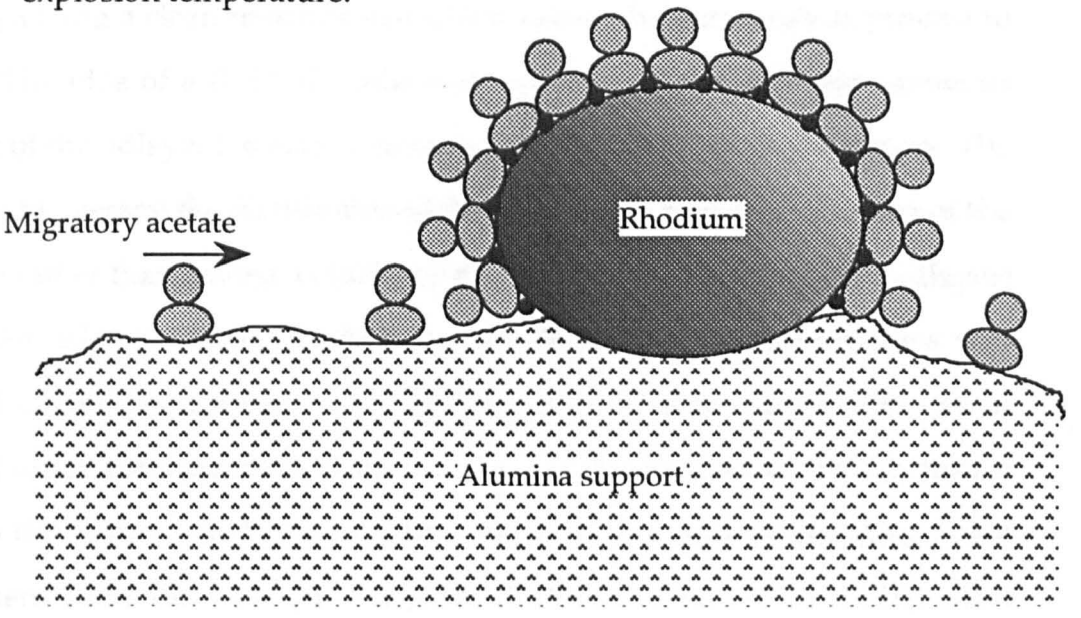

● Oxygen adatom.

Acetate group.

The idea that the initiation site is an abnormality in the surface structure, such as a defect or a kink, can still apply although on a heterogeneous particle, one would expect the concentration of these to be relatively high. Another possibility is that as the temperature increases, the mobility of the mixed adsorbate layer likewise is increased and at the temperature of the explosion it is far more fluid than static, under these conditions , some spill over at the metal-support boundary may well take place, yielding a clean rhodium site which allows the autocatalytic process to begin. The idea of a fluid-like adsorbate layer implies that a homogeneous mixing of the adlayer (acetate / oxygen) and rhodium vacancies occurs. The effect is to average the distribution of decomposition sites over the area of the particle rather than having a phase separation (which implies a static adlayer) as in the `island' model in which the number of decomposition sites was related to the circumference of a growing area of clean metal. The use of second order autocatalysis in order to describe the kinetics of the reaction is akin to the Falconer and Madix model, although the idea of islanding is not consistent with the physical make-up of the catalyst particle. The vital physical requirement, that of a dense area of acetate, is however achieved by the adsorption of oxygen onto the rhodium particles.

With the reversal in the order of adsorption, Figure 4.11. further evidence for acetates adsorbing on the alumina in the absence of an oxygen pre-dose and for the 'fluidity' of the adlayer is gained. If the acetate did adsorb onto the rhodium particles then a drop in the up-take of oxygen should be seen as the adsorption sites are occupied, this is not the case and further to this, as has been stated before, conventional (non-explosive) acetate decomposition occurs at below 100°C on rhodium single crystals. The fact that an explosion is seen, clearly shows that the acetates are able to move from the support to the oxygen covered rhodium particles and are stabilised there. The explosive peak is somewhat broader and indeed is disrupted. This

implies that although a fluid adlayer does form, it is not quite as homogeneously mixed as in the case with oxygen dosing preceding the acid dose.

Noticeable in the explosive T.P.D. spectra is that the broad desorptions are found to occur only after the explosion has occurred. The implication must be that the rhodium particles are poisoned by the dense layer of acetates and oxygen adatoms, as such decompositions are prevented from occurring. However, once the explosion has passed the rhodium is cleaned of the acetate adlayer and is available for reaction, although C(a) is left behind in the decomposition process..

The characteristic double desorption of CO_2, with water accompanying the lower temperature desorption and methane accompanying the higher CO_2 desorption is explained by the availability of oxygen on the rhodium catalyst. As the oxygen becomes scarce through water formation the destiny of the H(a) swings in favour of CH_4. Figure 4.13.(b) shows very clearly the two decomposition processes. The higher temperature CO_2 desorption is also evident when acetic acid decomposes without an oxygen pre-dose, as in figure 4.5. This is a further indication that the rhodium is depleted of oxygen at this stage , as

$$O(a) + CO(a) \text{-----} > CO_2(g)$$

is a facile reaction on this catalyst.

The sequence of T.P.D. experiments with varying oxygen doses figures 4.10.(a) - (g), reveals both the switch from water to methane desorption and the emergence of a second decomposition process at very low oxygen coverages, in which CO and H_2 desorb coincidentally. To explain the mechanism, firstly let us consider the manner in which the two adsorbates occupy the catalyst surface. Rhodium metal, as was shown in Chapter 3, adsorbs oxygen and at 50^{o}C, 0.5mls of oxygen is sufficient to saturate the metal. The catalyst bed is linear, therefore the front end of the bed interacts

Figure 4.20. Catalyst bed after ~ 0.1 ml of O_2.

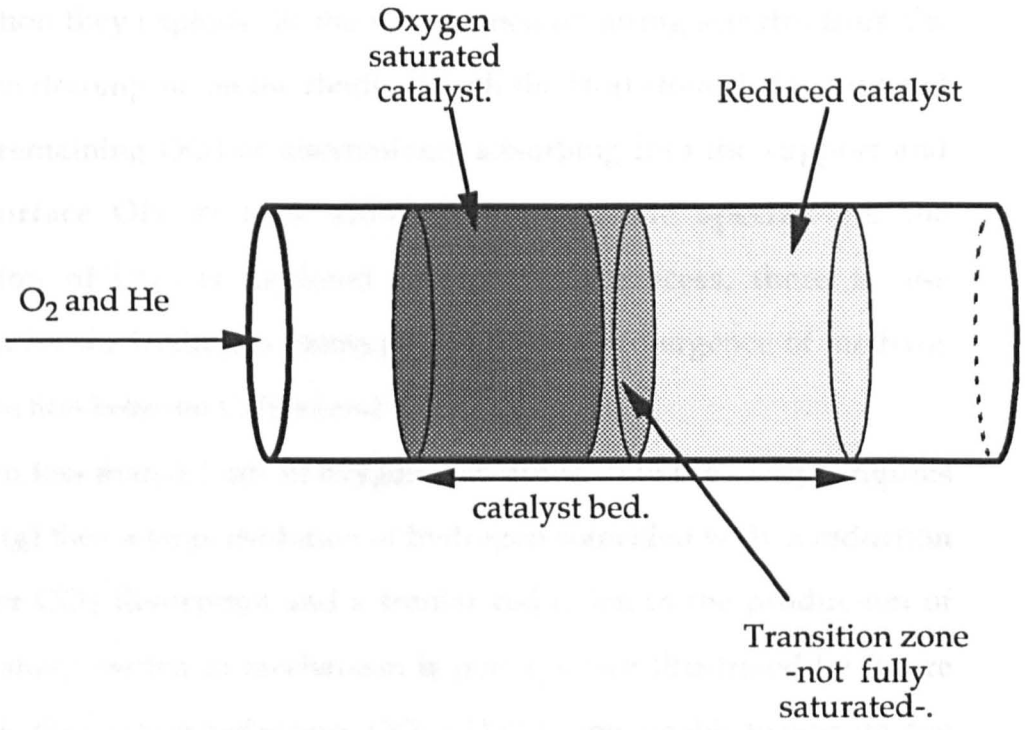

with the gas flow first, if the dose of oxygen is insufficient to saturate the catalyst bed then the result is not an evenly distributed, partially oxidised catalyst bed but one in which the front end of the bed has a full coverage of oxygen and the tail of the bed remains in a reduced state Figure 4.20. (catalyst bed) . Similarly with the acetic acid, more will adsorb at the front end of the bed than at the tail. When a rhodium particle is fully saturated with oxygen, acetate species are stabilised forming a dense 'clump' as in figure 4.17. and upon initiation they explode off the surface, neighbouring acetates from the support then decompose on the rhodium with the H(a) atoms being mopped up by the remaining O(a) or alternatively adsorbing into the support and forming surface OH or bulk aluminium hydroxide species. As the concentration of O(a) is depleted through this process, there is less competition for the hydrogen atoms and we see the emergence of methane from the reaction between CH_3(a) and H(a).

When less than 0.2 mls of oxygen was dosed onto the catalyst figures 4.10(f) and (g) then a large evolution of hydrogen coincided with a reduction of the lower CO_2 desorption and a similar reduction in the production of water, the sharp switch in mechanism is perhaps best illustrated by figure 4.10 (f) . The dissociation pathway to $CO_2 + H_2O$ is now unable to operate due to an abrupt lack of oxygen and the hydrogen atoms are seen to combine and desorb. There is also an increase in the methane yield due the more readily available H(a). This seems at first somewhat contradictory, since when no oxygen dose was introduced prior to acid adsorption, as described in section 4.2.2., no hydrogen was seen. The reason why hydrogen desorption is not seen in the absence of any oxygen pre-dose is because the acetate groups resides on the support, it is only when oxygen is present on the rhodium that acetates are stabilised there and at a critical concentration of oxygen to acetate (proposed to be located in a zone situated in the transition from fully saturated to a reduced catalyst) the acid adsorption and decomposition leads

to all the oxygens being reacted to water and hydrogen atoms then couple together and desorb before they have time to spill-over onto the support. From this result we can conclude that the acetates that decompose to yield the lower temperature broad CO_2 desorption, reside on or near the rhodium particles as in the absence of rhodium these processes are not seen. The acetates that produce the higher temperature CO_2 desorption reside on the support, as similar desorptions were observed with no oxygen pre-dose. It is due to the different acetate environments that different decomposition mechanisms are seen.

Water production occurs through various pathways due to the numerous origins of the two constituent atoms. The acid hydrogen is the first to become available and combines with either O(a) on the rhodium particle producing the most facile water species which desorbs first (inferred from the single crystal data where water desorbed at room temperature) or, forms a hydroxyl/water group on the alumina. The methyl hydrogen atoms are not available until after the acetate decomposition occurs and react with the available oxygen (which depends on the location of the decomposition as discussed above).

The experimental proof that an autocatalytic process is operating is that the rate of decomposition increases with no change in temperature. A kinetic model, describing both the TPD and the isothermal data has been used to simulate the desorption profiles. Figures 4.15. and 4.16. show the generated profiles using the autocatalytic model. The mathematical representations show a very similar line shape and indicate that indeed, classical second order autocatalytic kinetics does explain in general terms, the processes occurring. It is clear however that the model does not exactly fit the peak temperature or the line shape, the reason for this and indeed the apparent inconsistencies in the T.P.D. plots (for instance the slight variations in the explosive peak temperature) is due to the considerable increase in complexity of the reaction

processes caused by the nature of the support. Factors that contribute to the temperature of explosive and non-explosive desorptions are many, for example, the exact concentration of surface hydroxyl groups on the alumina. This will effect the adsorption and decomposition of the acetate on the support and may effect the state of the rhodium. For instance it is likely that the rhodium may be oxidised to some extent by excess hydroxyl groups. The concentration of surface hydroxyl groups depends critically on the reductive pre treatment of the catalyst prior to reactant adsorption and even though the same routine was followed, minor differences in reduction time and temperature did occur. Also related to the reductive catalyst pre treatment is the coverage of C(a) on the rhodium surface. From the single crystal data, C(a) was found to induce and alter the explosion temperature[38,50]. From this work, a build up of carbon has been shown to increase the decomposition temperature of the adsorbates, therefore if small amounts of C(a) are left behind on the catalyst after reduction then the desorption peak temperatures may be affected. It should be noted however that the reduction was continued each time until the production of methane could no longer be detected with the mass spectrometer as in Figure 4.9. However this said, from UHV studies it is known that only very tiny amounts of atomic adsorbates on platinum group metals can perturb the binding of other adsorbates. What is more, small rhodium particles are well known to be susceptible to morphological changes under different conditions of adsorbate concentration and temperature. It is possible that such factors are the cause of apparent inconsistencies in experimentally measured decomposition temperatures.

4.4. CONCLUSIONS

The results in this Chapter are significant in that they present an transfer of knowledge from surface science to catalysis, namely the phenomenon of surface carboxylate 'explosions'. It is true to say however that due to the far greater complexity of a high area supported catalyst at atmospheric pressure, in comparison to a well defined single crystal at U.H.V., some differences occur and direct comparisons are therefore dangerous. The differences however are due to the effect of the support, and the explosion reaction itself is analogous to the single crystal process as it occurs on the rhodium fraction only. Carboxylate 'explosions' from a supported catalyst have not been reported before in the literature and by analogy with the single crystal data, it has been shown that the explosive decomposition is described well by the kinetics of second order autocatalysis and therefore belongs in the mainstream of chemical reactivity rather than being an anomaly of well defined surfaces in U.H.V., as was suspected two decades ago. The near fit of the second order autocatalytic model in terms of both peak line shape and peak width - temperature change in the T.P.D. and time difference in the isothermal data - is encouraging considering the simplicity of the model in comparison to the complexity of the system and implies that over the time scale of the explosion, the adlayer made up of the acetates, oxygen adatoms and vacancies, are homogeneously mixed and in effect the acetates are able to 'sample' the whole rhodium particle surface.

This conclusion nullifies the static 'island' model described in the introduction to this chapter. Also more generally it is clear that acetate species can indeed reside on the rhodium part of a Rh/Al_2O_3 catalyst, provided it is stabilised by a co-adsorbate (in this case oxygen) and therefore cannot be ruled out as an intermediate in the rhodium catalysed ethanol synthesis

reaction from synthesis gas. This possibility has been dismissed by others from infra-red evidence showing a lack of response of acetate bonds to changes in the gas composition. Thus they labelled it a spectator species[60]. However it is likely that the infra-red spectrum was mainly contributed by the majority support phase and that acetates on the Rh phase were masked under that adsorption. The whole explosion phenomena may be closely related to that of oscillatory behaviour seen in certain catalytic reactions in that a feed-back loop connects the products of the reaction to the reactants themselves - in this case a free rhodium atom takes part in the feed-back loop, and the explosion is implicated in the acceleration phase of all oscillations.

Apart from its formation through the explosive decomposition, CO_2 is also formed in conjunction with H_2O in a slower decomposition and in a different decomposition pathway still, with CH_4. The mechanism change from CO_2 and H_2O production to CO_2 and CH_4 production can be explained through a picture of mobile acetate groups migrating to the rhodium particles and a depletion of O(a) at the rhodium surface.

4.5. REFERENCES.

1 Ying.D. and R.J.Madix., *J.Catal.*, **61**, 48 (1980).

2 Bowker.M. and Madix.R.J., *Surf.Sci.*, **102**, 542 (1981).

3 Bowker, M., Hadden, R., Houghton, K., Hyland, J. and Waugh, K.C., *J.Catal.*, **109**, 263 (1988).

4 Cassidy, T.J., Allen, T.J., Li, Y. and Bowker, M., *Catal. Lett.* , **21**, 321 (1993).

5 Bowker, M., Cassidy, T.J., Allen, M.D. and Li, Y., *Surf. Sci.*, **143**, 307 (1994).

6 Bhasin, M.M. and O'Connor, G.L., *Belgian Patent* 824, 823, July 28 (1975).

7 Bhasin, M.M., *Belgian Patent* 824, 823, July 28 (1975).

8 Bhasin, M.M., Bartley, W.J. and Wilson, T.P., *J.Catal.*, **54**, 120 (1978).

9 Gauthier-Lafayne,J. and Perron,R., '*Methanol and carbonylation*' Editors Technip, (1987).

10 Van Herwijnen, T. and de Jong, W.A., *J. Catal.*, **63**, 83 (1980).

11 Rethwisch, D.G. and Dumestic, J.A., *Applied. Catal.*, **21**, 97 (1986).

12 Kung, H.H., "*Transition Metal Oxides: Surface Chemistry and Catalysis*," p.245, Elsevier, Amsterdam, (1989).

13 Millar, G.J., Rochester, C.H., Bailey, S. and Waugh, K.C., *J. Chem. Soc. Faraday Trans.* **88**, 2085 (1992).

14 Shustorovich, E. and Bell, A.T., *Surf. Sci.* **253**, 386 (1991).

15 Orita, H., Naito, S. and Tamaru, K., *J. Catal.* **90**, 183 (1984).

16 Bowker, M., *Catal. Today*, **15**, 77 (1992).

17 Van der Lee, G., Bastein, A., Van der Boogert, J., Schuller, B., Luo, H. and Ponec, V., *J. Chem. Soc. Faraday Trans. 1*. **83**, 2103 (1987).

18 Force, E.L. and Bell, A.T., *J.Catal.* , **44**, 175 (1976).

19 Ai, M., *Catal. Today*, **13**, 679 (1992).

20 Kim, K.S. and Barteau, M.A., *J.Catal*. **125**, 353 (1990).

21 Sugiyama, S., Sato, K., Yamaski, S., Kawashiro, K. and Hayashi, H., *Catal. Lett.* **14**, 127 (1992).

22 Bailey, O.H., Montag, R.A. and Yoo, J.S., *Applied. Catal. A.* **88**, 163 (1992).

23 Madix, R. J., *Adv. Catal.* **29**, 1 (1980).

24 Barteau, M.A., *Catal. Lett.* **8**, 175 (1991).

25 Hindermann, J.P., Hutchings, G.J. and Kiennemann, A., *Catal. Rev.-Sci.Eng.*, **35**(1), 1 (1993).

26 Ichikawa,M., and Fukushima, T., *J. Chem. Soc. Chem. Commun.*, 321 (1985).

27 Ponec, V., Nonnemann, L.E.Y., in '*Natural Gas Conversion*', Elsevier, *Stud. in Surf. Sci.*, **61**, 225 (1991)

28 Ponec, V., *Catal. Today*, **12**, 227 (1992).

29 Koerts, T., Welters,W.J.J., van Santen, R.A., Nonnemann, L.E.Y., and Ponec, V. in '*Natural Gas Conversion*', Elsevier, *Stud. in Surf. Sci.*, **61**, 235 (1991).

30 Burch,R., and Petch, M.I., *Applied Catal. A.* **88**, 61(1992).

31 Diagne.C.,Idriss, H., Hindermann,J.P., and Kiennermann,A., *Applied Catal.* **51**, 165 (1989).

32 Diagne, C., Idriss, H., Pepin, I., Hindermann,J.P., and Kiennermann,A., *Applied Catal.* **50**, 43 (1989).

33 Kiennermann,A., Breault, R., and Hindermann,J.P. *J. Chem. Soc., Faraday 1*, **83**, 2119 (1987).

34 Bastein, T. *Ph.D. Thesis*, University of Leiden, The Netherlands (1988)

35 Underwood,R. and Bell,A.T., *J.Catal.*, **111**, 325 (1988).

36 Orita,H., Naito,S., and Tamaru,K., *J. Phys. Chem.*, **89**, 3066(1985)

37 Houtman, C. J., Brown N. F. and Barteau M. A., *J. Catal.*, **145**, 37(1994)

38 Bowker,M. and Li,Y. *Catal. Letts.*, **10**, 249 (1991).

39 Koerts,T., Welters,W.J.J., and van Santen,R.A., *J.Catal.*,**134** ,1 (1992).

40 Koerts,T., and van Santen,R.A., *J.Catal.*,**134** ,13 (1992).

41 Solymosi, F., Tambácz, I., and Kocsis, M., *J.Catal.* **75**, 78 (1982).

42 Erdöhelyi, A., Pásztor, M., and Solymosi, F., *J.Catal.* **98**, 169 (1986)

43 McCarthy,J., Falconer,J., and Madix,R., *J.Catal.* **30**,235 (1973).

44 Falconer, J.L., McCarty, J.G. and Madix, R.J., *Surf.Sci.*, **42**, 329(1974).

45 Falconer, J.L., and Madix, R.J., *Surf.Sci.*, **46**, 473 (1974).

46 Madix, R.J., Falconer, J.L., and Suszo, A.M., *Surf. Sci.*, **54**, 6 (1976).

47 Madix, R.J., Gland, J.L., Mitchell, G.E. and Sexton, B.A., *Surf. Sci.*, **125**, 481 (1983).

48 Benziger, J.B. and Schoofs, G.R., *J. Phys. Chem.* , **88**, 4439 (1984).

49 Bowker,M. and Li,Y., *Catal. Lett.*, **21**, 321 (1991).

50 Li, Y. and Bowker, M., *J.Catal.*, **142**, 630 (1993).

51 Li, Y. and Bowker, M., *Surf. Sci.*, **285**, 219 (1993).

52 Aas, N. and Bowker, M., *J.Chem. Soc. Faraday Trans.*, **89** (8), 1249 (1993).

53 Hoogers, G., Papageorgopoulos,D.C. and King,D.A., *J. Chem. Phys.*, submitted.

54 Anderson, J.A. and Rochester, C.H.,*J. Chem .Soc., Faraday Trans. 1*, **85**(5), 1117 (1989).

55 Kiselev,A.V. and Uvarov,A.V., *Surf. Sci.*, **6**, 399 (1967).

56 Evans.H.E. and Weinberg, W.H., *J. Chem. Phys.*, **71**(12), 4789 (1979).

57 Solymosi, F. and Erdöhelyi, A., *J. Catal.*, **91**, 327 (1985).

58 *See for instance,-* Frost, A.A. and Pearson, R.G., *Kinetics and Mechanism*, 2nd Edition, Whiley, New York, 19 (1961).

59 Efstathiou, A.M., Chafik, T., Bianchi, D and Bennett, C.O., *J. Catal.*, **148**, 224, (1994).

60 Fukushima, T. and Ichikawa,M., *J. Chem. Soc. Chem. Commun.*, 729 (1985).

CHAPTER 5.

EFFECTS OF POTASSIUM PROMOTION ON THE Rh/Al_2O_3 CATALYST.

5.1. INTRODUCTION.

5.1.1. PREAMBLE.

The term "promoter" is applied to substances that are not themselves catalytically active but which allow the active phase of the catalyst to function to its maximum capacity[1]. Almost every industrial catalyst has an added promoter and sometimes has many. The function of the promoter may be complex but in general terms normally falls into one or more of the following categories:

(i) Enhanced activity, in that the promoter increases the specific rate of the reaction by easing the rate determining step. Potassium is the most widely used promoter of this type, often referred to as an 'electronic' promoter.
(ii) Enhanced selectivity, such that the desired product of the reaction is produced at a relatively faster rate than the undesired products, for instance by hindering the rate of formation of the latter. Chlorine, normally a severe poison, is effective in suppressing the production of total combustion products in the production of ethylene oxide, and falls into this category of promoter.
(iii) Enhanced catalytic lifetime, making the catalysts' time on stream longer and therefore ensuring greater industrial efficiency by minimising plant shut-down. These are often referred to as 'textural' promoters as they inhibit sintering of the small particles making up the active phase of the catalyst. Alumina, used in the ammonia synthesis and steam reforming catalysts, falls into this category.
(iv) Physical modifications, for instance changing the metal surface area or the total surface area, altering the pore size distribution or perhaps influencing the catalyst texture on a macroscopic scale.

Table 5.1. gives a selection of some of the most important heterogeneous catalytic industrial catalysts that are promoted by alkali metals, adapted from Bowker[2]. There have been a number of reviews on the function of promoters, this introduction is intended as a brief overlook of their use and physical chemical properties, concentrating on potassium as this is the most widely used industrial promoter and indeed is the promoter used to alter the properties of the rhodium catalyst studied in this thesis.

Table 5.1. Important Alkali Promoted Industrial Reactions.

Industrial Process	**Basic catalyst**	**Promoter**	**Promoter Function**
Ammonia Synthesis ($N_2 + 3H_2$ -----> $2NH_3$)	Fe / Al_2O_3	K_2O	Activity
Fischer-Tropsch $xCO + 2xH_2$ ---> $C_xH_{2x} + xH_2O$	Fe / SiO_2	K_2O	Product Distribution
Methanation ($CO + 3H_2$ -----> $CH_4 + H_2O$)	Ni / Al_2O_3	Alkalis	Activity / Lifetime
Water Gas Shift $CO + H_2O$ -----> $CO_2 + H_2$	Iron Oxide / Al_2O_3	Alkalis	Activity / Lifetime
Ethylene Epoxidation $C_2H_4 + {}^1/_2\, O_2$ -----> C_2H_4O	Ag / Al_2O_3	K, Cs	Selectivity
Propene Ammox. ($C3H6 + {}^3/_2\, O_2 + NH_3$ -----> $C_2H_3CN + 3H_2O$	BiMo Oxide	K_2O	Selectivity

5.1.2. REDUCIBLE METAL OXIDE PROMOTERS.

Relatively recently there has been enormous interest in the use of oxidic transition and rare earth metal promoters in synthesis gas reactions over rhodium, as they promote the formation of oxygenates, particularly ethanol and ethanal[3]. The relationship between metal oxide promoters and oxygenate synthesis has been recognised for a long time. The typical promoters used to increase the selectivity and activity of synthesis gas towards oxygenates over rhodium catalysts are the oxides of; Ti, V, Mn, Fe, Co, Zr, Mo, Mg, La, and Ce. From a commercial point of view, interest in these types of processes has dwindled as it has become apparent that in order to gain high selectivity, very low conversions were required. However the fundamental role of the oxidic promoter is of great interest. The broad mechanistic aspects of hydrocarbon and alcohol formation has been recently reviewed[4]. It appears that the role of the promoter is to facilitate the formation of a 'tilted' CO species as proposed by Sachtler[5], with the carbon atom bonded to the metal and the oxygen atom of CO coordinated to the oxidic promoter. The existence of this species has been confirmed by IR studies[6]. This species can then be hydrogenated to form acyl-like intermediates as described in the introduction to Chapter 4, from which C_2^+ oxygenates can be formed, though the precise identity of the hydrogenated intermediate leading to specific products is still a matter of some debate.

Van Santen and Koerts[7] have recently studied the affect of vanadia promotion on a rhodium on silica catalyst in relation to the dissociation of CO. They concluded that CO dissociation was the rate limiting step in the methanation reaction and that the rate of CO dissociation was enhanced by the promoter with the activation energy being lowered from 90kJmol^{-1} to 67kJmol^{-1}. They also found that vanadia promotion reduces the rate of methane formation upon hydrogenation of surface carbon[8], due to an

enhanced metal-carbon interaction, and at the same time the probability of forming higher hydrocarbons is increased due to the greater residence time of the carbon fragments on the catalyst surface.

5.1.3. THE ELECTRONIC EFFECT of POTASSIUM.

As Table 5.1. shows, alkali metals and in particular potassium are very widely used to enhance the activity and selectivity of catalysts. The fundamental reasons for this is that they have a low ionisation potential and they induce electric field gradients at the catalyst surface. Because the 4s orbital of potassium is above the Fermi level of metals, the alkali atom will autoionise upon adsorption (certainly at low coverages in any case). This leads to in increase in electron density in the region around the atom and often causes an dramatic decrease in the work function of the metal. Taking CO adsorption as an example, the general effect of the promoter is to increase electron back-donation from the metal d-orbitals into the $2\pi^*$ anti-bonding orbital of the molecule (see Chapter 1) therefore weakening the CO bond, thereby easing dissociation. As can be seen from Table 5.1. potassium is not adsorbed in its ionic form in real catalytic systems, it is coadsorbed with anions (such as oxygen), the presence of the coadsorbate diminishes the overall electronic effect of the potassium, however it has been shown that even when adsorbed with anions the work function of the material is still decreased considerably[9], though to a lesser extent. Potassium is perhaps the most useful of the alkali metals because it forms many stable surface compounds such as K_2CO_3 and $K_2Al_2O_4$, what is more, because of its' ionic size, it is less prone to penetrating into the bulk of either the metal or the support.

All promoters above a certain coverage will poison a reaction by physically blocking surface adsorption sites. Promoters have their most marked influence on adjacent sites, that is, their effect is a localised one, with any delocalised effects being very slight. Bowker[10] illustrated this property clearly when he plotted the relationship between the number of activated sites and unaffected sites against promoter coverage, see Figure 5.1. In the figure, the five curves are generated by assuming that one promoter atom affects ensembles of 2, 4, 6, 8 and 10 sites adjacent to it. More theoretical calculations with and without coadsorbates have also shown the nature of the promoter affect to be localised[11,12].

5.2. RESULTS.

5.2.1. OXYGEN UP-TAKE.

In Chapter 3, figure 3.6. illustrated the effect that 0.25 monolayers of potassium has on the up-take of oxygen on the Rh/Al_2O_3 catalyst. The figure is printed again for convenience, Figure 5.2. Oxygen adsorption at 100°C revealed a decrease in up-take by a factor of 4. This decrease indicates that either oxygen requires an ensemble to dissociatively adsorb or that oxygen is bound to more than one rhodium atom. As the coverage of rhodium is 0.25 monolayers (assuming even distribution over the entire catalyst) then statistically all ensembles of 4 or more rhodium atoms will be disrupted, what is more, the potassium on the surface of the catalyst is more than likely to be in both potassium oxide and potassium carbonate form, which will further cover the surface of the catalyst. In a study on the state of potassium under CO hydrogenation conditions on a Ru(100) crystal, Hoffmann et al.[13] found

Figure 5.1.

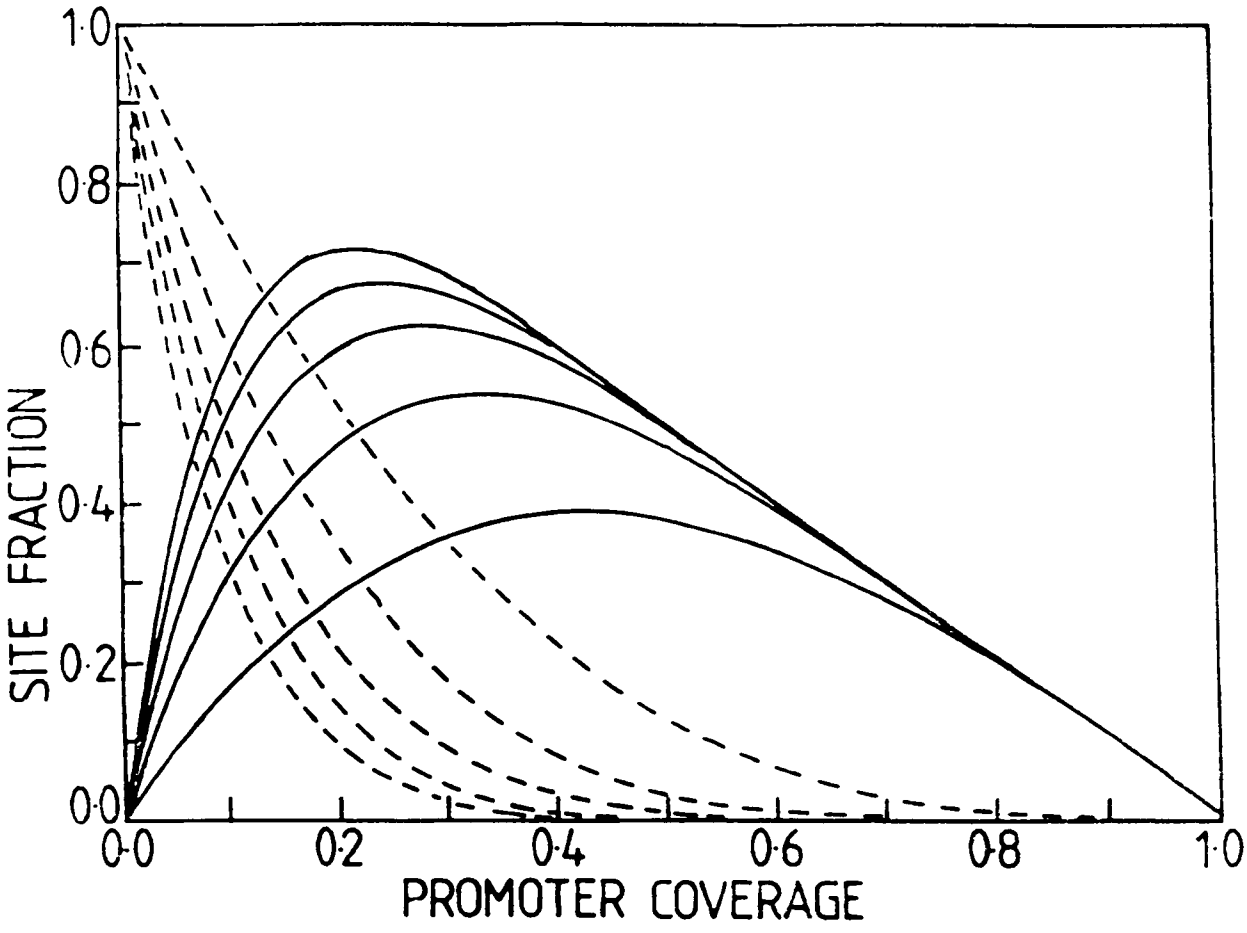

The figure shows the dependence of the fraction of promoted sites (solid lines) and unaffected sites (dashed lines) upon the surface coverage of promoter for ensembles of 2, 4, 6, 8 and 10 affected sites around a promoter atom. From Bowker[10].

Figure 5.2.
Oxygen take up versus temperature on
K promoted and unpromoted catalysts.

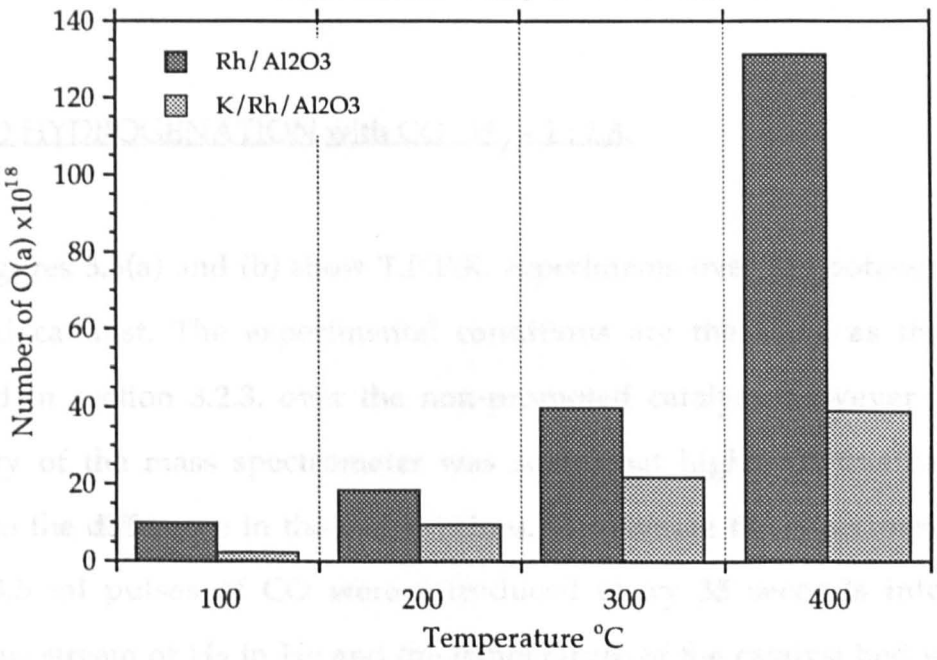

that three potassium states formed. At very low promoter coverages, < 0.1 monolayers, elemental ionic potassium was present. At higher promoter coverages, potassium carbonate and formate groups formed. The concentration of which varied with the gas composition. The ratio of oxygen up-take on the rhodium and promoted rhodium catalyst is not constant with the rise in temperature. This indicates that there are different activation energies for surface and bulk oxidation between the two catalysts.

5.2.2. CO HYDROGENATION with CO : H_2 = 1 : 1.8.

Figures 5.3(a) and (b) show T.P.P.R. experiments over the potassium promoted catalyst. The experimental conditions are the same as those described in section 3.2.3. over the non-promoted catalyst, however the sensitivity of the mass spectrometer was somewhat higher in this case, leading to the difference in the y-axis values. To reiterate the experimental set-up, 0.5 ml pulses of CO were introduced every 35 seconds into a continuous stream of H_2 in He and the temperature of the catalyst bed was ramped at ~0.4 ^{o}C per second. The CO pulse width is ~5 seconds at half maximum height and the H_2 : CO ratio is 1 : 1.8.

The temperature profile of the reaction over the promoted catalyst is broadly similar to that of that unpromoted catalyst (Figures 3.13.(a) and (b)) The onset of methane production is seen very slowly between 160^{o}C and 180^{o}C, if anything, this is fractionally later than the onset of methane on the unpromoted catalyst (by ~ 5^{o}C). The rate and yield of methane increase with the rise in temperature to between 300^{o}C-310^{o}C when the maximum yield under these conditions is reached. The rate of methanation however continues to increase with temperature, as evidenced by the ever sharper leading line shape. In the unpromoted case, the maximum yield of methane

Figure 5.3.(a)
T.P.P.R. CO hydrogenation over K promoted Rh/Al_2O_3
$CO:H_2 = 1:1.8$

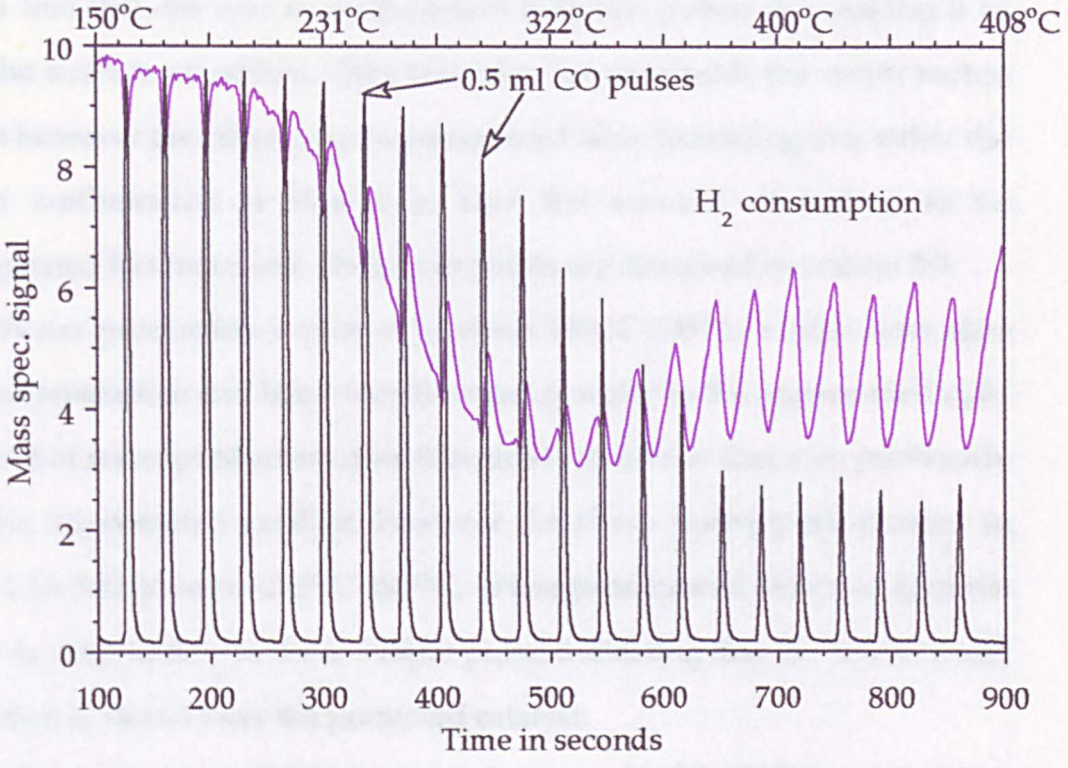

Figure 5.3.(b)
T.P.P.R. CO hydrogenation over K promoted Rh/Al_2O_3
showing products. $CO:H_2 = 1:1.8$

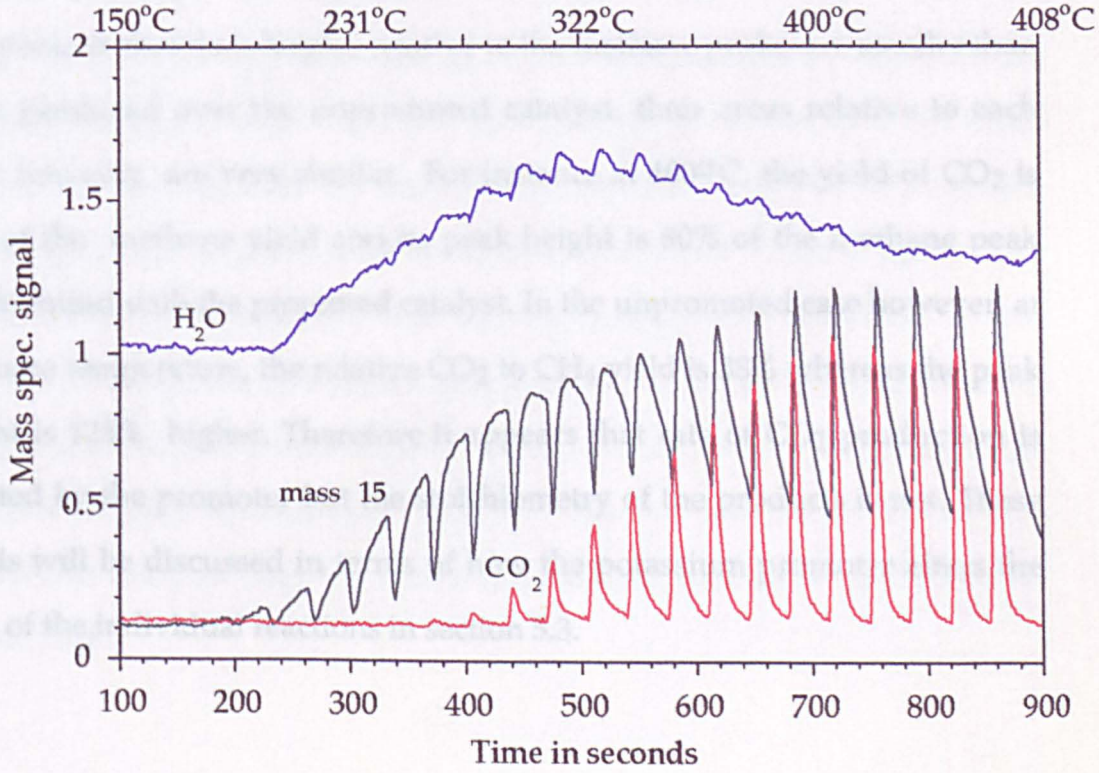

production was reached between 310°C-320°C. It can be seen from the mass 15 base line that the rate of methanation between pulses is insufficient to clean the surface of carbon. This was also the case with the unpromoted catalyst however the effect is more pronounced here, indicating that either the rate of methanation is slower or that the amount of carbon to be hydrogenated has increased. These two points are discussed in section 5.3.

Water production begins at between 180°C-200°C, a little later than methane production and later than the onset of water in the unpromoted case. The trend of water production once it begins is similar to that seen previously with the unpromoted catalyst, however the sharp water peak present in Figure 3.13.(b) between ~250°C-350°C, is less pronounced here and does not appear as close in time to the CO input pulse, indicating that the rate of water production is slower over the promoted catalyst.

The production of CO_2 begins at between 260°C-270°C, again this is similar though fractionally lower in temperature, than the on-set of CO_2 over the unpromoted catalyst (~270°C-280°C). It is apparent that the rate of CO_2 production is fast compared to both water and methane and that its yield increases steadily with temperature. An interesting point to note with the CO_2 peaks is that their height, relative to the methane peaks, are smaller than those produced over the unpromoted catalyst, their areas relative to each other however are very similar. For instance at 400°C, the yield of CO_2 is 34% of the methane yield and its peak height is 80% of the methane peak height found with the promoted catalyst. In the unpromoted case however, at the same temperature, the relative CO_2 to CH_4 yield is 38% whereas the peak height is 125% higher. Therefore it appears that rate of CO_2 production is affected by the promoter but the stoichiometry of the products is not. These trends will be discussed in terms of how the potassium promoter alters the rates of the individual reactions in section 5.3.

The conversion of CO begins very slowly at between 160°C-180°C evident through methane production, however the conversion doesn't reach appreciable levels until ~220°C. It is at this temperature that methane and water production begin to increase dramatically as a result of CO dissociation. There is a rapid increase in CO conversion over the temperature range of the T.P.P.R. experiment, a few comparable CO conversions for the promoted and unpromoted catalyst under these conditions are tabulated below. Evident from this data, and indeed simply from looking at the CO peaks in figure 5.3(a), is that CO conversion is similar in both cases up to ~310°C however it continues to rise with temperature in the promoted case whereas it levels off above 320°C in the unpromoted case.

Temperature °C	CO Conversion Rh/Al_2O_3	CO Conversion $K/Rh/Al_2O_3$
220°C	1%	1.7%
310°C	33%	34.7%
400°C	43%	77.3%

The general trends in product yields versus temperature and CO conversion versus temperature are illustrated more clearly in a bar chart format, Figures 5.4.(a) and (b). One obvious difference between the promoted and unpromoted catalysts is the continued high rate of methane production above 310°C in the promoted case. We saw in Chapter 3. figure 3.16.(b) that above 310°C methane production dropped as CO_2 production rose, because the CO conversion slowed above 310°C and there was a direct trade off between the two methanation reactions. Here we see that although CO_2 production rises, so does CO conversion, allowing methane production to remain high.

Figure 5.4.(a)
CO conversion with temperature rise.
$CO : H_2 = 1 : 1.8$

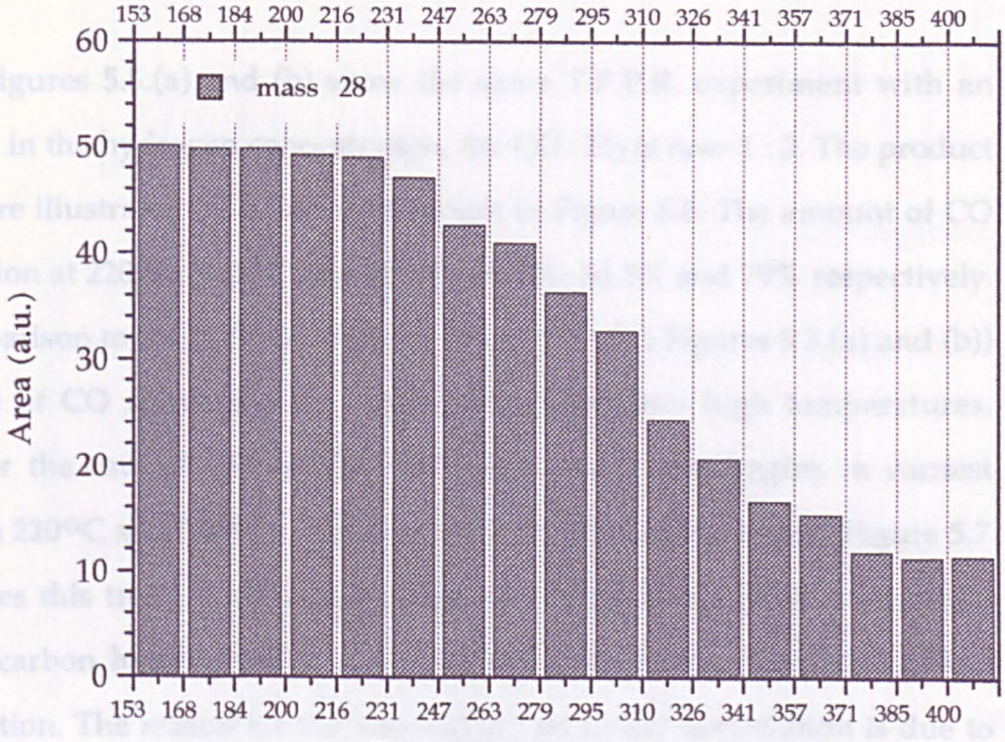

Figure 5.4.(b)
Product formation with temperature rise.
$CO : H_2 = 1:1.8$

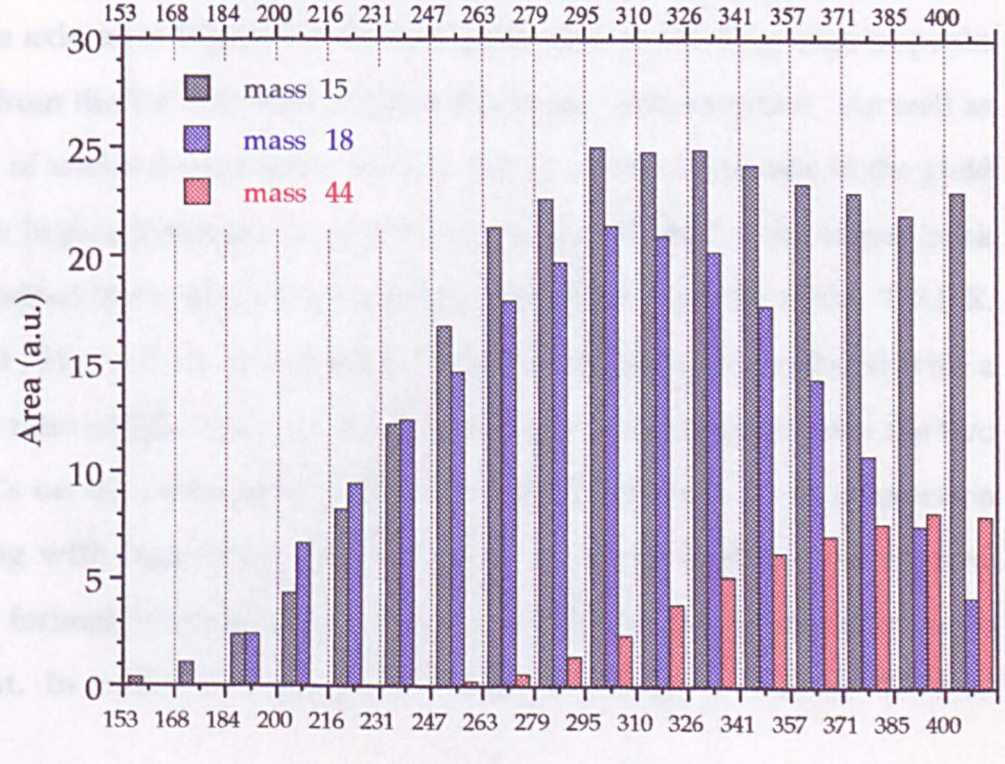

5.2.3. CO HYDROGENATION WITH HIGHER H_2 CONCENTRATIONS.

Figures 5.5.(a) and (b) show the same T.P.P.R. experiment with an increase in the hydrogen concentration, the CO : H_2 is now 1 : 3. The product yields are illustrated in a bar chart format in Figure 5.6. The amount of CO conversion at 220°C, 310°C and 400°C is 5.5%, 64.5% and 79% respectively. In comparison to the T.P.P.R. with CO : H_2 = 1 : 1.8, (Figures 5.3.(a) and (b)) the rate of CO conversion is similar at the low and high temperatures, however the rate of CO conversion, once dissociation begins in earnest between 220°C and 350°C, is faster with more hydrogen present. Figure 5.7. illustrates this trend more clearly. Evidently, more hydrogen increases the rate of carbon hydrogenation but does not lower the temperature of CO dissociation. The reason for the increase in rate of CO dissociation is due to the surface of the catalyst being cleaned of carbonaceous deposits faster as a result of the higher hydrogen concentration. The dramatic increase in C(a) hydrogenation as a function of hydrogen pressure is illustrated clearly when the mass 15 line shapes from Figure 5.3.(b) and Figure 5.5.(b) are plotted on the same axis, as in Figure 5.8. Evident is the sharper leading edge of peaks arising from the T.P.P.R. with a higher hydrogen concentration. As well as the rate of methane production there is also an apparent increase in the yield with the higher hydrogen concentration, as evidenced by the larger peak areas. Indeed the total yield of methane produced over the whole T.P.P.R. with CO : H_2 = 1 : 3 is 46% more than the total amount produced with a reactant ratio of CO : H_2 = 1 : 1.8. The total CO conversion between the two T.P.P.R.'s on the other hand differs by only 6.5 % (with more conversion occurring with higher H_2) . With a similar conversion of CO and no new product formed, it seems curious that the yield of methane appears to be so different. In order to explore this more thoroughly, further T.P.P.R.

Figure 5.5.(a)
T.P.P.R. CO hydrogenation over K promoted Rh/Al_2O_3
$CO : H_2 = 1 : 1.8$

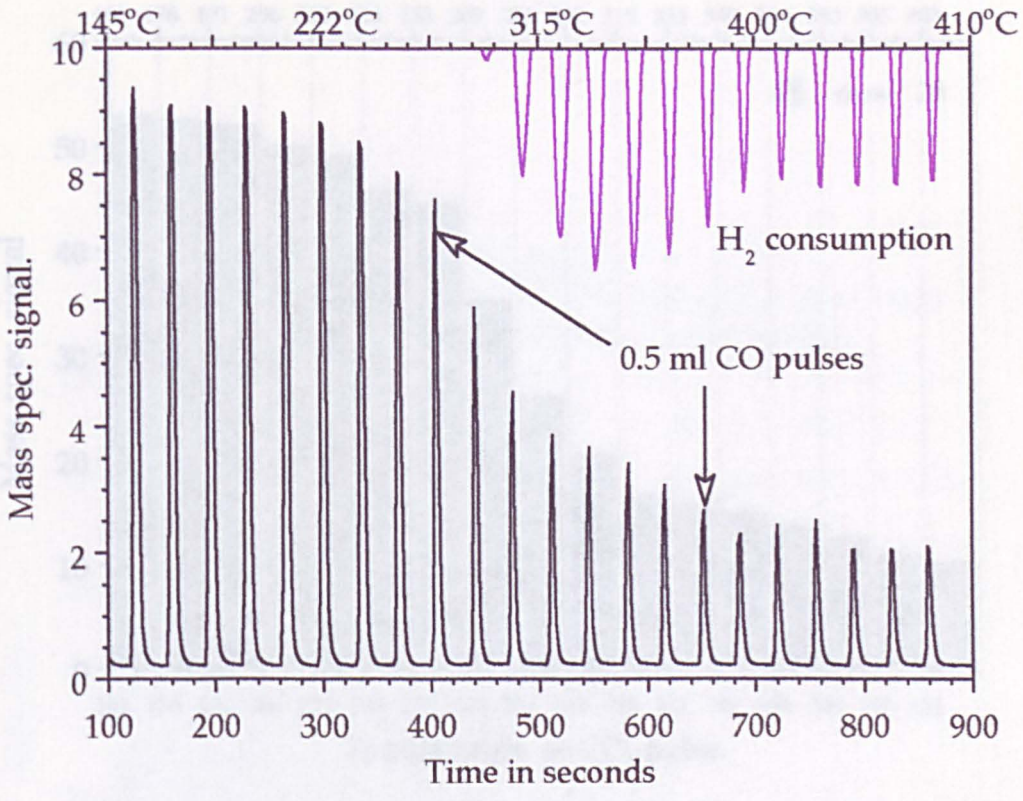

Figure 5.5.(b)
T.P.P.R. CO hydrogenation over K promoted Rh/Al_2O_3
showing products. $CO : H_2 = 1 : 3$

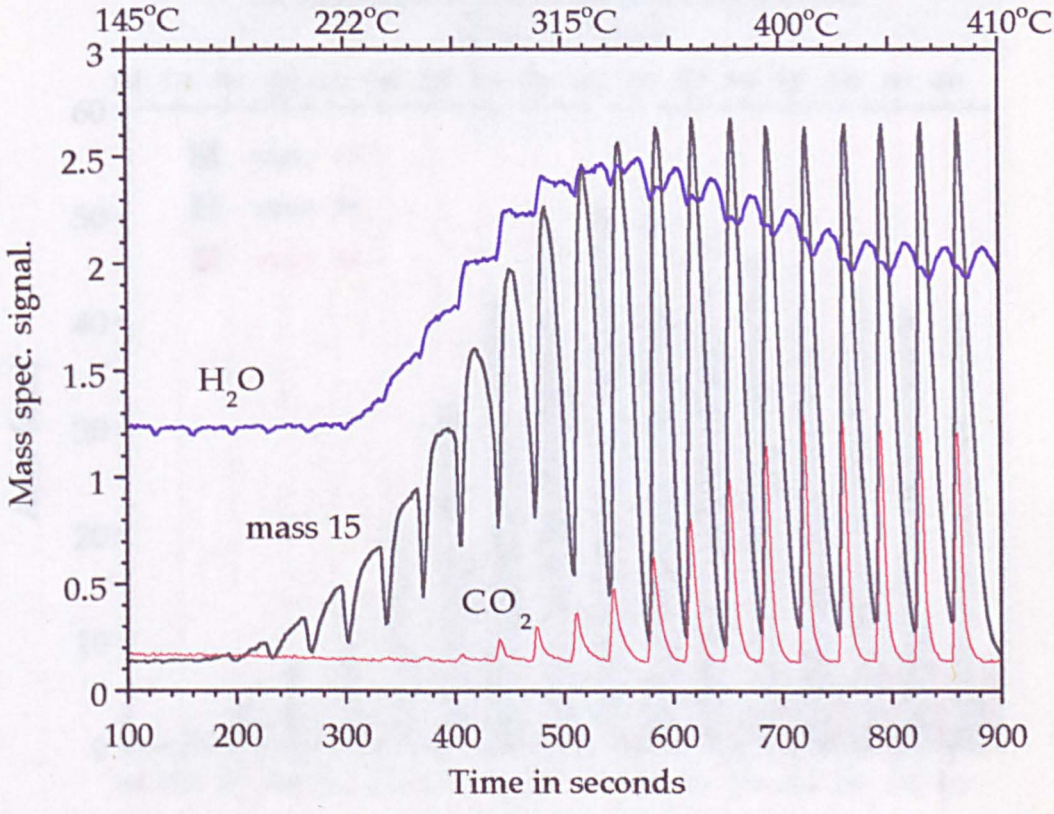

Figure 5.6.(a)
CO conversion with temperature rise.
$CO : H_2 = 1 : 3$

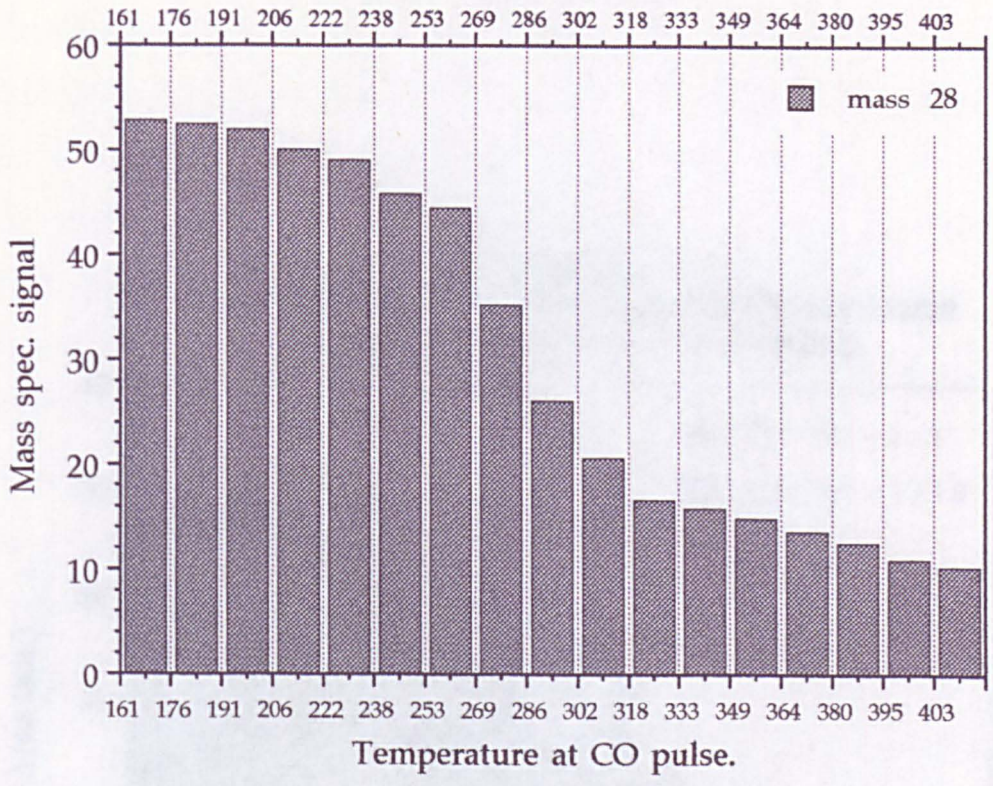

Figure 5.6.(a)
Product formation with temperature rise.
$CO : H_2 = 1 : 3$

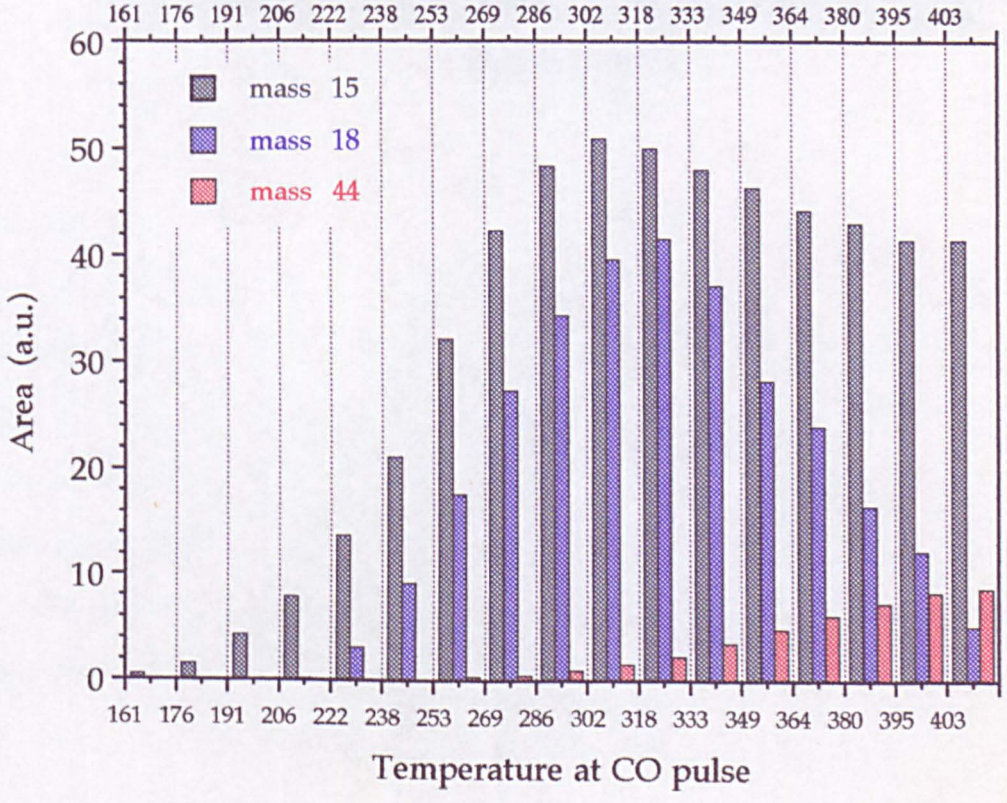

Figure 5.7.
A comparison of the change in rate of CO conversion with temperature and H_2 concentration.

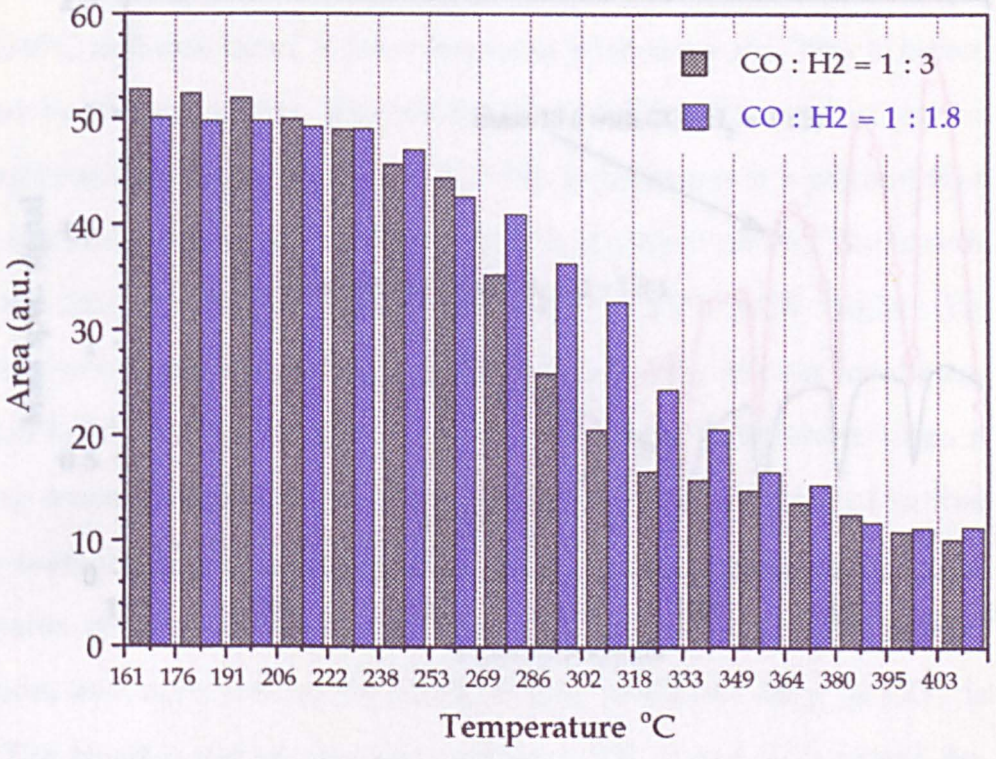

Figure 5.8.
Expanded view of methane production over promoted catalyst with different H_2 concentrations.

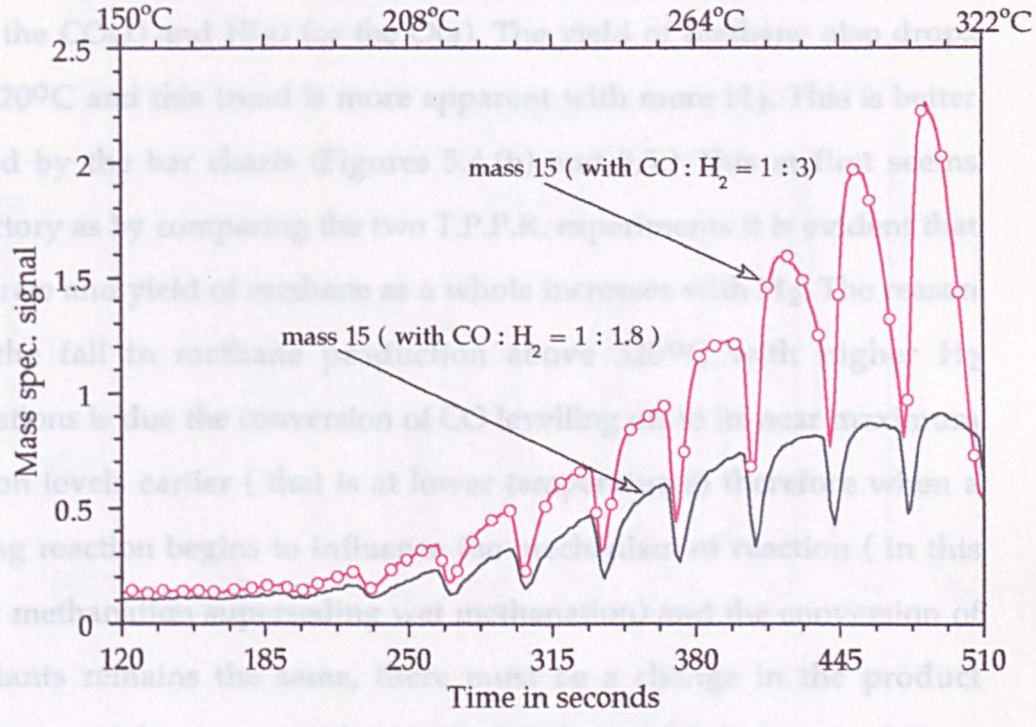

experiments and a series of isothermal pulsed experiments were conducted, and are described in section 5.2.5.

Noticeable from Figure 5.5.(b) is that with higher H_2, more methane and water is formed in the time between pulses, but the yield of CO_2 is practically the same as that seen with lower H_2. The water peak drops markedly with the onset of CO_2 production as there is direct competition between the CO(a) and H(a) for the O(a). The yield of methane also drops above ~320°C and this trend is more apparent with more H_2. This is better illustrated by the bar charts (Figures 5.4.(b) and 5.6.) This at first seems contradictory as by comparing the two T.P.P.R. experiments it is evident that both the rate and yield of methane as a whole increases with H_2. The reason behind the fall in methane production above 320°C with higher H_2 concentrations is due the conversion of CO levelling off to its near maximum conversion levels earlier (that is at lower temperatures) therefore when a competing reaction begins to influence the mechanism of reaction (in this case, dry methanation superseding wet methanation) and the conversion of the reactants remains the same, there must be a change in the product distribution, and here we see the yield of CH_4 and H_2O drop as CO_2 is formed. The trend is not as apparent in Figure 5.3.(a) and (b) because the conversion of CO is still rising throughout the experiment, therefore compensating this effect.

The CO_2 line shapes at first glance are very similar, however upon close inspection of the base line, slight differences appear with a change in H_2 concentration. Figure 5.9. shows the CO_2 production from Figures 5.3.(b) and 5.5.(b) plotted on the same page. When the hydrogen concentration is low, a broad background rise is evident, as was the case with the unpromoted catalyst. When the concentration of hydrogen rises, the background rise in CO_2 diminishes. The background is most likely to be the decomposition of a support species such as formate, that decompose to CO_2 at these

Figure 5.9.
Showing increased tail to CO_2 line shape during
CO hydrogenation with reduced H_2 concentration.

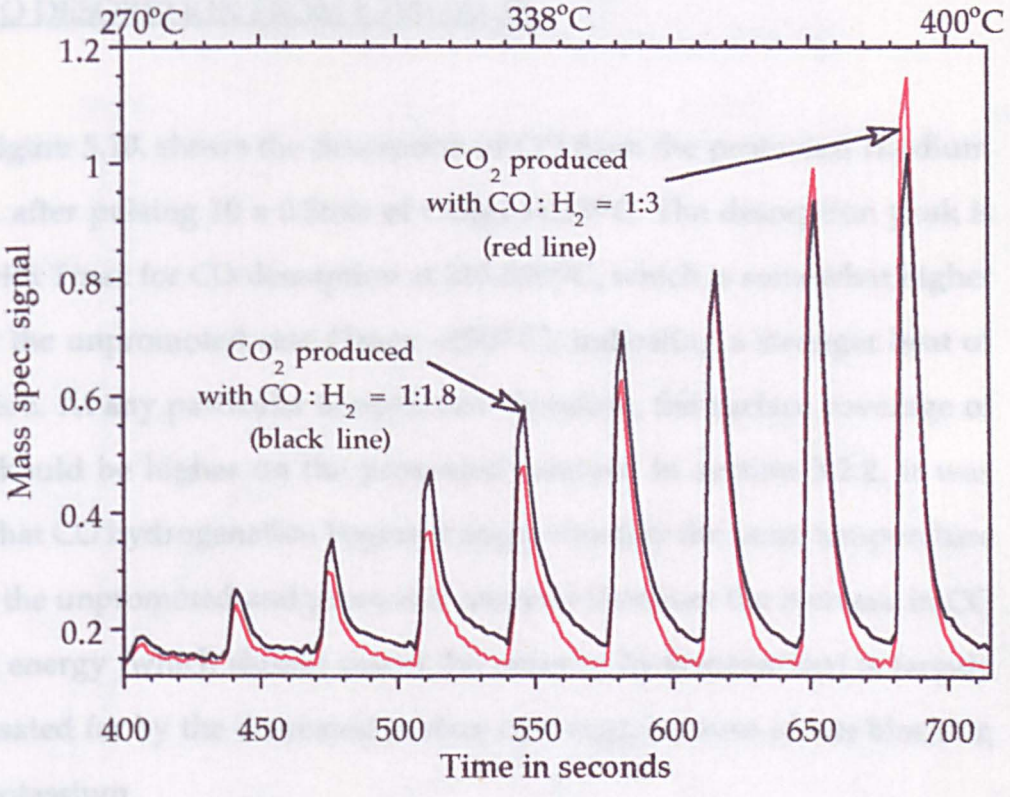

temperatures. With higher hydrogen concentrations, the formates are hydrogenated to methane readily and so do not cause a rise in the CO_2 baseline.

5.2.4. CO DESORPTION FROM $K/Rh/Al_2O_3$

Figure 5.10. shows the desorption of CO from the promoted rhodium catalyst, after pulsing 10 x 0.5mls of CO(g) at 35°C. The desorption peak is broad with Tmax for CO desorption at 210-220°C, which is somewhat higher than for the unpromoted case (Tmax ~180°C), indicating a stronger heat of adsorption. At any particular temperature therefore, the surface coverage of CO(a) should be higher on the promoted catalyst. In section 5.2.2. it was shown that CO hydrogenation begins at approximately the same temperature on both the unpromoted and promoted catalysts therefore the increase in CO binding energy (which should retard the onset of hydrogenation) is largely compensated for by the decreased surface coverage, because of site blocking by the potassium .

After depositing carbon on the surface of the catalyst by pulsing CO at 400°C, then cooling quickly to 50°C, it was hydrogenated away in a temperature programmed reaction (T.P.R.) experiment shown in Figure 5.11., it is analogous to Figure 3.9. in Chapter 3. The T.P.R. reveals a similar methane desorption profile to the unpromoted case however the peak Tmax for hydrogenation is higher over the promoted catalyst and the activation energy to hydrogenation of the C(a) has risen to 69kJmol^{-1} clearly demonstrating that the metal-carbon bond strength is increased with the addition of potassium. The activation energy for hydrogenation of C(a) over the unpromoted catalyst was 57kJmol^{-1}. The probable reason why the temperature required to hydrogenate C(a) laid down from CO pulses at

Figure 5.10.
CO desorption from $K/Rh/Al_2O_3$ catalyst

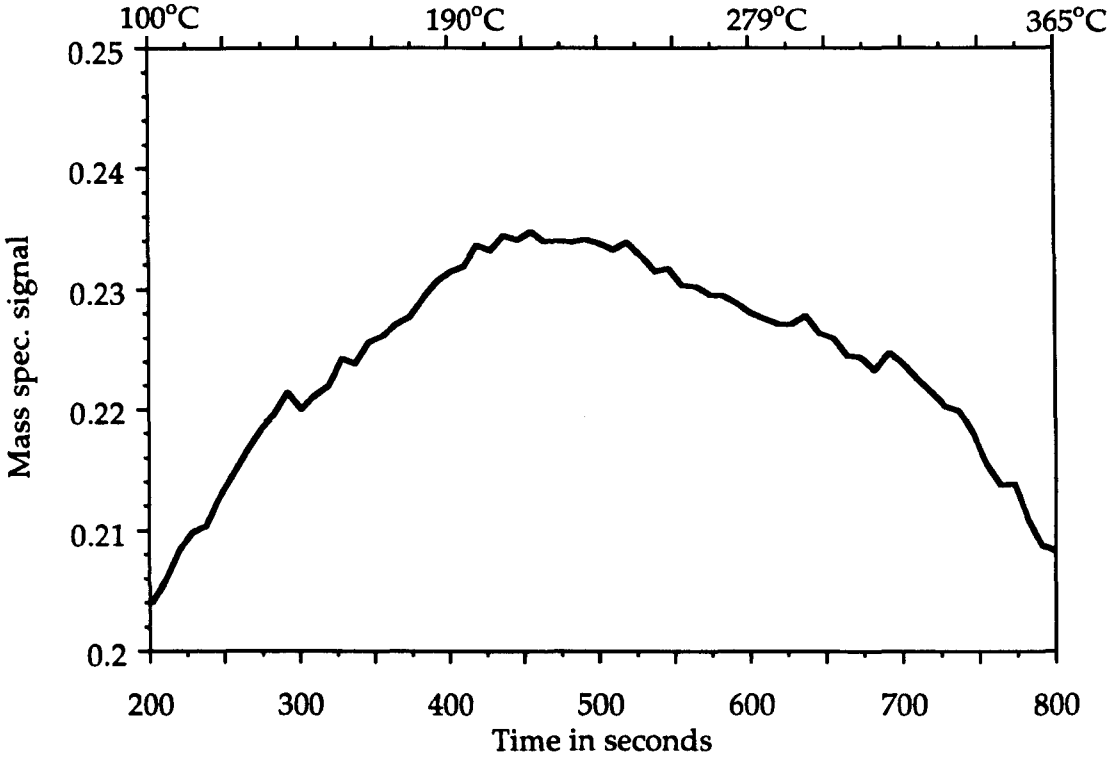

Figure 5.11.
T.P.R. with H_2 = 1 ml per minute showing carbon clean off from K/Rh/Al_2O_3 after CO pulses at 400°C.

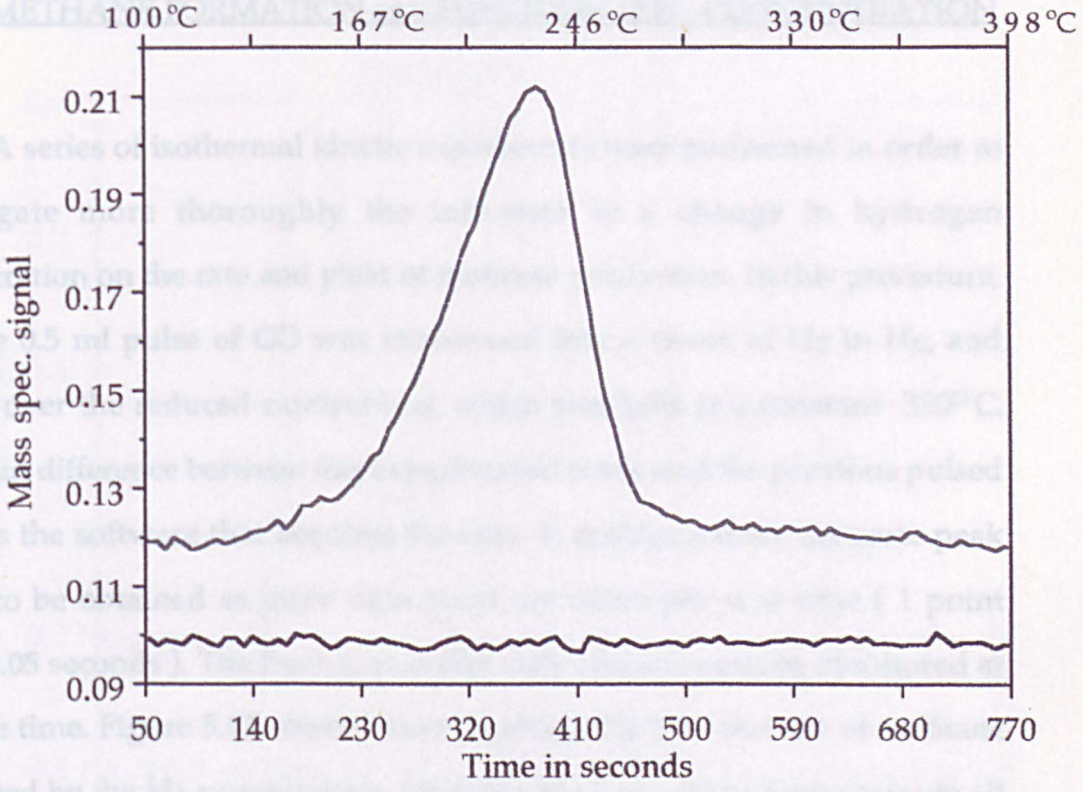

400°C is higher than the onset of methane production during the T.P.P.R. is because the C(a) has had time to age and in so doing has found the strongest binding sites such that the effect of the potassium is maximised.

5.2.5. METHANE FORMATION as a FUNCTION of H_2 CONCENTRATION

A series of isothermal kinetic experiments were performed in order to investigate more thoroughly the influence of a change in hydrogen concentration on the rate and yield of methane production. In this procedure, a single 0.5 ml pulse of CO was introduced into a steam of H_2 in He, and passed over the reduced catalyst bed, which was held at a constant 350°C. The main difference between this experimental mode and the previous pulsed mode is the software that acquires the data. It enables a more accurate peak shape to be obtained as more data point are taken per unit time (1 point every 0.05 seconds). The limitation is that only one mass can be monitored at any one time. Figure 5.12. shows more emphatically how the rate of methane is effected by the H_2 concentration. With the H_2 flow rate at 5 mls/minute all of the C(a) is hydrogenated away to methane within 25 seconds, whereas with H_2 = 2.5 mls per minute the rate is slowed so that ~42 seconds are required to hydrogenate away the C(a) and with H_2 at 1 ml per minute, ~100 seconds are required. However the reduction in hydrogen concentration does not markedly effect the extent of CO dissociation represented here as the yield of methane. The methane integrals with H_2 at 5 mls and 2.5 mls per minute are identical, the methane peak with H_2 = 1 ml per minute is slightly smaller due to the formation of CO_2, as seen in the T.P.P.R. experiments. As the dissociation of CO is not affected by a doubling of the hydrogen concentration, it is clear that H_2 does not assist in the dissociation step, its role in the reaction is to clean the surface of C(a) through hydrogenation and

Figure 5.12.
Change in methanation of CO pulse with H_2 concentration

Temperature = 350°C

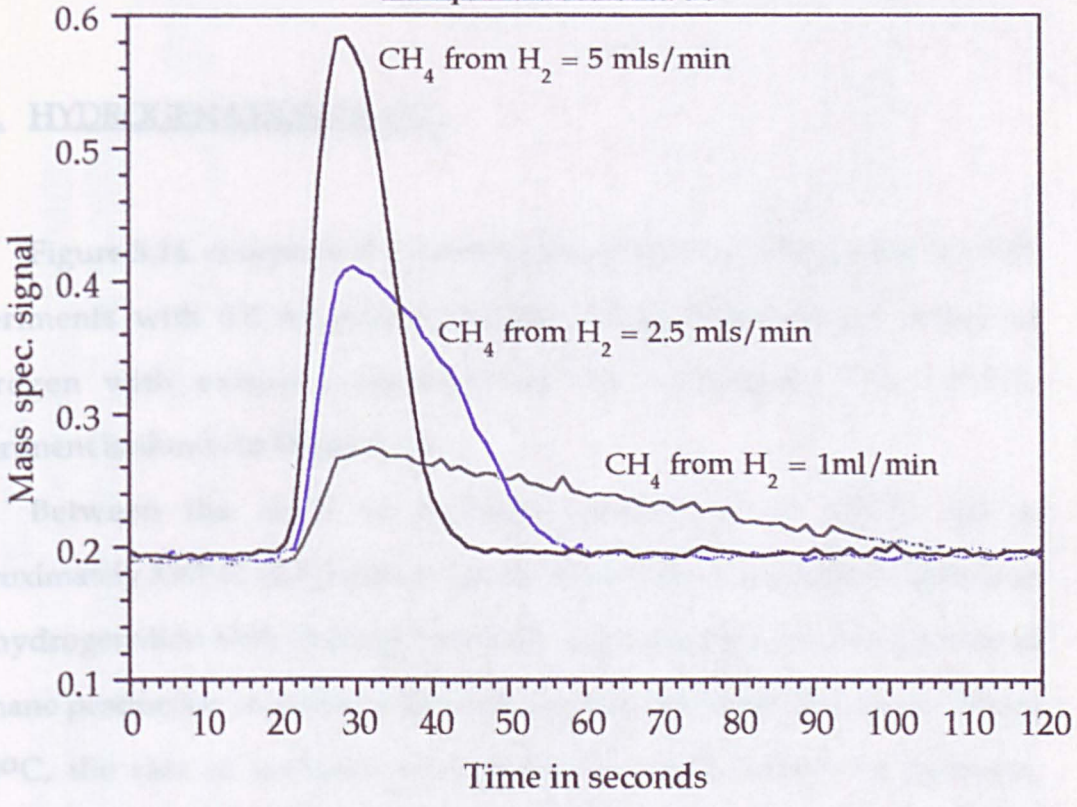

the rate of this process is determined by the H_2 concentration. These points are further clarified by the results shown in Figure 5.13. which shows the methane line shapes from a series of CO T.P.P.R. experiments in which the hydrogen concentration was varied from 1 ml per minute to 5 mls per minute. Note than the onset of methane production is the same temperature in each case but the rate of methanation varies remarkably.

5.2.6. HYDROGENATION OF CO_2

Figure 5.14. compares the methane line shapes resulting from T.P.P.R. experiments with 0.5 ml pulses of CO_2 being eluted into a stream of hydrogen with various concentrations. The analogous CO T.P.P.R. experiment is shown in Figure 5.13.

Between the onset of methane production at 170°C up to approximately 330°C, CO_2 hydrogenation follows the same general trends as CO hydrogenation with varying hydrogen concentrations, in that the rate of methane production increases with an increase in hydrogen. However above ~330°C, the rate of methane production from CO_2 begins to decrease, evidenced by the front edge of the line becoming less acute and the width of the peak broadening. This is particularly evident with the H_2 flow rate at 2.5 mls per minute, although the trend is seen with all the hydrogen concentrations tried. The rate of methanation of CO continues to rise with temperature. The onset temperature of methane production is the same in both CO and CO_2 hydrogenation and is ~180°C. The intrinsic rate of methane production from CO_2 hydrogenation is faster than that from CO hydrogenation. These trends were also observed with the unpromoted catalyst, see Chapter 3. From Figure 5.14. it is clear that with H_2 flow at ≥2.5 mls per minute the methane signal approaches the base-line between pulses

Figure 5.13.
T.P.P.R. of CO. Comparing methane production with various H_2 flow rates

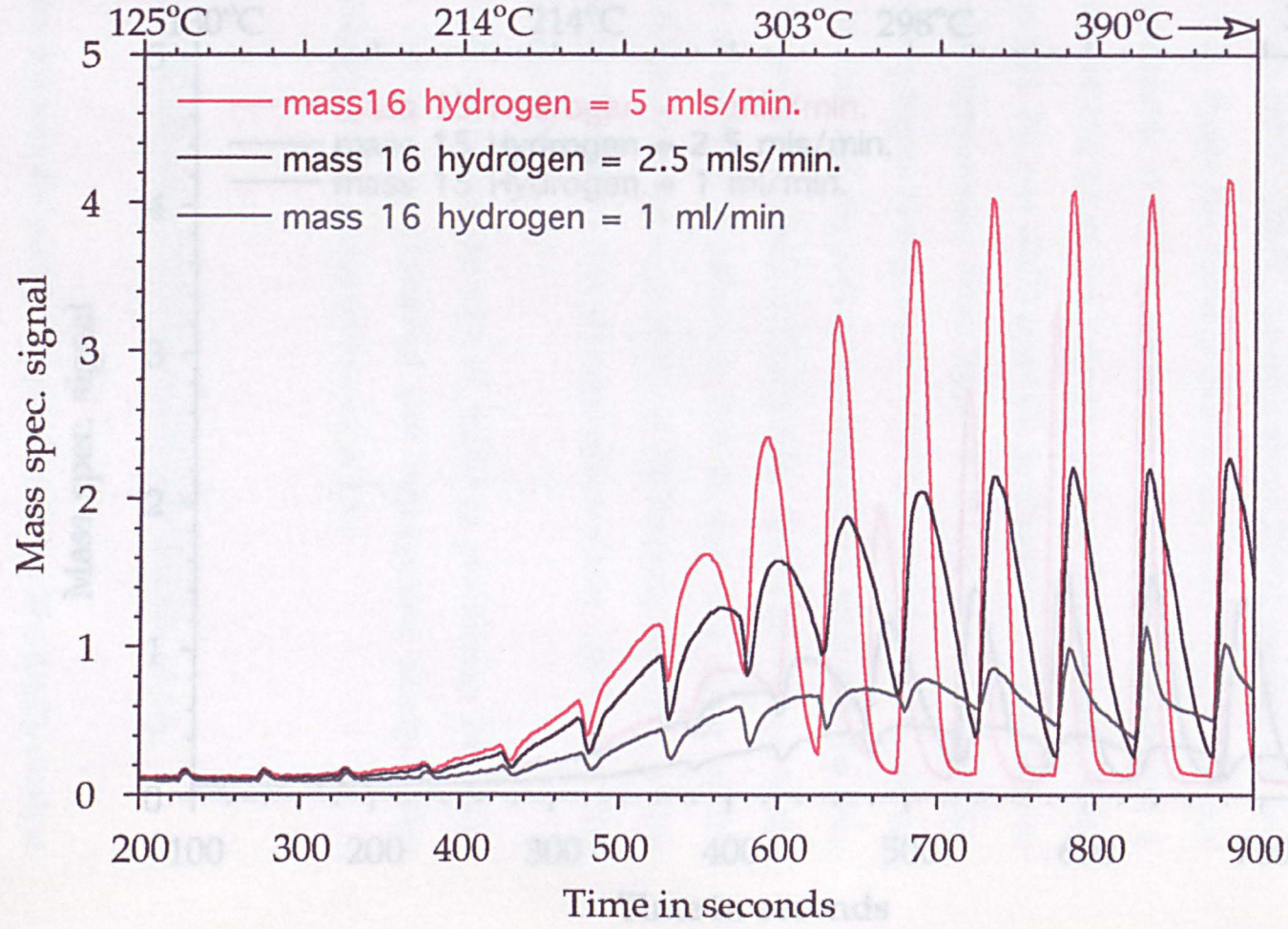

Figure 5.14.
T.P.P.R. of CO_2. Comparing methane production with various H_2 flow rates

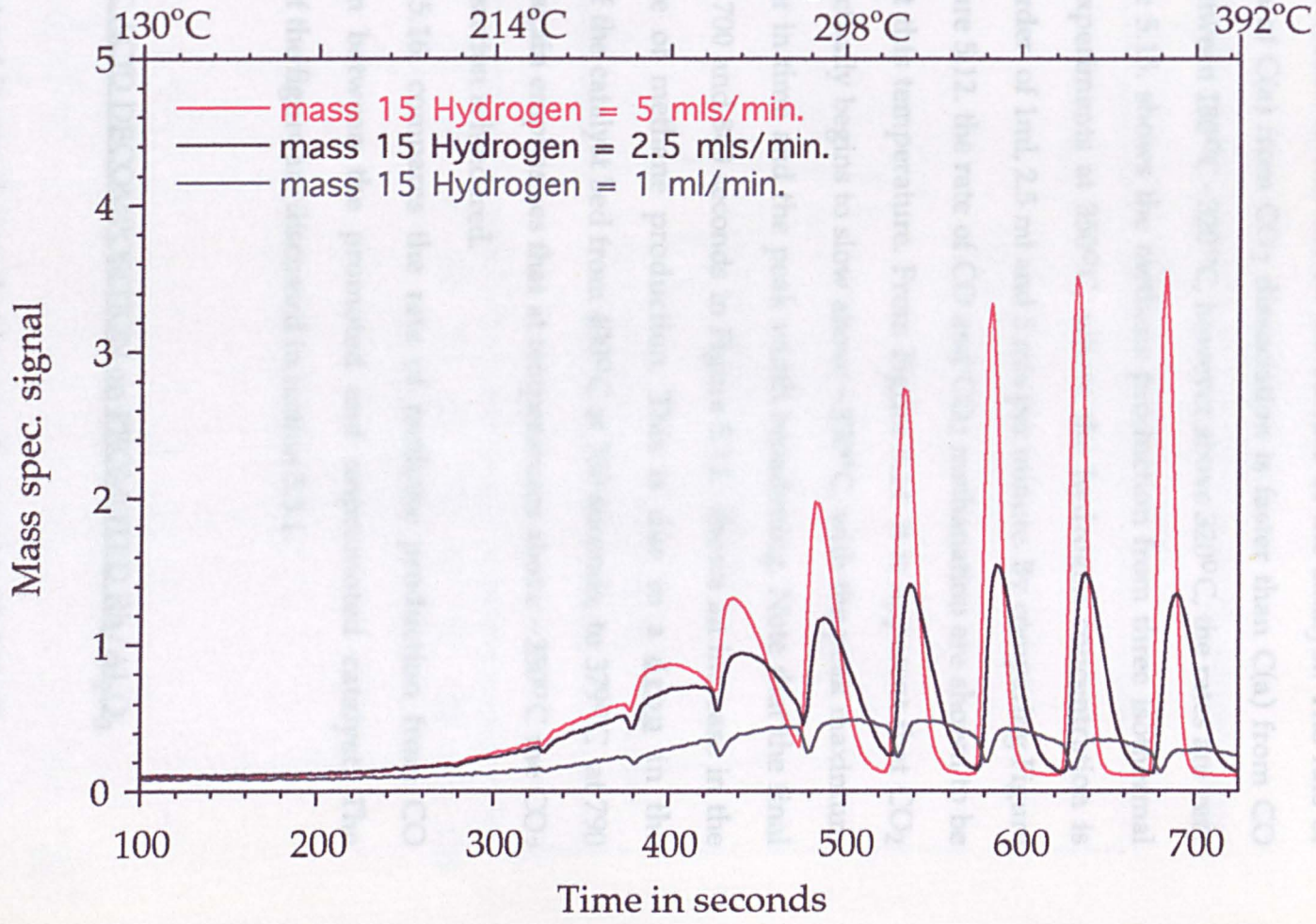

at ~ 300°C. In the case of CO hydrogenation, at the same temperature and hydrogen concentration, the methane production is still proceeding, indicating that carbon is still left on the surface of the catalyst. The rate of hydrogenation of C(a) from CO_2 dissociation is faster than C(a) from CO dissociation between 180°C - 320°C, however above 320°C, the rates are very similar. Figure 5.15. shows the methane production from three isothermal CO_2 pulsed experiments at 350°C, where the hydrogen concentration is varied in the order of 1ml, 2.5 ml and 5 mls per minute. By comparing Figure 5.15. with Figure 5.12. the rate of CO and CO_2 methanation are shown to be very similar at this temperature. From Figure 5.14. it is apparent that CO_2 methanation actually begins to slow above ~350°C, with the peak maximum appearing later in time and the peak width broadening. Note that the final peak between 700 and 800 seconds in Figure 5.14. shows an increase in the yield and rate of methane production. This is due to a drop in the temperature of the catalyst bed from 400°C at 730 seconds, to 379°C at 790 seconds. This again emphasises that at temperatures above ~350°C the CO_2 methanation reaction is hindered.

Figure 5.16. compares the rate of methane production from CO hydrogenation between the promoted and unpromoted catalyst. The implications of the figure are discussed in section 5.3.1.

5.2.7. ACETIC ACID DECOMPOSITION on PROMOTED Rh/Al_2O_3.

In Chapter 4 it was shown that by pre-dosing the Rh/Al_2O_3 catalyst with oxygen, a stable acetate intermediate can be formed on the rhodium phase, which autocatalytically decomposes once the decomposition process is initiated. The decomposition is manifested as an extremely narrow peak during T.P.D., termed a 'surface explosion'. The main factors in producing a

Figure 5.15.
Change in methanation of CO_2 pulse with H_2 concentration.

Temperature = 350°C

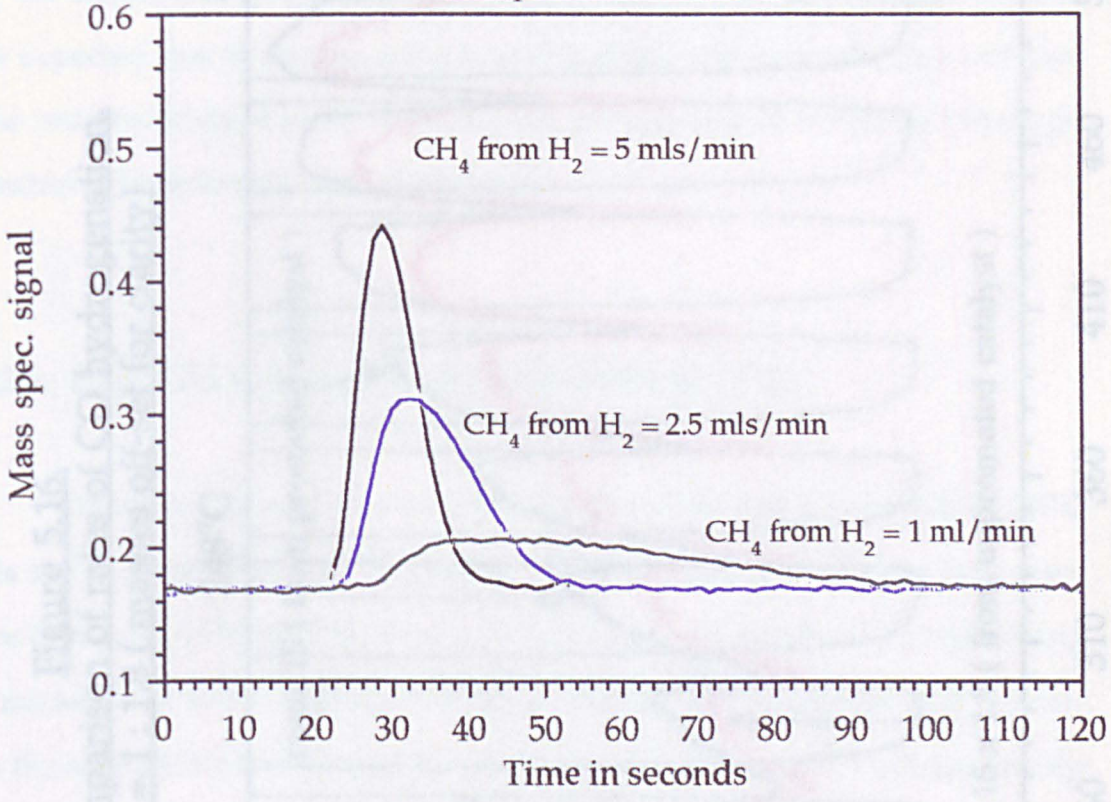

Figure 5.16.
Showing comparison of rates of CO hydrogenation.
$CO : H_2 = 1 : 1.8$ (masses off-set for clarity)

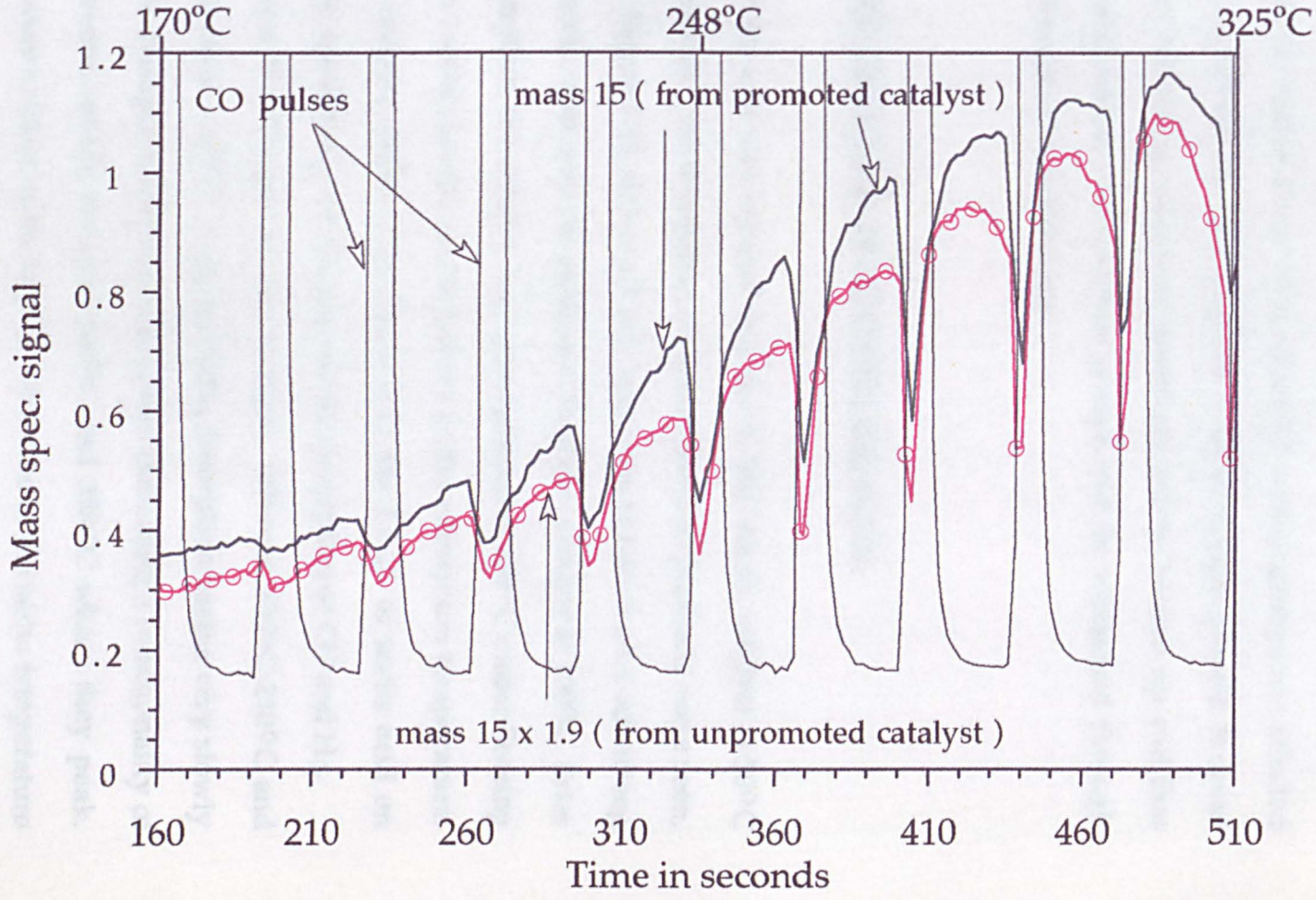

stable acetate on the rhodium phase were a 'site filling' by the oxygen adatoms, of free rhodium sites which initiate the decomposition, and a mutual electronic affinity between the oxygen adatoms and the acetate adlayer. As potassium alters the electronic state of a metal onto which it is absorbed, it was of interest to see how adsorbed acetate groups are affected by the addition of potassium, both with and without oxygen present. It could be expected that the dense adlayer of adsorbate will be broken up and that the intramolecular bonds of the acetate groups will be weakened through electronic backdonation from the metal.

5.2.8. REDUCED CATALYST - NO OXYGEN PRE-DOSE.

When acetic acid was injected onto the $K/Rh/Al_2O_3$ catalyst at 50°C via the PTFE septum , no desorption or decomposition products were seen, see Figure 5.17. Figure 5.18. shows a T.P.D. spectrum obtained after adsorbing 1 microlitre of acetic acid onto the promoted rhodium catalyst at 100°C. Prior to the acid adsorption, the catalyst had been reduced at 400°C under flowing hydrogen, then cooled quickly under helium to the adsorption temperature. The spectrum appears different to Figure 4.3., the T.P.D. of acetic acid on clean Rh/Al_2O_3, particularly with respect to the desorption of CO and H_2.

Desorption of hydrogen is seen to begin between 200°C-210°C and rises to a maximum at ~330°C. CO_2 and CH_4 desorption begins very slowly at ~220°C, their desorptions are near coincident indicating a commonality of origin and increase rapidly between 300°C and 350°C where they peak. These profiles were evident in the unpromoted case in the same temperature range, Figure 4.3. Water production is first seen at ~250°C and rises steadily up to 325°C-330°C when its production is altered by the appearance of a prominent CO desorption peak. The peak of the CO is coincident with the H_2

Figure 5.17.
No masses detected when 1 microlitre of acetic acid was dosed onto the catalyst at 50°C

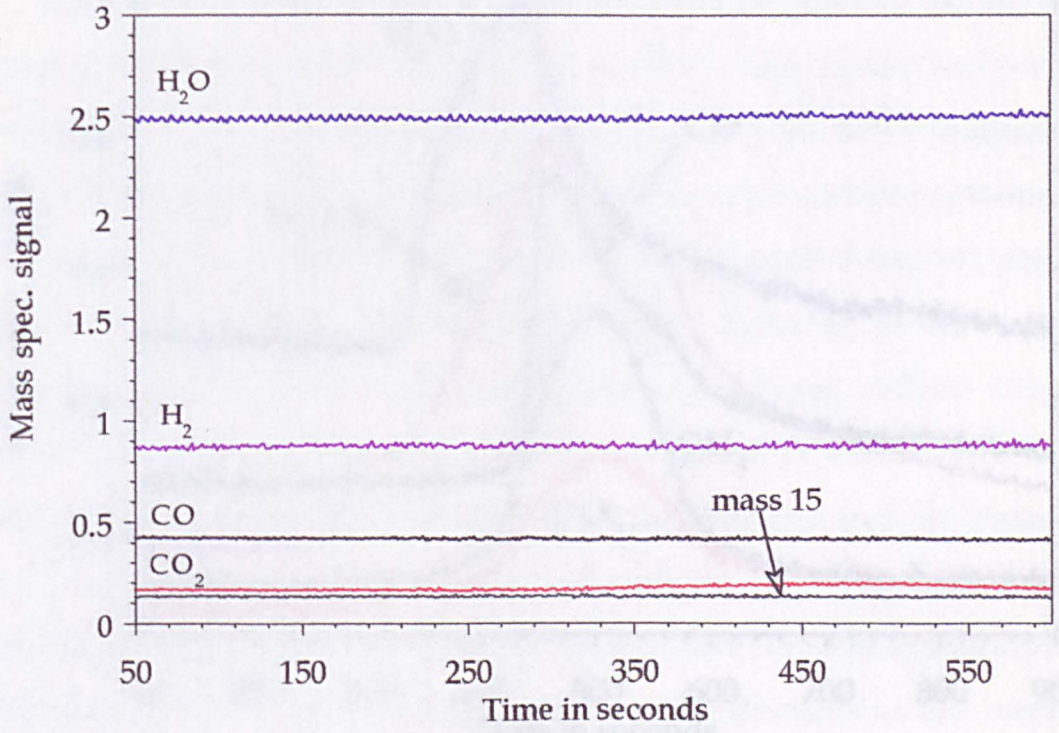

Figure 5.18.

1 microlitre of acetic acid onto reduced catalyst at 100°C then T.P.D. (no O_2 pre-dose)

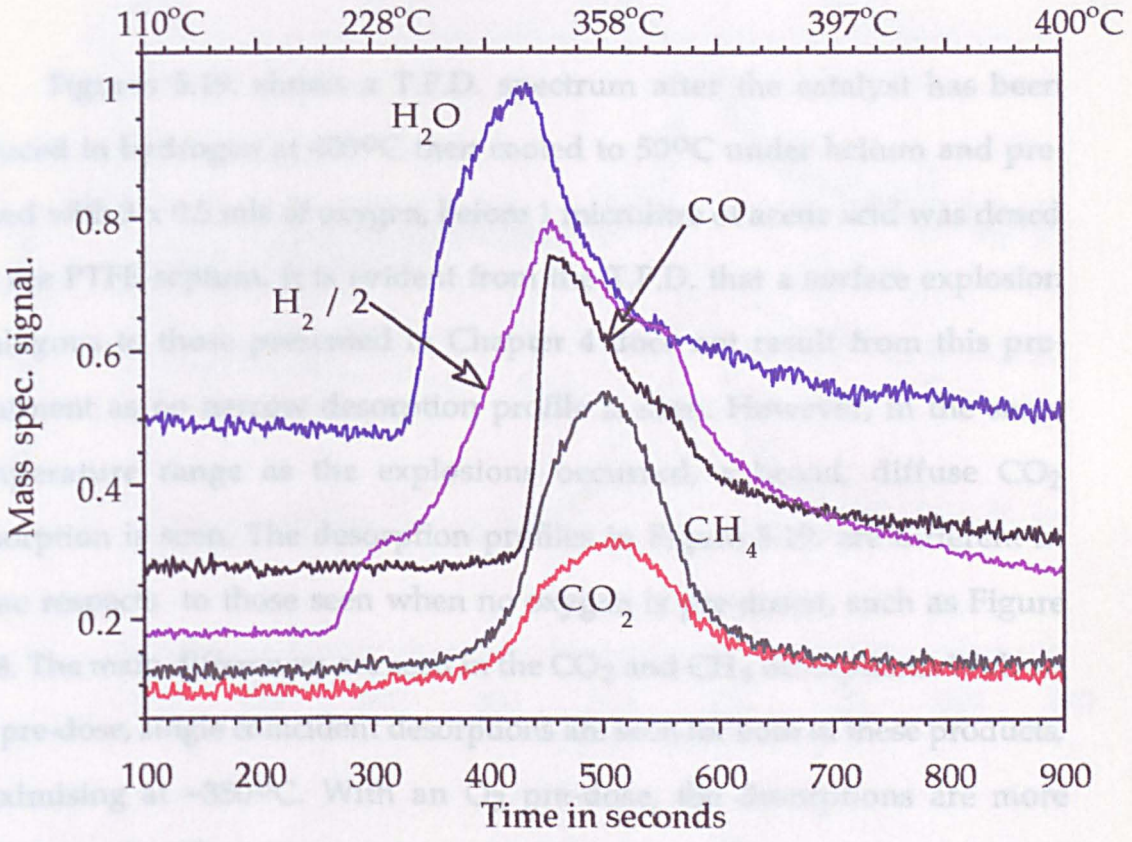

maxima and neither H_2 nor CO appeared in the T.P.D. spectrum of acetic acid on unpromoted Rh/Al_2O_3.

5.2.9. DECOMPOSITION of ACETIC ACID on O_2 PRE-DOSED $K/Rh/Al_2O_3$

Figures 5.19. shows a T.P.D. spectrum after the catalyst has been reduced in hydrogen at 400°C then cooled to 50°C under helium and pre-dosed with 3 x 0.5 mls of oxygen, before 1 microlitre of acetic acid was dosed via the PTFE septum. It is evident from the T.P.D. that a surface explosion analogous to those presented in Chapter 4 does not result from this pre-treatment as no narrow desorption profile is seen. However, in the same temperature range as the explosions occurred, a broad, diffuse CO_2 desorption is seen. The desorption profiles in Figure 5.19. are different in some respects to those seen when no oxygen is pre-dosed, such as Figure 5.18. The main differences are seen in the CO_2 and CH_4 desorptions. With no O_2 pre-dose, single coincident desorptions are seen for both of these products, maximising at ~350°C. With an O_2 pre-dose, the desorptions are more complicated with evidence of a small CO_2 desorption occurring between 220°C and 280°C then between ~280°C and 400°C the CO_2 and CH_4 desorptions coincide and show a double desorption akin to the post explosion desorptions found in the Rh/Al_2O_3 case (Chapter 4). Water desorption coincides with the lower temperature peak of the double desorption where as sharp coincident desorptions of H_2 and CO appear at ~350°C, and accompany the higher temperature CO_2 and CH_4 desorptions.

Figures 5.20. (a) - (d) show various T.P.D. experiments after carrying out the same reduction procedure, however here the temperature of adsorption of oxygen and acetic acid is 100°C rather than 50°C. The results are remarkable as simply with a change in adsorption temperature, an

Figure 5.19.

1.5 mls of O_2 on reduced catalyst at 50°C

Then 1 microlitre of acetic acid.

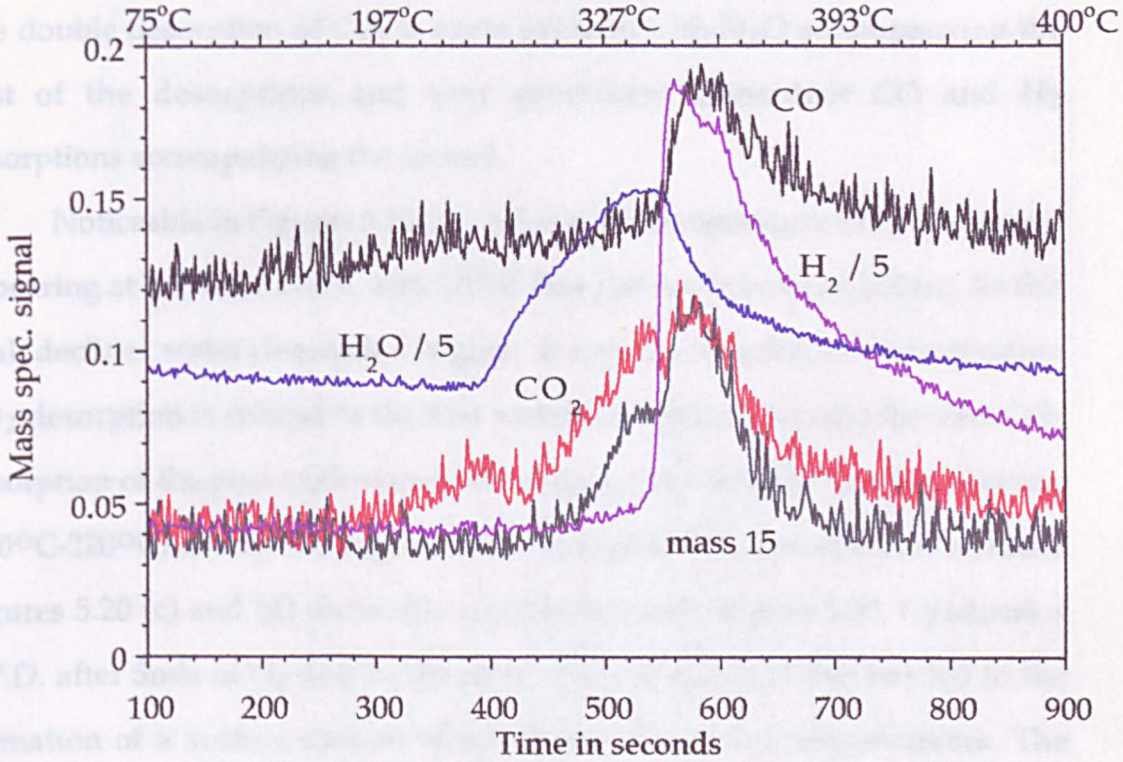

explosion is produced in the T.P.D. The explosion is less well defined than in the unpromoted cases, being somewhat more diffuse and having a wider half peak maximum width. The temperature of the explosions are not markedly different from those seen in the unpromoted case occurring within the same range (220°C - 260°C). they are however all in the upper range of those limits. The double desorption of CO_2 is again evident, with H_2O accompanying the first of the desorptions and very prominent coincident CO and H_2 desorptions accompanying the second.

Noticeable in Figures 5.20.(a) - (d) is a low temperature CO_2 desorption appearing at between 120°C and 220°C that has not been seen before. As this peak declines water desorption begins. It appears that this low temperature CO_2 desorption is related to the first water desorption and also the first CO_2 desorption of the post explosion double hump, as when the low temperature (120°C-220°C) desorption is prominent the higher CO_2 desorption is reduced. Figures 5.20 (c) and (d) show this relationship well. Figure 5.20. (c) shows a T.P.D. after 5mls of O_2 and 1 microlitre of acetic acid and this has led to the formation of a surface species which dissociates at low temperatures. The appearance of this low temperature peak is concurrent with a fall in a later CO_2 desorption and so it seems likely that the same acetates are responsible for both peaks. When the low temperature CO_2 peak is seen, a noticeable shoulder appears on the water desorption, this is shown most clearly when Figures 5.20.(c) and (d) are compared. In Chapter 4 is was suggested that acetates located close to the rhodium particles, migrated and reacted with O(a) adatoms on the rhodium, forming CO_2 and H_2O and this pathway is manifest as the first desorption of the double hump. In this case, it appears that with the addition of K, and a high oxygen predose, the decomposition of the same acetates can occur at a much lower temperature, however when the oxygen pre-dose is 1ml or less, the low temperature decomposition is not seen.

Figure 5.20. (a)

1ml O_2 at 100°C then 1 microlitre of acetic acid.

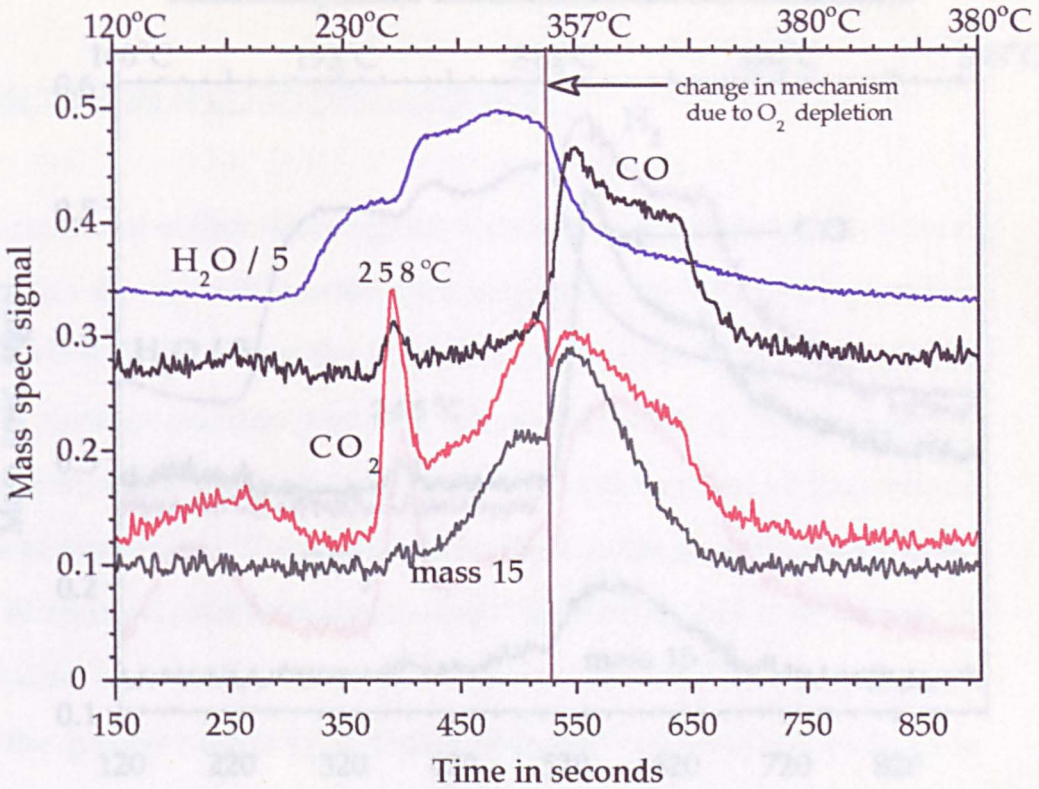

Figure 5.20.(b)

2 mls O_2 at 100°C then 1 microlitre of acetic acid.

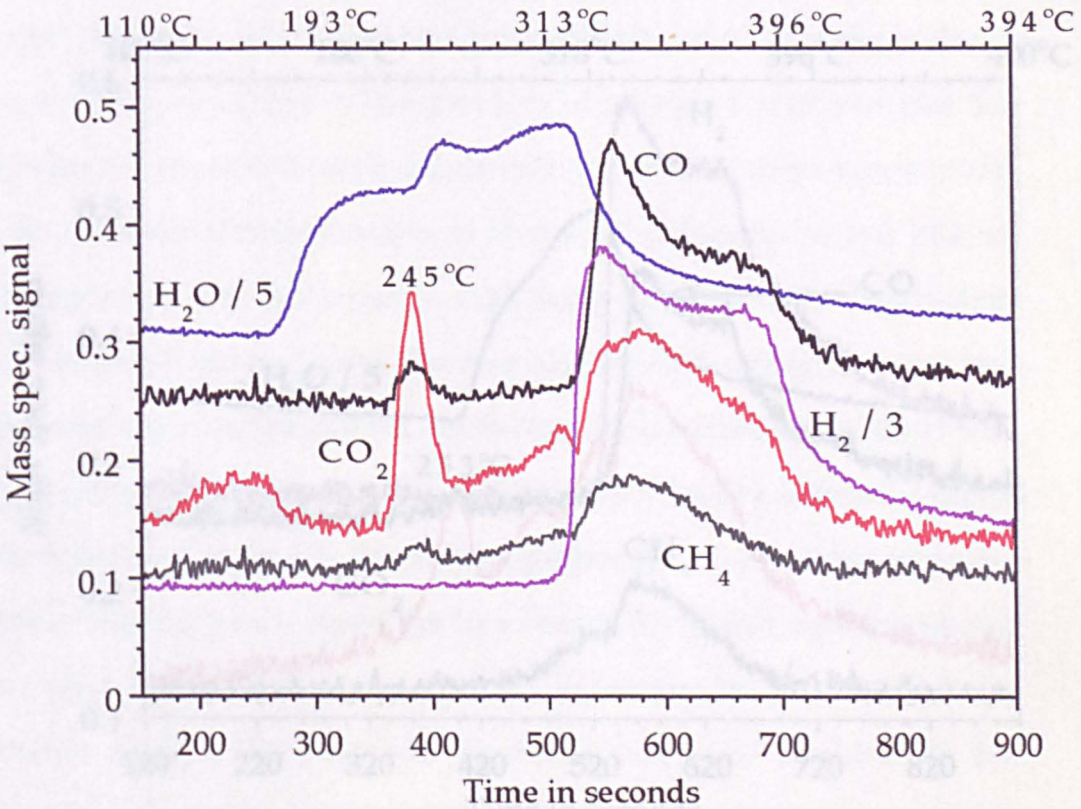

Figure 5.20. (c)

5 mls of O_2 at 100°C them 1 microlitre of acetic acid

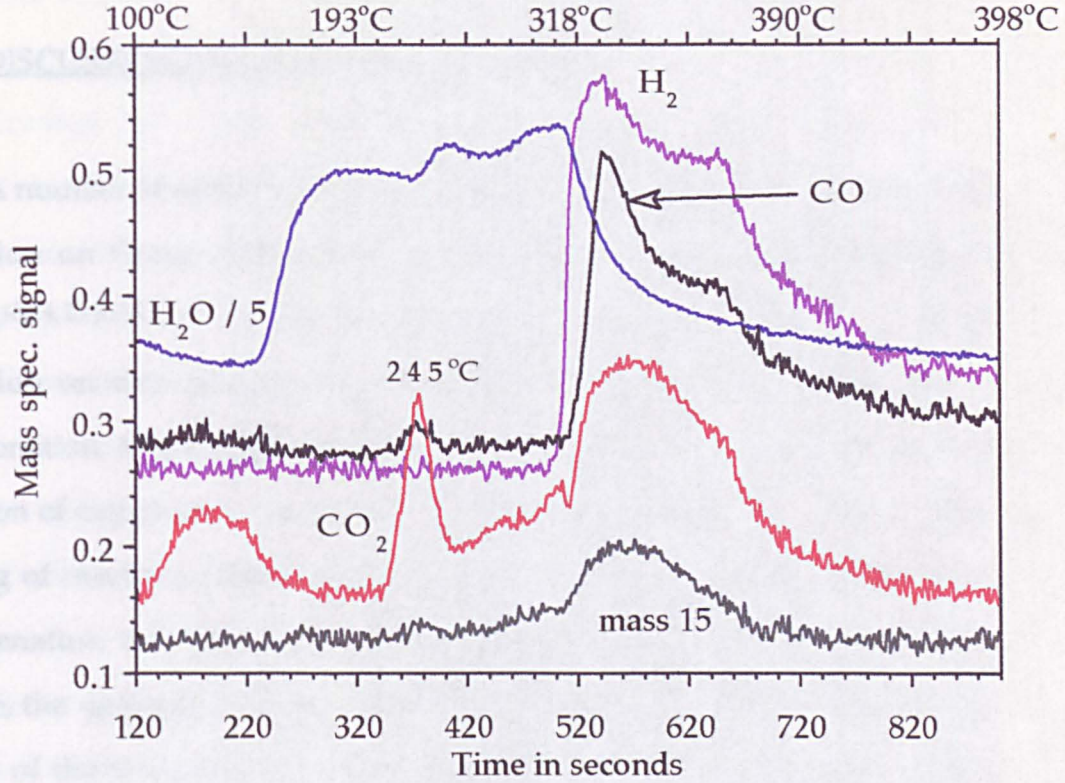

Figure 5.20. (d).

0.5 ml O_2 at 100°C then 1 microlitre of acetic acid

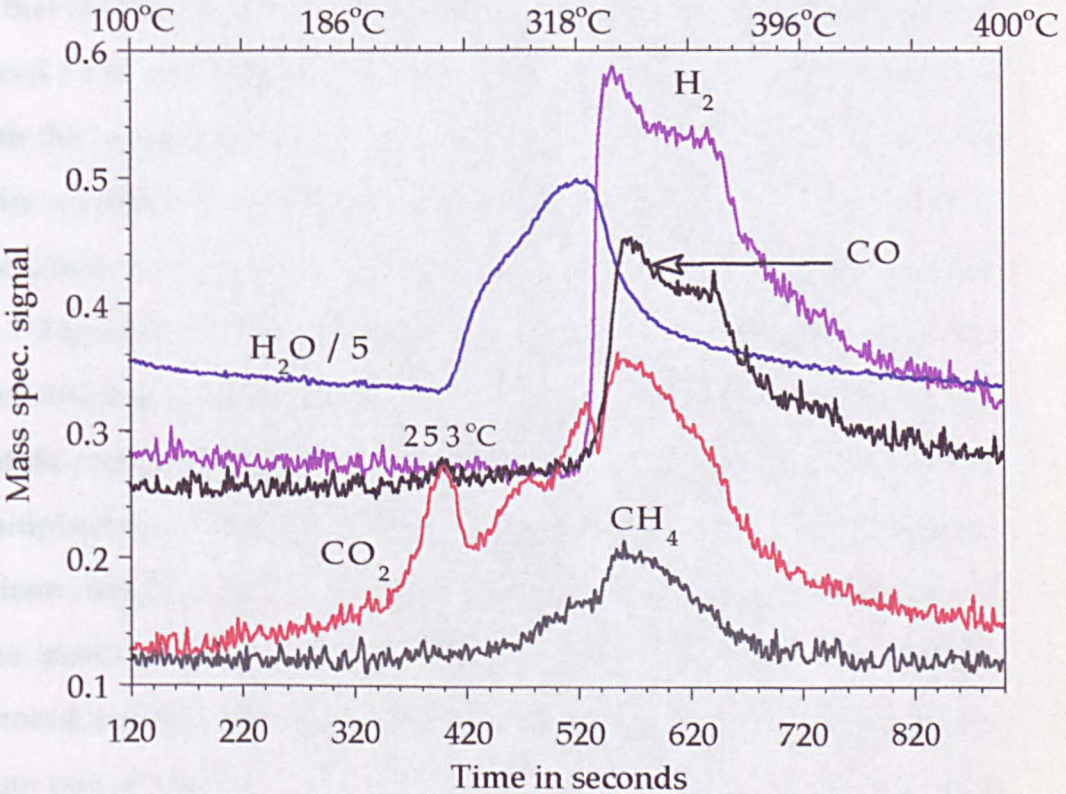

5.3. DISCUSSION

5.3.1. DISCUSSION of CO HYDROGENATION.

A number of authors have reported studies on the effect of alkali metal promotion on Group VIII metals with respect to the CO hydrogenation reaction[13,14,15,16,17,18,19]. From the literature, some general effects of alkali promotion on this reaction are; reduced overall activity, slower rate of hydrogenation, and a higher selectivity to C_2^+ hydrocarbons and also some formation of oxygenates. The main reasons cited for the loss of activity is the blocking of reaction sites by the promoter. The slowing down of the rate of hydrogenation was put down to the stronger metal to carbon bond and likewise, the greater selectivity to higher hydrocarbons was thought to be as a result of the increase in surface residence time of the carbon fragments, therefore increasing the probability of coupling .

Figure 5.3.(b) shows the T.P.P.R. of CO over the promoted catalyst. It is clear that the C(a) is not fully hydrogenated before the following pulse is introduced (the periodicity of the pulses is 35 seconds). This was also the case with the un-promoted catalyst, however the effect is more exaggerated here. The question is whether this is due to a reduction in the rate of hydrogenation, or is it due to more C(a) being laid down on the catalyst surface ? Figure 5.16. compares the rate of C(a) hydrogenation over the promoted and unpromoted catalyst. As the mass spectrometer sensitivity was different during the two experiments, the data from the unpromoted catalyst was multiplied by 1.9 for the illustration purposes, in order that an easier comparison may be made. From the line shapes it appears that the rate of methane production is broadly similar. However in the case of the unpromoted catalyst the peak can be seen to level off (indicating the maximum rate of reaction) at an earlier temperature than with the promoted

case. Therefore the rate of methanation has been slowed down by the potassium. This leads to the conclusion that 0.25 monolayers of potassium does slightly reduce the rate of methanation . It is worth considering the possibility that the catalyst does not have a homogeneous layer of potassium. Due to the acidic nature of the alumina support, the potassium may react with hydroxyl groups and bind more strongly to the alumina than to the rhodium, perhaps in the form of a stable potassium compound such as K_2CO_3. These compounds are known to be formed readily on alumina as well as other catalytic supports[20]. If this is indeed occurring the result would be a coverage of less than 0.25 monolayer on the rhodium particles and the promotion effect would be dampened. There is literature to suggest that this does take place in the case of Cs promotion[17], where the CO/H_2 reaction was relatively unchanged up to Rh:Cs promotion levels of 2:1. Also, in a study on the role of alkali metals as promoters in the Fischer Tropsch reaction over ruthenium[16], it was found that a sharp drop in methanation occurred when the composition of the surface was less than 80% Ru. Up to that point, the reaction was largely unaffected the conclusion was that at ~0.2 monolayers, a disruption of the Ru ensembles occurred, therefore the promoter effect was more a geometric one rather than electronic .

The conversion of CO is higher with the potassium present, especially at higher temperatures, this can be seen by comparing figures 3.13.(b) and 5.3.(b). As the concentration of hydrogen is the same in both T.P.P.R. experiments, the promoted catalyst takes longer to clean as there is more C(a) present. As the conversion of CO was seen to increase with potassium promotion, the site blocking effect cannot be a limiting factor. From the data presented in section 5.2. and with inference to the literature mentioned above, it clear that the potassium is not causing a <u>major</u> change in the CO/H_2 reaction.

The main points to note are; the conversion of CO has risen, CO dissociation starts at the same temperature (within 5°C in both the promoted and unpromoted cases). The rate of methane production is largely unaffected as is the selectivity to higher hydrocarbons and oxygenates, although the rate of methanation is slowed slightly. The concentration of hydrogen on the other hand, greatly influences the rate of hydrogenation but does not lower the activation energy to dissociation, as the on-set temperature of methanation is equal with varying H_2 flow rates.

5.3.2 DISCUSSION of ACETATE DECOMPOSITION.

As potassium is commonly used to lower the work function of metals onto which they adsorb by donating electrons into their conduction band, the expectation before this work was carried out was that the acetate groups would decompose at a lower temperature and would be unlikely to form dense stable clusters necessary for 'explosive' decompositions. In fact, since explosions were seen, it appears that a dense cluster of acetates must indeed be able to form on the rhodium, despite the presence of potassium.

With acetic acid adsorption at 50°C onto an oxygen pre-dosed catalyst, no explosion occurred. However a broad desorption between 200°C and 250°C suggests that acetate are adsorbed on the oxygen covered rhodium but are not able to decompose in a rapid ' explosive ' manner. The reason is clearly connected to the addition of K. The up-take of oxygen on the rhodium surface is reduced considerably by the presence of potassium . It appears that with the reduced level of oxygen up-take, an insufficient density of acetate groups are held on the rhodium surface to create the required conditions for an explosion when the adsorption temperature is 50°C. With the temperature of O_2 adsorption raised to 100°C we see remarkably that an explosion does

occur. The reason for this is that more oxygen is adsorbed onto the rhodium particles at higher temperatures as seen in figure 5.2., allowing a denser cluster of acetate to form on the particles. The effect of the potassium is to broaden the explosion width. This is understandable as the fluid like adlayer of acetate/oxygen atoms described in Chapter 4 is disrupted by the electropositive potassium compounds (such as the oxide and carbonate) which increase the metal - adsorbate bond and in doing so hinder the mobility of the acetate groups. As the temperature of the explosions are quite high it appears that the potassium/oxygen/acetate adlayer is stabilised, perhaps through a diversity of complementary dipole interactions such as $K(\delta+), O(-\delta)$.

In a study of the decomposition of acetate groups from a potassium doped Rh single crystal, Hoogers et al.[21] found that explosions did occur with co-adsorbed oxygen and therefore a dense mixed K/O/acetate adlayer can be formed. The reason they cited for the mixing of the acetate and potassium was their very different dipoles. Potassium destabilised the acetate group, however this effect could be balanced by the stabilising effect of oxygen. It appears in the cases presented here, that the oxygen clearly does compensate for any destabilising effect of the potassium, and the primary effect of the promoter is to broaden the explosion peak width by hindering the mobility and physical intimacy of the acetate groups.

The post explosion desorptions in Figure 5.20 (a) - (d) are similar to the desorptions found on a the Rh/Al_2O_3 catalyst with a very small amount of oxygen predosed onto it as shown in Figures 4.10.(f) and (g). There are clearly two CO_2 desorptions, the first one associated with a water desorption (and a methane desorption) the second associated with a sharp CO and H_2 desorption. It is likely that the H_2 is produced as a result of the lack of O(a) on the rhodium surface, as was seen in Chapter 4, and that CO is produced due

to the enhanced ability of the potassium doped catalyst to dissociate the surface acetates, once the stabilising effect of oxygen has been removed.

The low temperature CO_2 desorption (120°C-220°C) was not seen in the Rh/Al_2O_3 case and is observed here only when O_2 is dosed in quantities greater than 1 ml (that is, saturation). One explanation could be that potassium sites at the rhodium support interface may facilitate acetate decomposition, and this is manifested by the low temperature desorption. Also seen, although delayed by ~80°C due to the strong affinity of the alumina for hydroxyl groups, is a water peak. Figures 5.20 (c) and (d) illustrate that with no low temperature CO_2 desorption, there is no early shoulder to the water peak. The first post-explosion CO_2 desorption is reduced by the appearance of the low temperature CO_2 peak indicating that the same pool of acetates are responsible for both processes and these are the acetates located on the support that migrate to the rhodium particles and dissociate.

5.4. CONCLUSIONS.

The promotion of the Rh/Al_2O_3 catalyst with 0.25 monolayers of potassium changes the activity of the catalyst towards CO hydrogenation but does not change the selectivity. The CO conversion was found to be similar up to ~310°C but rose further at higher temperatures with the potassium promotion. The yield of products - methane , water and carbon dioxide - was higher with the promoter, however, as the leading edge of the line shapes for these masses were similar, the intrinsic rates at which they formed did not vary considerably, with only a slight slowing down of the rate of methane production. Conversely, the rate of CO dissociation increased with the

potassium promoter, as evidenced by the higher conversion. The mechanism of the reaction remains unchanged with CO dissociation being the rate determining step, and the rate of sequential hydrogenation of C(a) increases with both temperature and hydrogen concentration as it did in the unpromoted case.

The decomposition of acetic acid was more sensitive to the potassium promotion, with an obvious change in mechanism. An explosive decomposition only occurred when the temperature of oxygen dosing and acid adsorption was raised to ~100°C. It is believed that adsorption below this temperature does not lead to a sufficiently dense 'cluster' of acetates on the rhodium particles, for an explosion to occur. The mechanism of decomposition after the explosion has happened is akin to the situation present on the unpromoted catalyst, with CO and H_2 accompanying the high temperature decomposition. It is thought that the change in mechanism is caused by a reduction in the number of O(a) species on the rhodium particles.

5.5. REFERENCES.

1 Bond, G.C. *"Heterogeneous Catalysis: Principles and Applications"* 2nd Edn. Oxford University Press (1987)

2 Bowker M., 'Promoter Effects in Ammonia Synthesis' in *'The Chemical Physics of Solid Surfaces and Heterogeneous Catalysis.'* eds. King, D.A. and D.P.Woodruff, (Elsevier, Amsterdam, 1993), Vol 6, Ch. 7.

3 Ellgen, P.C., Bartley, W.J., Bhasin, M.M. and Wilson, T.P., *Adv. Chem.*, **178**, 147 (1979)

4 Hindermann, J.P., Hutchings, G.J. and Kiennemann, A., *Catal. Rev.-Sci. Eng.*, **35**(1), 1 (1993).

5 Sachtler, W.M.H., Schriver,D.F., Hollenberg, W.B. and Lang, A.F., *J.Catal.* **92**, 429 (1985)

6 Ichikawa, M. and Fukushima, T., *J. Phys. Chem.*, **89**, 1564 (1985)

7 Koerts, T., Welters, W.J.J. and Van Santen, R.A., *J. Catal.*, **133**, (1992).

8 Koerts, T. and Van Santen, R.A., *Catal. Letts.*, **6**, 49 (1990).

9 Paal, Z., Ertl, G. and Lee, L., *Appl. Surf. Sci.*, **8**, 231 (1981).

10 Bowker, M., *Appl. Catal.*, **45**, 115 (1988).

11 Holloway, S., Norskov, J. and Lang, N., *J. Chem. Soc. Faraday I*, **83**, 1935 (1987).

12 Holloway, S. and Norskov, J., *J. Electroanal. Chem.*, **161**, 193 (1984).

13 Hoffmann, F.M. and Weisel, M.D., *Surf. Sci.* **269/270**. 495 (1992).

14 Kagami, S., Naito, S., Kikuzono, Y. and Tamaru, K., *J. Chem. Soc. Commun.*, 256 (1983).

15 Chuang, S.C., Goodwin, Jr. J.G. and Wender, I., *J.Catal.*, **95**, 435 (1985).

16 Mori, T., Miyamoto, A, Takahashi, N., Niizuma, H., Hattori, T. and Murakami, Y., *J. Catal.*, **102**, 199 (1986).

17 McLaughlin Mclory,M. and Gonzales, R.D. *J.Catal*. **89**, 392 (1984).

18 Blackmond, D.G., Williams, J.A., Kesraoui, S. and Blazewick, D.S., *J. Catal.*, **101**, 496 (1986).

19 Hoost, T.E. and Goodwin,Jr. J.G., *J. Catal.*, **137**, 22 (1992).

20 Stork, W.H.J. and Pott. G.T. *J. Phys. Chem.* **78**, 2496 (1974).

21 Hoogers, G., Papageorgopoulos,D.C. and King,D.A., *J. Chem. Phys.*, submitted.

CHAPTER 6.

SUMMARY.

The aim of this final chapter is two-fold; to outline the main conclusions reached through the experiments highlighted in this thesis and, in doing so, to place the work in the correct context with respect to the literature. Secondly, the aim is to look towards the future and suggest useful and worthwhile science that leads on from this thesis, both in terms of the reactions studied and the experimental techniques employed.

A novel pulsed flow microreactor was used to perform all the experiments presented in this thesis. The microreactor is described in Chapter II. The catalyst under investigation was highly dispersed rhodium on alumina (1% by weight on alumina) and was studied with respect to the reactions of CO and H_2. These results are presented and discussed in chapter III. The decomposition of surface acetate groups, adsorbed by dissociative adsorption of glacial acetic acid, was also studied. These results are presented in chapter IV.

The experimental technique best described as Temperature Programmed Pulsed Reaction (T.P.P.R.) allows 0.5 ml pulses of CO to be eluted into a continuous gas stream, either a diluent or a H_2 diluent mix. The products evolved are monitored continuously, in real time, by quadrupole mass spectrometry. Therefore transient studies can be readily be done through the temperature range 20°C- 450°C.

Under the experimental conditions employed, the catalyst was 100% selective in the production of methane and water from synthesis gas between 160°C and 260°C. Above 260°C a gross change in the methanation mechanism occurred, with dry methanation becoming the more dominant process at higher temperatures. The two reactions are written below.

$CO + 3H_2$ ---------> $CH_4 + H_2O$ $\quad \Delta H_{1000K} = -225.4$ kJ mol^{-1}

$2CO + 2H_2$ ---------> $CH_4 + CO_2$ $\quad \Delta H_{1000K} = -260.5$ kJ mol^{-1}

The change in mechanism is caused by a change in the surface stoichiometries of the reactants as the temperature rises. This is due to the faster desorption rate of H_2 compared with CO.

There have been several proposals for hydrogen assisted CO dissociation cited in the literature. However, in the work presented in Chapter II, the onset of methane production, indicative of CO dissociation, does not vary with a change in H_2 concentration. Therefore H_2 does not lower the activation energy towards CO dissociation. The role of H_2 is to clean the surface of C(a) and O(a) and the rate of both methane and H_2O formation increases with H_2 concentration. Under T.P.P.R. conditions there was very little evidence for the production of higher hydrocarbons of C_2^+ oxygenates. It appears that the surface carbon species formed during a 0.5 ml pulse of CO are not in sufficient concentration and are hydrogenated off the surface too quickly for any coupling or insertion reactions to occur. Some surface species were formed, namely formate species and carbonate species. Under H_2 deficient conditions these surface species decomposed between 320°C and 450°C. This was apparent as there was a broad rise in the CO_2 base line and a tail accompanying the CO_2 peak resulting from the Boudouard reaction. With sufficient H_2 the surface species were hydrogenated away more rapidly such that no broad rise or obvious tail appeared in the CO_2 line shape. Without H_2 flowing, CO dissociation soon becomes poisoned over the catalyst as the rhodium surface is blocked with C(a). This amorphous carbon can be hydrogenated away to methane between 100°C and 350°C, with an activation energy of 57kJ/mol.

Pulses of CO_2 react with H_2 to yield CH_4 and H_2O with 100% selectivity between 150°C and 450°C, over the rhodium catalyst. The conversion of CO_2 is far less than CO under equivalent conditions of temperature and pressure. In agreement with the literature, the intrinsic rate of CH_4 formation once CO_2 has dissociated is faster than that from CO

dissociation. The main reason for this is that as less CO_2 dissociates, so the ratio of C(a) to $H_{(a)}$ will be small and so there is always plenty of hydrogen available to react with the C(a).

Looking towards the future, many useful experiments present themselves that would further clarify both the reactions of synthesis gas over rhodium catalysts and the usefulness of the pulsed flow microreactor. For instance, a more detailed kinetic study is needed in order to determine the exact reaction rates of the individual mechanistic steps. This can be done by fine tuning the microreactor such that the dead volume of the U-tube is essentially zero, to eliminate any diffusion effects and by modifying the acquisition data such that more detailed line shapes can be obtained. The latter suggestion is presently being carried out and the new software is able to collect data essentially as fast as the PC can process it. In practice, fifteen data points per mass, per second is easily attainable.

With a further modification to the reactor such that reactants can be continually dosed across the catalyst, isotopic studies incorporating labelled CO for instance, could give detailed kinetics of the reactions operating under steady state conditions. With a variety of reducible metal oxide promoters such as vanadia or iron, rhodium catalysts can become selective in higher oxygenate synthesis towards products such as ethanol and acetic acid. A transient study using labelled CO would help pin-point the mechanism of oxygenate synthesis and reveal the kinetics of the steps involved.

Chapter IV details an interesting example of a direct transfer of knowledge from surface science to catalysis. A phenomenon known as 'surface explosions' has been found to take place on the supported rhodium catalyst. The surface adsorbate that decomposes explosively is an acetate group. To our knowledge, this is the first example to be reported in the literature, of a carboxylate surface explosion occurring on a supported catalyst. It was found that the acetate group only resides on the rhodium

phase after oxygen was pre-adsorbed. With no oxygen pre-dose, no explosion occurred. The explosions are analogous to those reported in the surface science literature. A simple mathematical model of second order autocatalysis closely fits the experimental data in terms of line shape and width and thus best describes the kinetics taking place. In the model, a product of the decomposition is itself required for the forward reaction to take place. In this case the product is a clean rhodium atom, upon which a further decomposition takes place. The explosion itself occurs exclusively on the rhodium phase, however as much of the acetate resides on the support further decompositions occur at higher temperatures. To describe these processes, a mechanism is proposed incorporating a migration of support phase acetates to the rhodium particles. Available O(a) at the rhodium surface are reacted to H_2O during the acetate decomposition.

Practical applications of this discovery are seemingly few. However, from a fundamental point of view, there are many interesting avenues to explore. Presently, a detailed mathematical description of both the single crystal and the supported catalyst explosions is underway. It incorporates more parameters than the simple model described in chapter IV. The more localised nature of the processes, required by the small rhodium particles, is described by averaging the dispersion of the initiation sites. Also parameters such as staggered decomposition initiation, varying rates of decomposition and different initiation temperatures are built into the model.

The support clearly has an effect on the explosion and more noticeably on the higher temperature decompositions. An interesting study would be to extend the explosion phenomenon to a variety of supports in order to test the migrating acetate model and to clarify the synergy that exists between the support and metal phase. The potassium had a marked effect on the higher temperature decompositions and a more extensive study using a variety of promoters should shed further light on the decomposition pathways. As the

explosion phenomenon was extended to a number of metals and crystal planes in the surface science studies, it is possible that under the correct conditions explosions may occur on a similar variety of supported metal catalysts.